International Linear Collider Reference Design Report 2007

February 7, 2007

CONTENTS

LIST of FIGURES

LIST of TABLES

CHAPTER 1

Overview

This Chapter is published separately for the February 2007 release.

CHAPTER 2

Accelerator Description

2.1 BEAM PARAMETERS

The International Linear Collider (ILC) is designed to achieve the specifications listed in the ILCSC Parameter Subcommittee Report [5]. The three most important requirements are: (1) an initial center-of-mass (cms) energy up to 500 GeV with the ability to upgrade to 1 TeV, (2) an integrated luminosity in the first four years of 500 fb^{-1} at 500 GeV cms or equivalent at lower energies, and (3) the ability to scan in energy between 200 and 500 GeV cms.

The ILC Reference Design Report describes a collider that is designed to meet these requirements. The installed RF system is capable of accelerating beams for collisions at 500 GeV cms. The peak luminosity of $2 \times 10^{34}\,\mathrm{cm}^{-2}\mathrm{s}^{-1}$ at 500 GeV and a collider availability of 75% should enable the delivery of 500 fb^{-1} in the first four years of physics operation assuming an annual physics run of 9 months. The energy flexibility has been a consideration throughout the design and essential items to facilitate a future upgrade to 1 TeV, such as the length of the beam delivery system and the power rating of the main beam dumps, have been incorporated.

2.1.1 Collider and Beam Parameters

The ILC is based on 1.3 GHz superconducting RF cavities operating at a gradient of 31.5 MV/m. The collider operates at a repetition rate of 5 Hz with a beam pulse length of roughly 1 msec. The site length is 31 km for a cms energy of 500 GeV; the site would have to be extended to reach 1 TeV. The beams are prepared in low energy damping rings that operate at 5 GeV and are 6.7 km in circumference. They are then accelerated in the main linacs which are ∼11 km per side. Finally, they are focused down to very small spot sizes at the collision point with a beam delivery system that is ∼2.2 km per side. To attain a peak luminosity of $2 \times 10^{34}\,\mathrm{cm}^{-2}\mathrm{s}^{-1}$, the collider requires ∼230 MW of electrical power. A summary of the overall collider parameters appears in Table 2.1-1.

The beam parameters to reach a peak luminosity of $2\times10^{34}\,\mathrm{cm}^{-2}\mathrm{s}^{-1}$ are listed in Table 2.1-2. The table lists a set of nominal parameters and three other sets that define a 'parameter plane'. The collider has been designed to the nominal parameter set which was optimized considering aspects of the whole accelerator system such as: the beam instabilities and kicker hardware in the damping rings, the beam current and the pulse length in the linacs, and the kink instability and background in the final focus system. The parameter plane establishes

TABLE 2.1-1
Global Accelerator Parameters for 500 GeV cms.

Center-of-mass energy	500 GeV
Peak luminosity	2×10^{34} $\mathrm{cm}^{-2}\mathrm{s}^{-1}$
Availability	75%
Repetition rate	5 Hz
Duty cycle	0.005%
Main linacs	
Average accelerating gradient in cavities	31.5 MV/m
Length of each main linac	11 km
Beam pulse length	1 ms
Average beam current in pulse	9.0 mA
Damping rings	
Beam energy	5 GeV
Circumference	6.7 km
Length of beam delivery section (2 beams)	4.5 km
Total site length	31 km
Total site power consumption	230 MW
Total installed power	∼300 MW

a range of operating parameters that represent slightly different tradeoffs between these considerations. Experience with past accelerators indicates that there will be operational difficulties, which will be eased by modifying the beam parameters. The parameter plane provides flexibility to cope with such problems without sacrificing performance. It can also be useful during collider commissioning and when tuning the luminosity characteristics for different measurements and particle physics detectors.

2.1.1.1 The Nominal Parameter Set

The main linac RF system is designed to accelerate beam at a gradient of 31.5 MV/m. The nominal beam current is 9.0 mA and the beam pulse length is 970 μs so that the RF pulse length (including the fill time of the cavities) is 1.56 ms. The optimal single bunch charge is a balance between effects at the IP and in the damping ring; the choice of 2×10^{10} is similar to that specified in the TESLA TDR [2] and the US Technical Options Study [3].

The normalized vertical emittance at the IP is chosen to be 4×10^{-8} m·rad. This corresponds to a geometric emittance of ∼1 pm from the damping rings (5 GeV) and assumes 100% emittance growth during the transport to the IP. This damping ring emittance is slighty lower than what has already been achieved but is thought to be well within the present technology. The 100% emittance growth estimate is based on calculations made during the ILC Technical Review Report [1].

TABLE 2.1-2
Beam and IP parameters for 500 GeV cms

		Nominal	Low N	Large Y	Low P
Repetition rate	f_{rep} (Hz)	5	5	5	5
Number of particles per bunch	N (10^{10})	2	1	2	2
Number of bunches per pulse	n_b	2625	5120	2625	1320
Bunch interval in the main linac	t_b (ns)	369.2	189.2	369.2	480.0
in units of RF buckets		480	246	480	624
Average current in the main linac	I_{ave} (mA)	9.0	9.0	9.0	6.8
Normalized emittance at IP	$\gamma\epsilon_x^*$ (mm·rad)	10	10	12	10
Normalized emittance at IP	$\gamma\epsilon_y^*$ (mm·rad)	0.04	0.03	0.08	0.035
Beta function at IP	β_x^* (mm)	20	11	11	11
Beta function at IP	β_y^* (mm)	0.4	0.2	0.6	0.2
R.m.s. beam size at IP	σ_x^* (nm)	639	474	474	474
R.m.s. beam size at IP	σ_y^* (nm)	5.7	3.5	9.9	3.8
R.m.s. bunch length	σ_z (μm)	300	200	500	200
Disruption parameter	D_x	0.17	0.11	0.52	0.21
Disruption parameter	D_y	19.4	14.6	24.9	26.1
Beamstrahlung parameter	Υ_{ave}	0.048	0.050	0.038	0.097
Energy loss by beamstrahlung	δ_{BS}	0.024	0.017	0.027	0.055
Number of beamstrahlung photons	n_γ	1.32	0.91	1.77	1.72
Luminosity enhancement factor	H_D	1.71	1.48	2.18	1.64
Geometric luminosity	$\mathcal{L}_{geo}$ $10^{34}/\mathrm{cm}^2/\mathrm{s}$	1.20	1.35	0.94	1.21
Luminosity	$\mathcal{L}$ $10^{34}/\mathrm{cm}^2/\mathrm{s}$	2	2	2	2

2.1.1.2 Parameter Plane

The parameter sets labeled 'Low N' (low number of particles per bunch), 'Large Y' (large vertical emittance) and 'Low P' (low beam power) in Table 2.1-2 are representative points in the parameter plane. These parameter sets deliver essentially the same luminosity $2 \times 10^{34}\,\mathrm{cm}^{-2}\mathrm{s}^{-1}$ at 500 GeV but with different values for the specific beam parameters. The collider subsystems have been designed such that any point in the parameter plane is attainable. At present, it is not believed that there is a large cost impact of maintaining the parameter plane and there is a significant gain in operational flexibility; this will need to be examined again during the next phase of design optimization.

Low N

The bunch population of 2×10^{10} may lead to problems such as microwave instabilities in the damping rings, single bunch wakefield emittance dilutions, or a large disruption parameter at the IP which can cause a kink instability and may make the IP feedback difficult. In such cases, it could be desirable to reduce the bunch population.

The Low N parameter set addressed these possible difficulties with a reduced single bunch charge and reduced bunch length. Halving the bunch population with fixed current (twice the number of bunches and half the bunch interval) reduces the luminosity but this is compensated by focusing more tightly at the IP. These parameters also have lower beamstrahlung and possibly lower backgrounds in the particle physics detectors at the IP which may be desirable for some measurements. All these changes are beneficial, however, the Low N parameter set is more demanding in terms of the damping ring kicker, the bunch compressor, and the multi-bunch collective effects in the damping rings.

Large Y

The vertical emittance at the IP of 4×10^{-8} m·rad may not be achieved due to tuning difficulties in the damping rings and beam delivery system or wakefield effects in the linac. The Large Y parameters assume a vertical emittance that is twice the design and the luminosity is recovered by focusing more tightly in the horizontal at the IP and using a longer bunch to reduce the increased beamstrahlung. Unfortunately, the disruption parameter at the interaction point is increased and kink instability may be more pronounced.

Low P

Another condition that may arise are limitations due to the beam current or beam power. These may arise in the injector systems, damping rings, main linacs or beam delivery system. In this case, the collider could be optimized in the direction of the Low P parameters where the beam current is reduced by 30% and the beam power is reduced by a factor of two. Again, the luminosity is recoved with increased focusing at the IP in the horizontal plane. In this case, the beamstrahlung cannot be reduced by increasing the bunch length because of the tight focusing in the vertical plane. This results in a beamstrahlung that is roughly double that in the nominal parameters and this may limit the performance of the particle physics detector and the beam delivery extraction line.

2.1.1.3 Range of Parameters

The parameter plane described above defines a range of parameters as shown in Table 2.1-3. Note, however, the parameters, when they are varied, are correlated. For example, the shortest bunch length is required only when the bunch population is low.

TABLE 2.1-3
Range of parameters

		min		nominal		max	
Bunch population	N	1	-	2	-	2	$\times 10^{10}$
Number of bunches	n_b	1320	-	2625	-	5120	
Linac bunch interval	t_b	189	-	369	-	480	ns
Bunch length	σ_z	200	-	300	-	500	μm
Vertical emittance	$\gamma\epsilon_y^*$	0.03	-	0.04	-	0.08	mm·mrad
Beta function at IP	β_x^*	11	-	20	-	20	mm
	β_y^*	0.2	-	0.4	-	0.4	mm

2.1.1.4 Bunch Spacing and Path Length Considerations

In order to extract the bunches in the damping ring one by one and inject into the main linac there are certain constraints to satisfy among the DR circumference, number of bunches, RF frequencies and bunch distances in the DR and main linac. The present beam parameters do not meet all of the constraints needed to best facilitate injection and extraction from the damping rings [6]. The parameters will continue to be optimized during the next design phase to better satisfy the constraints, and it is expected that the damping ring circumference and linac bunch spacing will change by small amounts.

In addition, there is another another constraint due to the fact that the positrons are generated by electrons on the previous pulse. For flexible operation, it is highly desireable that the sum of certain beamline lengths such as the main linac and the transport lines be a multiple of the DR circumference. Because of this constraint, the exact location of the injector complex and the layout of the transport lines is a subject that can be fixed only after the final component lengths and the site are decided.

2.2 ELECTRON SOURCE

2.2.1 Overview

The ILC polarized electron source must produce the required train of polarized electron bunches and transport them to the Damping Ring. The nominal train is 2625 bunches of 2.0×10^{10} electrons at 5 Hz with polarization greater than 80%. The beam is produced by a laser illuminating a photocathode in a DC gun. Two independent laser and gun systems provide redundancy. Normal-conducting structures are used for bunching and pre-acceleration to 76 MeV, after which the beam is accelerated to 5 GeV in a superconducting linac. Before injection into the damping ring, superconducting solenoids rotate the spin vector into the vertical, and a separate superconducting RF structure is used for energy compression. A third polarized electron source (500 MeV) drives the Positron Keep Alive Source (KAS). Polarization is not required in the baseline, but will be required for either the e^--e^- or γ-γ options.

The SLC polarized electron source already meets the requirements for polarization, charge and lifetime. The primary challenge for the ILC source is the long bunch train, which demands a laser system beyond that used at any existing accelerator, and normal conducting structures which can handle high rf power. Both R$D developments are considered manageable.

2.2.2 Beam Parameters

The key beam parameters for the electron source are listed in Table 2.2-1.

TABLE 2.2-1
Electron Source System Parameters

Parameter	Symbol	Value	Units
Electrons per bunch (at gun exit)	n_e	3×10^{10}	Number
Electrons per bunch (at DR injection)	n_e	2×10^{10}	Number
Number of bunches	N_e	2670	Number
bunch repetition rate	$F_{\mu b}$	3	MHz
bunch train repetition rate	F_{mb}	5	Hz
bunch length at source	Δt	1	ns
Peak current in bunch at source	I_{avg}	3.2	A
Energy stability	S	<5	% rms
Polarization	P_e	80 (min)	%
Photocathode Quantum Efficiency	QE	0.5	%
Drive laser wavelength	Λ	790±20 (tunable)	nm
single bunch laser energy	E	5	μJ

2.2.3 System Description

Figure 2.2-1 depicts schematically the layout of the polarized electron source. Two independent laser systems are located in a surface building. The light is transported down an evacuated light pipe to the DC guns. The beam from either gun is deflected on line by a magnet system which includes a spectrometer, and it then passes through the normal-conducting subharmonic bunchers, traveling wave bunchers and pre-accelerating sections. This is followed by the 5 GeV superconducting linac. The Linac-to-Ring transfer line that brings the beam to the damping rings contains the spin rotators and energy compression.

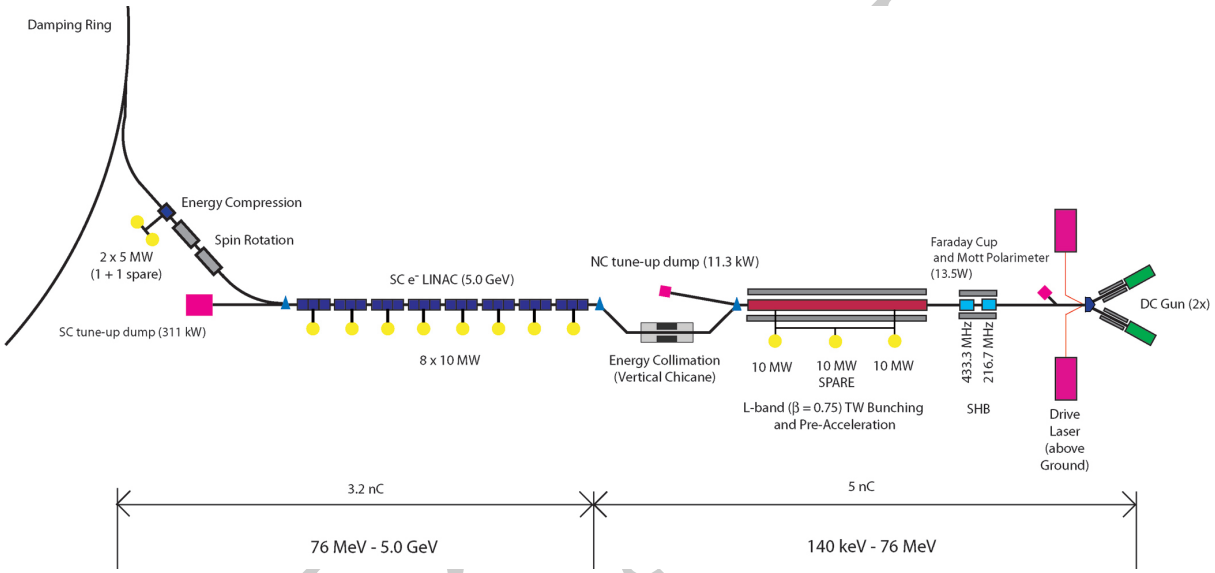

FIGURE 2.2-1. Schematic View of the Polarized Electron Source

2.2.3.1 Photocathodes for Polarized Beams

Photocathode materials have been the subject of intense *R&D* efforts for more than 15 years. The most promising candidates for the ILC polarized electron source are strained GaAs/GaAsP superlattice structures (see Figure 2.2-2). GaAs/GaAsP superlattice photocathodes routinely yield at least 85% polarization with a maximum QE of 1% (routinely 0.3 to 0.5%) [7, 8]. The present cathodes consist of very thin quantum well layers (GaAs) alternating with lattice-mismatched barrier layers (GaAsP). Each layer of the superlattice (typically 4 nm) is considerably thinner than the critical thickness (10 nm) for the onset of strain relaxation, while the transport efficiency for electrons in the conduction band still can be high. The structures are p-doped using a high-gradient doping technique, consisting of a thin (10 nm), very highly doped ($5 \times 10^{19}\ cm^{-3}$) surface layer with a lower density doping ($5 \times 10^{17}\ cm^{-3}$) in the remaining active layer(s). A high surface doping density is necessary to achieve high QE while reducing the surface-charge-limit problem. A lower doping density is used to maximize the polarization. With bunch spacing of 300 ns, the surface-charge-limit problem for the ILC is not expected to be a major issue. The optimum

doping level remains to be determined. An alternative under study is the InAlGaAs/GaAsP strained superlattice with minimum conduction band offset where a peak polarization of 91% has been observed [9]. Research continues on various cleaning and surface preparation techniques. Atomic hydrogen cleaning (AHC) is a well-known technique for removing oxides and carbon-related contaminants at relatively low temperatures [10] and will be further explored in the near future.

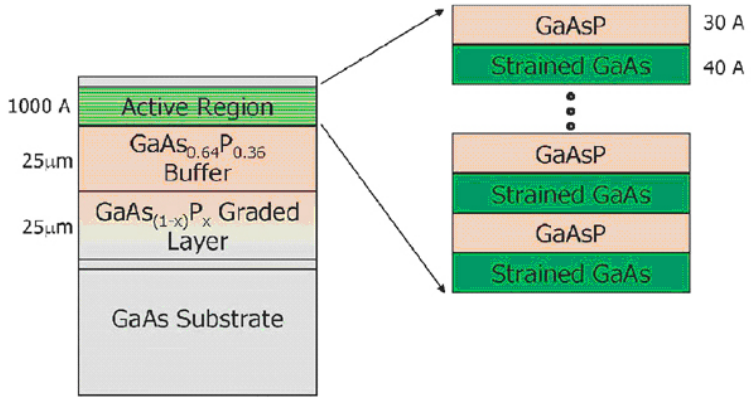

FIGURE 2.2-2. Structure of a Strained GaAs/GaAsP Superlattice Photocathode for Polarized Electrons

2.2.3.2 Polarized Electron Gun

The ILC polarized electron gun is a DC gun based on the design of the gun used for the SLC [11]. The ILC gun will be optimized for a space charge limited peak current of 4.5-5 A (4.5 - 5 nC/1ns). This provides overhead to compensate for losses that occur primarily through the bunching system. The gun power supply provides a cathode bias of -140 to 160 kV. An ultrahigh vacuum system with a total pressure $\leq 10^{-12}$ Torr (excluding H_2) is required to maintain the negative electron affinity (NEA) of the cathode. An SF_6/dry air gas system is used to maintain a high dielectric gun environment to avoid HV breakdown between ground and HV components. During HV operation the electric field on the cathode surface must be kept below 7 MeV/m to ensure low dark current (< 25 nC). Excessive dark current will lead to field emission resulting in molecular desorption from nearby surfaces. This process leads to deterioration of the gun vacuum and is destructive to the cathode's NEA surface.

The gun area will be equipped with a Mott polarimeter to measure polarization and a Faraday cup to measure the charge. Several Residual Gas Analyzers (RGAs) characterize the vacuum near the gun. Other special diagnostics for the DC gun include means to measure the quantum efficiency of the cathode (a cw diode laser integrated into the gun) and a nano-ammeter for dark current monitoring.

An NEA cathode requires periodic cesiation. Cesiator channels are located near the cathode to allow in situ cesiation of the photocathode. An improvement of the current

SLC gun design will be to locate the cesiation channels behind a retractable photocathode. This will eliminate the deposition of Cesium on electrode surfaces, thereby reducing the dark current of the gun. The SLC and subsequent polarized beam experiments at SLAC have demonstrated the operation of an efficient and highly automated cesiation system with minimal source downtime. The gun will have an integrated cathode preparation chamber and load-lock system. The activation chamber will be semi-permanently attached to the gun and both volumes will be semi-permanently maintained under high vacuum. The preparation chamber will allow the option of local cathode cleaning and activation as well as storage of spare cathodes. Cathodes may be rapidly exchanged between the gun and preparation chamber. The load-lock consists of a small rapidly-pumped vacuum chamber for transfering cathodes from an external atmospheric source into or out of the preparation chamber without affecting the latter's vacuum.

The dominant source of intensity variations and timing jitter is the laser system. A secondary source for intensity variations is the gun power supply and beam dynamics influenced by space charge forces within the gun and the low energy sections of the injector.

2.2.3.3 ILC Source Laser System

A conceptual layout schematic of the laser system is depicted in Figure 2.2-3. To match the bandgap energy of GaAs photocathodes, the wavelength of the laser system must be 790 nm and provide tunability (±20 nm) to optimize conditions for a specific photocathode. Therefore, the laser system is based on Ti:sapphire technology.

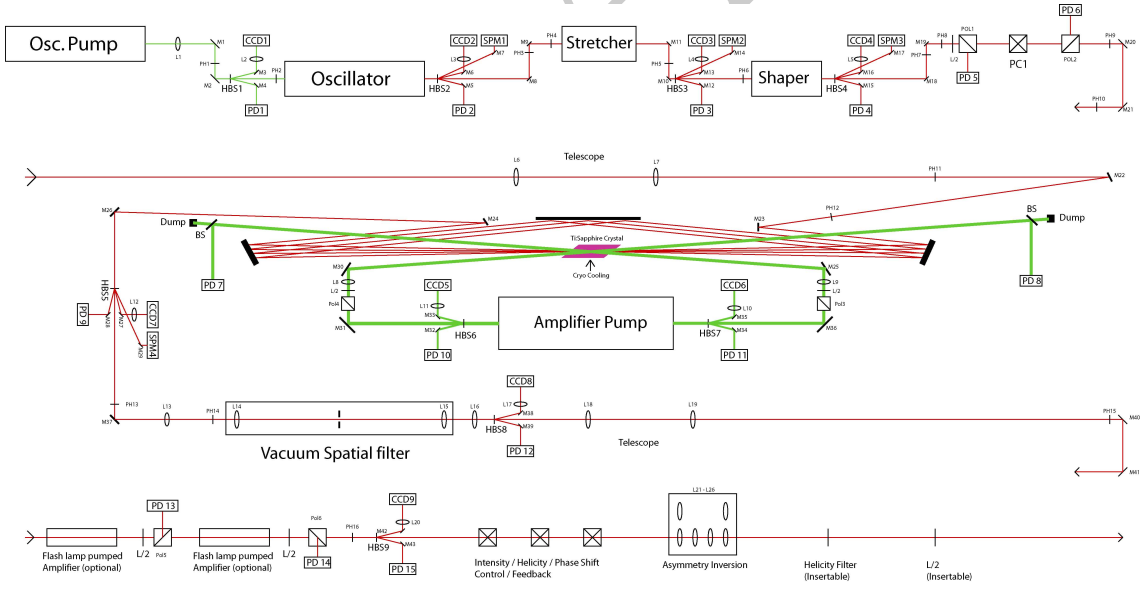

FIGURE 2.2-3. Schematic View of Source Drive Laser System

The 3 MHz pulse train is generated by a cavity-dumped mode-locked oscillator. After diffractive pulse stretching to 1 ns and temporal pulse shaping, the bunch train is amplified using a multi-pass Ti:sapphire amplifier. The amplifier crystal must be cryogenically

cooled to facilitate power dissipation and minimize instabilities caused by thermal lensing induced by the high power amplifier pump. A cw frequency-doubled Nd:YAG (or similar such as Nd:vanadate) diode pumped solid state (DPSS) laser provides the pump power for the Ti:sapphire amplifier. Additional amplification can be supplied by one or multiple flash-lamp pumped Ti:sapphire stages. Final laser pulse energy and helicity control is achieved by electro-optical techniques. This system can also be used as a feed-back device to compensate for the QE decay of the photocathode between cesiations, to remove slow intensity drifts of laser and/or electron beam, and to maintain the elliptical polarization state of the laser beam. Various optical techniques are used to cancel systematic effects caused by an asymmetric laser beam profile or effects associated with the sign of the helicity of the laser light.

2.2.3.4 Bunching and Pre-Acceleration

The bunching system compresses the 1 ns micro-bunches generated by the gun down to ∼20 ps FWHM. It includes two subharmonic bunchers (SHBs) and a 5 cell traveling wave β=0.75 L-band buncher. The SHB cavities operate at 216.7 MHz and 433.3 MHz, respectively. Together they compress the bunch to ∼200 ps FWHM. The L-band bunching system is a modification of the TESLA Test Facility [12] design with a traveling wave buncher to maximize capture efficiency. The buncher has 5 cells with β=0.75 and a gradient of 5.5 MV/m and compresses the bunch to 20 ps FWHM. The buncher and the first few cells of the following TW pre-accelerator are immersed in a 660 G solenoidal field to focus the beam. Two 50 cell β=1 normal conducting (NC) TW accelerating sections at a gradient of 8.5 MV/m increase the beam energy to 76 MeV. These structures must withstand very high RF power for the duration of the very long pulse but they are identical to those being developed for the positron source. Further details of the bunching system are summarized in reference [13].

2.2.3.5 Chicane, Emittance Measurement and Matching Sections

Immediately downstream of the NC pre-acceleration a vertical chicane provides energy collimation before injection into the SC booster linac. The chicane consists of four bending magnets and several 90° FODO cells. The initial dipole at the chicane entrance can be used as a spectrometer magnet (see Figure 2.2-1). A short beam line leads to a diagnostic section that includes a spectrometer screen. The injector beam emittance is measured by conventional wire scanners downstream of the chicane. Two matching sections combine the chicane and emittance measurement station with the downstream SC booster linac.

2.2.3.6 The 5 GeV Superconducting Pre-Acceleration (Booster) Linac

Twenty-one standard ILC-type SC cryomodules accelerate the beam to 5 GeV, and typical FODO cells integrated into the cryomodules transversely focus the beam. An additional string of three cryomodules is added to provide redundancy (total of 24 cryomodules). The booster linac consists of two sections. In the 1^{st} section, the e- beam is accelerated from 76 MeV to 1.7 GeV in cryomodules with one quadrupole per module. In the 2^{nd} section, the e^- beam is accelerated to the final 5 GeV in cryomodules with one quadrupole every other module.

TABLE 2.2-2
76 MeV Beam Parameters for the NC Bunching and Pre-Accelerating Electron Source (end of NC acceleration):

Parameters	$\beta = 0.75$ TW Buncher Design
Initial charge	4.5 - 5 nC
Transmitted charge	92%
Phase extension FWHM	9 deg L-band
Energy spread FWHM	<100 keV
Normalized rms emittance	70 μm-rad

2.2.3.7 Linac to Damping Ring Beamline and Main e^- Source Beam Dump

The Linac To Ring (LTR) beam line transports the beam to the damping ring injection point and performs spin rotation and energy compression. The 5 GeV longitudinally polarized electron beam is first bent through an arc. At 5 GeV, the spin component in the plane normal to the magnetic field precesses 90° in that plane for every n × 7.9° (n: odd integer) of rotation of momentum vector. An axial solenoid field integral of 26.2 T-m rotates the spin direction into the vertical [14]. A 5 GeV beam dump is installed near the LTR. To dump the 5 GeV beam, the first bend of the LTR is turned off, and the dump bend downstream energized. The dump drift is ∼12 m.

2.2.4 Accelerator Physics

Simulations indicate that >95% of the electrons produced by the DC gun are captured within the 6-D damping ring acceptance: $\gamma(A_x+A_y) \leq$0.09 m and ΔE x Δz $\leq$(±25 MeV) x (±3.46 cm). The starting beam size diameter at the gun is 2 cm, and this is focused to a few mm diameter before it is injected into the DR. Calculations in the low energy regions of the injector ($\leq$76 MeV) include space charge effects and use PARMELA [15]. The beam propagation through the superconducting booster linac and LTR beam line has been optimized using MAD [16] and tracked by the ELEGANT code [17].

2.2.4.1 DC Gun and Bunchers

The DC gun creates a 140-160 keV electron beam with a bunch charge of 4.5-5 nC with a bunch length of 1 ns and an unnormalized transverse edge emittance at the gun exit of 70 mm-mrad. To minimize longitudinal growth of the bunch it is desirable to locate the first subharmonic buncher as close to the gun as possible. However, the beam lines needed to combine both guns require a distance of ∼1-1.5 m between gun and first SHB. The SHBs capture almost 100% of the electrons generated at the gun. The beam parameters at 76 MeV are summarized in Table 2.2-2. A plot of the beam envelope from gun up through the bunching system is given in Figure 2.2-4.

2.2.4.2 The 5 GeV Booster Linac and Linac to Damping Ring Transfer Line (eLTR)

The optics of the superconducting booster linac are shown in Figure 2.2-5.

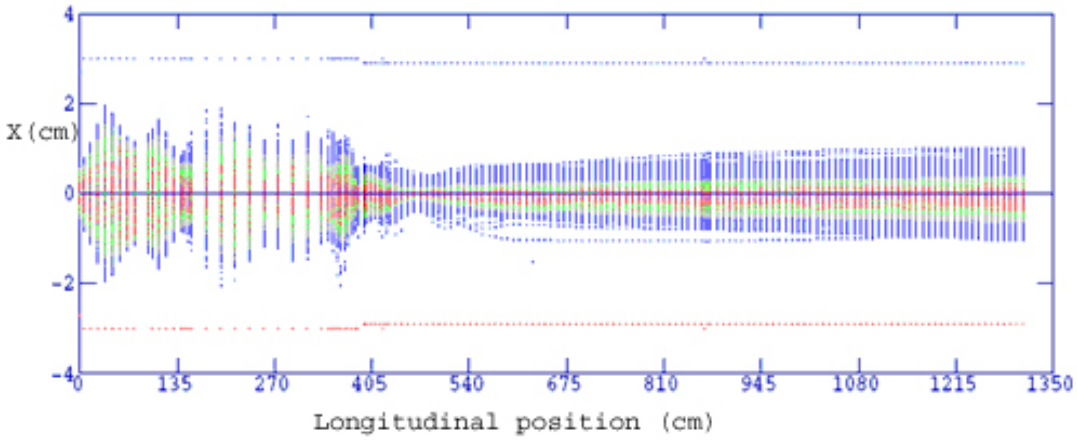

FIGURE 2.2-4. Beam Envelope along the 76 MeV Injector

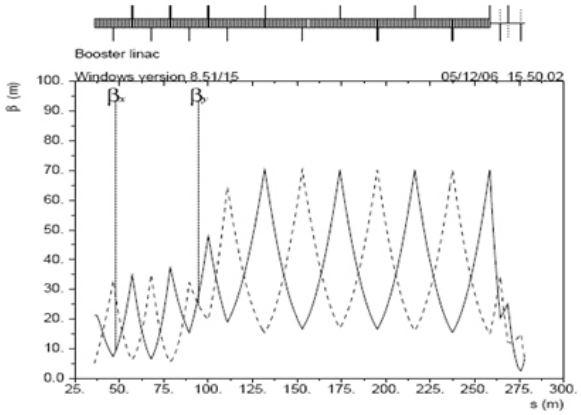

FIGURE 2.2-5. Optics of the SC Electron Booster Linac

At the dump window, the e-edge beam size σ_x/σ_y is 0.72 cm/1.4 cm and 13.9 cm/1.4 cm for 0% and ±10% energy spread, respectively. These beam sizes are within the dump window specifications. At the monitor location the dispersion dominates the beam size and thus the dump also serves as an energy spectrometer with 0.1% resolution.

The LTR arc consists of four FODO cells with eight bends. The total arc bending angle is $7 \times 7.9°$. The R_{56} (path length energy correlation) is adjustable, (86 ±40 cm). The arc is followed by the solenoid sections and RF unit, which occupy 5.5 m and 8.32 m, respectively. There are three PPS stoppers with 1 m space in the LTR arc. Two FODO cells upstream of the LTR arc have laser wire emittance measurement stations. The optics of the LTR system are shown in Figure 2.2-6.

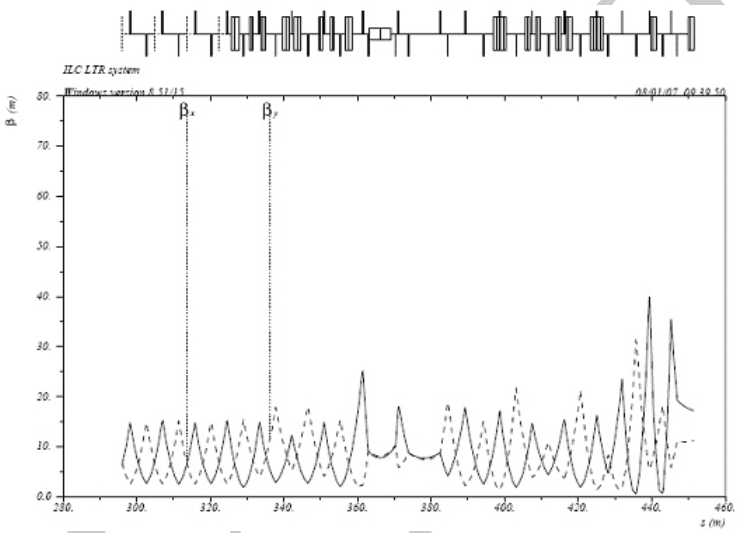

FIGURE 2.2-6. Optics of the LTR

The arc of the eLTR is designed to rotate the spin vector by 90 degrees from longitudinal into a horizontal position before injection into the damping ring and to provide the R56 necessary for energy compression. For a n × 90° of spin rotation, an arc angle of n × 7.9° is required. A 8.3-m-long superconducting solenoid with 3.16 T magnetic field solenoid rotates the spin vector into a vertical orientation. After the bunch is decompressed by the arc, an RF voltage of 180 MV provided by a 9-m-long 6-cavity superconducting linac, rotates the electrons in longitudinal phase space to match with longitudinal DR acceptance. The LTR also includes an additional 34.5° horizontal bend, a matching section with 4 quadrupoles and a double bend achromat to match Twiss parameters at the DR injection line [18].

2.2.5 Accelerator Components

2.2.5.1 Table of Parts Count

Magnets		Instrumentation		RF	
Bends	25	BPMs	100	216.7 SHB Cavity	1
Quads (NC)	76	Wirescanners	4	433.3 SHB Cavity	1
Quads (SC)	16	Laserwires	1	5 Cell L-band buncher	1
Solenoids(NC)	12	BLMs	5	L-band TW structure	2
Solenoids(SC)	2	OTRs	2	1.3 GHz Cryomodules	25
Correctors(SC)	32	Phase Monitors	2	L-band Klystrons/Modulators	13

TABLE 2.2-3
Total number of components for the polarized electron source.

Beam line section	Length
Gun Area	7 m
NC beam lines	14 m
Chicane + Emittance Station	54 m
SC beam lines	245 m
eLTR	157 m
Dumplines	12 m
Total beam line length	489 m
Total tunnel length	505 m

TABLE 2.2-4
System lengths for the e- source beamlines.

2.3 POSITRON SOURCE

2.3.1 Overview

The ILC Positron Source uses photoproduction to generate positrons. The electron main linac beam passes through a long helical undulator to generate a multi-MeV photon beam which then strikes a thin metal target to generate positrons in an electromagnetic shower. The positrons are captured, accelerated, separated from the shower constituents and unused photon beam and then are transported to the Damping Ring. Although the baseline design only requires unpolarized positrons, the positron beam produced by the baseline source has a polarization of ∼30%, and beamline space has been reserved for an eventual upgrade to ∼60% polarization.

The positron source must perform three critical functions:

- generate a high power multi-MeV photon production drive beam in a suitable short period, high K-value helical undulator;
- produce the needed positron bunches in a metal target that can reliably deal with the beam power and induced radioactivity;
- capture and transport the positron bunch to the ILC Damping Rings with minimal beam loss.

In addition, the Positron Source requires sufficient instrumentation, diagnostics and feedback (feedforward) systems to ensure optimal operation of the source and ILC.

2.3.2 Beam Parameters

The key parameters of the Positron Source are listed in Tables 2.3-1, 2.3-4 , 2.3-5. The source is required to deliver 2×10^{10} positrons per bunch at the IP with the nominal ILC bunch structure and pulse repetition rate. The source target system is designed with a 50% overhead and can deliver up to 3×10^{10} (13.5 mA) positrons per bunch to the 400 MeV point. There is sufficient RF power to accelerate 2.5×10^{10} (∼11 mA) to the damping ring within the 0.09 m-rad transverse dynamic aperture.

2.3.3 System Description

Figure 2.3-1 shows the layout of the ILC electron side and the relative positions of the major systems of the positron source. Figure 2.3-2 shows the major elements of the positron source. The positrons are produced, separated and accelerated to 400 MeV in the *Undulator* area of Fig. 2.3-2. They are then transported to the e^+ *Booster* area where they are further accelerated to the positron damping ring injection energy. The important lengths and distances associated with the positron source are summarized in Table 2.3-2.

Positrons are produced in electromagnetic showers when a multi-MeV photon beam impinges on a metal target. The photon beam is produced by passing the main electron linac beam through a long undulator. This photon beam is transported ∼ 500 meters to the positron source target hall where it hits a 0.4 radiation length thick Ti-alloy target producing showers of electrons and positrons. The resulting beam is matched using an optical matching device (OMD) into a normal conducting (NC) L-band RF and solenoidal focusing capture

TABLE 2.3-1
Nominal Positron Source Parameters († upgrade vales)

BEAM PARAMETERS	Symbol	Value	Units
Positrons per Bunch at IP	n_b	2×10^{10}	number
Bunches per Pulse	N_b	2625	number
Pulse Repetition Rate	f_{rep}	5	Hz
Positron Energy (DR Injection)	E_0	5	GeV
DR Transverse Acceptance	$\gamma(A_x+A_y)$	0.09	m-rad
DR Energy Acceptance	δ	$\pm$ 0.5	%
DR Longitudinal Acceptance	A_l	$\pm3.4 \times \pm25$	cm-MeV
Electron Drive Beam Energy	E_e	150	GeV
Electron Beam Energy Loss in Undulator		3.01	GeV
Positron Polarization †	P	$\sim$60	%

system and accelerated to 125 MeV. The electrons and used photons are separated from the positrons and dumped. The positrons are accelerated to 400 MeV in a NC L-band linac with solenoidal focusing. They are transported ~5 km to the central damping ring complex, where they are boosted to 5 GeV in a linac using superconducting (SC) L-band RF and injected into the positron damping ring.

The positron source system also includes a Keep Alive Source to generate a low intensity positron beam that can be injected into the SC L-band linac. This allows various beam feedbacks to remain active if the main electron beam, and hence the undulator based positrons, is lost. ILC availability studies (see Section 2.9.1) show that the Keep Alive Source makes a significant improvement in accelerator uptime and delivered luminosity. This source uses a 500 MeV electron drive beam impinging on a tungsten-rhenium target to produce positrons which are then captured and accelerated to 400 MeV similar to the main positron source. The Keep Alive Source is designed to produce 10% bunch intensity for the full 2625 bunch ILC pulse train at 5 Hz.

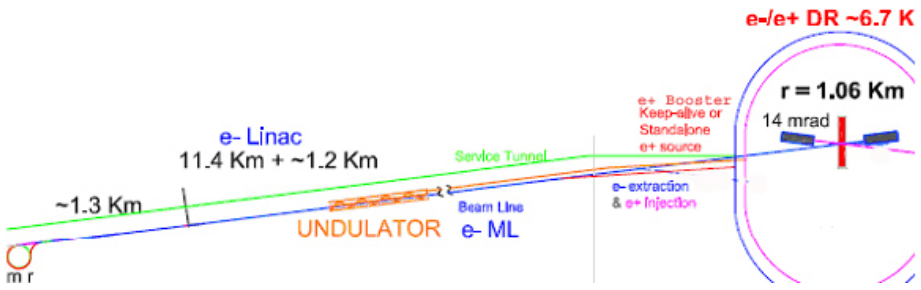

FIGURE 2.3-1. Layout of the Positron Source in the ILC

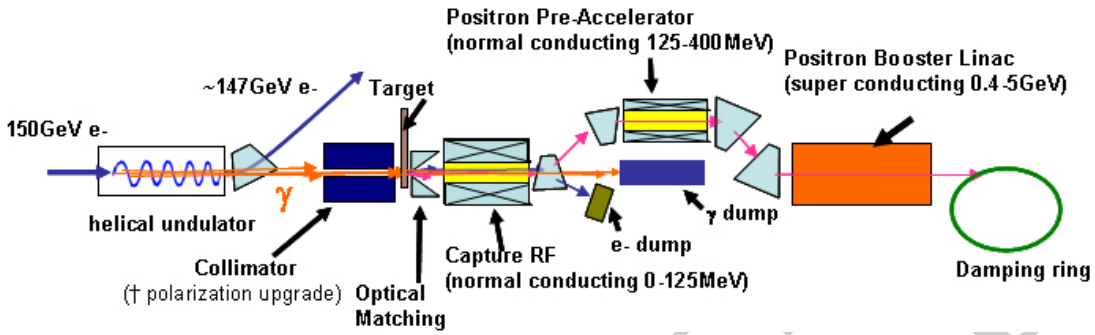

FIGURE 2.3-2. Overall Layout of the Positron Source

TABLE 2.3-2
Positron Source Beamline Lengths

AREA	LENGTH (meters)
Undulator Chicane Insert	1257
Undulator Center to Target	500
Undulator Length	200
Target Hall Length	150
400 MeV Long Transport Line	5032
Total RF Acceleration Length	350
Damping Ring Injection Line	431

2.3.3.1 Photon Production

The positron source relies upon an intense beam of high energy photons impinging upon a metal target. The photons must be of sufficient energy, typically of order 10 MeV, to generate electron-positron pairs that can escape from the target material and be captured and accelerated. The photons are generated by the radiation from relativistic electrons as they pass through the periodic, helical, magnetic field of the undulator. Details of the undulator are provided in Section 2.3.5.1. To generate the required photon energy, very high energy electrons are required. To avoid the expense of a dedicated electron beam, the undulator is installed part way along the electron main linac, where the electron energy has reached 150 GeV. After passing through the undulator the electrons continue through the remainder of the main electron linac, gaining energy up to 250 GeV. The first harmonic cut-off energy for the photon spectrum is 10.06 MeV.

A helical undulator generates twice the synchrotron radiation power per period than the equivalent planar undulator, enabling the overall undulator to be shorter for the same number of positrons. The helical device also produces circularly polarized light which in turn generates longitudinally polarized positrons.

2.3.3.2 Positron Production and Capture

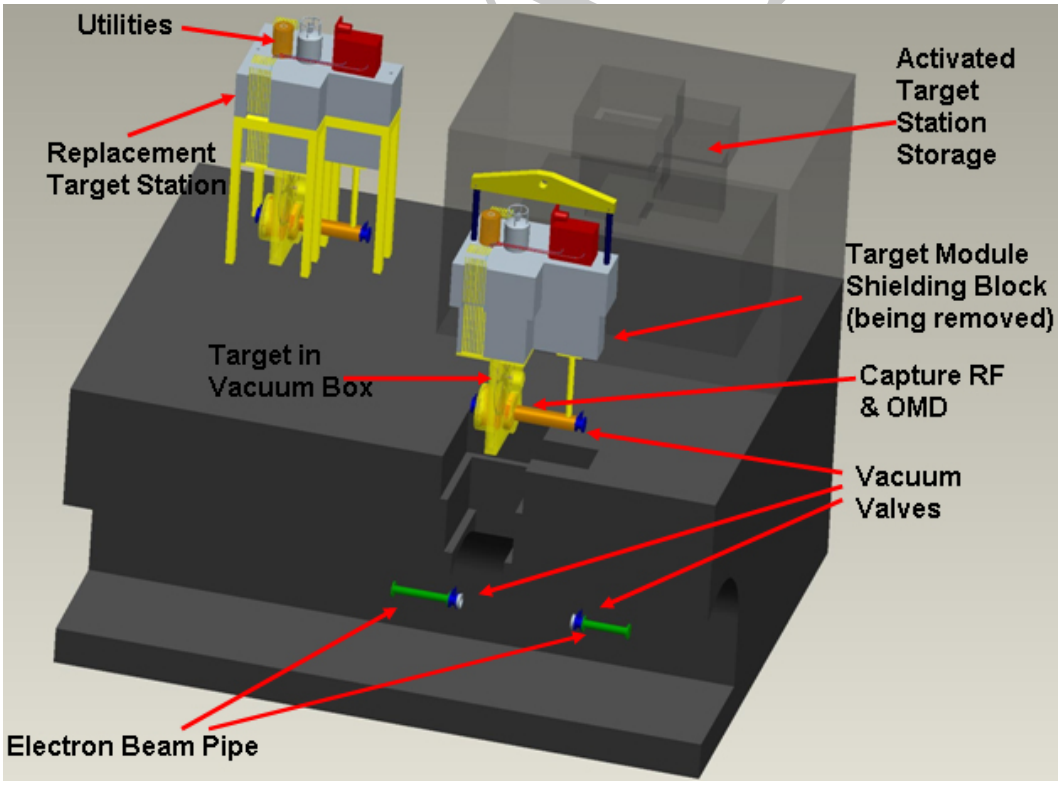

FIGURE 2.3-3. Target Removal Scheme (5-spoke target wheel, OMD and first RF section is seen being removed from the beamline)

The positron production, capture and transport to the damping rings are shown in Figure 2.3-2. The photon beam generated by the helical undulator is incident on the rim of a 0.4 X_0 thick rotating target (see Section 2.3.5.2) contained in a vacuum vessel. The photon beam has a transverse size of $\sim$ 1 mm rms and deposits $\sim$ 10.5 kW of power in the target. Photons up to the 8^{th} harmonic contribute to the positron generation. The particles emerging from the downstream side of the target are captured in the 0.09 m-rad transverse dynamic aperture defined by the positron damping ring. The energy of the beam coming out of the target is 3 - 55 MeV. The target is followed by the tapering magnetic field of an Optical Matching Device (OMD) (see Section 2.3.5.3) which has a field which decays from 5 - 0.5 T over 20 cm. The OMD matches the beam phase space from the target into the capture L-band RF which accelerates the beam to 125 MeV. The RF cavities have an average gradient of 9 MV/m and are located inside 0.5 Tesla solenoids which provide beam focusing. Details of the RF are given in Section 2.3.5.4.

The target and equipment immediately downstream are expected to become highly activated. A remote-handling system is used to replace the target, OMD and 1.3 meter NC RF cavities. Due to the underground location, the activated equipment needs to be removed vertically from the target vault. Figure 2.3-3 shows the conceptual design of such a system, where the target wheel, OMD and the first 1.3 meter NC RF cavity is shown being removed. This design does require special vacuum seals to enable speedy removal from the beam line, as the power deposition from the beam does not allow for windows in these lines.

2.3.3.3 Low Energy Positron Transport

Downstream of the capture RF, the positrons are separated from electrons and photons in an achromatic dogleg which horizontally deflects the positron line by 2.5 m. A set of collimators remove positrons with large diverging angles and large energy offsets. Normal conducting L-band RF structures embedded in a constant solenoid field of 0.5 T accelerate the positrons from 125 MeV to 400 MeV. The accelerating gradient is $\sim$8 MV/m and the length is 34.6 m.

A dogleg deflects the beam 5 m horizontally to the electron main linac tunnel and 2 m vertically to position the long positron transport line above the electron main linac. This beamline carries the positrons 4.09 km to the end of the main linac tunnel, then 941 m to the positron booster linac in a separate tunnel.

2.3.3.4 Keep Alive Source

The Keep Alive Source (KAS) is designed to deliver a low intensity ($\sim$10%) beam of positrons at 400 MeV to the positron booster linac in case the primary positron beam is unavailable. It occupies $\sim$500 meters of tunnel just before the booster linac. A 500 MeV electron beam impinges on a tungsten-rhenium target to produce positrons. The electron drive beam is similar to the electron source. The KAS positron target has a simpler design because of the lower incoming beam power, but still requires remote handling. The positrons are captured, separated and accelerated to 400 MeV using the same system as for the primary positron beam.

2.3.3.5 5-GeV SC Booster Linac

The SC booster linac accelerates the beam from 400 MeV to 5 GeV in three sections of periodic FODO lattice. The first section up to 1083 MeV has four non-standard cryomodules, each

containing six 9-cell cavities and six quadrupoles. The quad field strength ranges from 0.88-2.0 T. The second section up to 2626 MeV has six non-standard cryomodules, each containing eight 9-cell cavities and two quadrupoles . The quad strength ranges from 0.62-1.3 T. Finally, the positrons are accelerated to 5 GeV using twelve standard ILC-type cryomodules, each with eight 9-cell cavities and one quadrupole with strength ranging from 0.95-1.63 T.

2.3.3.6 Linac to Damping Ring Beam Line

The Linac to Ring (LTR) brings the positrons from the booster linac to the Damping Ring (DR) injection line. In addition, the LTR orients the beam polarization and compresses the beam energy to improve acceptance into the DRs. The LTR design is the same as for the electron source 2.2.4.2. The longitudinal polarization of the positrons from the target is preserved to the LTR. If polarization is needed at the IP it must be preserved through the DR. This is achieved by rotating the spin to vertical before injection into the DR. The LTR contains bending magnets which rotate the spin vector from longitudinal to horizontal, followed by solenoids, if turned on, that rotate from horizontal to vertical. At 5 GeV, the total bending angle must be an odd integer multiple of 7.9° to produce a net 90° of spin rotation. 26.23 T-m of solenoidal field is required to produce the horizontal-to-vertical spin rotation which is provided by two 2.5 meter 5.2 T solenoids.

2.3.4 Accelerator Physics Issues

2.3.4.1 Photon Drive Beam

The photon drive beam is generated by passing the main electron beam through a long, small-aperture undulator which sits in the middle of a magnetic chicane. The design of this system has to ensure that this does not compromise the main electron beam quality, and hence the ILC luminosity. In addition the undulator system and the main linac downstream of the undulator need to be protected from any beam failures.

The electron beam transport through the complete undulator system is based upon a simple FODO arrangement with quadrupole spacing of ∼12 m (again in the room temperature section). There are beam position monitors (BPM) at every quadrupole and Horizontal and vertical corrector magnets in each cryomodule. A recent study indicated that a quadrupole to BPM misalignment of 10 um leads to an emittance growth of less than 1%, mostly due to the undulator. The undulator increases the energy spread of the electron beam 0.16% to 0.23%.

The baseline pressure requirement of 10^{-8} Torr has been set to avoid fast ion instability problems. Vacuum calculations confirm that the cryopumping will be adequate provided that photons with energy >10 eV are intercepted by absorbers spaced approximately every 12 m to shadow the cold vessel surfaces. These absorbers are in room temperature sections.

To protect the undulator and downstream linac from beam failure, there is a fast extraction system before the chicane that can dump the main electron beam into a full power beam dump. A collimator in front of the undulator can intercept a few bunches before the dump system fires.

2.3.4.2 Positron Generation

The primary issue for positron production is to efficiently capture the positrons which are produced with a small spatial extent and large angles. Point-to-parallel focusing immediately after the target increases the positron capture. An Optical matching Device (OMD) placed immediately after the target produces a longitudinal field that decays from 5 Tesla to 0.5 Tesla in $\sim$ 20 cm. Calculations show a factor of two improvement in positron capture from the OMD.

2.3.4.3 Beam Transport

The positron beam transport must efficiently bring the large emittance beam from the target through several km of beamline. The beam at damping ring injection must match the damping ring phase space to avoid beam losses in the damping ring. Beam outside the acceptance must be absorbed on collimators to localize radioactivation.

The linac transfer line that takes the 400 MeV positron beam from the target hall to the booster linac has 16.8 m long FODO cells with 90 degree phase advance per cell and $\sim$28.5 m maximum β-function. It follows the earths curvature as does the linac tunnel. The vertical dogleg which brings the positron beam 8 m vertically from the linac tunnel to the booster tunnel, has at each end a double bend achromat to provide 17.1 mrad of bending angle. Four quads are inserted in between two bends to create 180° phase advance between the two bends and cancel the dispersion. The last section connects to the positron booster linac.

In order to match the positron beam into the longitudinal acceptance of the damping ring, the beam energy spread is reduced from $\pm$2.8% to $\pm$0.5%. The energy compression and spin rotation takes place in four FODO-like cells with 8 bends in the first arc of the LTR. The total bending angle is 55.5°. The nominal momentum compaction, R_{56}, is 86 cm but it is adjustable. After the bunch decompression, a 9-m-long 6-cavity superconducting linac at an RF voltage of 180 MV rotates the positrons in longitudinal phase space to match the DR acceptance. The rest of the LTR includes a section with an additional 34.5° horizontal bend, a matching section with 4 quadrupoles and a double bend achromat used to match into the DR injection line. The geometry is shown in Figure 2.3-4.

Multi-particle tracking has been performed from the target to the DR injection. The ELEGANT code, [19] was chosen to track the unique positron beam with large angular divergence and long low-energy tails. The LTR energy compression was optimized to maximize the positron beam within the 6-D acceptance in the DR equal to $\gamma(A_x+A_y) < 0.09$ m and ($\pm$ 25 MeV)$\times$($\pm$ 3.46 cm). 55% of positrons from the target survive the transport through the complete beamline based on the physical apertures of the beam pipes [20] and $\sim$50% of the positrons are within the DR 6-D acceptance. An energy collimator in the LTR second arc reduces the number of unwanted particles reaching the DR from 5.6% to 1.1%. Additional betatron and energy collimators may be required to collimate the rest of the unwanted 1.1% of particles, 0.8% of which are outside of the transverse DR acceptance. Tracking with realistic magnet errors shows similar results after orbit correction. Figure 2.3-5 shows the positron yield in various parts of the ILC Positron Source.

2.3.5 Accelerator Components

Table 2.3-3 lists the components for the positron source. In addition to this there are two target stations, the first of which is the main production target and the second used in the

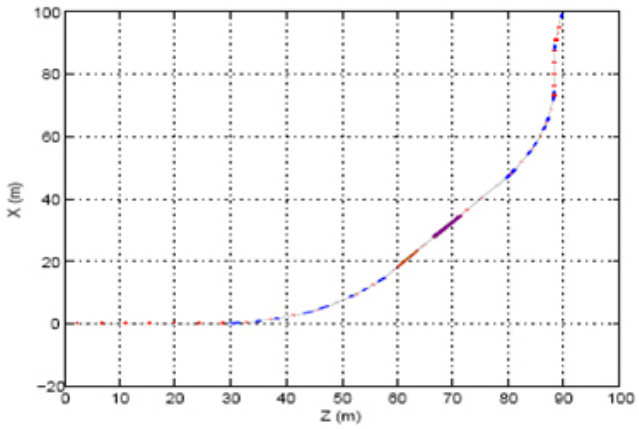

FIGURE 2.3-4. Optics of the LTR Beamline (Matching happens from 1-25 meters and DR injection is at z=90meters

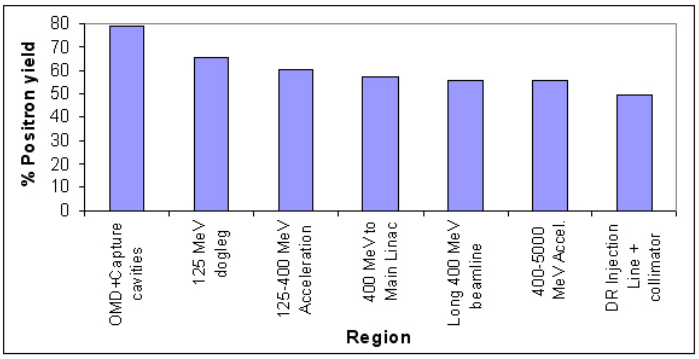

FIGURE 2.3-5. Positron Yield in Various Parts of the Positron Source

Keep Alive Source, and their associated instrumentation. Except for the target, remote handling and the OMD, costing for the positron source system were done by the global systems groups. The target and OMD costs were estimated by the design engineers and the remote handling system costs were projected from costs associated with remote handling in other accelerator facilities.

MAGNETS	#	INSTRUMENTATION	#
Dipoles	157	BPM x,y pairs	922
NC Quads	871	BPM Readout Channels	922
SC Quads	51	Wire Scanners	29
Sextupoles	32	Beam Length Monitors	2
NC Solenoids	38	Profile Monitors	7
SC Solenoids	2	Photon Profile Monitors	3
NC Correctors	840		
SC Correctors	102	RF	#
Kickers	15	NC L-band Structures	26
Septa	4	1.3 GHz SC Cavities	176
SC Undulator Cryomodules	27	1.3 GHz Cryomodules	23
OMD	2	1.3 GHz Klystrons/Modulators	9

TABLE 2.3-3
Total Number of Components in the Positron Source.

2.3.5.1 Undulator

The undulator must be superconducting to achieve the required parameters of high field and short period. The present baseline parameters are given in Table 2.3-4. Two interleaved helical windings of NbTi spaced half a period apart generate the transverse helical field. Figure 2.3-6 is a picture of some short sample undulator prototypes showing the forms for the helical windings. The 147 m of undulator is supplied by forty-two 4 m long cryomodules containing two separate undulators with an active undulator length per cryomodule of ∼3.5 m. Figure 2.3-7 shows the cryomodules with the two undulators running along the center.

The undulator vacuum chamber has a nominal inner diameter of 5.85 mm and is made of copper. The extremely high conductivity of copper at cryogenic temperatures mitigates resistive wall effects. The material between the superconducting windings is soft magnetic iron which also serves as an outer yoke to increase the field and provides additional support. Each cryomodule contains a liquid helium bath and in-situ cryocooler are used to achieve zero liquid boil off.

Since the electron vacuum vessel is at cryogenic temperatures, each module effectively acts as a long cryopump. Roughing pumps are installed in room temperature sections between cryomodules (approximately every 12 m) but achieving UHV conditions relies upon

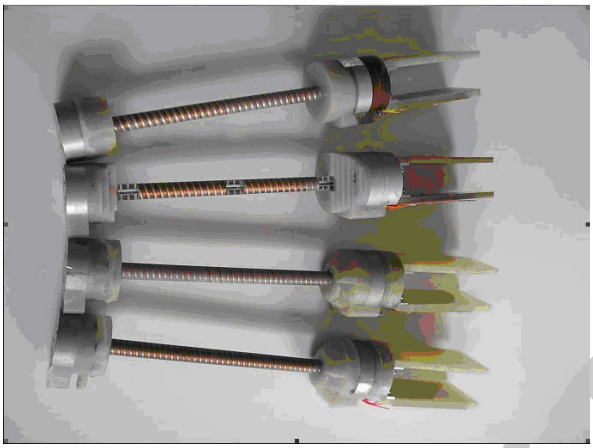

FIGURE 2.3-6. Short Sample Undulator Prototypes

cryopumping. To achieve the baseline pressure requirement of 10^{-8} Torr absorbers to clean up the soft photon flux at large angles are placed every 12 meter in room temperature section.

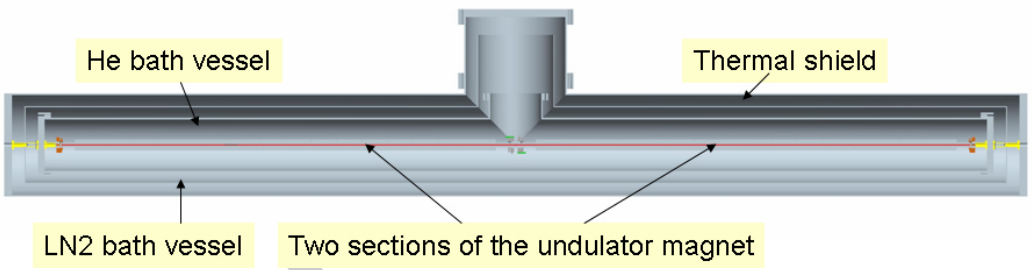

FIGURE 2.3-7. 4-meter Undulator Cryomodule

2.3.5.2 Target

The ILC positron target parameters are shown in Table 2.3-5. The positron production target is a rotating wheel made of titanium alloy (Ti-6%Al-4%V). The photon beam is incident on the rim of the spinning wheel, whose diameter is 1 m and thickness is 0.4 radiation lengths (1.4 cm). During operation the outer edge of the rim moves at 100 m/s. This combination of wheel size and speed offsets radiation damage, heating and the shock-stress in the wheel from the ∼131 kW photon beam. A picture of the conceptual target layout is shown in Figure 2.3-8. A shaft that extends on both sides of the wheel with the motor mounted on one shaft end, and a rotating water union on the other end to feed cooling water. The target wheels sit in a vacuum enclosure at 10^{-8} torr (needed for NC RF operation), which requires vacuum seals to enable access to the chamber. The rotating shaft penetrates the enclosure using two vacuum pass-throughs, one on each end. The optical matching device (OMD -

TABLE 2.3-4
Nominal Positron Source Parameters († upgrade vales)

UNDULATOR PARAMETERS	Symbol	Value	Units
Undulator Period	λ	1.15	cm
Undulator Strength	K	0.92	
Undulator Type		helical	
Undulator Length	L_u	147	m
Field on Axis	B	0.86	T
Beam Aperture		5.85	mm
Photon Energy (1^{st} harmonic cutoff)	E_{c10}	10.06	MeV
Photon Beam Power	P_γ	131	kW

TABLE 2.3-5
Nominal Positron Source Parameters († upgrade vales)

TARGET PARAMETERS	Symbol	Value	Units
Target Material		Ti-6%Al-4%V	
Target Thickness	L_t	0.4 / 1.5	r.l. / cm
Target Power Adsorption		8	%
Incident Spot Size on Target	σ_i	>0.75	mm, rms

see Section 2.3.5.3), is mounted on the target assembly, and requires an additional liquid nitrogen cooling plant. The motor driving the target wheel is sized to overcome forces due to eddy currents induced in the wheel by the OMD.

The target wheel assembly is designed for an operational life of two years. In the event that the target fails during a run, the assembly can be replaced by a new assembly in about a day using vertical remote handling.

A series of sensors provide information on the target behavior. An infrared camera tracks temperatures on the wheel, to allow for quick shutdown in the case of a cooling failure. Flowmeters monitor cooling water flow in and out of the wheel (to watch for leaks), along with thermocouples to check ingoing and outgoing flow temperature. A torque sensor is placed on the shaft, with vibration sensors on the wheel to report mechanical behavior. Finally, the wheels rotational speed is monitored.

2.3.5.3 Optical Matching Device

The OMD generates a solenoidal magnetic field which peaks in strength at 5 Tesla close to the target and falls off to 0.5 Tesla to match the solenoidal field at the entrance of the capture section. The OMD increases the capture efficiency by a factor of 2. The OMD is a normal conducting pulsed flux concentrator based on an extrapolation of a magnet created for a hyperon experiment [21].

The magnetic field of the OMD interacts with the spinning metal of the target to create

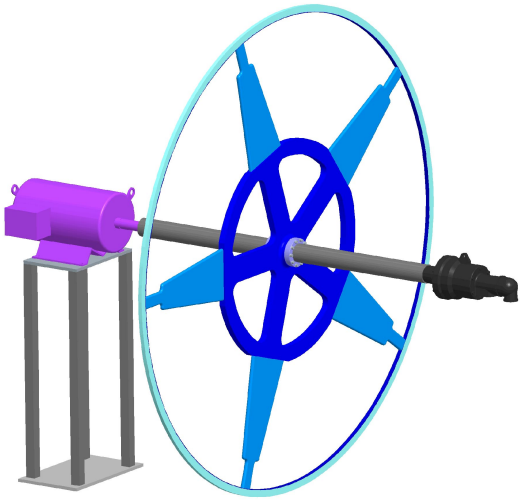

FIGURE 2.3-8. Target Station Layout

eddy currents. The target design must accommodate this drag force which increases the average heat load and requires a stronger target drive motor. The OMD may possibly induce 5 Hz resonance effects in the target that will need to be mitigated.

2.3.5.4 Normal Conducting RF Accelerator System

Due to the extremely high energy deposition from positrons, electrons, photons and neutrons behind the positron target, normal conducting structures must be used up to an energy of 125 MeV. This normal-conducting section is challenging but feasible, and a prototype test structure is under construction. It must sustain high accelerator gradients during millisecond-long pulses in a strong magnetic field, provide adequate cooling in spite of high RF and particle loss heating, and produce a high positron yield with the required emittance. The design contains both standing-wave (SW) and traveling-wave (TW) L-band accelerator structures [22]. The capture region has two 1.27 m SW accelerator sections at 15 MV/m and three 4.3 m TW accelerator sections at 8.5 MV/m accelerating gradient. All accelerator sections are surrounded with 0.5 T solenoids. Figure 2.3-9 shows the schematic layout.

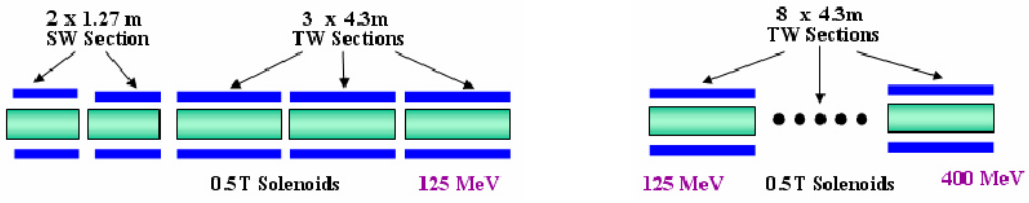

FIGURE 2.3-9. Layout of the Capture Region (left) and Pre-Accelerator Region (right)

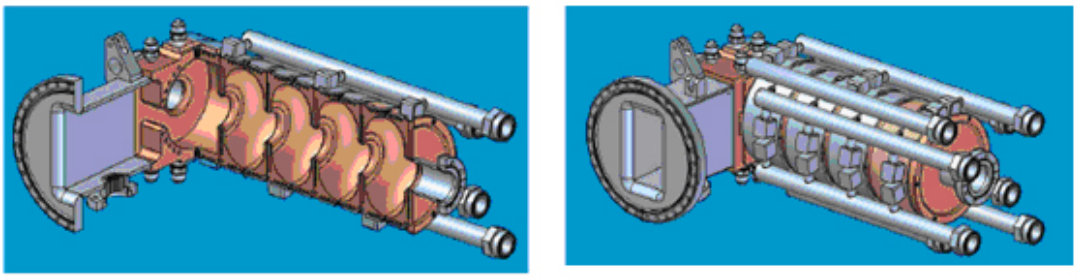

FIGURE 2.3-10. SW Structures - Cut-away and External Views

The high gradient (15 MV/m) positron capture sections are 11-cell π mode SW accelerator structures. The SW structures have a more effective cooling system and higher shunt impedance with larger aperture (60 mm), but require RF circulators to protect the klystrons from reflected power. The mode and amplitude stability under various cooling conditions for this type of structure have been theoretically verified. Figure 2.3-10 shows engineering drawings of the SW structures.

The TW sections are 4.3 m long, $3\pi/4$ mode constant gradient accelerator structures. The phase advance per cell has been chosen to optimize RF efficiency for a large aperture TW structure. The TW structures allows easy installation for long solenoids and do not need circulators. Each accelerator section has an individual 1.3 GHz RF power source.

2.3.5.5 Magnets

The Positron Source has more than 2000 magnets, see Table 2.3-3, but most of the magnet designs are quite straightforward. The large aperture DC solenoids, surrounding the L-band capture RF must be normal conducting because of the high beam losses in the target region and as such use a large amount of electrical power. In addition, there are two long high field SC solenoids for spin rotation in the LTR.

2.3.5.6 Diagnostics

The Positron Source has the normal complement of beamline instrumentation to measure orbit, emittance, charge and energy spread. Specialized diagnostics are designed into the unique positron systems, e.g. target. The major cost is in the BPM system because of the large channel count coming from the long beamlines. The number of readout channels is halved by processing only one transverse plane of the BPM x,y pair at each quadrupole. Performance specifications for the diagnostics are in most cases equal to or less than the Main Linac or RTML.

2.3.5.7 Electron and Photon Beam Dumps

There are 9 beam dumps, 16 variable aperture collimators, 1 fixed aperture collimator and 5 stoppers with burn through monitors planned for the positron source system. Three of the beam dumps must absorb sufficiently large beam power that they require dump designs with

water in the path of the beam. The plumbing to cool and treat the resulting radioactive water is the dominant cost.

There is a tune-up dump at the 150 GeV pre-undulator extraction point of the electron linac. For tune-up, the number of bunches per train is limited to 100; with absorbed power of 240 kW at nominal beam parameters. This dump, roughly in line with the linac, also serves as the abort dump for up to a full train of electrons (1.35 MJ) to protect the undulator. The dump consists of a 40 cm diameter by 250 cm long stainless vessel filled with 10 mm diameter aluminum balls through which flows $\sim$ 30 gallons per minute of water; it is backed by a short length of peripherally cooled solid copper. The dump is shielded from the access passageway by 10 cm of steel and 40 cm of concrete. A service cavern houses a heat exchanger, pumps and a system to treat the water for hydrogen, oxygen and ^7Be. A second dump, technically identical (225 kW at nominal beam parameters), is located near the dampping ring to tune the 5 GeV positrons before injection.

The most challenging dump in the positron production system absorbs the non-interacting undulator photons from the target. This dump must absorb up to 300 kW (upgrade value) continuously (1.9 x 10^{17} photons/sec of 10 MeV average energy). The primary absorber in this case must be water, contained in a vessel with a thin window. For a dump located 150 m downstream of the target, calculations indicate that the power density on a 1 mm Ti window is 0.5 kW/cm^2, the resultant temperature rise after the passage of one bunch train is 425°C, and in the core of the beam the rise in the water temperature is 190°C. With this geometry, a compact (10 cm diameter by 100 cm long) pressurized (12 bar) water vessel and Ti window, with a radioactive water processing system, is required. Lengthening the target to dump distance by several hundred meters would ease requirements on the dump, but incur the expense of a longer transport.

The remaining dumps and collimators in the positron system all are based on peripherally cooled solid metal construction, with the cooling water supplied directly from the accelerator low conductivity water (LCW) system and do not present technical or cost challenges.

2.4 DAMPING RINGS

2.4.1 Overview

The ILC damping rings include one electron and one positron ring, each 6.7 km long, operating at a beam energy of 5 GeV. The two rings are housed in a single tunnel near the center of the site, with one ring positioned directly above the other. The damping rings must perform three critical functions:

- Accept e- and e+ beams with large transverse and longitudinal emittances and produce the low-emittance beams required for luminosity production
- Damp incoming beam jitter (transverse and longitudinal) and provide highly stable beams for downstream systems
- Delay bunches from the source to allow feed-forward systems to compensate for pulse-to-pulse variations in parameters such as the bunch charge.

The damping ring system includes the injection and extraction systems, which themselves include sections of transport lines matching to the sources (upstream of the damping rings) and the RTML system (downstream of the damping rings).

2.4.2 Beam Parameters

The key parameters for both the electron and positron damping rings are listed in Table 2.4.3.

2.4.3 System Description

The configuration of the damping rings is constrained by the timing scheme of the main linac. In particular, each damping ring must be capable of storing a full bunch train (roughly 3000-6000 bunches) and reducing the emittances to the required level within the 200 ms interval between machine pulses. In addition, the relatively large bunch separation in the main linacs means that the damping rings must be capable of injecting and extracting individual bunches without affecting the emittance or stability of the remaining stored bunches.

Several configuration options capable of satisfying the various constraints were evaluated in 2005 on the basis of cost and technical risk, and the 6.7 km ring was selected [23]. The exact circumference has been chosen to provide flexibility in the operational timing scheme, allowing variation in the bunch charge and number of bunches per pulse, for a fixed total number of particles per pulse and constant pulse length in the linac [23]. The superconducting RF system is operated at 650 MHz. To achieve the short damping times necessary to reduce the emittances (by five orders of magnitude in the case of the positron vertical emittance) within the allowed 200 ms interval, superconducting wigglers of total length roughly 200 m are used in each damping ring.

As noted in Section 2.1.1.4, there are significant constraints on the DR circumference, the fill patterns and the bunch spacing in the main linac. These issues will need to be optimized during the next design hase and it is likely that small changes will be made to the DR circumference and the bunch spacing.

TABLE 2.4-1
Positron damping ring parameters. The electron damping ring is identical except for a smaller injected emittance.

Parameter	Value
Energy [GeV]	5.0
Circumference [km]	6.695
Nominal # of bunches	2625
Nominal bunch population	2.0×10^{10}
Maximum # of bunches	5534
Bunch population at max # of bunches	1.0×10^{10}
Average current [A]	0.40
Energy loss per turn [MeV]	8.7
Beam power [MW]	3.5
Nominal bunch current [mA]	0.14
RF Frequency [MHz]	650
Total RF voltage [MV]	24
RF bucket height [%]	1.5
Injected beam emittance, $A_x + A_y$ [m.rad]	0.09
Equilibrium $\gamma\epsilon_x$ [μm.rad]	5.0
Chromaticity, Ξ_x/Ξ_y	-63/-62
Partition Numbers, $J_x/J_y/J_E$	0.9998/1.0000/2.0002
h	14,516
ν_s	0.067
f_s [kHz]	3.0
α_c	4.2×10^{-4}
ν_x/ν_y	52.40/49.31
σ_z [mm]	9.0
σ_p/p	1.28×10^{-3}
τ_x [ms]	25.7
τ_s [ms]	12.9

2.4.3.1 Lattice Design Considerations

The ring lattice satisfies the basic requirements of damping time, normalized horizontal emittance and bunch length, has sufficient aperture for injecting a large emittance positron beam, and has a sufficiently large momentum compaction factor to maintain single bunch stability. However, there remains design work to be done on the lattice, for example to optimize the dynamic aperture to ensure efficient acceptance of the large emittance beam from the positron source, and to minimize sensitivity to tuning and alignment errors that could degrade the emittance.

The ring is divided into six arcs and six straight sections (see Figure 2.4-1). The arcs are composed of Theoretical-Minimum-Emittance (TME) cells to give low quantum excitation, and the straight sections are composed of FODO cells for the damping wigglers, RF cavities, and injection and extraction sections. Optical parameters are shown in Figure 2.4-2. The parameters of the TME cells and the wigglers (peak field of 1.67 T) were selected to obtain the required damping time, momentum spread, and normalized horizontal emittance.

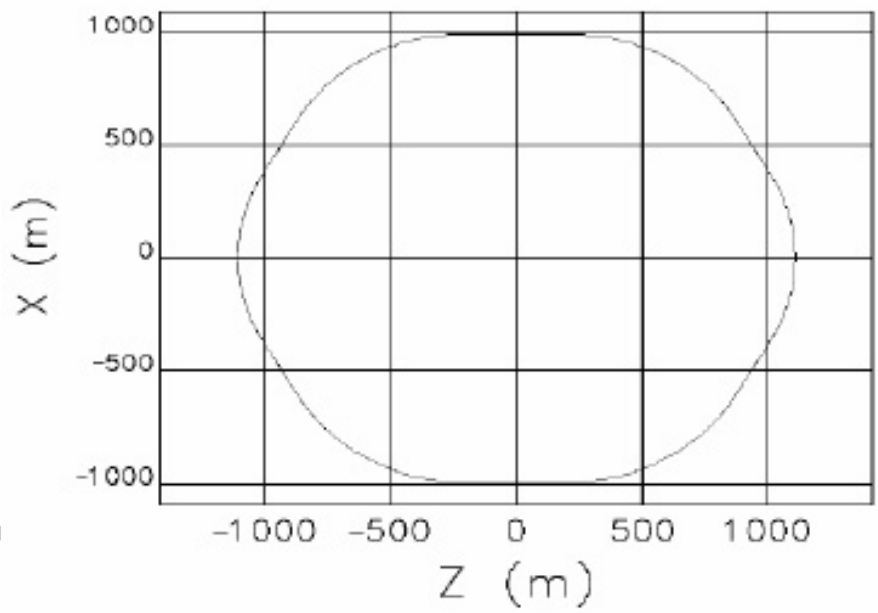

FIGURE 2.4-1. Layout of ILC Damping Ring.

Two families of sextupole magnets are inserted in the TME cells for correcting the first-order chromatic effects of the linear optics. To reduce nonlinear effects of the sextupoles, the betatron phase advance of the TME cells was set to 90° in each plane. The resulting dynamic and momentum apertures (see Figure 2.4-3) were found to depend on the number of straight sections (i.e., the symmetry of the lattice) and on the betatron phase advances of the straight sections. The straight section betatron phase advances were adjusted for maximum dynamic aperture. While a larger number of straight sections was found to improve the

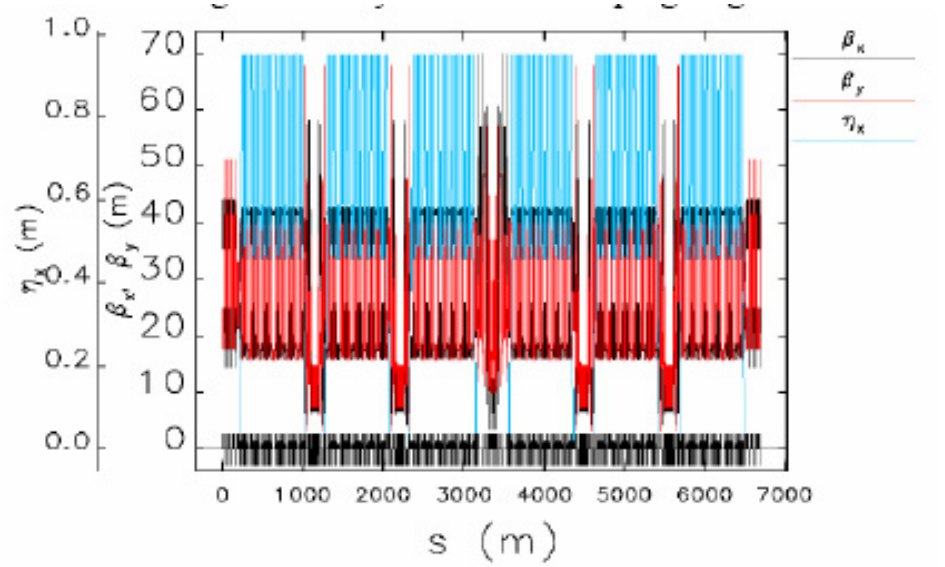

FIGURE 2.4-2. Optical functions of ILC Damping Ring.

nonlinearities, this comes at a higher cost for subsystems. A compromise configuration of six straight sections was eventually chosen for the baseline lattice.

The choice of momentum compaction factor, controlled chiefly by the total number of TME cells, results from a balance between competing requirements: single-bunch stability against the impedance of the vacuum chamber (favoring a high value of α_c) and a lower cost RF system (favoring a low value of α_c) . The value 4.2×10^{-4} is somewhat on the high side to reduce the risk of single-bunch instability. Unfortunately, a high momentum compaction factor makes it difficult to achieve a low equilibrium emittance and strong damping wigglers are required. The Twiss parameters in the wiggler region were adjusted to produce the required equilibrium emittance.

The injection/extraction sections accommodate a large number of fast stripline kickers (their large number being due to their inherent weakness). Optical functions were designed to ensure that the beam goes through the stripline kickers without hitting their apertures. For the injection section, the beam traverses the kickers at an angle but with a small trajectory offset.

2.4.3.2 Fast Ion Instability

Of significant concern to the electron damping ring is the fast ion instability. As opposed to the more familiar ion-trapping effect, where ions oscillate stably for long periods in the potential well of the stored beam, the fast ion instability is associated with ions created in the beam path by interaction with the circulating beam during a single turn. Ions created at the head of the bunch train move slowly, and remain in the beam path, influencing the motion of subsequent bunches. The resultant ion-induced beam instabilities and tune shifts are critical issues for the electron damping ring due to its ultra-low vertical emittance. A low base vacuum pressure at the 1 nTorr level is essential to reduce the number of ions formed.

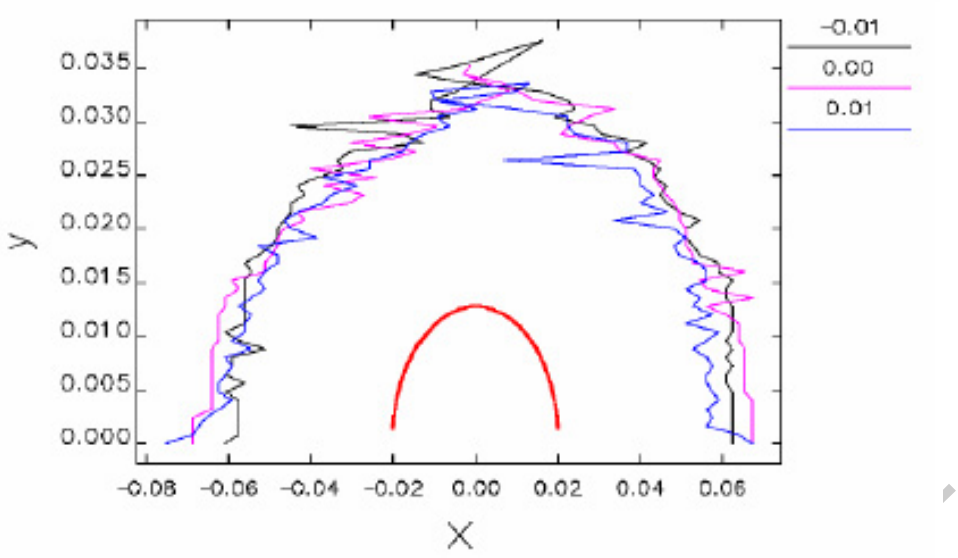

FIGURE 2.4-3. Dynamic aperture of the ILC damping ring (without field and alignment errors) for relative momentum errors of -1%, 0% and 1% at x = 44 m and y = 18 m. The thick red line represents the size of the injected positron beam.

To mitigate bunch motion, we also employ bunch-by-bunch feedback systems with a damping time of ≈ 0.1 ms.

To further reduce the core ion density, short gaps are introduced in the electron beam bunch train by omitting a number of successive bunches. The use of such "mini-gaps" in the train significantly mitigates the fast ion instability by reducing the core ion density and by inducing tune variation along the train. Figure 2.4-4 shows the buildup of the ion cloud in the case of a particular multi-train pattern with 118 bunch trains and 49 bunches per train. In this case, the reduction in the core ion density is a factor of 60 compared with a fill consisting of a single long bunch train. It is worth pointing out that the effect of train gaps is a function of beam size, so they are less effective early in the damping cycle. The simulated growth time for the beam pattern corresponding to Fig. 2.4-4 is 280 μs.

The tune spread due to both linear and nonlinear tune shifts provides Landau damping that helps control ion-induced instabilities [25]. With a multi-train fill pattern, the size of the ion cloud is much larger than the vertical beam size, so there is a larger tune spread. When the oscillation amplitude of the beam reaches the beam size, the nonlinearity effectively saturates the instability.

2.4.3.3 Electron Cloud Instability

Electron cloud instabilities and tune shifts are critical issues for the positron damping ring. The electron cloud develops quickly as photons striking the vacuum chamber wall knock out electrons that are then accelerated by the beam, gain energy, and strike the chamber again, producing more electrons. The peak secondary electron yield (SEY) of typical vacuum chamber materials is > 1.5 even after surface treatment, leading to amplification of the

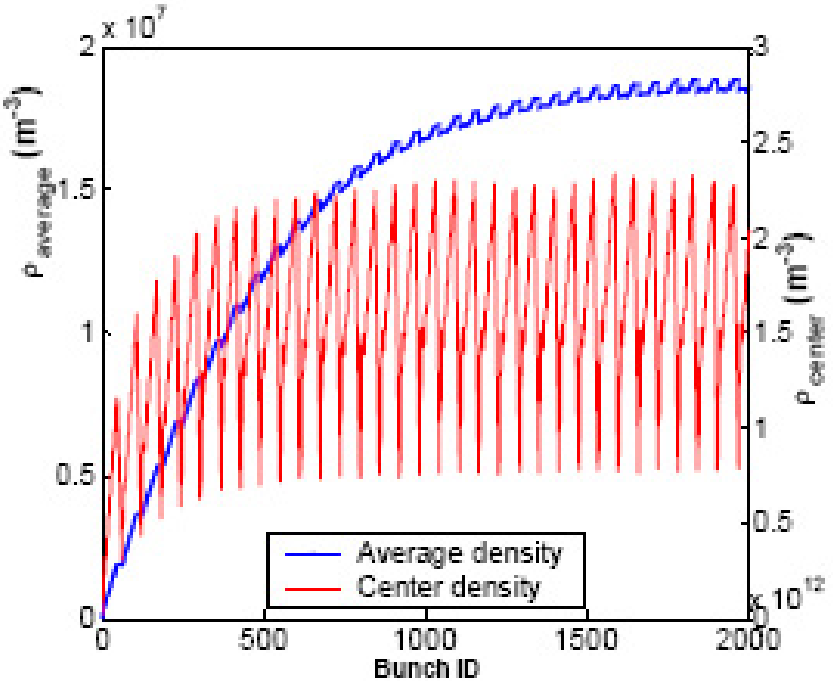

FIGURE 2.4-4. Buildup of CO^+ ion cloud at extraction. The total number of bunches is 5782 (118 trains with 49 bunches per train). The beam has a bunch separation of two RF bucket spacings, and a train gap of 25 RF bucket spacings. There are 0.97×10^{10} particles per bunch, and the partial vacuum pressure is 1 nTorr.

cascade. Once the cloud is present, coupling between the electrons and the circulating beam can cause a single-bunch (head-tail) instability and incoherent tune spreads that may lead to increased emittance, beam oscillations, or even beam losses. Because the electron cloud is difficult to suppress in the dipole and wiggler regions of the ring, this is where its effects are expected to be most severe. A large synchrotron tune is beneficial, as it raises the threshold for the electron cloud head-tail driven instability.

Single-bunch instability simulations for the 6.7 km damping ring lattice show that the instability sets in above an average cloud density of 1.4×10^{11} e-/m^3, where an incoherent emittance growth is observed, see Figure 2.4-5. Analytic calculations give higher density thresholds by roughly a factor of 4 [27, 28]. Tune shifts on the order of 0.01 are expected near threshold.

Simulations indicate that a peak secondary electron yield of 1.2 results in a cloud density close to the instability threshold. Based on this, the aim of ongoing experimental studies is to obtain a surface secondary electron yield of 1.1. Simulations also indicate that techniques such as grooves in the chamber walls or clearing electrodes will be effective at suppressing the development of an electron cloud [29, 30]. Figure 2.4-6 shows the buildup of the electron cloud and the suppression effect of clearing electrodes in an arc bend of the 6.7 km ring. A clearing electrode bias potential of +100 V is sufficient to suppress the average (and central) cloud density by more than two orders of magnitude. Techniques such as triangular or rectangular

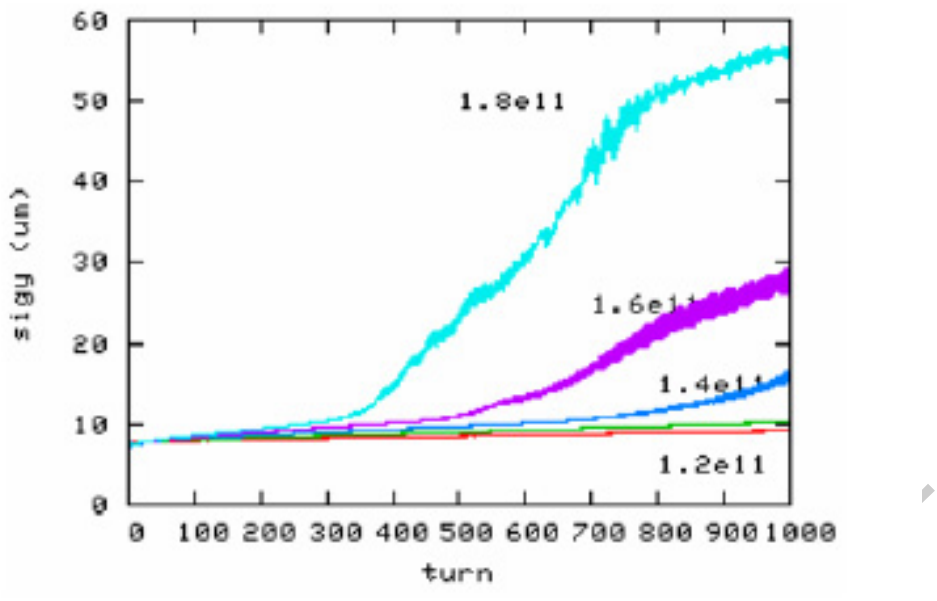

FIGURE 2.4-5. Emittance growth from single-bunch instability driven by electron cloud in the 6.7 km OCS ring. Electron cloud densities in e-/m^3 are indicated.

fins or clearing electrodes need further R&D studies and a full demonstration before being adopted. Nonetheless, mitigation techniques appear to be sufficient to adopt a single 6.7 km ring as the baseline design for the positron damping ring.

2.4.3.4 Injection and Extraction

The bunch separation in the main linacs is much longer than in the damping rings, so individual bunches must be injected and extracted without affecting the emittance or stability of the remaining stored bunches. For this to be the case, the kicker field must be negligible for any stored bunch upstream or downstream of the injected or extracted bunch, requiring that the effective kicker pulse width be less than twice the bunch spacing. Injection is interleaved with extraction, to minimize excursions in beam loading of the RF system.

Extraction is located near the center of one long straight section. A set of kickers deflects a single damped bunch horizontally. A horizontally defocusing quadrupole increases the deflection. About 90° of betatron phase downstream of the kickers, the bunch passes through the bending fields of a pair of septum magnets. These deflect the trajectory further horizontally, so it passes outside of the next focusing quadrupole and into the extraction line optics. The stored orbit is located in the nominally field-free region of the septum magnets and is not significantly affected. The extraction straight section also includes an abort dump.

Injection is located near the center of the opposite long straight section. The injection line grazes the outside of a quadrupole, and is deflected horizontally by a pair of septum bend magnets so the trajectory passes inside the aperture of the next quadrupole. This horizontally defocusing quadrupole makes the trajectory nearly parallel to the stored orbit. About 90° of

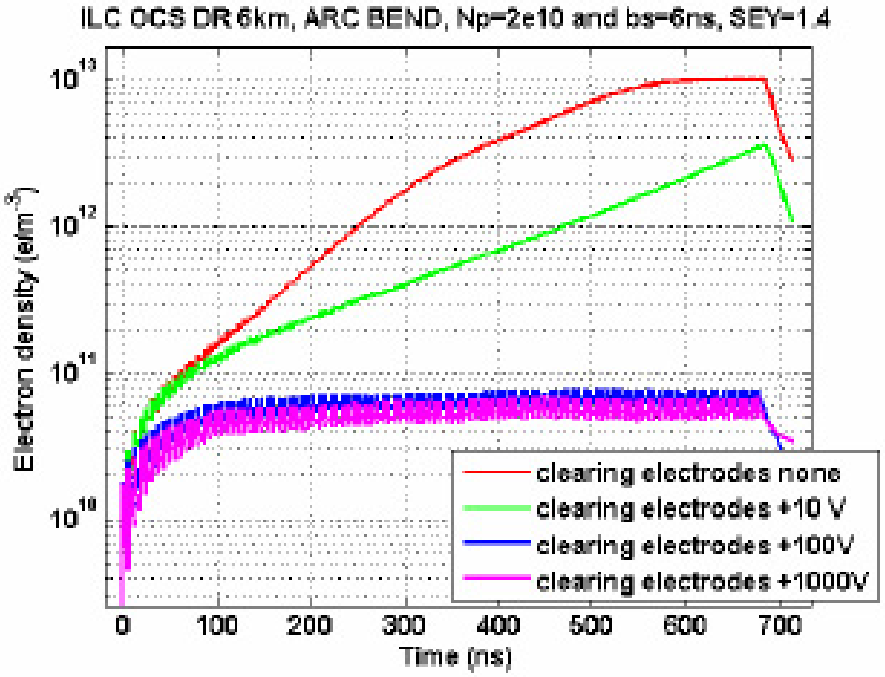

FIGURE 2.4-6. Electron cloud buildup in an arc bend of the 6.7 km ring and suppression effect of clearing electrodes biased at the indicated voltages.

betatron phase downstream from the septa, where the injection trajectory crosses the stored orbit, a set of kickers deflects the single injected bunch onto the stored orbit. As mentioned previously, the kicker is distributed into several modules at the axis-crossings of the injected trajectory, so the module aperture can be minimized.

The kicker modules are 50 Ω stripline structures inside the vacuum pipe, each 30 cm long, operating at a voltage of 22 kV, provided as +11 and -11 kV pulses on opposite electrodes. Twenty modules are required; two extra kickers are included to ensure adequate availability. The 30 cm stripline gives a 2 ns contribution to the kicker pulse width, leaving less than 10 ns for the electrical pulse width at the nominal ring bunch spacing of 6 ns. The kickers pulse about every 300 ns during the linac pulse of about 1 ms. For the low bunch charge parameters, the ring bunch spacing is 3 ns, requiring an electrical pulse width of less than 4 ns and a pulse about every 150 ns. The electrical pulser requirements are challenging, and the subject of an extensive R&D program.

Figure 2.4-7 shows beam deflection vs. kicker time measured at the ATF storage ring at KEK with 33 cm striplines and a 5-kV 3-MHz pulser built by FID GmbH. The main pulse easily meets the width and rate requirement for 6 ns bunch spacing, although at half the desired amplitude and with undesireable structure before and after the main pulse.

The positron injection kick amplitude is $\approx 20\sigma_x$ of the damped beam, so if the extraction kick amplitude is the same, a 0.05% amplitude jitter would give a 1 σ horizontal beam jitter. This results in an extraction kicker amplitude jitter tolerance in the 10^{-3} range. A similar tolerance applies to the kicker amplitude for bunches before and after the target bunch in

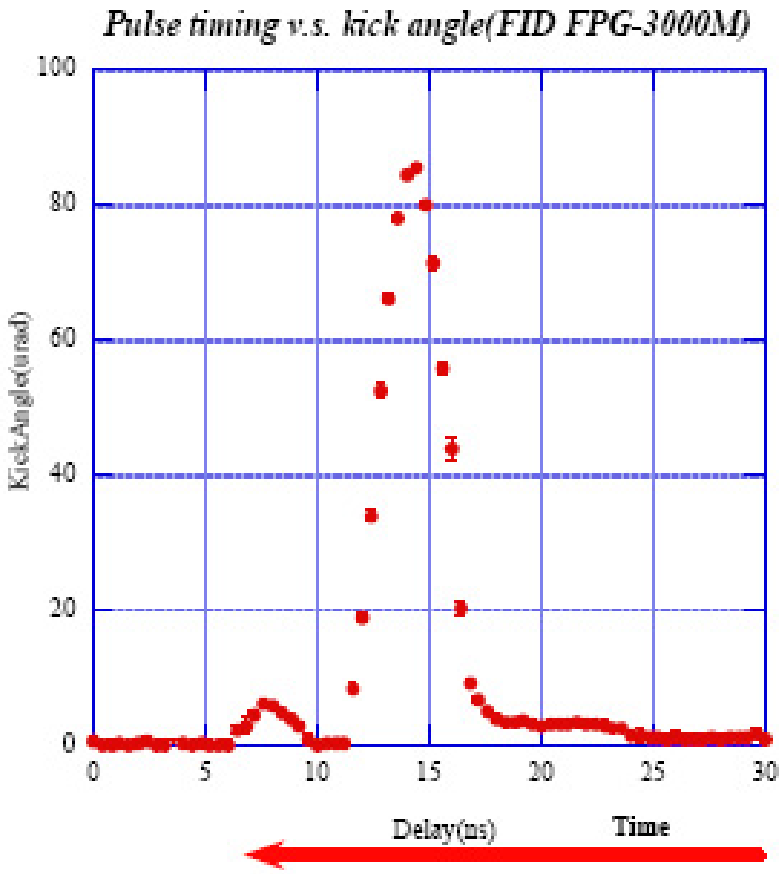

FIGURE 2.4-7. Kick angle vs. time. Note that time increases to the left here.

the ring bunch train. As a tolerance on the absolute kicker field before and after the pulse, this is very difficult to achieve and is the subject of ongoing R&D.

The septum magnets are modeled after the Argonne APS injection septa. The thin (2 mm) septum magnet has a 0.73 T field, and the thick (30 mm) septum magnet has a 1.08 T field. Each magnet has an effective length of 1 m. Both magnets are pulsed once per linac cycle to reduce power dissipation, with eddy currents in the septum shielding the circulating beam. A half-sine pulse of about 10 ms width is used, and post-regulation is required to produce a 1 ms plateau flat to 10^{-4}.

2.4.4 Accelerator Components

The damping ring has conventional electromagnets for the dipole, quadrupole, sextupole, and corrector magnets. This technology choice offers flexibility for tuning and optimizing the rings as well as for adjusting the operating beam energy by a few percent around the nominal value of 5 GeV. Superconducting wigglers based on the CESR-c design [31] provide sufficient field quality that the wigglers impose no limitation on the damping ring dynamic

TABLE 2.4-2
Magnet types and counts for a single ILC Damping Ring using the OCS6 lattice. These counts do not include injection and extraction line magnets nor magnets, kickers, and septa associated with the damping ring abort beam dump. Wiggler magnets are superconducting, all others are room-temperature.

Type	Number	Power Method
Dipoles (6 m)	114	6 strings, 1 per arc
Dipoles (3 m)	12	6 strings, 1 per arc
Quadrupoles	747	Individual
Sextupoles	504	Individual
Horizontal correctors	150	Individual
Vertical correctors	150	Individual
Skew quadrupoles	240	Individual
Wigglers	80	Individual
Kickers	64	Individual
Septa	4	Individual

aperture. The large wiggler aperture improves the ring acceptance for the large injected positron beam and reduces the growth of the electron cloud in the wiggler region. Power supplies and controllers are located in alcoves at the centers of the RF-wiggler straights. Magnet counts are shown in Table 2.4.4. Table 2.4.4 gives the key magnet parameters and maximum higher-order harmonic content specifications.

The superconducting damping wigglers are 4.5 K devices with static heat loads of 2 W/m or less, based on CESR-c experience. To avoid a significant dynamic heat load, care must be taken to ensure that only tiny amounts of scattered synchrotron radiation reach the cold mass. Two of the wigglers are co-located in the damping ring straight sections with the superconducting RF cavities, where the necessary crygenic infrastructure is readily available. The other wigglers are fed by transfer lines, with a single transfer line infrastructure for both rings.

All quadrupoles, sextupoles, wigglers and corrector magnets (dipole, skew quadrupole, and possibly other multipoles yet to be specified) have individual power supplies. Individual control of the quadrupole and sextupole magnets significantly enhances the ability to tune and locally correct the machine optics in a ring with very aggressive operating parameters. Individual power supplies for the wigglers offer simplified control in the event of a magnet quench by eliminating the power system coupling between magnets. Because of the long distances between individually powered magnets and the alcoves, the power supply system uses bulk supplies located in the main alcoves that power a master "bus" from which DC-to-DC converters supply power to individual magnets. This design minimizes cable heat loads in the ring and provides a more efficient power system. For the dipole magnets, each arc section is powered separately. The pulsed power supplies for the stripline kickers require short cable runs to preserve the necessary timing synchronization, and must be located in the tunnel or in small secondary alcoves near each group of kickers.

TABLE 2.4-3
Target field tolerances at a reference radius of 20 mm for damping ring magnets. Magnet aperture radii are 30 mm except for the wigglers. For the wigglers, the operating field is 1.67 T and the field quality is specified by the observed roll-off for a horizontal displacement from the beam axis by the indicated distance. The maximum KL-value specifies the nominal strength of the strongest magnet of each magnet type. *(Wigglers have reference radius 20 mm (H); aperture radius 37.5 mm (H), 45 mm (V))*

Type	Max KL	L [m]	Max field error	# of types
Dipoles	0.0524	6 ; 3	2×10^{-4}	2
Quadrupoles	0.31 m^{-1}	0.3	2×10^{-4}	4
Sextupoles	0.24 m^{-2}	0.25	2×10^{-3}	1
H correctors	0.002	0.25	5×10^{-3}	1
V correctors	0.002	0.25	5×10^{-3}	1
Skew quads	0.03 m^{-1}	0.25	3×10^{-3}	1
Wigglers	–	2.5	3×10^{-3}	1

2.4.4.1 RF System

The damping ring RF frequency of 650 MHz has a simple relationship with the main linac RF (1.3 GHz) to accommodate varying bunch patterns. While high power 650 MHz RF sources are not commercially available, several major klystron manufacturers can develop them by modifying 500 MHz klystrons of equivalent power level. Similarly, the RF cavity units can be designed by scaling from existing 500 MHz superconducting module designs currently in operation at CESR, KEK, and elsewhere. The RF cryomodule dimensions are 3.5 m in length and 1.5 m in diameter.

For either ring, the beam power and the total RF voltage is shared among 18 superconducting cavities. These are located in two RF straight sections roughly 40 m long. Operating 18 SC-cavity modules per ring ensures adequate energy and beam power margin in case of an RF station fault, and permits continued operation with 14 cavity modules at full performance by increasing the RF field in the remaining units. Table 2.4.4.1 summarizes the RF system main features and compares the parameters for the nominal case with that when one RF station is off. Parameters are scaled from the 500 MHz units developed by industry and being operated in various laboratories.

Two or three RF stations are located in each RF-wiggler straight section, as indicated schematically in Figure 2.4-8. Each klystron can feed 4 SC cavities by means of a distribution system having magic-tees for power splitting and 3-port circulators for protecting the klystron. To guarantee sufficient power margin in case of a klystron fault, the power sources are 1.2 MW CW. One "hot-spare" station in each ring is operated with only two cavities, rather than four. The stations are upstream of the wigglers at opposite ends of the straight section tunnel, with waveguides connecting them to the klystrons housed in centrally located alcoves having access shafts to the surface.

The selection of 650 MHz requires a redesign of existing 500-MHz sources, cavities and cryomodules. A critical element is the input coupler because the power handling capability must be kept at a level of about 260 kW CW, comparable to presently operating 500 MHz

TABLE 2.4-4
Estimated 650 MHz SC cavity parameters (scaled from 500 MHz model) for both electron and positron damping rings.

Parameter	All Stations On	One Station Off
Frequency [MHz]	650	
Active cavity length [m]	0.23	
R/Q [Ω]	89	
Operating Temperature [K]	4.5	
Standby losses at 4.5 K [W]	30	
Operating SC modules per ring	18	14
Accelerating gradient [MV/m]	5.8	7.5
Accelerating voltage [MV]	1.33	1.72
Q_0 at operating gradient [10^9]	1.0	0.9
RF cyrogenic losses per cavity [W]	20	33
Total cryo losses per ring [W]	900	925
Beam power per cavity [kW]	194	250
Klystrons per ring	5	4
Klystron emitted power [kW]	780	1000

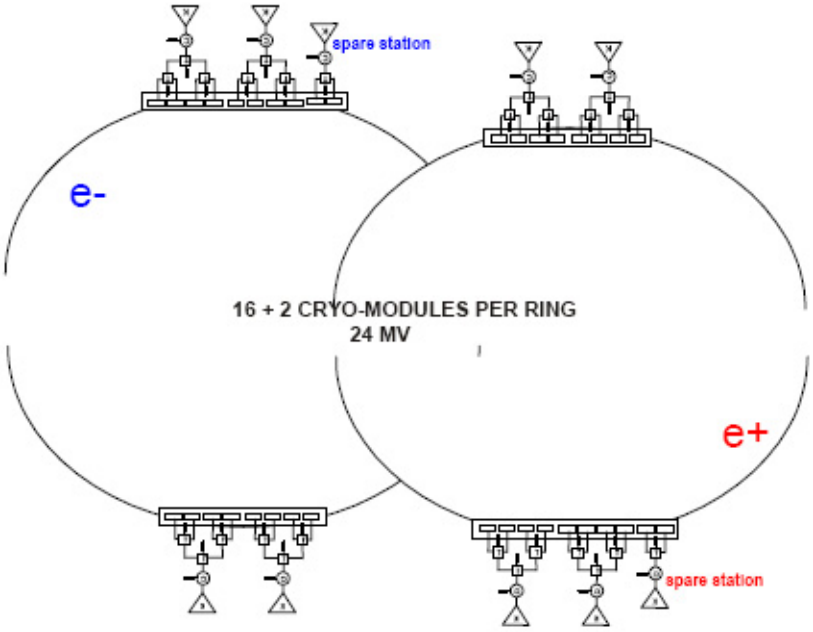

FIGURE 2.4-8. Schematic layout of DR RF systems. Each of the two RF-wiggler sections accommodates three stations from one ring, and two from the other. All stations are situated upstream of the wiggler in that ring.

systems. The HOM dampers and cryostat mechanical details must also be revised.

2.4.4.2 Cryogenic Plant

The DR cavities operate at 4.5 K and the total cryogenic losses per ring are approximately 900 W with 14 modules operating in case of one klystron fault. The design has one cryogenic plant in each RF straight section. With this choice, the helium transfer lines to the RF are not very long and do not impact the cryogenic plant cost. The cryogenic plant capability must be sufficient to handle the worst-case scenario of one klystron fault, where the cryogenic power in the other straight section could increase to a total of 925 W. With the standard refrigerator efficiency of 0.3% at 4.5 K, the total wall-plug power for each straight-section refrigerator is about 300 kW. Table 2.4.4.2 summarizes the specifications of the cryogenic system.

2.4.4.3 Fast Feedback System

With thousands of bunches circulating in the ring, wakefields induced in vacuum chamber components can give rise to coupled-bunch instabilities that cause bunch jitter and/or emittance growth. To combat this, the rings have fast bunch-by-bunch feedback systems in all three oscillation planes (longitudinal, horizontal and vertical). Modern commercial FPGAs (Field Programmable Gate Arrays) can easily manage the requirements of the feedback systems in terms of speed and number of bunches. The bandwidth of the fast feedback system

TABLE 2.4-5
Main specifications of the RF cryogenic system, with 18 modules per ring.

Nominal cryogenic losses per straight section [W]	900
Design cryogenic losses per straight section [W]	925
Wall plug power per cryogenic plant [kW]	300
Total number of cryogenic plants	2

must be at least f_{RF} (that is, 650 MHz). This means that every block of the system must have the capability to manage the full bandwidth except for the power section (amplifiers and kickers), where half bandwidth is sufficient. The main elements of each system are the analog front end, digital processing unit, analog back end, amplifier and kicker.

The pickups are 4-button monitors (two or three for each beam line) with at least full bandwidth and adequate dynamic range. The analog front ends must be capable of extracting the oscillation signals from the monitors in each of the three planes (L, H, V) and giving them to the digital sections with a swing in the range of ~ 0.5 V (typical of many analog-to-digital converters).

To minimize the quantization noise and have an adequate dynamic range, the digital units are based on a 16-bit signal processing system. The processing is able to compute the correction signal for all buckets (including the empty ones) to decouple the feedback behavior from the fill pattern. This means that all feedback systems must have the capability to process, in real time, 14,516 input/output channels, although the real bunches are in, at most, 5,534 buckets. The digital unit sampling frequency is 650 MHz. A real time FIR (finite impulse response) filter (with ≥ 50 taps) provides the correction synchrotron or betatron phase advance using only one pickup for each system. The feedback setup should be easily configurable using software tools. A down-sampling feature is also needed to manage very low oscillation frequencies.

The analog back-end systems adapt the output correction signals to the power section. The longitudinal kicker (a cavity) works at a frequency between 800 and 1600 MHz, whereas the transverse kickers (striplines) operate at baseband (from 10 kHz up to half the bandwidth of the fast feedback system). Each power section has four 250 W amplifiers (1 kW total), with the bandwidth required by the kicker.

2.4.4.4 Vacuum System

The vacuum design for the damping rings is similar to those for modern storage rings and synchrotron radiation sources. The need to avoid the fast ion instability leads to very demanding specifications for the vacuum in the electron damping ring: < 0.5 nTorr CO-equivalent in the arc cells, < 2 nTorr CO-equivalent in the wiggler cells, and < 0.1 nTorr CO-equivalent in the straight sections [32]. A combination of coatings, grooved chamber profiles, and clearing electrodes is required to suppress the electron cloud in the positron damping ring. The baseline design uses a non-evaporable getter (NEG) coated aluminum tubular vacuum chamber. With NEG coating, fewer pumps with lower pumping speed are required. Issues associated with the ultimate lifetime of the NEG material, its regeneration, and the synchrotron radiation power density on the chamber walls need further study. Each of the 120 arc cells requires one sputter ion pump with an effective pumping speed of 20 L/s installed immedi-

ately downstream of the dipole. In the long straight sections, similar sputter ion pumps are required every 10 m for $0 < z < 80$ m, every 20 m for $80 < z < 160$ m, and every 40 m for $160 < z < 400$ m.

The wiggler straight section vacuum system consists of separate chambers for the wiggler and quadrupole sections. A cross section of the wiggler chamber is shown in Figure 2.4-9. The chamber is a machined and welded aluminum unit, designed as a warm-bore insert, mechanically decoupled from the wiggler and cryogenic system. A NEG pumping system and photon absorber are incorporated in antechambers. Integral cooling is incorporated to minimize distortion of the chamber and thermal load on the wiggler cryostat during NEG regeneration. A TiZrV NEG surface coating is used on the main chamber bore to minimize secondary electron yield [33]. Clearing electrodes are also incorporated to reduce the electron cloud.

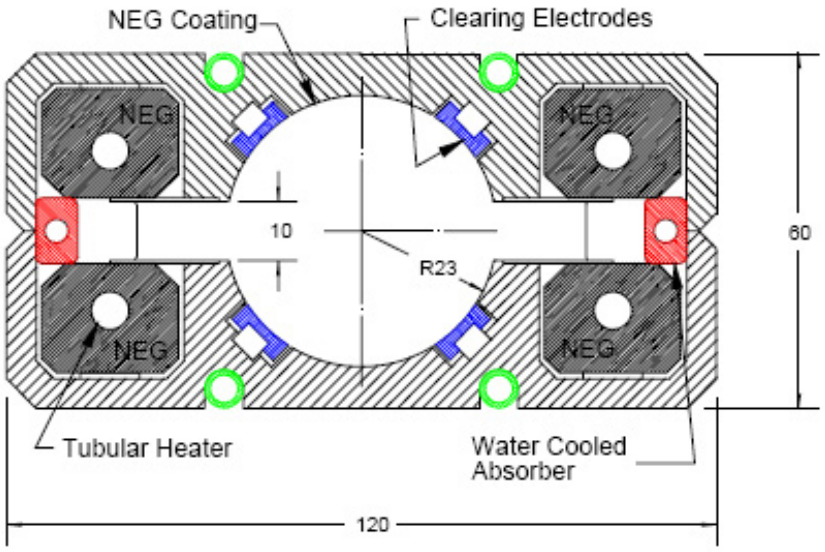

FIGURE 2.4-9. ILC damping ring wiggler chamber; dimensions in mm.

The photon absorbers are hollow water-cooled copper conductor designed to absorb photon power from upstream wigglers in the same straight section. Power radiated from the first wiggler in the straight section is intercepted initially by wiggler number three. Intercepted power increases for successive wigglers up to number nine; thereafter, a constant 3 W/mm^2 peak power density is reached. The total power absorbed per wiggler is 26 kW, that is, 13 kW per absorber.

The NEG pumping system is similar to that designed for the PEP-II B Factory. The assembly consists of NEG-coated fins and an integral heating rod for regeneration. The estimated pumping speed for CO is 1000 L/s/m. With a total incident photon flux of 2×10^{18} photons/s/m, the estimated yield of CO is 2×10^{13} molecules/s/m. This results in an equilibrium CO partial pressure of 7×10^{-10} Torr.

Between each wiggler chamber is a separate chamber for the quadrupole section. This chamber is welded aluminum, incorporating TiZrV NEG coating for secondary electron yield reduction. Bellows, a BPM assembly, and an ion pump for pumping non-reactive gases are included. The ion pump also serves as a vacuum gauge. The quadrupole chamber is completely shadowed by the wiggler chamber photon absorbers and does not absorb any of the photon power from upstream wigglers.

2.4.4.5 Cost Methodology

Several of the technical subsystems in the damping rings have specific requirements that distinguish them from corresponding subsystems in other parts of the ILC; generally, this is because of the relatively high average current and synchrotron radiation power (for the vacuum system, wigglers, and fast feedback systems), CW operation (for the RF system), or unique functionality (for the injection/extraction kickers). The cost estimates for these damping-ring-specific designs were developed by the damping ring group.

The RF system is CW and operates at 650 MHz, a different frequency from the RF systems used elsewhere in the ILC. The designs of high-power RF components, such as klystrons and circulators, were scaled from commercially available 500 MHz devices. Estimates from klystron manufacturers indicated that development costs would increase the total cost by roughly the cost of one additional unit at the standard catalog price. Manufacturing costs for the cavity cryomodules were assumed to be the same as for commercial versions of 500 MHz systems developed at Cornell and KEKB, with increased engineering effort to account for the rescaling, or in some cases redesign, of the existing subcomponents.

A preliminary design for the vacuum system was based on estimates for required vacuum levels (set by ion instabilities in the case of the electron damping ring), handling of synchrotron radiation, aperture requirements, and conditioning rates. Standard commercial component costs were used for extruded aluminum vacuum chambers, bellows, pumps, valves, and bake-out systems. Coating the chambers with NEG was assumed to be done with in-house labor. The cost estimate for the complex damping wiggler vacuum chamber was based on fabrication of similar systems for other projects.

The engineering and fabrication experience for the CESR-c wigglers were used to provide reliable cost estimates for the ILC damping wigglers, taking proper account of the well-defined differences in specification. Costs for the kicker pulser were based on a commercially available pulser (a fast ionization dynistor, or FID, device) that comes close to meeting the specifications for the damping ring injection/extraction kickers; this cost dominates the total cost of the injection/extraction system. Other components, including the stripline electrodes and the septa, are relatively conventional, and costs were based on similar existing devices.

Costs of the ILC damping ring fast feedback systems were taken directly from comparable systems in existing machines. Power amplifiers dominate the cost of the fast feedback systems. Amplifiers operating in the appropriate parameter regime are available commercially, and costs for these were obtained from an experienced manufacturer.

2.5 RING TO MAIN LINAC

2.5.1 Overview

The ILC Ring to Main Linac (RTML) is responsible for transporting and matching the beam from the Damping Ring to the entrance of the Main Linac. The RTML must perform several critical functions:

- transport of the electron and positron beams from the damping rings, at the center of the ILC accelerator complex, to the upstream ends of their respective linacs ("geometry matching");
- collimation of the beam halo generated in the damping ring;
- rotation of the spin polarization vector from the vertical to any arbitrary angle required at the IP;
- compression of the long Damping Ring bunch length by a factor of $30 \sim 45$ to provide the short bunches required by the Main Linac and the IP;

In addition, the RTML must provide sufficient instrumentation, diagnostics and feedback (feedforward) systems to preserve and tune the beam quality.

2.5.2 Beam Parameters

The key beam parameters of the RTML are listed in Table 2.5-1. Parameters are shown for the nominal configuration and for the "low charge" configuration (which requires a shorter bunch at the IP).

Parameter	Nominal value	Low Charge value
Initial energy	5.0 GeV	
Initial energy spread	0.15%	
Initial emittances	8.0μm $\times$ 20 nm	
Initial horizontal beam jitter	1 σ	
Initial bunch length	9.0 mm	
Final bunch length	0.3 mm	0.2 mm
Final energy	15.0 GeV	13.7 GeV
Final energy spread	1.5%	2.7 %
Final horizontal beam jitter	0.1σ	
ISR emittance growth	1.2 μm	1.0 μm
Emittance budget	1μm $\times$ 4 nm	

TABLE 2.5-1
Basic beam parameters for the RTML. This table assumes the 9 mm RMS DR bunch length, which is not yet baseline. This table needs to be updated prior to final publication.

2.5.3 System Description

2.5.3.1 Layout

Figure 2.5-1 depicts schematically the layout and location of the various sub-beamlines of the RTML. The RTML includes the long low-emittance transport from the Damping Ring, followed by a 180° turn-around, the spin-rotation and two-stage bunch compression sections. The beamlines upstream of the turnaround are collectively known as the "upstream RTML," while those from the turnaround to the launch into the main linac are collectively known as the "downstream RTML." In order to accommodate the different damping ring elevations and linac lengths, the electron and positron RTMLs have slight differences in their long transport sections, but are otherwise identical.

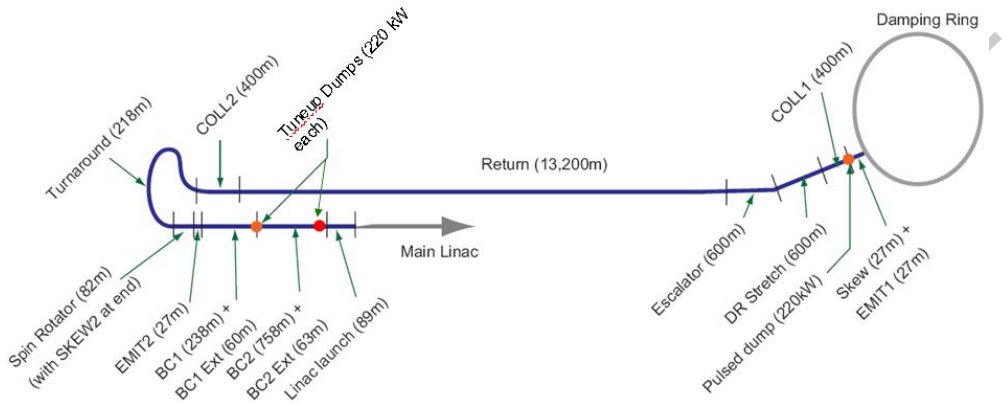

FIGURE 2.5-1. Schematic of RTML, indicating the various functions described in the text.

Each of the key functions of the RTML listed in 2.5.1 is supported by several of the sub-beamlines shown in Figure 2.5-1.

2.5.3.2 Geometry Match

Following extraction from the damping rings, the beams are brought parallel to the long axis via the 90° arcs in the Arc sections; transported from the the damping ring elevation to the main linac tunnel elevation via the vertical doglegs in the Escalator sections; transported out to their respective ends of the site via the Return lines, which are suspended from the ceiling of the main linac tunnel; and reversed in direction by the Turnaround sections. In addition, small vertical and horizontal doglegs at the upstream end of the Turnaround change the beam elevation from the ceiling of the linac tunnel to the nominal linac elevation, and adjust the horizontal position between the Return line axis and the main linac axis.

2.5.3.3 Collimation

The RTML's betatron collimation section is downstream of the damping ring extraction arc. It is constructed from two sets of thin spoiler and thick absorber pairs, placed 90° apart

Parameter	Nominal BC1 value	Nominal BC2 value
Initial Energy	5 GeV	4.88 GeV
Initial Energy Spread	0.15%	2.5%
Initial Bunch Length	9 mm	1.0 mm
RF Voltage	448 MV	11.4 GV
RF Phase	-105°	-27.6°
Wiggler R_{56}	-376 mm	-54 mm
Final Energy	4.88 GeV	15.0 GeV
Final Energy Spread	2.5%	1.5%
Final Bunch Length	1.0 mm	0.3 mm

TABLE 2.5-2
Key parameters for the two-stage bunch compressor in the nominal configuration, when compression to 0.3 mm RMS length is desired.

in betatron phase. This is considered sufficient to reduce the halo density by 3-4 orders of magnitude. The thin spoilers are needed to protect the absorbers from a direct hit from an errant beam in the event of some machine error [36]. The spoilers in the upstream section are protected by their proximity to the damping ring, which permits extraction to be halted prior to spoiler damage if the beam begins to hit the spoiler. There are additional collimators for energy collimation placed in the Turnaround, and in the wigglers of the Bunch Compressor.

2.5.3.4 Spin Rotation

The beam polarization in the damping rings is vertical, and this polarization is transported with negligible loss or precession to the end of the Turnaround. At that point it is necessary to be able to reorient the spin vector to any direction required by the experimental physicists. To achieve this, both the electron and positron RTMLs have a complete spin rotation system. Each system includes a pair of superconducting solenoids, followed by an arc with a net 7.9° bend angle, which is in turn followed by another pair of solenoids. By adjusting the excitation in the solenoid pairs, the spin vector at the end of the spin rotator can be oriented in any desired direction. In order to rotate the spin without introducing undesired x-y coupling, the solenoid-based rotators each use a pair of identical solenoids separated by a quadrupole lattice which introduces a $+I$ transformation in the horizontal plane and a $-I$ transformation in the vertical plane [37], the net effect of which is to cancel the cross-plane coupling.

2.5.3.5 Bunch Compression

In order to achieve the required bunch compression factor of 30-45, a two-stage system is adopted. A single-stage compressor would produce a beam with a relative energy-spread that is unacceptably high, leading to unachievable alignment tolerances in both the RTML and the early stages of the Main Linac.

Table 2.5-2 summarizes the important parameters for both the first-stage (BC1) and second-stage (BC2) compressor.

In addition to flexibility in the final bunch length, the two-stage bunch compressor allows some flexibility to balance longitudinal and transverse tolerances by adjustment of the wiggler magnet strengths, RF voltages, and RF phases. The nominal compressor configurations ease tolerances on damping ring extraction phase, damping ring bunch length, and bunch compressor phase stability, at the expense of tightening the tolerances on transverse alignment of accelerator components. There are also alternate configurations which loosen transverse alignment tolerances but tighten the longitudinal (i.e. phase) tolerances.

The linacs in both compressor stages use standard SCRF cryomodules and an RF power unit configuration similar to that of the Main Linac (i.e. one klystron driving three cryomodules). The first-stage compressor has a single RF unit with 8 cavities and one quadrupole in each of its 3 cryomodules; the second-stage compressor uses 14 RF units (plus one redundant spare) which are identical to the main linac configuration (*i.e.*, 26 cavities and 1 quad per unit, arranged in 3 cryomodules). The stronger focusing in the first stage is necessary to mitigate the higher wakefields and cavity-tilt effects resulting from the longer bunch length in the compressors. The first-stage has no spare RF unit; instead, a spare klystron and modulator are connected via a waveguide switch to provide some degree of redundancy.

Each bunch compressor stage includes a 150 m lattice of bend magnets("wiggler") which provides the momentum compaction required for bunch compression. As implied by the name, the wigglers introduce no net offset or angle to the beam.

2.5.3.6 Tuning, Correction, and Operations

The diagnostic, correction, and operational requirements of the RTML have been carefully integrated into the design of the entire beamline.

Global Dispersion Correction: The Arc, the BC1 wiggler, and the BC2 wiggler contain normal and skew quads in regions of horizontal dispersion which are used to tune any residual dispersion due to misalignments and errors. The quads are arranged in pairs, with an optical $-I$ transform between the two quads in a pair; this permits the tuning of the dispersion without introducing any betatron coupling or beta beats. The dispersions in the Turnaround are adjusted by tuning normal quads in the horizontal and vertical doglegs at the upstream end of the Turnaround; similarly, tuning the normal quads in the Escalator allows its vertical dispersion to be tuned.

Global Coupling Correction: There are two decoupling regions: the first is immediately downstream of the Arc, and the second is immediately downstream of the Spin Rotator. Each decoupling region contains 4 orthonormal skew quads in regions of zero dispersion, which allow complete and independent control of the 4 betatron coupling terms. The first station is conceptually intended to correct the coupling introduced by the damping ring extraction system, while the second corrects coupling generated by errors in the spin rotation system, as well as the remaining betatron coupling from small rotation errors on the RTML quads.

Emittance Measurement: There are three emittance measurement stations: the first is between the first decoupling section and the first collimation section, the second is between the second decoupling station and the bunch compressor, and the third is between the bunch compressor and the linac. Each of these stations contains 4 laser wire scanners embedded in a FODO lattice with 45° betatron phase; each station can therefore measure the projected x and y emittances of the beam. The first station can be used to tune the Arc dispersion and the skew quads in the first decoupler; the second station can be used to tune the Turnaround dispersion and the skew quads in the second decoupler; the third station can be used to tune

the dispersion correction in the Bunch Compressor wigglers. Although none of the systems have the capability to directly measure normal-mode emittances and coupling parameters, the optics of the first two stations are compatible with a later upgrade if needed.

Beam Position Monitors: There are cavity-type beam position monitors (BPMs) with horizontal and vertical readout at each quadrupole, with additional units close to the laser wires, at high-dispersion regions in the Bunch Compressor wigglers, and at other critical locations. The BPMs in the room-temperature sections of the RTML almost all operate in the 6 GHz frequency band ("C-band"), while the BPMs in the cryomodules and at a handful of other locations use the 1 GHz frequency band ("L-band"). At the nominal bunch charge of 3.2 nC, these BPMs can achieve sub-micron single-bunch resolution. The standard RTML BPM requires high precision and stability of the BPM's offset with respect to the device's mechanical center; a few of the BPMs have other requirements, such as high bandwidth or low latency.

Longitudinal Diagnostics: Each stage of the Bunch Compressor contains arrival-time (phase) monitors, beam position monitors at dispersive locations, X-ray synchrotron light monitors, and two types of bunch length monitors (a passive device based on measuring the RF spectrum of the bunch, and an active device based on transverse deflecting cavities [38]). The active bunch length monitor can also measure the correlation between energy and transverse position within a bunch.

Feedback and Feed-Forward: The RTML is not expected to require any intra-train trajectory feedback systems, although there will be a number of train-to-train (5 Hz) trajectory feedbacks. In addition, the beam energy at BC1 and BC2 will be controlled by a 5 Hz feedback, as will the electron-positron path length difference through their respective bunch compressors (see 2.5.4). There is also a trajectory feed-forward that uses BPMs at the end of the Return line to make bunch-by-bunch orbit measurements, which are fed forward to a set of fast correctors downstream of the Turnaround. The speed-of-light travel time between these two points is about 600 nanoseconds, and the actual distance between them is on the order of a few tens of meters; the resulting delay of the beam relative to the propagated signal is more than adequate for a digital low-latency orbit correction system [39].

Intermediate Extraction Points: There are 3 locations where the beam in the RTML may be directed to a beam dump: downstream of the first collimation section, downstream of BC1, and downstream of BC2. At each of these locations, there are both pulsed kickers and pulsed bends for beam extraction. The kickers are used when an intra-train extraction is required, for example during a machine protection fault, while the bends are used to send entire trains to their beam dumps. The pulsed bends can also be energized by DC power supplies if a long period of continual dump running is foreseen. All 3 dumps are capable of absorbing 220 kW of beam power. This implies that the first 2 dumps, which are at 5 GeV, can absorb the full beam power, while the third dump, at 15 GeV, can absorb only about 1/3 of the nominal beam power. Full trains can be run to this dump at reduced repetition rate, or short trains at full rate.

Access Segmentation: During personnel access to the main linac or downstream RTML beam tunnels, the beam can be sent to the first RTML dump. For additional safety, the bend magnets in the Escalator are switched off and additional personnel protection stoppers are inserted into the beamline. This allows the damping ring complex, the Arc dispersion tuning, the first decoupler, and the first emittance measurement station to be used at full beam power during linac access.

Path Length and Timing Adjustment: to be filled in later.

2.5.4 Accelerator Physics Considerations

A number of beam dynamics issues were considered in the design and specifications of the RTML.

Incoherent (ISR) and Coherent (CSR) Synchrotron Radiation: Current estimates indicate that the horizontal emittance growth from ISR will be around 80 nm (1%) in the Arc, 400 nm (5%) in the Turnaround, and 480 nm (6%) in the Bunch Compressor in its nominal configuration. Vertical emittance growth from ISR in the Escalator is negligible.

Studies of the ILC Bunch Compressor indicate that there are no important effects of coherent synchrotron radiation, primarily because the longitudinal emittance of the beam extracted from the damping ring is so large [40].

Stray Fields: Studies have found that fields at the level of 2.0 nTesla will lead to beam jitter at the level of 0.2 σ_y [41]. This is considered acceptable since the orbit feed-forward will correct most of this beam motion. Measurements at existing laboratories [42] indicate that 2 nTesla is a reasonable estimate for the stray field magnitude in the ILC. Emittance growth considerations also place limits on the acceptable stray fields, but these are significantly higher.

Beam-Ion Instabilities: Because of its length and its weak focusing, the electron Return line will have potential issues with ion instabilities. To limit these to acceptable levels, the base pressure in the Return line must be limited to 20 nTorr [43].

Static Misalignments: The main issues for emittance growth are: betatron coupling introduced by the Spin Rotator or by rotated quads; dispersion introduced by rotated bends, rotated quads in dispersive regions, or misaligned components; wakefields from misaligned RF cavities; and time-varying transverse kicks from pitched RF cavities.

Studies of emittance growth and control in the region from the start of the Turnaround to the end of the second emittance region have shown that a combination of beam steering, global dispersion correction, and global decoupling can reduce emittance growth from magnetostatic sources to negligible levels, subject to the resolution limits of the measurements performed by the laser wires [44]. Although the upstream RTML is much longer than the downstream RTML, its focusing is relatively weak and as a result its alignment tolerances are actually looser. Studies have shown that the same tuning techniques can be used in the upstream RTML with the desired effectiveness [45]. The tolerances for RF cavity misalignment in the RTML are large (0.5 mm RMS would be acceptable) because the number of cavities is small and the wakefields are relatively weak [46]. Although in principle the RF pitch effect is difficult to manage, in practice it leads to a position-energy correlation which can be addressed by the Bunch Compressor global dispersion correction [47]. A full and complete set of tuning simulations have not yet been performed, but it is expected that the baseline design for the RTML can satisfy the emittance preservation requirements.

Phase Jitter: Phase and amplitude errors in the bunch compressor RF will lead to energy and timing jitter at the IP, the latter directly resulting in a loss of luminosity. Table 2.5-3 shows the RMS tolerances required to limit the integrated luminosity loss to 2%, and to limit growth in IP energy spread to 10% of the nominal energy spread [48]. The tightest tolerance which influences the arrival time is the relative phase of the RF systems on the two sides: in the nominal configuration, a phase jitter of the electron and positron RF systems of 0.24° RMS, relative to a common master oscillator, results in 2% luminosity loss. The tight tolerances will be met through a three-level system:

- Over short time scales, such as 1 second, the low-level RF system will be required to

Parameter	Arrival Time Tolerance	Energy Spread Tolerance
Correlated BC Phase Errors	0.24°	0.35°
Uncorrelated BC Phase Errors	0.48°	0.59°
Correlated BC Amplitude Errors	0.5%	1.8%
Uncorrelated BC Amplitude Errors	1.6%	2.8%

TABLE 2.5-3
Key tolerances for the two-stage bunch compressor.

keep the two RF systems phase-locked to the level of 0.24 degrees of 1.3 GHz. See Section 3.9 for a fuller description of the low-level RF system.

- Over longer time periods, the arrival times of the two beams will be directly measured at the IP and a feedback loop will adjust the low-level RF system to synchronize the beams. This system is required to compensate for drifts in the low-level RF phase-locking system which occur over time scales long compared to a second.

- Over a period of many minutes to a few hours, the arrival time of one beam will be "dithered" with respect to the arrival time of the other beam, and the relative offset which maximizes the luminosity will be determined. This offset will be used as a new set-point for the IP arrival-time feedback loop, and serve to eliminate drifts which arise over time scales long compared to a minute.

Halo Formation from Scattering: Halo formation is dominated by Coulomb scattering from the nuclei of residual gas atoms, and it is estimated that 100 nTorr base pressure will cause approximately 9×10^{-7} of the beam population to enter the halo [49]. A similar calculation was performed for the upstream RTML, which indicates that 20 nTorr base pressure will cause approximately 2×10^{-6} of the beam population to enter the halo. This is well below the budget of 10^{-5} which has been set for all beamlines between the damping ring and the BDS collimators [50].

Space Charge: In the long, low-energy, low-emittance transfer line from the damping ring to the bunch compressor, the incoherent space-charge tune shift will be on the order of 0.15 in the vertical. The implications of such large values in a single-pass beamline have not been studied.

Collimator Wakefields: Assuming collimation of the beam extracted from the damping ring at $10\sigma_x$, $60\sigma_y$, and $\pm 1.5\%$ ($10\sigma_\delta$) in momentum, the worst-case jitter amplification for untapered, "razor-blade" spoilers is expected to be around 10% in x, around 75% in y, and the contribution to x jitter from energy jitter is expected to be negligible [51, 52]. The vertical jitter amplification figure is marginal, but can be substantially improved through use of spoilers with modest longitudinal tapers. The other collimator wakefield "figures of merit" are acceptable even assuming untapered spoilers.

2.5.5 Accelerator Components

Table 2.5-4 shows the total number of components of each type in each RTML. The number of quadrupoles, dipole correctors, and BPMs is larger in the electron RTML than in the positron RTML due to the longer electron Return line; for these 3 component classes, the

different totals for each side are shown in Table 2.5-4. Each quadrupole and dipole has its own power supply, while other magnets are generally powered in series with one power supply supporting many magnets. The cost estimate for the S-band dipole-mode structures was developed by the RTML Area Systems group based on recent experience with accelerator structure construction at IHEP; all other component cost estimates were developed by the ILC Technical and Global Systems groups.

Magnets		Instrumentation		RF	
Bends	362	BPMs	772/740	1.3 GHz Cavities	414
Quads	789/752	Wires	12	1.3 GHz Cryomodules	48
Dipoles	1185/1137	BLMs	2	1.3 GHz Sources	$16+1$
Kickers	17	OTRs	5	S-band Structures	2
Septa	7	Phase Monitors	3	S-band Sources	2
Rasters	6	Xray SLMs	2		
Solenoids	4				

TABLE 2.5-4
Total number of components in each RTML. Where 2 totals are shown, the larger number refers to the longer electron-side RTML, the smaller number refers to the shorter positron-side RTML.

Table 2.5-5 shows the system lengths for the RTML beamlines.

Upstream RTML	Turn	Spin	Emit	BC	Dumplines
15,447 m / 14,247 m	275 m	82 m	47 m	1,105 m	180 m
Total				17,136 m / 15,936 m	
Total, excluting extraction lines				16,956 m / 15,756 m	
Footprint length				1,301 m	

TABLE 2.5-5
System lengths for each RTML beamline. Where 2 values are shown, the larger number refers to the longer electron-side RTML, the smaller number refers to the shorter positron-side RTML.

2.5.5.1 Vacuum Systems

The base pressure requirement for the downstream RTML is set by limiting the generation of beam halo to tolerable levels, while in the upstream RTML it is set by the necessity of avoiding beam-ion instabilities. As described in 2.5.4, the base pressure requirement for the downstream RTML is 100 nTorr, while in the upstream RTML it is 20 nTorr. Both upstream and downstream RTML vacuum systems will be stainless steel with 2 cm OD; the upstream RTML vacuum system will be installed with heaters to allow *in situ* baking, while the downstream RTML vacuum system will not. The bending sections of the turnaround

and bunch compressors are not expected to need photon stops or other sophisticated vacuum systems, as the average beam current is low, and the fractional power loss of the beam in the bending regions is already small to limit emittance growth from ISR.

2.5.5.2 Service Tunnel

There is a service tunnel that runs parallel to the beam tunnel for the full length of the RTML and is shared with other systems. All of the power supplies, RF sources, and rack-mounted instrumentation and controls equipment and computers are installed in the service tunnel This configuration allows repairs and maintenance to be performed while minimizing disruption to the accelerator itself.

2.6 MAIN LINACS

2.6.1 Overview

The two main linacs accelerate the electron and positron beams from their injected energy of 15 GeV to the final beam energy of 250 GeV over a combined length of 23 km. This must be accomplished while preserving the small bunch emittances, which requires precise orbit control based on data from high resolution beam position monitors. The linacs utilize L-band (1.3 GHz) superconducting technology, with nine-cell standing-wave niobium cavities operating at an average gradient of 31.5 MV/m in a 2K superfluid helium bath. The choice of operating frequency is a balance between the high cavity cost due to size at lower frequency and the lower sustainable gradient due to increased surface resistivity at higher frequency. The accelerator gradient is somewhat higher than that typically achievable today and assumes that further progress will be made during the next few years in the aggressive program that is being pursued to improve cavity performance.

2.6.2 Beam Parameters

Table 2.6-1 lists the key beam parameters in the main linac. A description of the tradeoffs which led to the selection of the parameters can be found in Section 2.1.

TABLE 2.6-1
Nominal beam parameters in the ILC Main Linacs.

Parameter	Value	Parameter	Value
Initial beam energy	15 GeV	Initial $\gamma\epsilon_x$	8.4 μm
Final beam energy	250 GeV	Final $\gamma\epsilon_x$	9.4 μm
Particles per Bunch	2×10^{10}	Initial $\gamma\epsilon_y$	24 nm
Beam current	9.0 mA	Final $\gamma\epsilon_y$	34 nm
Bunch spacing	369 ns	σ_z	0.3 mm
Bunch train length	969 μs	Initial σ_E/E	1.5%
Number of bunches	2625	Final σ_E/E	0.10%
Pulse repetition rate	5 Hz	Beam phase wrt RF crest	5°

The rms bunch length remains constant along the linacs, while the bunch fractional energy spread decreases roughly as E_0/E, where E is the beam energy and E_0 is the initial main linac beam energy. The bunches are phased 5° off-crest to minimize their energy spread. No BNS energy spread is included to suppress resonant head-to-tail bunch trajectory growth as the short-range wakefield is fairly weak. For this same reason, the focusing strength of the quadrupole lattice in the linacs is kept fairly weak to reduce emittance growth from quadrupole misalignments.

2.6.3 System Description

2.6.3.1 RF Unit

The main linacs are composed of RF units whose layout is illustrated in Figure 2.6-1 and whose parameters are listed in Table 2.6-2. Each unit has a stand-alone RF source that powers three contiguous cryomodules containing a total of 26 cavities (with 9, 8 and 9 cavities in each cryomodule, respectively). The RF source includes a high-voltage modulator, a 10 MW klystron and a waveguide system that distributes the RF power to the cavities. It also includes the low-level RF (LLRF) system to regulate the cavity field levels, interlock systems to protect the source components, and the power supplies and support electronics associated with the operation of the source. To facilitate maintenance and limit radiation exposure, the RF source is housed mainly in a separate service tunnel that runs parallel to the beam tunnel.

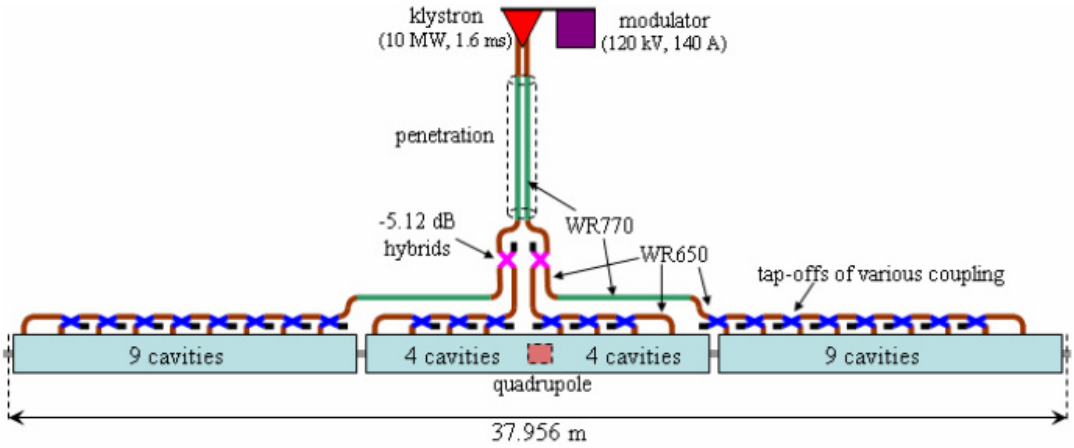

FIGURE 2.6-1. RF unit layout.

The modulator is a conventional pulse-transformer type with a bouncer circuit to compensate the voltage droop that occurs in the main storage capacitor during the pulse. The modulator produces 120 kV, 130 A, 1.6 ms, 5 Hz pulses with an efficiency of 83%, including the charging supply and rise time losses. These high voltage pulses power a multi-beam klystron (MBK) that amplifies $\sim$ 100 W, 1.6 ms RF pulses from the LLRF system up to 10 MW. This klystron has higher power and improved efficiency (65% goal) relative to commercial 5 MW tubes (40-45%). Two waveguides transport the power from the dual MBK outputs through a penetration to the beam tunnel where the power in each waveguide is then split to feed half of the middle cryomodule and one end cryomodule (see Figure 2.6-1).

The distribution system is composed primarily of aluminum WR650 (6.50" x 3.25") waveguide components. For long runs, WR770 is substituted to minimize distribution losses, estimated to be 7%, including 2% in the circulators. Along each cryomodule, RF power is equally distributed among the cavities through a series of hybrid-style 4-port tap-offs, each with appropriate fractional coupling (e.g. 1/9, 1/8, ...1/2). Between each tap-off output and its associated cavity power coupler, there are a bend, a semi-flexible section, a circulator,

TABLE 2.6-2
RF unit parameters.

Parameter	Value
Modulator overall efficiency	82.8%
Maximum klyston output power	10 MW
Klystron efficiency	65%
RF distribution system power loss	7%
Number of cavities	26
Effective cavity length	1.038 m
Nominal gradient with 22% tuning overhead	31.5 MV/m
Power limited gradient with 16% tuning overhead	33.0 MV/m
RF pulse power per cavity	293.7 kW
RF pulse length	1.565 ms
Average RF power to 26 cavities	59.8 kW
Average power transferred to beam	36.9 kW

a three-stub tuner, and a diagnostic directional coupler. The three-stub tuner allows fine adjustment of cavity phase and can be used to adjust the cavity Q_{ext}, although this is mainly adjusted via motor control of the position of the inner conductor in the cavity power coupler. The circulator, with a load on its third port, absorbs the RF power reflected from the cavities during filling and discharge, and so provides protection to the klystron and isolation between cavities.

The cryomodule design is a modification of the Type-3 version developed and used at DESY (see Figure 2.6-2). Within the cryomodules, a 300 mm diameter He gas return pipe serves as a strongback to support the cavities and other beam line components. Invar rods are used to maintain the spacing between the components when the cryomodule cools down, which requires roller-type support fixtures. The gas return pipe itself is supported at three locations off of the top of the outer vacuum vessel, with only the center support fixed. The middle cryomodule in each RF unit contains eight cavities, rather than nine, to accommodate a quad package that includes a superconducting quadrupole magnet at the center, a cavity BPM, and superconducting horizontal and vertical corrector magnets. All cryomodules, whether with or without the quad package, are 12.652 m long so the active length to actual length ratio in a 9-cavity cryomodule is 73.8%. Each also contains a 300 mm long HOM beam absorber assembly that removes energy through the 40-80K cooling system from beam-induced higher order modes above the cavity cutoff frequency.

The cavities illustrated in Figure 2.6-2 are "dressed" in that the cells are enclosed in a titanium vessel containing the liquid helium, a tuner system is mounted around the center to control the cavity length, and a coaxial power coupler (not shown) connects the cavity to the external waveguide feed. The cavity spacing within the cryomodules is 5 3/4 λ_0 = 1.326 m, which facilitates powering the cavities in pairs via 3 db hybrids as an alternate distribution scheme that eliminates or reduces the number of circulators. However, the spacing would not be significantly reduced otherwise due to the required length of bellows between cavities and

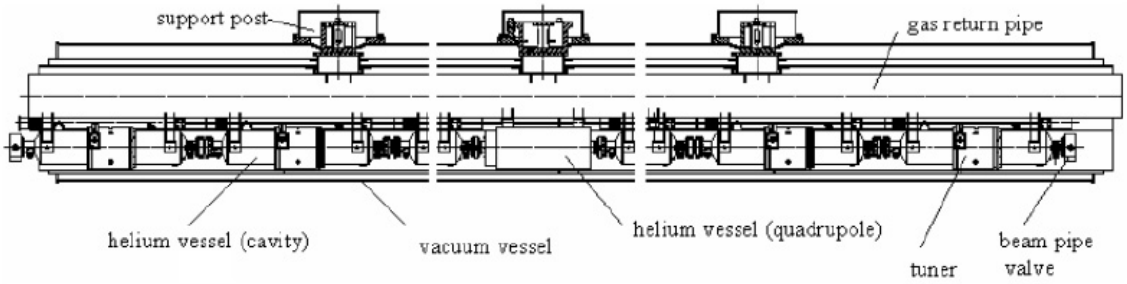

FIGURE 2.6-2. Side view of a cryomodule with a quadrupole magnet in the center. The figure has been compressed as indicated by the two white gaps, so not all eight cavities are shown.

space for flange accessibility.

To operate the cavities at 2K, they are immersed in a saturated He II bath, and helium gas-cooled shields intercept thermal radiation and thermal conduction at 5–8 K and at 40–80 K. The estimated cryogenic heat loads per RF unit are listed in Table 2.6-3, and were obtained by scaling the TESLA TDR estimates. Also, for each of the three cooling systems, the associated cryoplant power is listed for both the static and dynamic contributions from an RF unit and associated transfer line and distribution components, including a 50% overcapacity factor. The dynamic 2 K heat loss, attributable mainly to the RF and beam HOM losses in the cavities, constitutes about half the total installed power.

TABLE 2.6-3
RF cryogenic heat loads and installed AC cryogenic plant power to remove the heat.

	40–80 K		5–8 K		2 K		Total
	Static	Dynamic	Static	Dynamic	Static	Dynamic	
Heat load (W)	177.6	270.3	31.7	12.5	5.1	29.0	
Installed power	4.4	6.2	9.6	3.5	8.1	28.5	60.4

2.6.3.2 Linac Layout

The Main Linac components are housed in two tunnels, each of which has an interior diameter of 4.5 meters. The tunnels are separated from one another by 5.0 m to 7.5 m depending on the geology at the ILC site. As illustrated in Figure 2.6-3, the cryomodules occupy the beam tunnel while most of the RF system, including modulators, klystrons, power supplies, and instrumentation racks, are located in the service tunnel. This arrangement permits access to the equipment in the service tunnel for maintenance, repair, or replacement during beam operation and limits radiation exposure to most of the electronics (except motors in or near the cryomodules). The two tunnels are connected by three penetrations along each RF unit: one for the waveguide, one for signal cables, and one for power and high voltage cables. Personnel access points between the two tunnels are located at roughly 500 meter intervals.

Rather than being "laser straight", the tunnels are curved in the vertical plane, with a radius of curvature slightly smaller than that of the Earth. This allows the beam delivery system to lie in a plane at the center of the site, while the cryomodules nearly follow a gravitational equipotential to simplify distribution of cryogenic fluids.

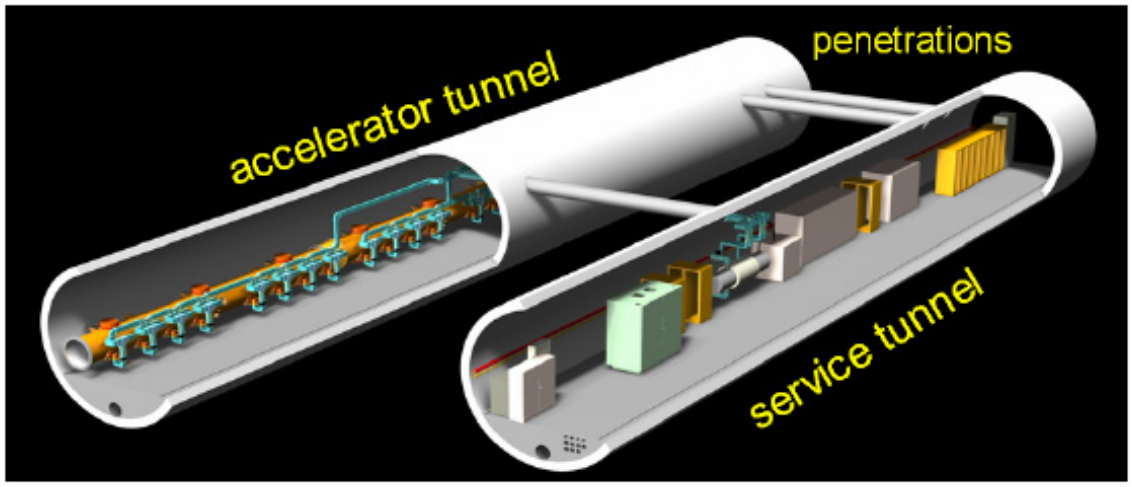

FIGURE 2.6-3. Cutaway view of the linac dual-tunnel configuration.

The positron linac contains 278 RF units, and the electron linac has 282 RF units; the four additional RF units are needed to compensate for the beam energy lost in the undulator that is used to generate gamma rays for positron production. The positron system section within the electron linac is 1,257 m long and is located near the 150 GeV point (see Section 2.3). Coasting sections, about 400 m long, are included at the end of the linacs so that additional RF units can be installed as an upgrade to provide up to 3.5% energy overhead during 500 GeV CM operation. No additional tunnel is included for a future upgrade to higher energies, although the site is sized to allow expansion for 1 TeV CM operation.

The tunnels in the present sample sites are 100-150 meters underground and are connected to the surface through vertical shafts. Each of the main linacs includes three shafts, roughly 5 km apart as dictated by the cryogenic system. The upstream shafts in each linac have diameters of 14 m to accommodate lowering cryomodules horizontally, and the downstream shaft in each linac is 9 m in diameter, which is the minimum size required to accommodate tunnel boring machines. At the base of each shaft is a 14,100 cubic meter cavern for staging installation and housing utilities and parts of the cryoplant, most of which are located on the surface.

The layout of the RF units in the main linac is not uniform, but includes an additional 2.5 m long "end box" after every 4 RF units that terminates the 2K He distribution to the upstream cavities and restarts it from the main 2K feed line for the downstream cavities. The linac section from one such end boxe to the next is called a "cryo string." In a few locations, cryo-strings of three RF units are used instead of four RF units. Cryo-strings are arranged in groups of 10 to 16 to form a cryogenic unit which is supported by a single cryoplant. Each cryogenic unit also includes 2.5 m long "service boxes" on each end (one service box replaces

a cryo-string end box), and is separated from the next cryogenic unit by a 7.7 m warm section that includes vacuum system components and a laser wire to measure beam size. Accounting for these additional sections and the quad package length, the active to actual length ratio in the linacs is 69.7% (excluding the undulator section and the coasting section at the end of each linac). Table 2.6-4 summarizes the linac component lengths and numbers.

TABLE 2.6-4
Subdivision lengths and numbers in the two main linacs. Total linac lengths exclude the length of the positron production insertion and the coasting length at the end of each linac.

Subdivision	Length (m)	Number
Cavities (9 cells + ends)	1.326	14,560
Cryomodule (9 cavities or 8 cavities + quad)	12.652	1,680
RF unit (3 cryomodules)	37.956	560
Cryo-string of 4 RF units (3 RF units)	154.3 (116.4)	71 (6)
Cryogenic unit with 10 to 16 strings	1,546 to 2,472	10
Electron (positron) linac	10,917 (10,770)	1 (1)

There are five, 4 MW-size cryoplants in each linac that also provide cooling for the RTML and undulator region. The total cryogenic capacity of the ILC linacs is comparable to that of the LHC. The plants are paired at each linac shaft, one feeding downstream cryomodules and the other upstream cryomodules, except for the downstream most shaft, where there is only one plant that feeds upstream cryomodules. The plants are sized with a 40% overcapacity to account for degradation of plant performance, variation in cooling water temperature, and operational overhead.

Conventional water cooling towers are also located on the site surface near each linac shaft. Through various distribution loops, they provide 35°C process water that removes most of the heat generated by the RF system, and 8°C chilled water for heat exchangers that maintain the tunnel air temperature at 29°C and cool electronics racks via closed, circulated-air systems. In each RF unit, roughly 10 kW of heat are dissipated in the racks, and another 10 kW are dissipated into the air from convection off of the RF source components.

The electrical requirements of the main linac are supplied by two high-voltage cable systems. One of the systems supports the conventional services, while the other supports the RF system. Table 2.6-5 summarizes the combined power consumption of the two main linacs. Of this power, 20.5 MW is transferred to the beams, for a net efficiency of 13.7%.

2.6.4 Accelerator Physics

2.6.4.1 Optics

The main linac lattice uses a weak focusing FODO optics, with a quad spacing of 37.956 m, corresponding to one quad per RF unit. Each quadrupole magnet is accompanied by horizontal and vertical dipole correctors and a cavity BPM which operates at 1.3 GHz. Because of the aperiodicity conditions imposed by the cryogenic system, the lattice functions are not perfectly regular. The mean phase advance per cell is 75° in the horizontal plane and 60° in the

TABLE 2.6-5
AC power consumption of the two main linacs.

System	AC Power (MW)
Modulators	81.4
Other RF system and controls	8.4
Conventional facilities	25.7
Cryogenic	33.8
Total	149.3

vertical plane. The vertical curvature is provided by the vertical correctors at the quadrupole locations, rather than by dedicated bend magnets. Dispersion matching and suppression at the beginning and end of the linac and around the undulator insertion are achieved by supplying additional excitation to small numbers of correctors in "dispersion-bump" configurations. Figure 2.6-4 shows the optical functions of the electron linac, including the undulator insertion. The functions for the positron main linac are basically the same except that the undulator insertion is not present.

2.6.4.2 Beam Dynamics

A key requirement of the main linacs is that they preserves the small emittances which are produced in the damping rings and transported through the RTMLs. This is particularly true for the vertical emittance, which is smaller than the horizontal emittance by a factor of 400. The main obstacles to emittance preservation in the linacs are transverse wakefields, betatron coupling, and dispersion.

The short-range transverse wakefields in the ILC cavities are quite weak compared to the wakefields typically associated with higher-frequency RF cavities. Alignment tolerances for cavities and cryomodules in the range of 200-300 μm RMS are expected to yield emittance growth on the order of 2 nm (10%) in the vertical plane. It is possible that even this small amount of emittance dilution can be corrected by the use of "wake bumps" (local orbit distortions which excite wakefields but not other aberrations).

The long-range wakefields in the ILC cavities are potentially more harmful given the high Q values typical in superconducting cavities. These wakefields are mitigated through HOM damping ports on the cavities, additional HOM absorbers in each RF unit at the location of the quadrupole magnet package, and detuning of the HOM's at the level of 10^{-3}. The combination of damping and detuning reduces the multi-bunch emittance growth to 0.5 nm (2.5%).

Azimuthal deformations to the cavities from construction errors or from the placement of the HOM and fundamental mode ports can cause the HOM's to develop diagonal polarizations instead of horizontal and vertical polarizations. Diagonally-polarized (or "mode-rotation") HOM's can couple beam jitter from the horizontal to the vertical, resulting in unacceptable vertical emittance dilution. This is mitigated in the main linacs by making the horizontal and vertical betatron tunes highly unequal. Setting the horizontal phase advance per cell to 75° and the vertical to 60° limits emittance growth from this effect to 5 nm (25%).

Betatron coupling between the relatively large horizontal mode and the relatively small

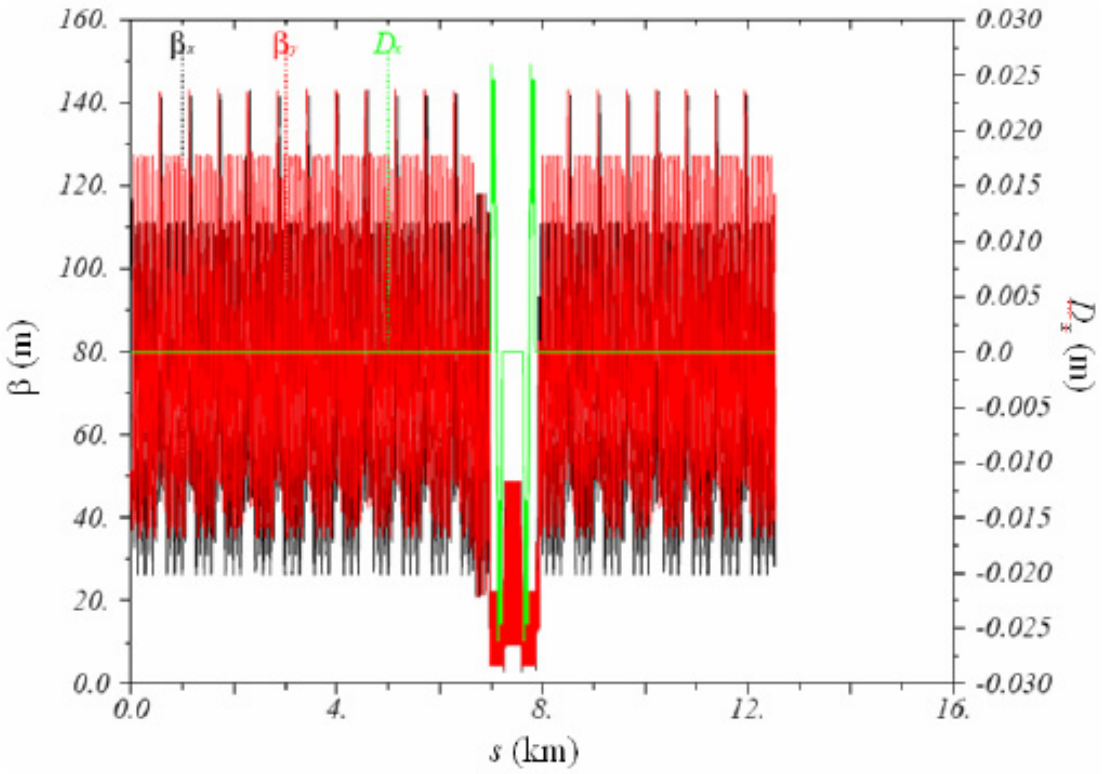

FIGURE 2.6-4. Beam optics functions for the electron main linac. The discontinuity of the pattern around s$\sim$ 8 km represents the undulator section for positron production.

vertical mode is driven by unwanted rotations of the main linac quadrupole magnets. By limiting the rms rotations of the quads to 0.3 mrad, the resulting emittance growth can be limited to 2 nm (10%). Most of this emittance growth can be globally corrected by the decoupler at the start of the beam delivery section (see Section 2.7.3.1.2), subject to the resolution limits of the laser wire profile monitors in the BDS.

Dispersion in the main linac is created by misaligned quadrupole magnets and pitched RF cavities. Emittance growth from this effect is mainly corrected through local or quasi-local steering algorithms such as Ballistic Alignment (BA), Kick Minimization (KM), or Dispersion Free Steering (DFS), with additional correction achieved through local orbit distortions which produce measured amounts of dispersion in a given phase ("dispersion bumps"). Simulations indicate that emittance growth from dispersion can be limited to about 5 nm (25%) through combinations of these techniques.

The principal main linac beam diagnostic is the suite of beam position monitors: a BPM with horizontal and vertical readout and sub-micron single-bunch resolution is located adjacent to each quadrupole magnet. For beam size monitoring, a single laser wire is located in each of the warm sections between main linac cryogenics units (about every 2.5 km). Upstream quadrupole magnets are varied to make local measurements of the beam emittances.

The main linacs do not contain any equipment for intra-train trajectory control. Such trajectory control is implemented only in the warm regions upstream and downstream of the main linacs and in the undulator section. There are no diagnostics for measuring energy or

energy spread in the main linacs. These measurements are made upstream and downstream of the main linacs and in the undulator section. There are no beam abort systems in the main linacs. Machine protection in the linac is ensured by verifying the state of the main linac hardware (both RF and magnets) prior to beam extraction from the RTML, and by verifying that the orbit in each damping ring is correct. The limiting aperture along the main linacs is the 70 mm diameter cavity iris.

2.6.4.3 Operation

Within each RF unit, a low level RF (LLRF) system monitors the vector sum of the fields in the 26 cavities. It makes adjustments to flatten the energy gain along the bunch train and keeps the beam-to-rf phase constant. It compensates for perturbations including cavity frequency variations (e.g. due to microphonics and residual Lorentz force detuning after feed-forward piezo-electric controller compensation), inter-pulse beam current variations, and non-flatness of the klystron pulse. In addition to the phase and amplitude of the klystron, this system has remote control over individual cavity phases (through the RF distribution system), external quality factors $Q_{\rm ext}$ (through the moveable coupler center conductor), and resonant frequencies (through slow and faster tuners).

The cavities are qualified at 35 MV/m or greater during initial testing (i.e. so-called "vertical" tests) prior to installation in cryomodules. This should allow them to run at 31.5 MV/m on average, installed, although the variation of sustainable gradients may be significant according to current data. Some cryomodule gradient variation within an rf unit can be accommodated by one-time adjustments in the main feed line power splitters and the in-line attenuators in each of the two feed lines.

For 500 GeV operation, there is no energy overhead if the average sustainable cavity gradient is the design value of 31.5 MV/m. With failed RF units, the ILC can only reach 500 GeV if the cavities achieve a higher average gradient (power limited to 33 MeV/m) or if additional RF units are eventually installed in the reserved drift region at the end of the linacs. The beam energy is coarsely adjusted by turning on or off RF units, each of which contributes about 0.3% of the beam energy, and finely adjusted by cross-phasing RF units near the end of the linacs.

2.6.5 Accelerator Components

2.6.5.1 Cavities and Cryomodules

The 1.3 GHz superconducting accelerating cavity is the fundamental building block of the ILC main linacs. Its parameters are listed in Table 3.6-1. A partially "dressed" cavity for installation in a cryomodule is shown Figure 2.6-5, together with the power coupler schematic. Each cavity is qualified for installation in the main linac in a vertical test stand; cavities which can sustain a gradient in excess of 35 MV/m with a Q value in excess of 0.8×10^{10} are then installed in cryomodules for use in the main linac. More information on the construction and testing of cavities can be found in Section 3.6.

2.6.5.2 Quad Package

In addition to cavities, the center cryomodule in each RF unit contains a 1.2 m long quad package that includes a quadrupole magnet, combined horizontal and vertical corrector mag-

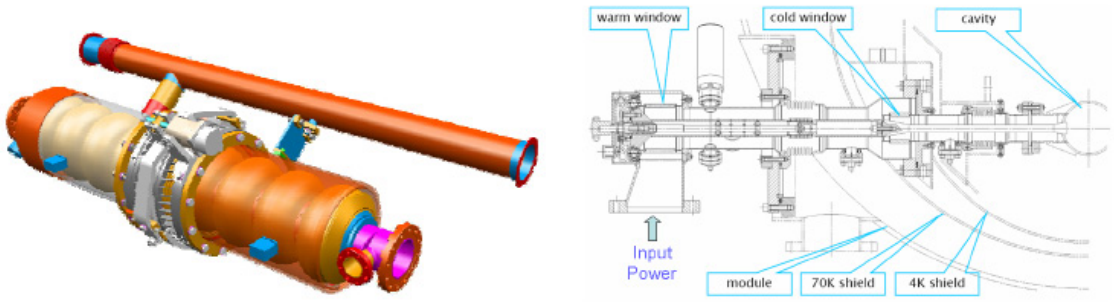

FIGURE 2.6-5. Left: A partially dressed cavity including the helium vessel, 2K He feed line and frequency tuners. Two HOM couplers and an RF pickup (not visible) are located near the ends of the cavity. Right: Schematic of the coaxial power coupler that attaches to the off-axis port shown in the left figure.

TABLE 2.6-6
Cavity parameters.

Parameter	Value
Type	9 cell, π-mode
R/Q of fundamental mode	1036 Ω
Iris diameter	70 mm
Cell-to-cell coupling	1.9%
Average Q_0	1.0×10^{10}
Average $Q_{\rm ext}$	3.5×10^6
Fill time	596 μs
Cavity resonance width	370 Hz

nets, and a cavity beam position monitor. At the low-energy end of the linac the quadrupoles and correctors are superferric types, while $\cos(2\theta)$ and $\cos(\theta)$ superconducting magnets are used at the high-energy end of the linac. The maximum gradient required in the quadrupoles at the high energy end of each linac is 60 T/m, while the maximum dipole integrated strength required is about 0.05 T-m. The beam position monitor is an L-band design capable of measuring horizontal and vertical positions with 1 micrometer resolution for a single bunch at full charge. All of the elements in the quad package have an aperture which is larger than the 70 mm aperture of the superconducting cavities.

2.6.5.3 Vacuum System

There are three independent vacuum systems along the accelerator: the beamline system that includes the volume in the cavities and other beamline components, the coupler system that includes the volume between the two windows in each coupler, and the insulation system that

includes the volume within the cryomodule vacuum vessel. The beamline system runs the length of the linacs and includes slow valves with second-scale response times in each 154 m cryo-string plus fast valves with ms-scale responses in the warm sections between cryogenic units. In the event of a major vent, these systems will limit the length of linac which is exposed to air to one or two cryo strings. Finally, the coupler vacuum system is segmented by cryomodule, and all couplers therein are pumped in common. With this system, a leak in one of the cold windows is fairly benign.

2.6.5.4 Beamline Components

Table 2.6-7 lists the basic beamline components and the total number of each contained in the two main linacs, excluding those in the positron production undulator region.

TABLE 2.6-7
Main Linac Beamline Components.

Component	Number (total)
Cavities	14,560
SC quadrupole magnets	560
X-correctors	560
Y-correctors	560
SRF BPMs	560
Laser wire scanners	7

2.7 BEAM DELIVERY SYSTEMS

2.7.1 Overview

The ILC Beam Delivery System (BDS) is responsible for transporting the e^+/e^- beams from the exit of the high energy linacs, focusing them to the sizes required to meet the ILC luminosity goals ($\sigma_x^* = 639$ nm, $\sigma_y^* = 5.7$ nm in the nominal parameters), bringing them into collision, and then transporting the spent beams to the main beam dumps. In addition, the BDS must perform several critical functions:

- measure the linac beam and match it into the final focus;
- protect the beamline and detector against mis-steered beams from the main linacs;
- remove any large amplitude particles (beam-halo) from the linac to minimize background in the detectors;
- measure and monitor the key physics parameters such as energy and polarization before and after the collisions;

The BDS must provide sufficient instrumentation, diagnostics and feedback systems to achieve these goals.

2.7.2 Beam Parameters

Table 2.7-1 shows the key BDS parameters. The IP beam parameters are shown for the nominal parameter set at 500 GeV CM.

2.7.3 System Description

The main subsystems of the beam delivery starting from the exit of the main linacs are the diagnostics region, the fast extraction and tuneup beamline, the betatron and energy collimation, the final focus, the interaction region and the extraction line. The layout of the beam delivery system is shown in Figures 2.7-1 and 2.7-2. The BDS is designed for 500 GeV center of mass but can be upgraded to 1 TeV with additional magnets.

There is a single collision point with a 14 mrad crossing angle. To support future energy upgrades, the beam delivery systems are in line with the linacs and the linacs are also oriented at a 14 mrad angle. The 14 mrad geometry provides space for separate extraction lines and requires crab cavities to rotate the bunches horizontally for head-on collisions. There are two detectors in a common IR hall which alternately occupy the single collision point, in a so-called "push-pull" configuration. The detectors are pre-assembled on the surface and then lowered into the IR hall in large subsections once the hall is ready for occupancy.

2.7.3.1 Diagnostics, Tune-up dump, Machine Protection

The initial part of the BDS, from the end of the main linac to the start of the collimation system (known for historical reasons as the Beam Switch Yard or "BSY"), is responsible for measuring and correcting the properties of the beam before it enters the Collimation and Final Focus systems. In addition, errant beams must be detected here and safely extracted in order to protect the downstream systems. Starting at the exit of the main linac, the system includes the MPS collimation system, skew correction section, emittance diagnostic section, polarimeter with energy diagnostics, fast extraction/tuning system and beta matching section.

TABLE 2.7-1
Key parameters of the BDS. The range of L*, the distance from the final quadrupole to the IP, corresponds to values considered for the existing detector concepts.

Length (linac exit to IP distance)/side	m	2226
Length of main (tune-up) extraction line	m	300 (467)
Max Energy/beam (with more magnets)	GeV	250 (500)
Distance from IP to first quad, L*	m	3.5-(4.5)
Crossing angle at the IP	mrad	14
Nominal beam size at IP, σ^*, x/y	nm	639/5.7
Nominal beam divergence at IP, θ^*, x/y	μrad	32/14
Nominal beta-function at IP, β^*, x/y	mm	20/0.4
Nominal bunch length, σ_z	μm	300
Nominal disruption parameters, x/y		0.17/19.4
Nominal bunch population, N		2×10^{10}
Beam power in each beam	MW	10.8
Preferred entrance train to train jitter	σ_y	< 0.5
Preferred entrance bunch to bunch jitter	σ_y	< 0.1
Typical nominal collimation aperture, x/y		8–10/60
Vacuum pressure level, near/far from IP	nTorr	1/50

2.7.3.1.1 MPS collimation At the exit of the main linac is a short 90° FODO lattice, composed of large bore quadrupoles, which contains a set of sacrificial collimators of decreasing aperture. The purpose of this system is to protect the 12 mm aperture BDS from any beam which develops an extremely large trajectory in the 7 cm aperture main linac (the effective aperture is $R/\beta^{1/2}$, which is 3–4 times smaller in the BDS than in the linac). This section also contains kickers and cavity BPMs for inter- and intra-train trajectory feedback.

2.7.3.1.2 Skew Correction The skew correction section contains 4 orthonormal skew quadrupoles which provide complete and independent control of the 4 betatron coupling parameters. This scheme allows correction of any arbitrary linearized coupled beam.

2.7.3.1.3 Emittance Diagnostics The emittance diagnostic section contains 4 laser wires which are capable of measuring horizontal and vertical RMS beam sizes down to 1 μm. The wire scanners are separated by 45° in betatron phase to allow a complete measurement of 2D transverse phase space and determination of the projected horizontal and vertical emittances.

2.7.3.1.4 Polarimeter and Energy Diagnostics Following the emittance diagnostic section is a magnetic chicane which is used for both Compton polarimetry and beam energy diagnostics. At the center of the chicane is the Compton IP, a BPM for measuring relative beam energy changes, and a sacrificial machine protection system (MPS) energy collimator which defines the energy acceptance of the tune-up extraction line. The length of the chicane

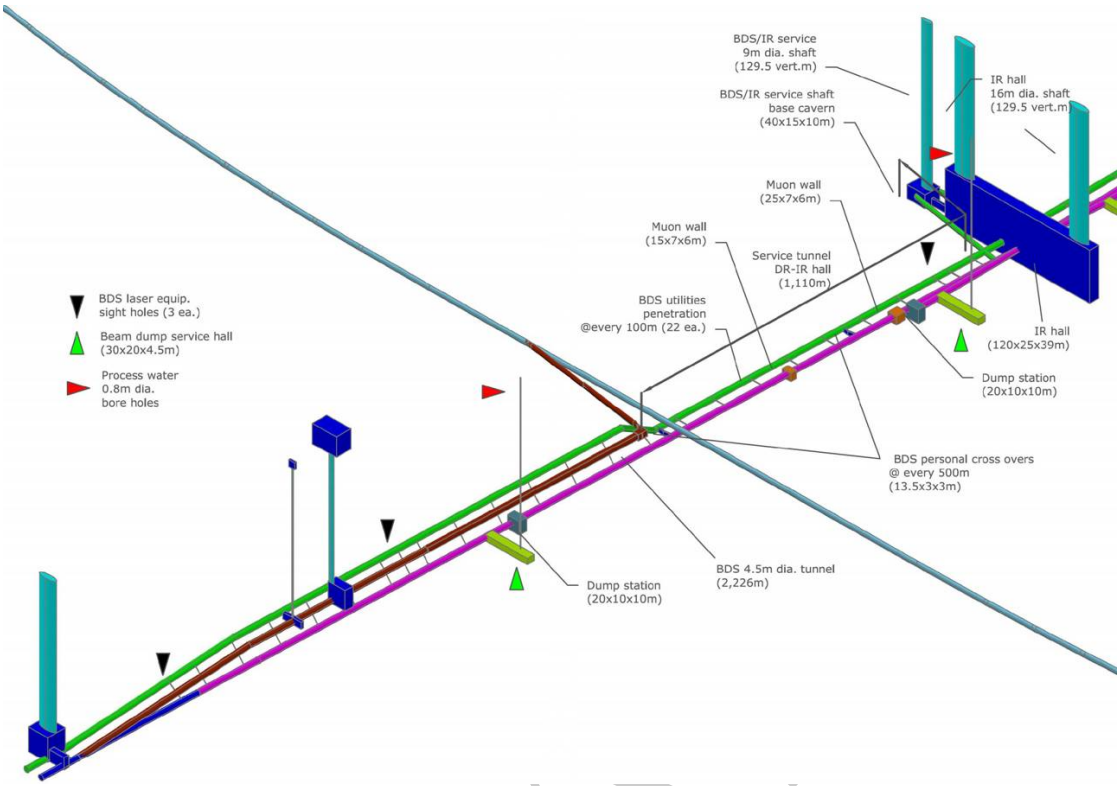

FIGURE 2.7-1. BDS layout, beam and service tunnels (shown in magenta and green), shafts, experimental hall.

is set to limit horizontal emittance growth due to synchrotron radiation to less than 1% with a 500 GeV/beam. A detector for the Compton-scattered photons from the laser wires is included in the chicane.

2.7.3.1.5 Tune-up and Emergency Extraction System

The BSY pulsed extraction system is used to extract beams in the event of an intra-train MPS fault. It is also used any time when beams are not desired in the collimation, final focus, or IR areas, for example during commissioning of the main linacs. The extraction system includes both fast kickers which can rise to full strength in the 300 ns between bunches, and pulsed bends which can rise to full strength in the 200 ms between trains. These are followed by a transfer line with ±10% momentum acceptance which transports the beam to a full-beam-power water-filled dump. There is a 125 m drift which allows the beam size to grow to an area of $2\pi\ mm^2$ at the dump. A set of rastering kickers sweep the beam in a 3 cm radius circle on the dump window. By using the nearby and upstream BPMs in the polarimeter chicane and emittance sections, it is possible to limit the number of errant bunches which pass into the collimation system to 1–2.

2.7.3.2 Collimation System

Particles in the beam halo produce backgrounds in the detector and must be removed in the BDS collimation system. One of the design requirements for the ILC BDS is that no particles are lost in the last several hundred meters of beamline before the IP. Another requirement is

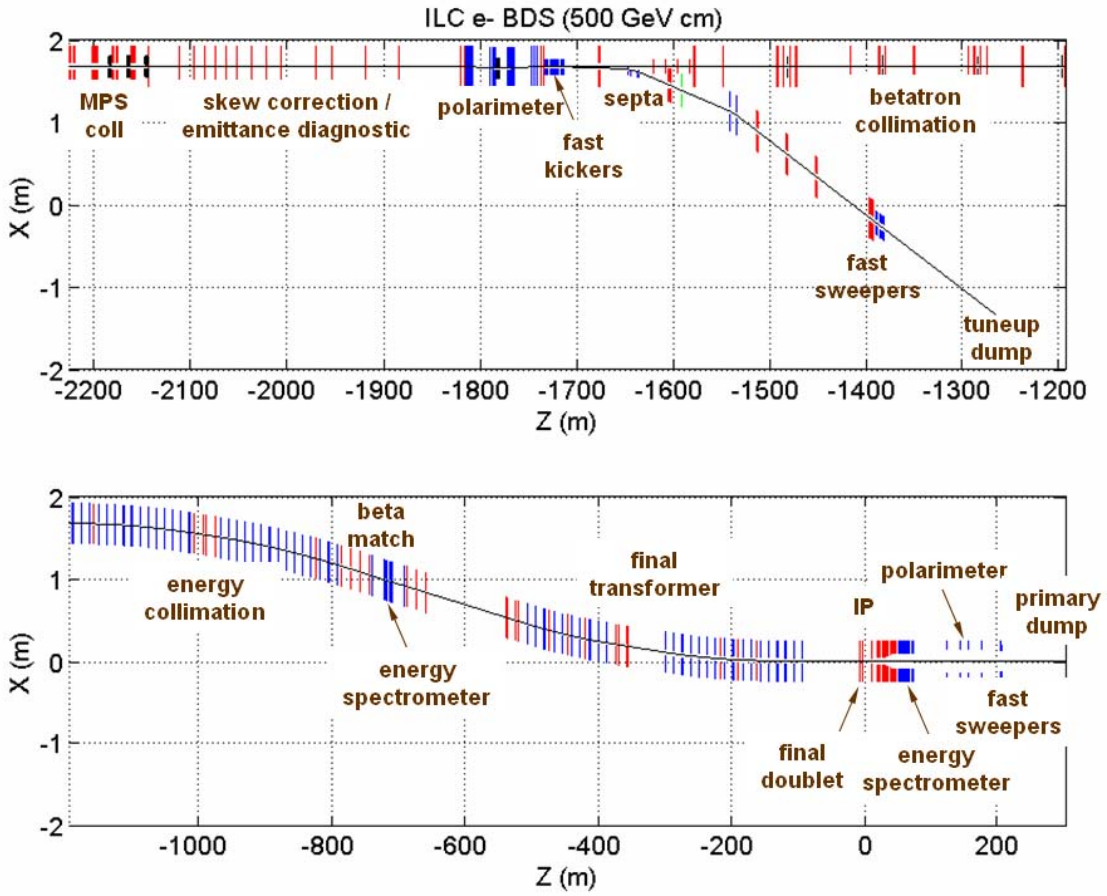

FIGURE 2.7-2. BDS layout showing functional subsystems, starting from the linac exit; X – horizontal position of elements, Z – distance measured from the IP.

that all synchrotron radiation passes cleanly through the IP to the extraction line. The BDS collimation must remove any particles in the beam halo which do not satisfy these criteria. These requirements define a system where the collimators have very narrow gaps and there are significant machine protection, survivability and beam emittance dilution issues.

The collimation system has a betatron collimation section followed by energy collimators. The downstream energy collimators help to remove the degraded energy particles originating from the betatron collimation section but not absorbed there. The betatron collimation system has two spoiler/absorber x/y pairs located at high beta points, providing single-stage collimation at each of the final doublet (FD) and IP betatron phases. The energy collimation section has a single spoiler located at the central high dispersion point (1530 μm/%). All spoilers and absorbers have adjustable gaps. Protection collimators (PC) are located throughout to provide local protection of components and additional absorption of scattered halo particles.

The spoilers are 0.5 to 1 X_0 (radiation length) thick, the absorbers are 30 X_0, and the protection collimators are 45 X_0. The betatron spoilers as well as the energy spoiler are "survivable" – they can withstand a hit of two errant bunches of 250 GeV/beam, matching the emergency extraction design goal. With 500 GeV beam, they would survive only one bunch, and would therefore require more effective MPS or the use of a pre-radiator scheme.

The collimation apertures required are approximately $\sim 8 - 10\sigma_x$ in the x plane and

$\sim 60 - 80\sigma_y$ in the y plane. These correspond to typical half-gaps of betatron spoiler of $\sim$1 mm in the x plane and $\sim$0.5 mm in the y plane.

Wakefield calculations for the BDS spoilers and absorbers give IP jitter amplification factors [54] of $\mathcal{A}_x = 0.14$ and $\mathcal{A}_y = 1.05$. Estimated as $\delta\varepsilon/\varepsilon = (0.4 n_{\rm jitter}\mathcal{A})^2$ this gives emittance dilutions of 0.08% and 4.4% in the x and y planes respectively, for 0.5 σ incoming beam jitter. Energy jitter at the collimators also amplifies the horizontal jitter at the IP. An energy jitter of 1% produces a horizontal emittance growth of 2.2%.

2.7.3.2.1 Muon suppression Electromagnetic showers created by primary beam particles in the collimators produce penetrating muons which can easily reach the collider hall. The muon flux through the detector is reduced by a 5 m long magnetized iron shield 330 m upstream of the collision point which fills the cross-sectional area of the tunnel and extends 0.6 m beyond the ID of the tunnel. The shield has a magnetic field of 1.5 T, with opposite polarities in the left and right halves of the shield such that the field at the beamline is zero. The shield also provides radiation protection for the collider hall during access periods when beam is present in the linac and beam switch yard.

2.7.3.2.2 Halo power handling The power handling capacity of the collimation system is set by two factors: the ability of the collimators to absorb the incident beam power, and the ability of the muon suppression system to reduce the muon flux through the detector. In the baseline design, the muon suppression system presents the more restrictive limitation, setting a tolerance of $1 - 2 \times 10^{-5}$ on the fraction of the beam which is collimated in the BDS. With these losses and the 5 m wall, the number of muons reaching the collider hall would be a few muons per 150 bunches (a reduction of more than 10^{-2}). Since the actual beam halo conditions are somewhat uncertain, the BDS includes caverns large enough to increase the muon shield from 5 m to 18 m and to add an additional 9 m shield downstream. Filling all of these caverns with magnetized muon shields would increase the muon suppression capacity of the system to 1×10^{-3} of the beam. The primary beam spoilers and absorbers are water cooled and capable of absorbing 1×10^{-3} of the beam continuously.

2.7.3.2.3 Tail-folding octupoles The final focus includes two superconducting octupole doublets. These doublets use nonlinear focusing to reduce the amplitude of beam halo particles while leaving the beam core untouched [55]. This "tail-folding" would permit larger collimation amplitudes, which in turn would dramatically reduce the amount of beam power intercepted and the wakefields. In the interest of conservatism the collimation system design described above does not take this tail folding into account in the selection of apertures and other parameters.

2.7.3.3 Final focus

The role of the final focus (FF) system is to demagnify the beam to the required size ($\sim$639 nm (horz) and $\sim$5.7 nm (vert)) at the IP. The FF optics creates a large and almost parallel beam at the entrance to the final doublet (FD) of strong quadrupoles. Since particles of different energies have different focal points, even a relatively small energy spread of $\sim$0.1% significantly dilutes the beam size, unless adequate corrections are applied. The design of the FF is thus mainly driven by the need to cancel the chromaticity of the FD. The ILC FF has local chromaticity correction [53] using sextupoles next to the final doublets. A

bend upstream generates dispersion across the FD, which is required for the sextupoles to cancel the chromaticity. The dispersion at the IP is zero and the angular dispersion is about $\eta'_x \sim 0.009$, i.e. small enough that it does not significantly increase the beam divergence. Half of the total horizontal chromaticity of the whole final focus is generated upstream of the bend in order for the sextupoles to simultaneously cancel the chromaticity and the second-order dispersion.

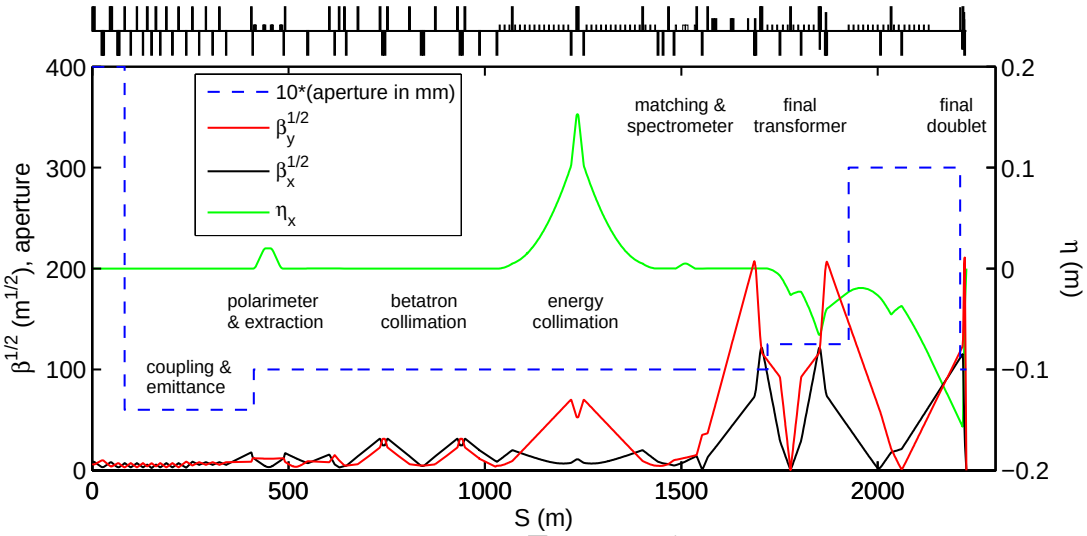

FIGURE 2.7-3. BDS optics, subsystems and vacuum chamber aperture; S is distance measured from the entrance.

The horizontal and the vertical sextupoles are interleaved in this design, so they generate third-order geometric aberrations. Additional sextupoles upstream and in proper phases with the FD sextupoles partially cancel the third order aberrations. The residual higher-order aberrations are minimized further with octupoles and decapoles. The final focus optics is shown in Figure 2.7-3.

Synchrotron radiation from the bending magnets causes emittance dilution, so it is important to maximize the bending radius, especially at higher energies. The FF includes sufficient bend magnets for 500 GeV CM and space for additional bend magnets which are necessary at energies above 500 GeV CM. With the reserved space filled with bends, the emittance dilution at 1 TeV CM is about 15%.

In addition to the final doublet and chromaticity correction optics, the final focus includes: an energy spectrometer (see Section 2.7.4.3.1); additional absorbers for the small number of halo particles which escape the collimation section; tail folding octupoles (see Section 2.7.3.2); the crab cavities (see Section 2.7.4.1); and additional collimators for machine protection or synchrotron radiation masking of the detector.

2.7.3.4 IR design and integration to detector

The ILC final focus uses independently adjustable compact superconducting magnets for the incoming and extraction beam lines. The adjustability is needed to accommodate beam en-

ergy changes and the separate beamline allows optics suitable for post IP beam diagnostics. The BNL direct wind technology is used to produce closely spaced coil layers of superconducting multi-strand cable. The design is extremely compact and the coils are almost touching in shared cold mass volumes. Cooling is provided by superfluid helium at 2 K. The technology has been demonstrated by a series of short prototype multi-pole coils. The schematic layout of magnets in the IR is shown in Figure 2.7-4 and Figure 2.7-9. The quadrupoles closest to the IP are actually inside the detector solenoidal field and therefore cannot have magnetic flux return yokes; at the closest coil spacing the magnetic cross talk between the two beam apertures is controlled by using actively shielded coil configurations and by use of local correction coils, dipole, skew-dipole and skew-quadrupole or skew-sextupole, as appropriate.

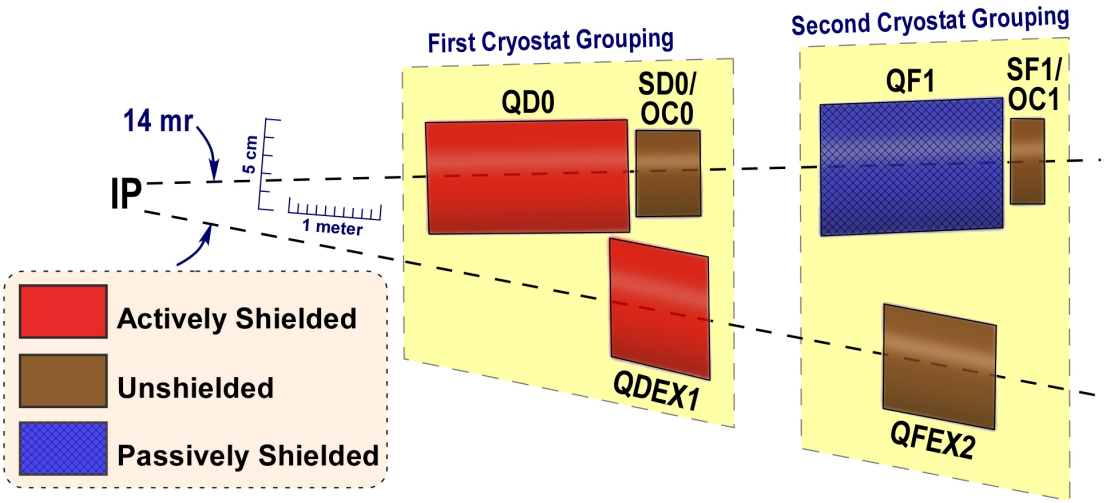

FIGURE 2.7-4. Schematic layout of magnets in the IR.

To facilitate a rapid, "push-pull" style exchange of detectors at a shared IP, the superconducting final focus magnets are arranged into two groups so that they can be housed in two separate cryostats as shown in Figure 2.7-4, with only warm components and vacuum valves placed in between. The cryostat on the left in Figure 2.7-4 moves with the detector during switchover, while the cryostat on the right remains fixed on the beamline.

Additional optical elements are required in the IR to compensate the effects of the detector solenoid field interacting with the accelerator IR magnets. The first is a large aperture anti-solenoid in the endcap region to avoid luminosity loss due to beam optics effects [58]. The second is a large aperture Detector Integrated Dipole (DID) [59] that is used to reduce detector background at high beam energies or to minimize orbit deflections at low beam energies.

The vertical position of the incoming beam line quadrupole field center must be stable to order of a few tens of nanometers, in order to stay within the capture range of the intra-train collision feedback (see 2.7.4.2). This requirement is well beyond experience at existing accelerators and is being addressed in ongoing R&D.

2.7.3.5 Extraction line

The ILC extraction line [56, 57] has to transport the beams from the IP to the dump with acceptable beam losses, while providing dedicated optics for beam diagnostics. After collision, the beam has a large angular divergence and a huge energy spread with very low energy tails. It is also accompanied by a high power beamstrahlung photon beam and other secondary particles. The extraction line must therefore have a very large geometric and energy acceptance to minimize beam loss.

The optics of the ILC extraction line is shown in Figure 2.7-5. The extraction line can transport particles with momentum offsets of up to 60% to the dump. There is no net bending in the extraction line, which allows the charged particle dump to also act as a dump for beamstrahlung photons with angles of up to 0.75 mrad.

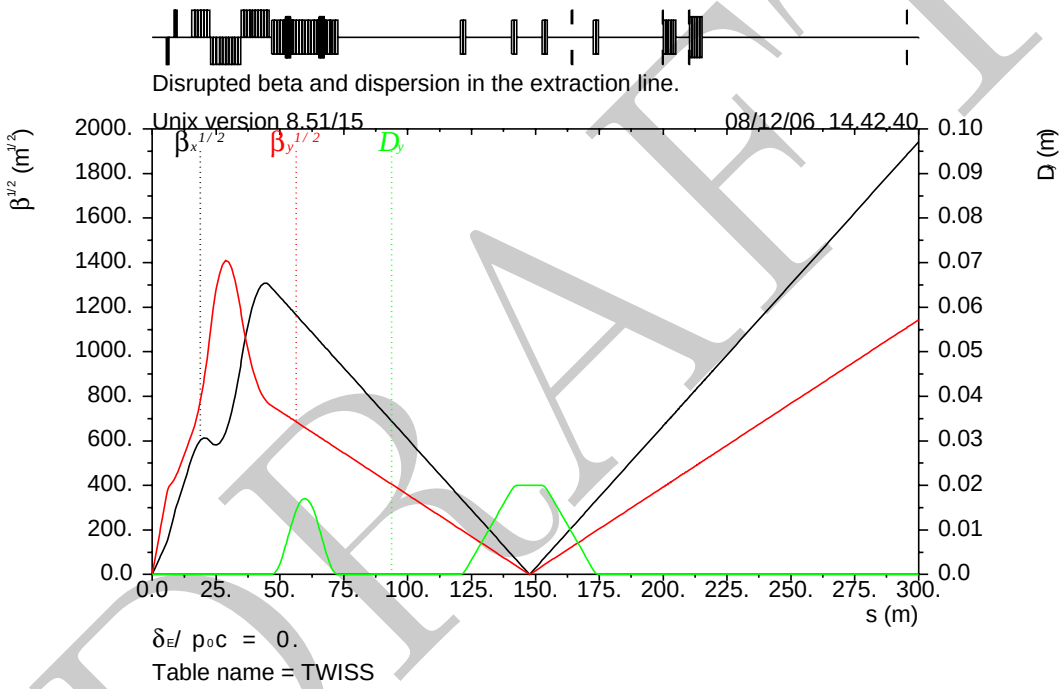

FIGURE 2.7-5. Disrupted β-functions and dispersion in the extraction line for the nominal 250 GeV beam.

The first quadrupole is a superconducting magnet 5.5 m from the IP, as shown in Figure 2.7-4. The second quadrupole is also superconducting, with a warm section between the cryostats for these two quadrupoles. The downstream magnets are normal conducting, with a drift space to accommodate the crab cavity in the adjacent beamline. The quadrupoles are followed by two diagnostic vertical chicanes for the energy spectrometer and Compton polarimeter, with a secondary focal point in the center of the latter. The horizontal angular amplification (R_{22}) from the IP to the Compton IP is set to -0.5 so that the measured Compton polarization is close to the luminosity weighted polarization at the IP. The lowest energy particles are removed by a vertical collimator in the middle of the energy chicane. A large chromatic acceptance is achieved through the soft D-F-D-F quadruplet system and careful optimization of the quadrupole strengths and apertures. The two SC quadrupoles are compatible with up to 250 GeV beam energy, and the warm quadrupoles and the chicane

bends with up to 500 GeV beam.

The diagnostic section is followed by a 100 m long drift to allow adequate transverse separation (>3.5 m) between the dump and the incoming line. It also allows the beam size to expand enough to protect the dump window from the small undisrupted beam. A set of rastering kickers sweep the beam in a 3 cm circle on the window to avoid boiling the water in the dump vessel. Three protection collimators in the 100 m drift remove particles that would hit outside of the 15 cm radius dump window and protect the rastering kicker magnets.

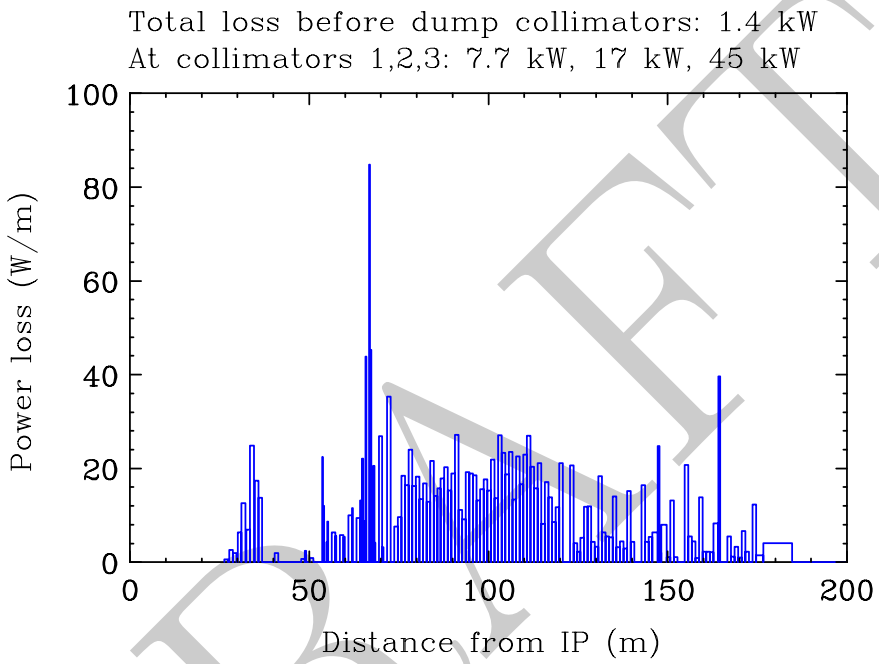

FIGURE 2.7-6. Power loss density in the magnet region for disrupted beam at 250 GeV, with an extreme choice of parameters.

Extraction beam loss has been simulated for realistic 250 GeV GUINEA-PIG beam distributions [60], with and without beam offset at the IP. No primary particles are lost in the SC quadrupoles, and all particles above 40% of the nominal beam energy are transmitted cleanly through the extraction magnets. The total primary loss on the warm quadrupoles and bends is a few watts, and the loss on the protection collimators is a few kW for the nominal beam parameters. Figure 2.7-6 shows that even for an extreme set of parameters, with very high beamstrahllung energy loss, the radiation deposition in the magnet region is manageable.

2.7.4 Accelerator Components

The BDS accelerator components are described in the following sections and the total counts are shown in Table 2.7-2.

2.7.4.1 Crab cavity system

With a 14 mrad crossing angle, crab cavities are required to rotate the bunches so they collide head on. Two 3.9 GHz SC 9-cell cavities in a 2–3 m long cryomodule are located 13.4 m from

the IP. The cavities are based on the Fermilab design for a 3.9 GHz TM_{110} π mode 13-cell cavity [61]. The three cell prototype of this cavity is shown in Figure 2.7-7. The ILC has two 9-cell versions of this design operated at 5 MV/m peak deflection. This provides enough rotation for a 500 GeV beam and 100% redundancy for a 250 GeV beam.

FIGURE 2.7-7. Photo of a 3.9GHz 3 cells deflecting cavity built at Fermilab, which achieved 7.5MV/m.

The most challenging specification of the crab cavity system is on the uncorrelated phase jitter between the incoming positron and electron cavities which must be controlled to 61 fsec to maintain optimized collisions [62]. A proof-of-principle test of a 7 cell 1.5 GHz cavity at the JLab ERL facility [63] has achieved a 37 fsec level of control, demonstrating feasibility. The higher- and lower-order modes of the cavity must be damped effectively to limit unwanted vertical deflections at the IP, as must the vertical polarization of the main deflecting mode.

Couplers with lower Q_{ext} and greater power handling capability are required to handle beam loading and LLRF feedback for off-axis beam. The crab cavity needs ∼3 kW per cavity for about 10 msec, with a Q_{ext} of $\sim 10^6$ [64]. The crab cavity is placed in a cryostat with tuner, x-y and roll adjustment which provides proper mechanical stability and microphonic rejection. The cryostat also accommodates the beampipe of the extraction line which passes about 19 cm from the center of the cavity axis.

2.7.4.2 Feedback systems and Stability

Maintaining the stability of the BDS is an essential prerequisite to producing luminosity. Since the beams have RMS vertical sizes of 5.7 nm at the IP, vertical offsets of about 1 nm will noticeably reduce the luminosity. In addition, especially for parameter sets with higher disruption, the beam-beam interaction is so strong that the luminosity is extremely sensitive to small variations in the longitudinal shape of the bunch caused by short-range wakefields. Finally, the size of the beam at the IP is sensitive to the orbit of the beam through the final doublet quads, the sextupoles, and other strong optical elements of the BDS. Care must be taken to minimize thermal and mechanical disturbances, by stabilizing the air temperature to 0.5°C and the cooling water to 0.1°C, and by limiting high frequency vibrations due to local equipment to the order of 10 nm.

Beam-based orbit feedback loops are used to maintain the size and position of the beam at the IP. All of the feedback loops use beam position monitors with micrometer-level resolution to detect the beam position, and dipole magnets or stripline kickers to deflect the beam. There are two basic forms of feedback in the BDS: train-by-train feedbacks, which operate at the 5 Hz repetition rate of the ILC, and intra-train feedbacks, which can apply a correction to the beam between bunches of a single train.

2.7.4.2.1 Train-by-train feedback A train-by-train feedback with 5 correctors controls the orbit through the sextupoles in the horizontal and vertical planes, where the optical tolerances are tightest. Additional correctors throughout the BDS help reduce long-term beam size growth. The orbit control feedback can maintain the required beam sizes at the IP over periods from a few hours to several days depending on details of the environment. On longer timescales, IP dispersion and coupling knobs need to be applied.

2.7.4.2.2 Intra-Train IP position and angle feedbacks The intra-train feedbacks use the signals detected on early bunches in the train to correct the IP position and angle of subsequent bunches. The offset of the beams at the IP is determined by measuring the deflections from the beam-beam interaction; this interaction is so strong that nm-level offsets generate deflections of tens of microradians, and thus BPMs with micron-level resolution can be used to detect offsets at the level of a fraction of a nanometer. Corrections are applied with a stripline kicker located in the incoming beamline between SD0 and QF1. The angle of the beams at the IP is determined by measuring the beam positions at locations 90° out of phase with the IP; at these locations the beam is relatively large so micron resolution is sufficient to directly measure the beam position (and hence the IP angle) to a small fraction of its RMS size. A stripline kicker is located at the entrance to the FF causing a latency of about 4 bunch spacings.

The position feedback BPM is located near the IP in a region where electromagnetic backgrounds or particle debris from the collisions are a concern. Preliminary results from simulations and from a test-beam experiment indicate that backgrounds are an order of magnitude too small to cause a problem [65].

2.7.4.2.3 Luminosity feedback Because the luminosity may be extremely sensitive to bunch shape, the maximum luminosity may be achieved when the beams are slightly offset from one another vertically, or with a slight nonzero beam-beam deflection. After the IP position and angle feedbacks have converged, the luminosity feedback varies the position and angle of one beam with respect to the other in small steps to maximize the measured luminosity.

2.7.4.2.4 BDS Entrance Feedback ('train-straightener') A bunch-to-bunch correction at the end of the Linac removes systematic transverse position offsets within the train due to long-range wakefield kicks in the accelerating cavities. This system consists of two kicker-BPM systems similar to those described above. Each pair operates at a different phase to null the orbit in both vertical degrees of freedom.

For stripline kickers the maximum correction would be about 8–10 μm, and the BPM resolution requirements are about 200 nm. This requires cavity BPMs that are read out in bunch-bunch mode and processed with low-latency electronics. The kicker-BPM separations imply latencies of about 400 ns, allowing feedback on every-other bunch.

2.7.4.2.5 Hardware Implementation for intra-train feedbacks High bandwidth, low-latency (∼5 ns) signal processors for stripline and button BPMs have been tested at the NLCTA and ATF [66]. The feedback processor has been prototyped using fast state of the art FPGAs; a system prototype has been demonstrated with a FB board latency of ∼70 ns [67]. Commercial boards that meet the latency requirement are not available without custom firmware modification; one such board has been tested by the FONT group and would meet the ILC latency specification for bunch-bunch operation.

2.7.4.3 Energy, Luminosity and polarization measurements

2.7.4.3.1 Energy measurements Absolute beam energy measurements are required by the ILC physics program to set the energy scale for particle masses. An absolute accuracy better than 200 ppm is required for the center-of-mass energy, which implies a requirement of 100 ppm on determination of the absolute beam energy. The intra-train relative variation in bunch energies must be measured with a comparable resolution. Measurements of the disrupted energy spectrum downstream of the IP are also useful to provide direct information about the collision process.

To achieve these requirements, there are two independent and complementary detectors for each beam. Upstream from the IP, a spectrometer based on the LEP-II energy spectrometer is capable of making high-precision bunch-to-bunch relative measurements in addition to measuring the absolute beam energy scale. A four-magnet chicane in the instrumentation region provides a point of dispersion which can be measured using triplets of high-precision RF BPMs. The maximum displacement of the beam is a few millimeters and must be measured to a precision below 100 nanometers. Precision movers keep the beam nearly centered in the BPMs in order to achieve this accuracy.

Downstream from the IP, there is a synchrotron radiation spectrometer. A three-magnet chicane in the extraction line provides the necessary beam deflection, while the trajectory of the beam in the chicane is measured using synchrotron radiation produced in wiggler magnets imaged ∼70 meters downstream at a secondary focus near the polarimeter chicane.

2.7.4.3.2 Luminosity measurements The ILC luminosity can be measured with a precision of 10^{-3} or better by measuring the Bhabha rate in the polar-angle region from 30-90 mrad. Two detectors are located just in front of the final doublets as shown in Figure 2.7-9. The *LumiCal* covers the range from 30-90 mrad and the *BeamCal* covers the range from 5-30 mrad. At 500 GeV center-of-mass energy, the expected rate in the *LumiCal* region is ∼10 Bhabhas per bunch train, which is too low to permit its use as an intra-train diagnostic for tuning and feedback. At smaller polar angles of 5-30 mrad the rate or energy deposition of beamstrahlung e+e- pairs can be measured for a fast luminosity diagnostic. The expected rate in this region is 15,000 pairs (and 50 TeV energy deposition) per bunch crossing. Furthermore, the spatial distributions of pairs in this region can be used to determine beam collision parameters such as transverse sizes and bunch lengths.

2.7.4.3.3 Polarization measurements Precise polarimetry with 0.25% accuracy is needed to achieve the ILC physics goals [68]. Compton polarimeters [69, 70] are located both ∼1800 m upstream of the IP, as shown in Figure 2.7-2, and downstream of the IP, as shown in Figure 2.7-8, to achieve the best accuracy for polarimetry and to aid in the alignment of the spin vector.

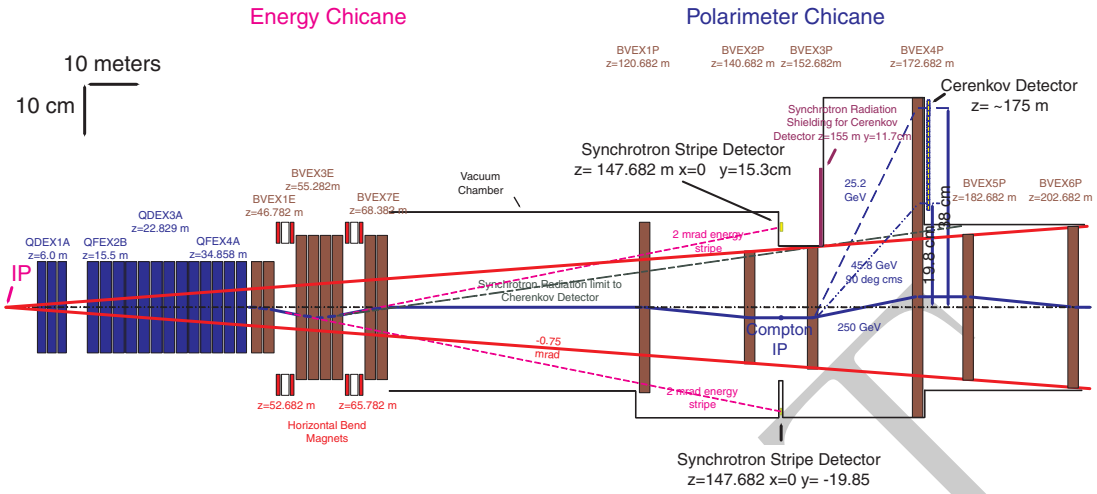

FIGURE 2.7-8. Schematics of energy and polarimeter chicanes in the 14 mrad extraction line, shown in a configuration with two additional bends at the end. Longitudinal distances are given from the IP. Also shown is the 0.75 mrad beam stay-clear from the IP.

The upstream polarimeter measures the undisturbed beam before collisions. The relatively clean environment allows a laser system that measures every single bunch in the train and a large lever arm in analyzing power for a multi-channel polarimeter, which facilitates internal systematic checks. The good field region of the individual dipoles is wide enough to accommodate the lowest expected beam energy of 45.6 GeV. The downstream polarimeter measures the polarization of the outgoing beam after collision. The estimated average depolarization for colliding beams is 0.3%, and for the outgoing beam 1%. A schematic drawing of the extraction line is shown in Figure 2.7-8.

Each polarimeter has a dedicated 4-bend chicane to facilitate injection of the laser light and extraction of the Compton signal. The upstream polarimeter uses a horizontal chicane to minimize emittance growth from synchrotron radiation, while the downstream polarimeter uses a vertical chicane to maximize analyzing power. The systems are designed to meet the physics requirements at all energies from the Z pole to the full energy of the ILC.

2.7.4.4 Beam dumps and Collimators

The beam delivery system contains two tune-up dumps and two main beam dumps. These four dumps are all designed for a peak beam power at nominal parameters of 17 MW at 500 GeV per beam. These dumps consist of 1.5 m diameter cylindrical stainless steel high pressure (10 bar) water vessels with a 30 cm diameter 1 mm thick Ti window; and also include their shielding and associated water systems.

The dumps absorb the energy of the electromagnetic shower cascade in 6.5 m (18 X_0) of water followed by 1 m of water cooled Cu plates (22 X_0). Each dump incorporates a beam sweeping magnet system to move the charged beam spot in a circular arc of 3 cm radius during the passage of the 1 ms long bunch train. Each dump operates at 10 bar pressure and also incorporates a vortex-flow system to keep the water moving across the beam at 1.0-1.5 m/s. In normal operation with 250 GeV beam energy, the combination of the water velocity and the beam sweepers limits the water temperature rise during a bunch train to

40°C. The pressurization raises the boiling temperature of the dump water; in the event of a failure of the sweeper, the dump can absorb up to 250 bunches without boiling the dump water.

The integrity of the dump window, the processing of the radiolytically evolved hydrogen and oxygen, and containment of the activated water are important issues for the full power dumps. The dump service caverns include three loop pump driven 2300 gallon per minute heat exchanger systems, devices to remotely exchange dump windows as periodic maintenance, catalytic H_2-O_2 recombiners, mixed bed ion exchange columns for filtering of ^{7}Be, and sufficient storage to house the volume of tritiated water during maintenance operations.

In addition to the main dumps, the BDS contains 16 stoppers, of which 14 are equipped with burn-through monitors, and the extraction lines have 6 fixed aperture high power devices composed of 10 mm aluminum balls immersed in water. The beam delivery system contains 32 variable aperture collimators and 32 fixed aperture collimators. The devices with the smallest apertures are the 12 adjustable spoilers in the collimation system. To limit their impedance to acceptable levels, these 0.6-1.0 X_0 Ti spoilers have longitudinal Be tapers.

TABLE 2.7-2
BDS components, total counts.

Magnets		**Instrumentation**		**Dumps & Collimators**	
Warm dipoles	190	BPMs C-band	262	Full power dumps	4
Warm quads	204	BPMs L-band	42	Insertable dumps	2
Warm sextupoles	10	BPMs S-band	14	Adjustable collim.	32
Warm octupoles	4	BPMs stripline/button	120	Fixed apert. collim.	32
SC quads	32	Laser wire	8	Stoppers	14
SC sextupoles	12	SR transv. profile imager	10		
SC octupoles	14	OTR screens	2	**Vacuum**	
Muon spoilers	2	Crab & deflection cavities	4	Pumps	3150
Anti-solenoid	4	Loss monit. (ion chamb., PMT)	110	Gauges	28
Warm correctors	64	Current monitors	10	Gate valves	30
SC correctors	36	Pick-up phase monitors	2	T-connections	10
Kickers/septa	64	Polarimeter lasers	3	Switches	30

2.7.4.5 BDS Magnets

The BDS has a wide variety of different magnet requirements, and the most distinct magnet styles (67) of any ILC area, even though there are only 636 magnets in total. Of these, 86 are superconducting magnets clustered into 4 cryostats close to the IP, as described in section 2.7.3.4, and the tail-folding octupoles described below. There are 64 pulsed magnets: 5 styles of abort kickers, sweepers and septa. These are used to extract the beams to a fast extraction/tuning dump and to sweep the extracted beam in a 3 cm circle on a dump window.

The remaining 474 magnets are conventional room temperature magnets, mostly with water-cooled hollow copper conductor coils and low carbon steel cores. The bend magnets in the final focus have fields of less than 0.5 kG to minimize synchrotron radiation that would cause beam dilution; they use solid wire coils. The quadrupoles and sextupoles have straightforward designs adequate for up to 500 GeV beam. The extraction line magnets have large apertures, e.g. over 90 mm and up to 272 mm, to accommodate the disrupted beam and the photons emerging from the IP. These magnets must fit in alongside the incoming beamline.

The main technical issue with the BDS magnets is their positional stability. All the incoming beamline quadrupoles and sextupoles sit on 5 degree of freedom magnet movers with a 50 nm smallest step size. BPMs inserted in the magnet bores provide data on the relative position of each magnet with respect to the beam so that it can be moved if necessary. The absolute field strength of the BDS magnets has a tight tolerance, requiring power supplies with stability of a few tens of ppm. Magnet temperature changes lead to strength and position variations so the ambient temperature in the tunnel must be controlled to within about 0.5°C and the cooling water to within 0.1°C.

2.7.4.5.1 BDS Magnets: Tail Folding Octupoles The tail folding octupoles are the only superconducting magnets in the BDS (other than the FD and extraction quadrupoles) and have the smallest, 14 mm ID, clear working aperture in order to reach the highest practical operating gradient. The magnets are energized via NbTi conductor cooled to 4.5 K. With such a small aperture, the beam pipe must have high conductivity to minimize the impact of wakefields. This can be achieved with a cold aluminum beam pipe at 4.5 K or a cold stainless steel beam pipe with a high conductivity coating. Because these magnets are isolated in the BDS, being far from either the IP or the end of the linac, cryocoolers are used to provide standalone cooling.

2.7.4.6 Vacuum system

While the aperture of the BDS vacuum chamber is defined by the sizes of the beam, its halo and other constraints, the design of the chambers and vacuum level are governed mainly by two effects: resistive and geometric wakes and the need to preserve the beam emittance; beam-gas scattering and minimization of detector background.

2.7.4.6.1 Wakes in vacuum system The resistive wall (RW) wakefield of the BDS vacuum system and the geometric wakefield of the transitions in the beam pipe may cause emittance growth due to incoming (transverse) jitter or drift, or due to beam pipe misalignment. In order to limit these effects to tolerable levels, the BDS vacuum chamber must be coated with copper, the vacuum chambers must be aligned with an RMS accuracy of ~ 100 μm [71], and incoming beam jitter must be limited to $0.5\sigma_y$ train-to-train and $0.25\sigma_y$ within a train, to limit the emittance growth to 1-2%.

2.7.4.6.2 Beam-gas scattering The specification for the pressure in the BDS beam pipe is driven by detector background tolerance to beam-gas scattering. Studies have shown that electrons which are scattered within 200 m of the IP can strike the beam pipe within the detector and produce intolerable backgrounds, while electrons which scatter in the region from 200 to 800 m from the IP are much more likely to hit the protection collimator upstream

of the final doublet and produce far less severe detector backgrounds [72]. Based on these studies, the vacuum in the BDS is specified to be 1 nTorr within 200 m of the IP, 10 nTorr from 200 m to 800 m from the IP, and 50 nTorr more than 800 m from the IP.

In the extraction lines the pressure is determined by beam-gas scattering backgrounds in the Compton Polarimeter [68] located about 200 m from the IP. Here the signal rates are large enough that 50 nTorr would contribute a negligible background in the detectors.

2.7.4.6.3 Vacuum system design The BDS vacuum is a standard UHV system. The main beampipes are stainless steel, copper coated to reduce the impedance, with the *option* of an aluminum alloy chamber. In locations where there is high synchrotron radiation (SR) power ($\geq$10 kW/m) (e.g. in the chicanes or septa regions), the beampipe is copper with a water-cooled mask to intercept the photons. The beampipes are cleaned and baked before installation. There is no *in situ* baking required except possibly for the long drift before the IP.

The required maximum pressure of 50 nTorr (N_2/CO equivalent) can be achieved by standard ion pumps located at appropriate intervals. The beampipe near the IP must have pressure below 1 nTorr for background suppression, and may be baked *in situ* or NEG-coated.

2.7.4.7 IR arrangements for two detectors

There are two detectors in a common IR hall which alternately occupy the single IR, in a so-called "push-pull" configuration. The detector hall is 120 m (long) $\times$ 25 m (wide) $\times$ 38 m (high). The layout of the hall is compatible with surface assembly of the detectors. The previous layout with two 14 mrad IRs is kept as an *alternative configuration*, and is about 50% more expensive than the single IR.

To facilitate the exchange of detectors, there is a breakpoint in the beam line near the edge of the detector, between the two final doublet cryostat halves as shown in Figure 2.7-4 and Figure 2.7-9. A necessary condition for efficient push-pull operation is to avoid disconnecting any of the systems for the detectors during the exchange. One possible solution is to equip each detector with an adjacent services platform which moves together with the detector. The platforms would house the cryogenic systems, high current power supplies for solenoids and FD, and detector electronics. All the connections between the platform and detector would be fixed and not disconnected during the exchange. The movable detector service platform would have flexible connections to fixed services (including high voltage AC, room temperature high pressure He supply and return, data I/O, etc.), that do not need to be disconnected during the exchange.

The FD alignment and support system is designed to be compatible with rapid exchange, in particular, an interferometer network between the two parts of the FD and the walls may be needed. The push-pull arrangement of two detectors implies specific requirements for the radiation safety design of the detector and of the collider hall shielding. Since the off-beam axis detector needs to be accessible during beam operation, the detectors either need to be self shielded or there must be a shielding wall between them.

Several technical solutions for moving the detectors are under consideration, including rails, Hilman Rollers or air pads. A guiding mechanism is needed to determine the path for the detector motion and its accurate positioning. The motion of a heavy detector (up to 14 kton) in the collider hall produces deformations, which are estimated to be less than a millimeter [73]. The detector support system must ensure that those deformations, as well

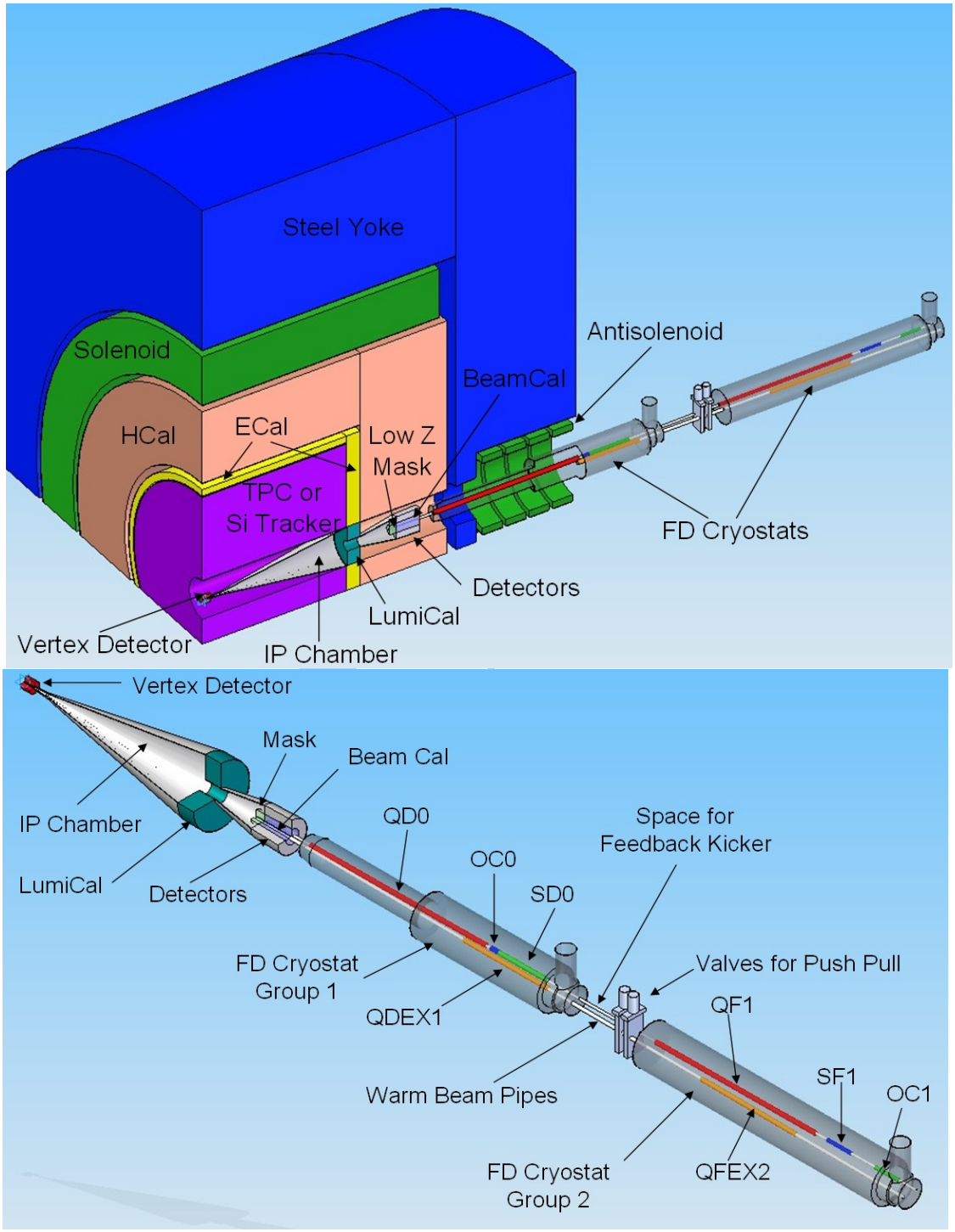

FIGURE 2.7-9. Generic detector and IR arrangements, showing the location of beamline elements near the IR and their integration with the detector.

as possible deformations during lifting, do not affect its internal alignment. To minimize deformations, the detector may require a support platform. The 5 cm thick steel plates covering most of the experimental hall area also facilitate stability and allow the use of air-pads.

2.7.4.8 Diagnostic and Correction devices

Each quadrupole, sextupole, and octupole magnet in the incoming BDS beamlines is placed on an x/y/roll/pitch/yaw mover, and has an associated BPM. There are also several tens of correctors in the incoming beamlines for 5 Hz feedback, and in the extraction lines, where there are no movers. The BPMs in the incoming beamline are RF-cavities, either S, C or L-band, depending on the beamline aperture. Long chains of bends or kickers have sparsely placed BPMs. BPMs in the extraction lines are button or strip-line design.

Additional instrumentation in the BDS includes a deflecting cavity to measure Y-T correlation, ion chamber and PMT loss monitors, X-synchrotron light transverse profile monitors, OTR monitors, current monitors, pickup phase monitors, etc.

2.8 ACCELERATOR PHYSICS

This section still under review. Draft to be released by April 1, 2007.

2.9 AVAILABILITY, COMMISSIONING AND OPERATIONS

This section still under review. Draft to be released by April 1, 2007.

CHAPTER 3

Technical Systems

3.1 MAGNET SYSTEMS

3.1.1 Overview

The ILC has $\sim$ 80 km of beamlines which require magnets for focusing and steering the beams. There are over 13000 individual magnets, of which approximately 18% are superconducting and the rest "conventional" warm iron-dominated magnets with copper coils. About 40% are low-current corrector magnets. Superconducting technology is primarily used for the magnets located in the RF cryomodules, but it is also required for the spin rotation solenoids, damping ring wigglers, positron source undulator and beam delivery octupoles, sextupoles and final doublet quadrupoles.

3.1.2 Technical Description

The scope of the Magnet Technical System includes the magnets and their power systems, as well as the magnet support stands and positioning devices needed for precise magnet alignment in the beamlines. Power systems include the power supplies, cabling to the magnets, sensors and systems for local control, monitoring, and magnet protection. Pulsed kicker and septum magnets used for beam injection, extraction, and/or protection are particularly challenging. Almost all of the room temperature magnets have easily achievable requirements. The major technical issues, challenges and special purpose magnet systems are presented below. Challenging technical issues unique to particular Areas (especially BDS and DR) are discussed in those sections.

The magnet design process starts with the Area System leaders who specify a standard set of requirements based upon the lattice designs, machine layout, and envisioned operating scenarios. Conceptual magnet designs follow primarily from the specified integrated strength, field quality, clear bore aperture, and slot length constraints. Given the conceptual magnet design, a power supply (PS) design is developed based on the magnet-specific current, voltage and stability requirements, and the need to power magnets individually or in series.

3.1.3 Technical Issues and Challenges

3.1.3.1 High Availability and Low Cost

A major criterion for ILC magnet design is to achieve very high availability in spite of the very large number of magnets. The "availability" goal of the ILC is 75% (or better) and the magnets have been budgeted to incur no more than 0.75% down time. The availability "A" of a component is given as A = MTBF/(MTBF+MTTR), where MTBF is Mean Time Between Failures, and MTTR is Mean Time To Repair a magnet, turn it back on and restore the beam. Detailed studies of magnet failures at three high energy physics labs indicate that most failures are with conventional water-cooled magnets, which had an MTBF ranging from about 0.5 million to 12 million hours based on tens of millions of integrated magnet-hours. The ILC has 6873 such magnets. With an MTTR of 16 hours, the MTBF of each one must be longer than 18 million hours in order to achieve the desired availability.

This reliability level should be achievable, without incurring a significant increase in cost, by applying the assembled magnet design, production and operation experience at existing HEP accelerators. The approach is to apply best modern magnet engineering practices, ensure adequate quality control of materials and procedures during fabrication, and use established guidelines for operating within reasonable environmental limits (such as ambient temperature and allowed temperature rise, maintaining proper water flow conditions, and keeping electronic components out of radiation areas where possible). Power system electronic components typically have much lower MTBF values of around 100,000 hours. Here, the solution is to build in redundancy for crucial elements, and use "smart" electronics that can detect failure and rapidly switch to redundant units. Replacement of failed units can then be scheduled to occur during beam downtimes. Comprehensive failure mode and effects analyses (FMEA) are thus viewed as an essential part of the magnet system engineering effort.

3.1.3.2 Field Quality and Alignment

The field quality requirements in most normal-conducting ILC magnets are similar to those at other accelerators currently in operation, and not particularly challenging. Higher order harmonics must be on the order of a "few units" (1 unit = 10^{-4}) of the main field strength, and are most stringent in the Damping Rings where beam circulates for many turns. For corrector magnets, a few tens of units is characteristic. In warm iron-dominated electromagnets, these levels are achieved through careful control of pole shapes and their positioning. Similarly, control of coil position is important for superconducting magnet field quality, and is achievable with proper mechanical design and tooling. Large room temperature magnets have a split yoke design to reduce repair time in the tunnel; experience shows that field quality can be maintained with proper design and care in re-assembly.

Alignment and mechanical stability requirements in many areas are very challenging. In the BDS, beam positions must be maintained at sub-micron levels to collide the beams, so precision 5-axis magnet positioning mounts, or "movers," are needed for continuous adjustment of all the quads and sextupoles in the final focus region – the development of movers and control programs is an area of active R&D. For the regions where movers are not required, room temperature and cryogenic magnet stands use a robust and precisely adjustable design. In some areas, pedestals are required to offset the precision stands from the tunnel floor. Alignment tolerances on the relative positions of Beam Position Monitors (BPMs) to

quadrupoles differ by area ($\sim$ 10 μm in BDS, $\sim$ 100 μm in ML). In the BDS this results in stringent temperature control requirements locally, where geometry-sensitive cavity style BPMs are affixed to the thermally active magnets.

3.1.3.3 Superconducting Magnets

There are 2318 superconducting (SC) magnets in a variety of applications throughout the ILC, but fewer than 10% of them require high integrated field strength in limited space and about 60% are correcting coils wound in the same physical space as the main coils. Most of the SC magnets are not very strong and are located in the RF cryomodules. A package containing a focusing quadrupole (quad), steering dipole correctors and a Beam Position Monitor is located at the center of every third main linac cryomodule. This location makes it challenging to maintain the quad positions during thermal cycles and to measure and relate the quad positions to external survey fiducials and to the BPMs used to keep the beam centered in the quads (at the 100 micron level, over a distance of $\sim$ 6 meters). The resulting magnetic center in nested dipole and quad designs may also be affected by persistent current effects. Alternative designs and further research are needed to understand these issues and develop the magnet support and measurement techniques; there could be significant advantages to moving the magnets and BPMs from the RF cryomodule out to a separate cryostat.

The superconducting wigglers in the damping rings and the superconducting undulators in the positron source also require great mechanical precision; their particular challenges are described in their respective chapters. The most challenging superconducting magnets, those just before the interaction point, are described in the BDS chapter. They have strong gradient fields with many layers of correcting coils, and must fit into as small a radius possible to not interfere with the detector. In the ILC sources, there are superconducting solenoids for spin rotation and a few large aperture magnets that may be either conventional or superconducting, depending on detailed optimization of operating versus capital cost.

3.1.3.4 Power Systems Design

The non-pulsed ILC magnets operate with DC currents, with set points that may be adjusted periodically but only slowly ($\sim$ 5A/s or less). Most magnets are individually powered to allow independent control. Power supply stability requirements are assumed to be comparable to performance of existing commercial units. The design of a power system, whether for an individual or a string of magnets, requires a conceptual magnet design which determines the required operating current, defines the coil resistance and inductance and cooling requirements (air or water). The magnet position, with respect to power supplies located in alcoves, defines the cable length; cables are sized for the maximum operating current using two sizes above the NEC rated minimum, to reduce voltage drop and heat generation. The required maximum power supply voltage is then determined by the cable and coil resistive drop at maximum current, plus the inductive drop at the maximum ramp rate. The supply is sized with a 10% margin on the power rating, to accommodate uncertainties in magnet strength, inductance, cable lengths, etc. The summed power ratings set requirements for AC power, air and water conditioning in each area.

Power systems are classified by their size and type, and standard models were developed for each of the various system categories: they are distinguished by “normal” versus “superconducting”, “individually powered” versus “series connected”, “rack mounted” versus “free

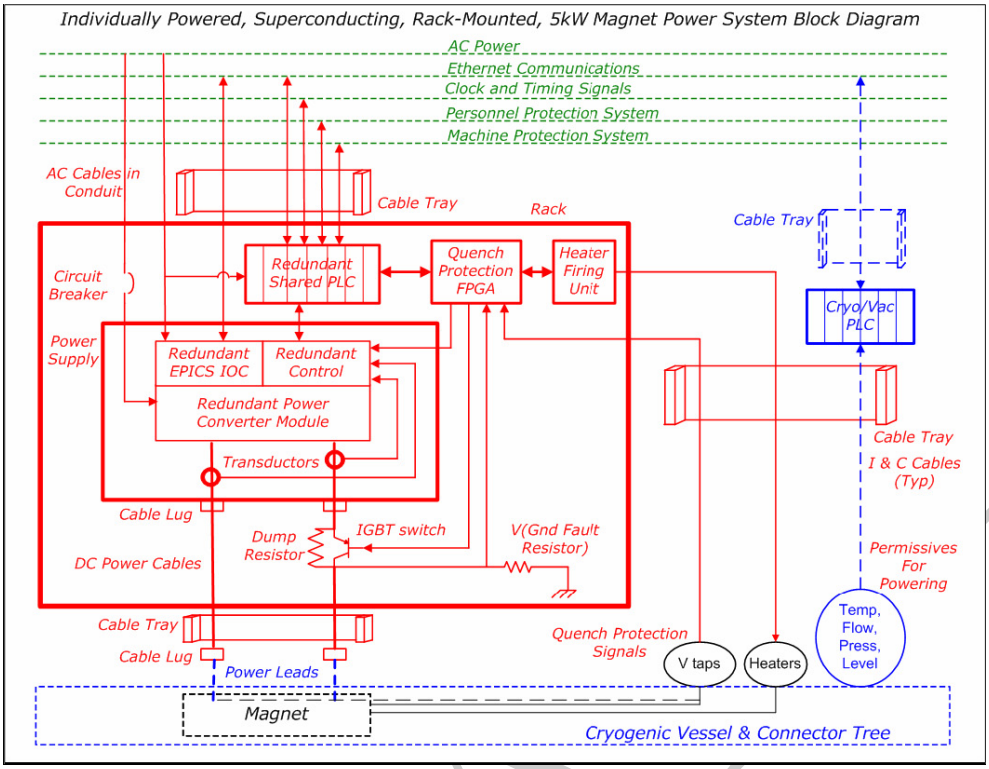

FIGURE 3.1-1. An example DC power system style: items in red are specific to the power system, magnet elements are in black; relevant interfaces are shown, where blue and green lines are responsibility of other groups (global controls, cryogenics, vacuum, facilities, etc.)

standing". These styles have certain elements in common, but may differ in detail (water versus air cooling, for example); Figure 3.1-1 shows one example which contains all of the power system elements, and illustrates interconnections between components and systems. Each power system provides local control and magnet protection (via PLCs and FPGAs), and has the capability of diagnostic data capture. The design incorporates redundant current transductors, controllers, and Ethernet IOCs, which are utilized for communication with machine control, protection, and other technical systems (e.g., to obtain cryogenic or LCW process variables for operating permissive). Smaller rack-mount supplies can accommodate a redundant supply within the rack, for automatic switch-over in case of a failure. The conceptual design for the superconducting magnets is based on the generic model shown, although the protection elements may be simplified after detailed magnet design.

3.1.3.5 Kicker, Septum, and Pulsed Magnets

A kicker is a device that makes fast time-dependent changes in the beam path. A septum magnet has regions with very different magnetic field with a material septum between them. A kicker diverts the beam from one side of the septum to the other, and the much higher field of the septum diverts the beam by a much larger angle, typically around some downstream obstacle like a quadrupole magnet. A pulsed magnet changes its field as part of normal

operation, but less rapidly than a kicker. The high power beam dumps have pulsed magnets upstream to sweep the beam across the dump to avoid localized damage. Fast actuators in the beam feedback systems in the damping rings and at the IP, which are also sometimes called "kickers," are described in the area chapters.

There are several classes of kickers in the ILC. The damping ring injection and extraction kickers are pulsed every few hundred ns for single bunches during each millisecond linac pulse, and need rise and fall times of a few ns. A damping ring abort kicker is only fired when an abnormal beam condition is detected, to divert the stored beam to a dump, and avoid damage to machine components. The rise time must be less than the ion-clearing or abort gap in the ring filling pattern, with a pulse width of a full ring turn (≈ 22 μs).

There are other abort kickers at several locations outside the damping rings, with rise times of less than the time between bunches (≈ 100 ns). When used as abort kickers, the pulse rate is nearly zero, and the pulse width need only be long enough for the bunches that cannot be stopped upstream. An abort kicker can also be used to limit the beam power downstream, by firing it after a fraction of the beam bunches in the train have passed. In this application, the kicker may be fired on every linac pulse, for the full linac pulse duration.

The ILC kickers are all stripline structures inside the vacuum chamber, driven by pulsed power supplies. The injection and extraction kickers have short strips and extremely fast pulsers to achieve fast rise and fall times. The required total kicker strength (kilovolt-meters) is set essentially by the beam size and energy, with the result that a large number of stripline and pulser units are needed for each installation. The damping ring abort kickers use more conventional thyratron or FET pulsers and longer strips since the rise time can be longer, the pulse length is moderate, and the rate is low. The other abort kickers have relaxed rise time requirements, but the pulse may need to be a millisecond long at full linac rate, and higher beam energies require more kicker field energy. The pulser power required scales inversely with the cube of the available length, and can be quite high. The beam delivery system abort kicker installations each require several pulsers of the scale of main linac modulators.

The baseline design has a thin and a thick pulsed eddy-current septum magnet for each damping ring kicker. This design is inspired by the Argonne APS septa, but R&D is required to make a millisecond flat top to the required tolerance. An alternative optics design is under consideration for injection and extraction that allows a DC current-sheet septum of moderate current density to be used. An abort septum must be DC, and could be a current sheet septum, or an iron magnet with a beam-hole in its pole region (Lambertson septum). The damping ring abort region optics, and thus the type and parameters of its septum, are discussed in the Damping Ring chapter. The RTML and beam delivery abort septa are DC current sheets. The undulator protection abort septa are dogleg bend magnets modified to be Lambertson septa. All of the abort dumps downstream of the damping ring require sweeper magnets.

3.1.3.6 Fabrication, Test, and Storage

The program of fabrication and testing of ILC magnets follows a 7 year schedule, with one year of preparation, five years of production and testing, and (overlapping) four years of installation. Magnet fabrication utilizes industrial suppliers world-wide; tooling developed for ILC magnet fabrication belongs to ILC for future use. A large fraction of solid-wire corrector magnets are tested by manufacturers, and all non-corrector magnets are tested and magnetically measured at the ILC test facility. Superconducting test stands share cryogenic

resources with nearby SRF test facilities and have both production and special measurement areas and test systems. The conventional magnet measurement area is large, with multiple stands for efficient and high throughput, with space for temporary magnet storage. Alignment and survey capabilities are needed for all magnet styles. In the long term, some space could be converted for storage of tooling and spare magnets (or coils and parts), and part of the facility could be devoted to repair and new magnet fabrication. Also an area remains dedicated to making tests and measurements, and conducting R&D for later machine improvements. Such a facility is necessary to ensure the initial high quality of ILC magnets.

3.1.4 Cost Estimation

The cost estimate is based on the conceptual designs for magnets, power systems, stands and movers described above, with additional assumptions about estimated costs of material and labor. Given time and resource limitations, detailed conceptual designs were developed for only a small number of the magnet styles. The majority of estimates are "engineering estimates" based on existing designs with similar requirements. Standardized labor rates were determined from laboratory and industrial sources[1]. In order to determine the material costs, the weights of magnet and cable materials, primarily copper and iron, have been estimated and summed, and current world commodity prices obtained. Similarly, prices have been obtained for commercially available electronic components such as power supplies, FPGAs and PLCs, controllers and Ethernet interfaces.

In one instance, a design and a complete set of drawings was developed for a e^+ Source transfer line quadrupole (a large quantity item) and a request for quote sent to a number of magnet vendors. The cost estimates obtained were in reasonable agreement with an internal estimate: the average agreed within a few percent of the internal estimate, with a spread of $\sim 25\%$. For a few magnet systems, more detailed cost estimates were provided based on either existing designs (Cornell wigglers) or R&D prototypes already in progress (Daresbury/Rutherford undulators); in a similar fashion, Brookhaven provided detailed cost estimates for the superconducting insertion magnets at the IR based on experience with similar magnet designs.

Estimates of EDIA labor costs were based upon reviews of recent large accelerator magnet and power supply projects at SLAC and Fermilab, where the materials, fabrication and EDIA labor fractions are well known. The fractional distribution of EDIA among several types of laborers, which were costed at the standardized labor rates, was assigned on the basis of project management experience.

3.1.5 Component Counts

The number of conventional and superconducting magnets and magnet styles in each of the ILC Areas is shown in Table 3.1-1. There are compelling reasons to reduce the number of magnet styles - to reduce cost and increase maintainability and reliability - and this process is an iterative one, that has not yet been fully optimized.

[1]It should be noted that rates for different world regions have not been incorporated at this time. It should also be recognized that labor rates and production hours are not necessarily uncorrelated: the lowest labor rates are quite often in regions with less automation and infrastructure resulting in longer task times.

Magnet Type	Grand Totals		Sources			Damping Rings					2 RTMLs		2 Linacs		2 BDS	
				e-	e+		e- DR	e+ DR	e- Inj/Ext	e+ Inj/Ext						
	Style	Qty	Style	Qty	Qty	Style	Qty	Qty	Qty	Qty	Style	Qty	Style	Qty	Style	Qty
Dipole	22	1356	6	25	157	2	126	126	8	8	6	716	0	0	8	190
NC Quad	37	4165	13	76	871	4	747	747	76	76	5	1368	0	0	15	204
SC Quad	16	715	3	16	51	0	0	0	0	0	0	56	3	560	10	32
NC Sextupole	7	1050	2	0	32	2	504	504	0	0	0	0	0	0	3	10
SC Sextupole	4	12	0	0	0	0	0	0	0	0	0	0	0	0	4	12
NC Solenoid	3	50	3	12	38	0	0	0	0	0	0	0	0	0	0	0
SC Solenoid	4	16	1	2	2	0	0	0	0	0	1	8	0	0	2	4
NC Corrector	9	4016	1	0	840	3	540	540	0	0	4	2032	0	0	1	64
SC Corrector	14	1374	0	32	102	0	0	0	0	0	0	84	2	1120	12	36
Kickers/Septa	11	227	0	0	19	5	46	46	0	0	1	52	0	0	5	64
SC Wiggler	1	160	0	0	0	1	80	80	0	0	0	0	0	0	0	0
NC Octupole/Muon Spoiler	3	8	0	0	0	0	0	0	0	0	0	0	0	0	3	8
SC Octupole	3	14	0	0	0	0	0	0	0	0	0	0	0	0	3	14
SC Undulator	1	27	1	0	27	0	0	0	0	0	0	0	0	0	0	0
Overall Totals	135	13190	30	163	2139	17	2043	2043	84	84	17	4316	5	1680	66	638
Totals w/o Correctors	112	7800														
Total NC	92	10872														
Total SC	43	2318														

TABLE 3.1-1
Numbers of Conventional and Superconducting Magnets and Magnet Styles in ILC Areas

3.2 VACUUM SYSTEMS

3.2.1 Overview

The ILC has over $\sim$ 80 km of beamlines which must be kept under vacuum to limit the beam-gas scattering and operate the RF cavities. Different areas of the machine present different challenges but fortunately, there is an experience base at existing accelerators for essentially all of the systems, to facilitate design and costing. The largest and most complex are the vacuum systems for the cryomodules containing superconducting cavities that accelerate the beam. There are $\sim$ 2000 cryomodules in the main linacs, electron and positron booster linacs and bunch compressors. There are also single cavity cryomodules in the damping rings and beam delivery systems. These cryogenic units require separate vacuum systems for the beam line, the insulating vacuum and the waveguides.

Other beamlines throughout the ILC pose particular challenges. The lifetime of the electron source photocathode requires a vacuum in the range of a pico-Torr. The superconducting undulator for the positron source is a warm bore chamber with a very small aperture. Chambers for bending magnets in the damping rings and elsewhere require antechambers and photon absorbers for the synchrotron radiation. The presence of electron cloud in the positron damping ring and ions in the electron damping ring can seriously impact performance and requires mitigation. Beam-gas scattering in the beam delivery must be limited to reduce backgrounds in the experimental detectors. The designs for each system and costing approach are discussed in more detail below.

3.2.2 Technical Issues

3.2.2.1 Linac Cryomodules

There are $\sim$ 20 km of cryomodules in the main linac and another $\sim$ 1.6 km of modules in the sources and bunch compressors. Each cryomodule has separate vacuum systems for the accelerating structures, the insulating vacuum and the transmission waveguides. The structure vacuum vessel holds the niobium cavities and is at 2K cryogenic temperature. This system must produce very low quantities of particulates as these can contaminate the cavities causing field emission and lowering the available gradient. The system must also be able to produce ultra-high vacuum at room temperature to eliminate the risk of residual gases condensing on the niobium walls during cooldown. The beamline vacuum is segmented into strings of 142 m. Each string has an insulating vacuum break and a port for valves and ion pumps. Every other string has additional valves, pumps, leak detection, and vacuum diagnostics. Each group of 4 strings (571 m) has cold vacuum isolation valves. A vacuum/diagnostics station is installed between every 16 strings (2.288 km). These stations have slow start turbo-molecular pumps, leak detection, clean venting systems, and warm isolation valves.

The insulating vacuum system must maintain a typical pressure of $\sim$ 0.1 mTorr, a regime where high voltage breakdown is a serious issue. It is complicated by the pump cabling from the main system which must pass through the insulating vacuum. The system is segmented into 142 m strings consistent with the beamline vacuum. Each string has valves, a turbo-molecular pump, and bypass valves. Every other string additionally has a leak detector and a large screw pump.

Much of the transmission waveguide vacuum is at room temperature, but it must transition to helium temperatures at the couplers. In addition, the rf power being transmitted is

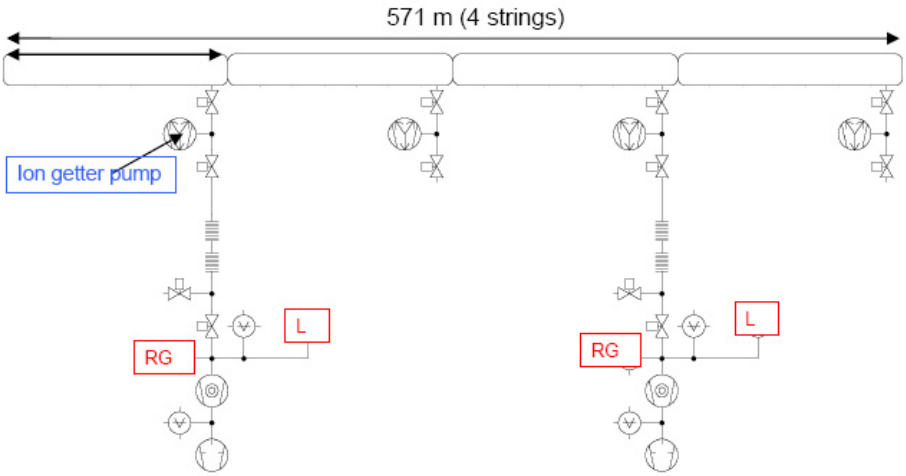

FIGURE 3.2-1. Beamline vacuum system – 2 turbo-molecular pumps (TMP) with high sensitivity leak detector (LD) and residual gas analyzer (RGA), safety, clean venting system, slow start pumping etc.

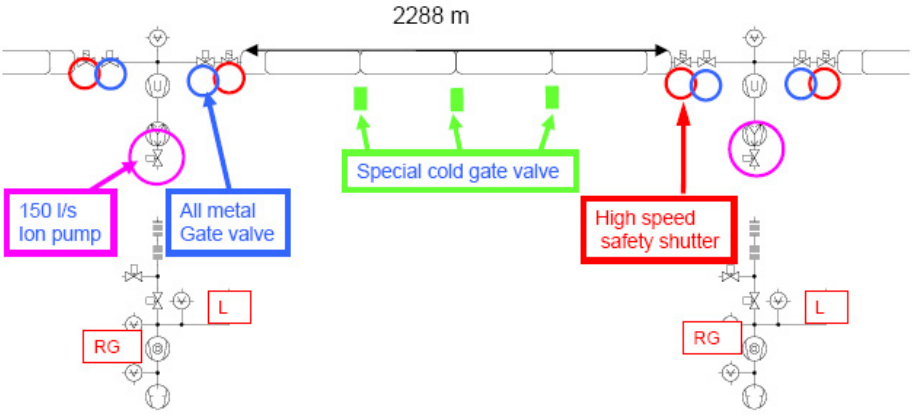

FIGURE 3.2-2. Beamline vacuum system gates and valves.

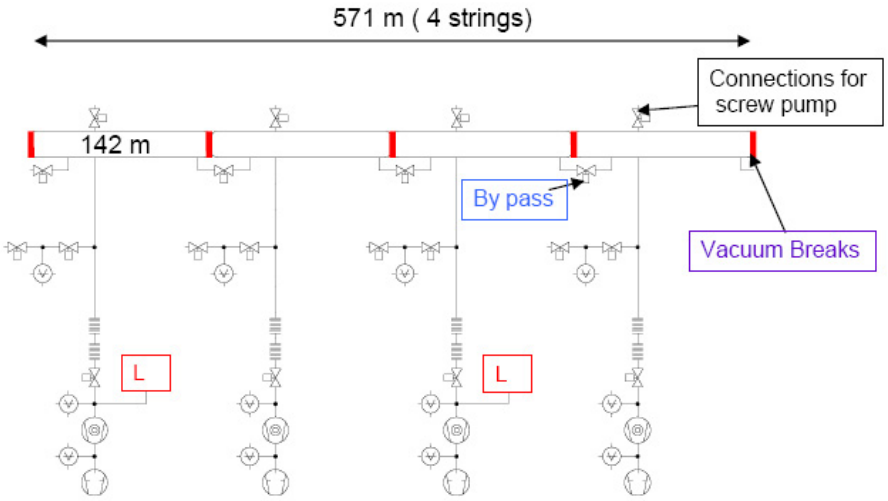

FIGURE 3.2-3. Insulating vacuum system – 4 TMP pumping units: 2 with LD (leak detector) + 2 large screw pump for fore pumping.

very high, so multipactoring and arcing must be considered in the design. There is a valve for each coupler. Every cryomodule has an ion pump and titanium sublimation pump, and every 3 cryomodules have a turbomolecular pump, a scroll fore pump and a leak detector.

While the cryomodule vacuum system is complex, costs can be estimated from work done for the TESLA TDR proposal and from recent projects such as SNS. Standard parts, were estimated from vendor quotations and from recent large quantity procurements.

3.2.2.2 Damping Ring and Beam Delivery Cryomodules

The damping ring accelerating rf is single 650 MHz cavities in individual cryomodules. The beam delivery also uses superconducting crab cavities with individual cryomodules. (See Sections 2.4 and 2.7.4.1 for a description of damping ring cryomodules and crab cavity cryomodules.)

3.2.2.3 Polarized Electron Source

The electron source is a DC gun with a laser illuminated photocathode similar to the electron guns at SLAC and Jefferson Lab. To maintain photocathode lifetime, the pressure must be $< 3 \times 10^{-11}$ torr. This is achieved by incorporating large ion pumps and non-evaporable getter (NEG) pumps.

3.2.2.4 Positron Source

The positron source undulator and target vacuum systems are particularly challenging. Electrons are transported through a superconducting undulator to produce γ-rays. The superconducting undulator is a cold bore chamber with a small aperture. The γ-rays are then

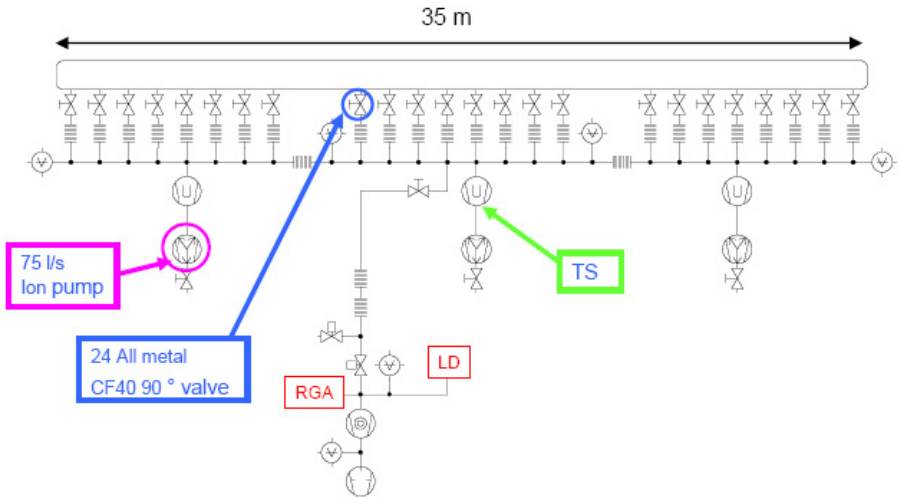

FIGURE 3.2-4. Waveguide and coupler vacuum system.

Beamline	Max Pressure (nTorr)	Aperture Diameter (cm)	Length (m)	Number of Beamlines	Comments
Gun	10^{-3}	4	0.2	2	Integrated into Gun Design
Gun combining beam line	10^{-3} to 0.1	3	1	2	Differential pumping needed to protect gun vacuum
Transport through Bunching System	1	4	~ 15	1	
NC beam lines	10	4	~ 17.5	1	
SC RF	< 1	7	~ 273	1	8 strings (of 3) cryomodules, adopt vacuum specification for main linac
Dump beam line	10	4	12	1	
ELTR	10	4	~ 140	1	Linac to Ring beam line

TABLE 3.2-1
Transport lines for the ILC Electron Source System. Vacuum specifications, beam aperture inner diameters, and lengths are noted. Except in the case of the accelerator sections, the vacuum chamber material is stainless steel.

Beamline	Max Pressure (nTorr)	Aperture (cm)	Length (m)	Comments
Chicane 1	50	2	300	halo generation
Undulator	100	0.6	290	fast ion, Daresbury
Chicane 2	50	20	300	halo generation
Photon line	1000	4.5	500	
Positron transport	100	15	5,100	
NC RF	20	6 and 6-4.6	115	1.27 m and 4.3 m sections
SC RF	< 1	7	280	12.6 m sections
Linac-to-Ring	50	2	80	
Other	100	6	300	

TABLE 3.2-2
Transport lines for the ILC Positron System. The reasoning behind the specification is noted and is subject to discussion. Vacuum specifications and aperture inner diameters are noted. Except in the case of the accelerator sections, the vacuum chamber material is stainless steel.

directed onto a target to produce positrons. The positron target has a very large power load deposted into the target and nearby structures.

3.2.2.5 Damping Ring Issues

The most challenging issues for the damping ring vacuum systems are suppression of the electron cloud in the positron damping ring and ions in the electron damping ring. A variety of techniques are used, including low residual pressure, low SEY coatings, and possibly grooved chambers or clearing electrodes. Lifetime considerations require pressures of less than 1 nTorr which is achieved with neg coated chambers. The bend magnet vacuum pipe requires an antechamber with a photon absorber to collect synchrotron radiation emitted. (For details see 2.4.)

The wiggler straight vacuum system for the ILC damping rings consists of separate chambers for the wiggler and quadrupole sections. A schematic cross-section of the wiggler chamber is shown Figure 3.2-5. The chamber is a machined and welded aluminum unit designed as a warm bore insert which is mechanically decoupled from the wiggler and cryogenic system. A NEG pumping system [99] and photon absorber are incorporated in ante chambers. Integral cooling is incorporated to minimize distortion of the chamber and thermal load on the wiggler cryostat during NEG regeneration. A NEG surface coating will be used on the main chamber bore to minimize secondary electron yield [100]. Clearing electrodes will also be incorporated to reduce the electron cloud.

The quadrupole chamber is welded aluminum, also incorporating NEG coating for secondary electron yield reduction. Bellows, a BPM assembly and an ion pump are incorporated. The quadrupole chamber is completely shadowed by the wiggler chamber photon absorbers and does not absorb any of the photon power from upstream wigglers.

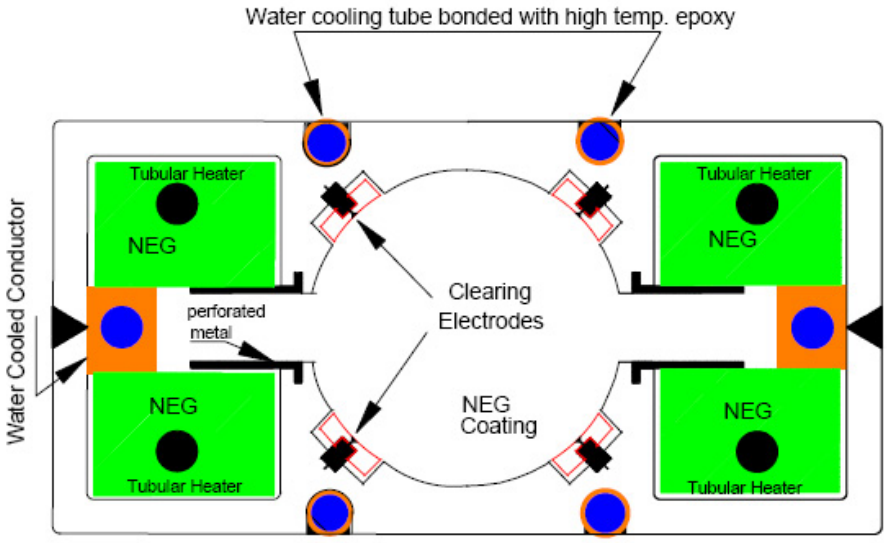

FIGURE 3.2-5. ILC damping ring wiggler chamber.

3.2.2.6 Ring to Main LINAC

Each of the two Ring to Main Linac transport sections contains a room temperature transport line of $\sim$ 15 km length, superconducting RF sections of $\sim$ 0.5 km length, and additional room temperature beamlines of $\sim$ 1.0 km length. The vacuum level in the long room temperature transport line is set by requirements on the beam-ion interaction in the electron system to $\sim$ 20 nTorr. The vacuum level in the remaining room temperature beamlines is set by beam scattering requirements to 100 nTorr, at which level about 1×10^{-6} of the beam population is scattered out of the acceptance. The superconducting RF sections have vacuum requirements and system designs which are identical to those of the main linac, i.e., beamline and isolation vacuum systems. Although the RTML contains room temperature bending sections they are not expected to need photon stops or other photon power absorbers because the average current is low and the bending radii in the RTML are kept large to limit emittance growth from incoherent synchrotron radiation effects.

3.2.2.7 Beam Delivery System

The beam delivery system transport requires special attention to limit backgrounds in the experimental detectors. In order to reduce the residual beam-gas scattering to acceptable levels, the line pressure near the interaction region needs to be $<$ 1 nTorr. The design is complicated by the requirement for small chamber diameters. The small chamber diameter and the low pressure require close spacing of the ion pumps, bake-outs and the use of neg coated chambers.

3.2.3 Cost Estimation

The main parts of the vacuum systems were obtained from quotations from vendors and from recent large quantity procurements. "Consumables," such as flanges, gaskets, bolts and nuts, cables, etc, were either not yet included or were estimated for quantity discounts of catalog items.

3.3 MODULATORS

3.3.1 Overview

The accelerating gradient for the ILC main linacs is supplied by superconducting 1.3 GHz cavities powered by 560 10 MW RF stations, each with a modulator, klystron and RF distribution system. Another 86 similar stations are used in the e+ and e- Sources and RTML bunch compressors. The damping ring RF power is supplied by 650 MHz superconducting cavities powered by 1.2 MW peak power klystrons. These are fed from a DC supply and do not have pulsed modulators. There are also a few special purpose S-band RF stations for instrumentation and a 3.9 GHz RF station to power the crab cavities near the Interaction Point. This section describes only the 1.3 GHz modulators, Damping Ring HVPS system and associated components.

3.3.2 Technical Description

The 10 MW L-Band RF power stations for the ILC are installed in the support tunnel, spaced approximately 38 meters apart. The L-Band Modulator baseline design was developed for the TESLA Test Facility at DESY, and has been adopted for the European XFEL. Three FNAL units and 5 commercial units have brought online at DESY starting in 1993. The design has a series on-off solid state switch with partial capacitor discharge. The ILC unit varies from this design in two minor ways: (1) A new solid state redundant switch is employed to form the 1.7 msec output pulse, for better reliability; and (2) the input charger will operate from a voltage of 8 kV instead of 480 V to eliminate the AC input step-up transformer in the current design. The modulator specifications and requirements are summarized in Table 3.3-1.

The block schematic is shown in Figure 3.3-1. Photos of current prototypes are shown in Fig. 3.3-2. Operation is straightforward: The charger delivers a DC voltage to the storage capacitors of approximately 11 KV. The modulator main switch is then triggered and held closed for 1.7 msec. Capacitor current flows through the switch to the step-up transformer input. At the same time, an auxiliary droop compensation "Bouncer" circuit is fired to maintain the pulse top flat to within +/- 0.5% during the RF drive period. The slightly above 10 KV drive pulse (to compensate for Bouncer voltage) is delivered to the input of the pulse transformer in order to produce at least 115.7 kV 133.0 A to the klystron for rated 10 MW peak output.

The Damping Rings have 650 MHz CW stations using 1.2 MW peak power klystrons, 20 in total for 2 rings. Power is supplied from a DC supply of 2.0 MW delivering 50-75vkV at 17-10vA DC. The RF envelope is controlled by the low level RF control and timing to maintain stability and clearing gaps as needed. The station block diagram is shown in Figure 3.3-3.

3.3.3 Technical Issues

3.3.3.1 L-Band

There are no major technical issues with the L-Band modulator as long as the entire system has sufficient overhead (redundancy) to compensate for a failed station. To achieve an acceptable availability, the linac energy and beam current parameters must be chosen to provide some RF spare stations. Redundancy of internal components such as IGBT switches

	Typical	Maximum
Charger input voltage kV RMS	7.67	8
Charger average power input kW	147.9	161.7
Charger efficiency	0.93	0.93
Charger DC output voltage = Modulator kVin	10.8	11.3
Charger DC avg output current = Modulator Ain	13.26	13.26
Charger average power output @ 5 Hz kW	137.5	150.3
Modulator efficiency	0.94	0.94
Modulator pulse voltage output = Pulse Transformer kVin	10.16	10.18
Modulator pulse current output = Pulse Transformer Ain	1560	1680
Modulator average power output @ 5 Hz kW	129.3	141.3
Pulse transformer step-up ratio	12	12
Pulse transformer efficiency	0.97	0.97
Pulse transformer voltage out = Klystron kVpk	115.7	120
Pulse transformer current out = Klystron Apk	133.0	140
Pulse transformer average power output @ 5 Hz kW	125.4	137.1
High voltage pulse duration (70% to 70%) ms	1.631	1.7
High voltage rise and fall time (0 to 99%) ms	< 0.23	0.23
High voltage flat top (99% to 99%) ms	1.565	1.565
Pulse flatness during flat top %	$< \pm 0.5$	± 0.5
Pulse to pulse voltage fluctuation %	$< \pm 0.5$	± 0.5
Energy deposit in klystron from gun spark J	< 20	20
Pulse repetition rate, Hz	5	5
Klystron filament voltage V	9	11
Klystron filament current A	50	60

TABLE 3.3-1
Modulator Specifications & Requirements Assuming Klystron μP=3.38, Effy=65%

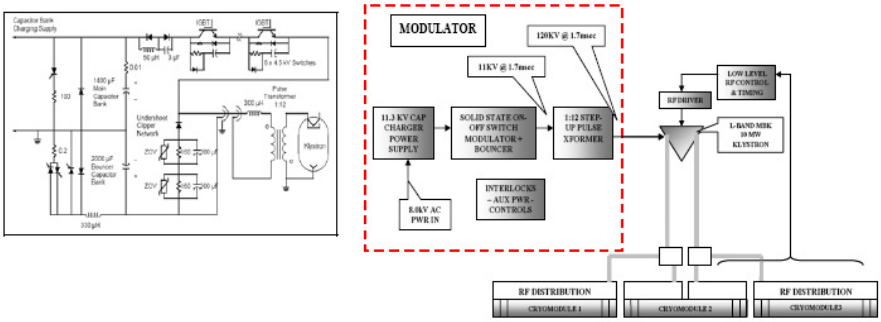

FIGURE 3.3-1. Modulator schematic and L-Band RF station block diagram (1 of 646).

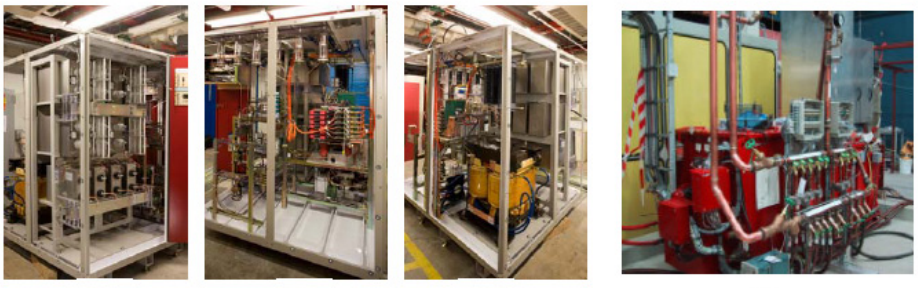

FIGURE 3.3-2. (a) Capacitor stack, (b) Dual IGBT switch, (c) Bouncer choke, (d) Pulse transformer.

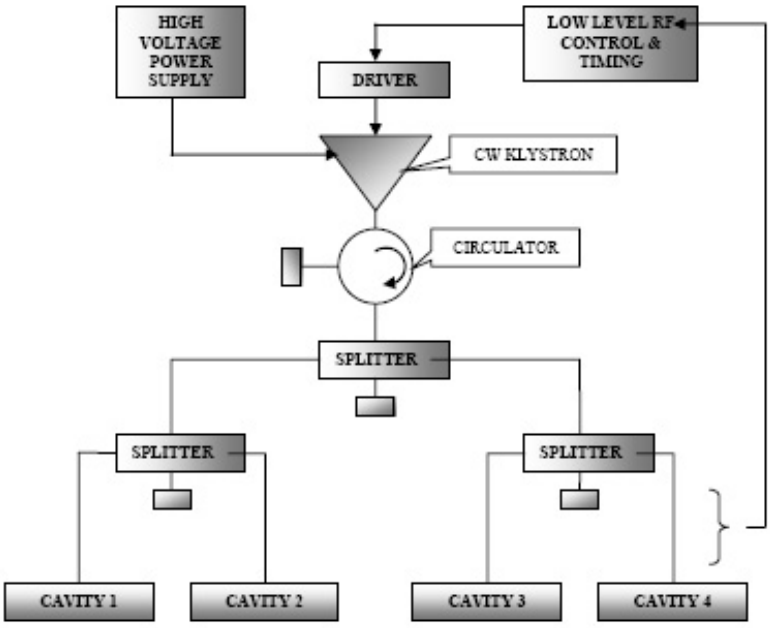

FIGURE 3.3-3. Damping Ring 1.2vMW RF station (1 of 20).

and sectioning of chargers for N+1 redundancy[2] is also important. Currently this is only partially implemented in the prototypes.

The present design which develops the drive pulse at low voltage and high current has larger losses than would be experienced with a higher voltage design. This is not a major technical issue, but a cost, size and weight issue. Installation and repair during operations will be more difficult with multi-ton components such as the transformer and main capacitor-switch multi-cabinet assembly.

An alternative modulator design is being investigated to address these issues, including the possibility of significant cost reduction. The design would reduce the overall footprint and eliminate the step-up transformer and other oil-filled components.

3.3.3.2 Damping Rings 650 MHz

The Damping Ring stations are modeled after similar stations in operation in Italy, Japan and the US. The power supply systems are very well understood. The only change desired would be to make them N+1 redundant internally for higher reliability. This will be investigated and will not have a large cost impact.

[2]N+1 design segments a single unit such as a power supply into N parallel or series smaller modules components plus an additional spare so one module can fail without interrupting operation. N+1 design is used in stacked or parallel power supplies, capacitors and IGBT's. Such designs can achieve much higher overall Availability especially if modules can be exchanged without interrupting operation (Hot Swap capability). This is only possible in lower voltage units.

Modulator Type	Total	e- Inj	e+ Inj	e- RTML	e+ RTML	e- Linac	e+ Linac	e- DR	e+ DR
10 MW 1.3 GHz 5 Hz	646	11	39	18	18	282	278	0	0
1.2 MW 650 MHz CW	20	0	0	0	0	0	0	10	10

TABLE 3.3-2
Modulator distribution by type and area.

3.3.4 Cost Estimation

The L-Band modulator cost model was derived directly from the latest FNAL design, extrapolated as needed to fit the ILC specifications. A traditional bottom-up estimate was made and learning curves applied to first-unit costs for an estimated manufacturing cost. Both single and dual source factory models were examined, as well as sensitivity to learning curve assumptions. These costs were also compared with industrial estimates from both Europe and Japan. In general, the US estimated cost lies between the two offshore commercial estimates. Conservative learning curve exponents (alphas[3]) were used for both parts and labor. Profit and factory support costs were than applied, as well as the staging costs of preparing the units for installation and final system checkout. These costs were compiled in M&S and FTE's. The factory models were documented in detail for each Area subsystem and given to the responsible managers for the Area rollups.

The modulator and charger costs were based on recent fabrication of units at SLAC in partnership with LLNL. All parts were recently purchased or fabricated at outside shops, and small additional extrapolations were made for the total quantities.

The cost of the HV power supply for the Damping Ring CW tubes was estimated based on recently built PEPII stations at SLAC, and separate estimates from Italy and Japan. All estimates were in reasonable agreement. The CW power rating needed is 25% lower than for PEP but there will be some additional cost for the N+1 implementation. Again a conservative learning curve was applied for 20 units.

3.3.5 Table of Components

Table 3.3-2 shows the modulator component counts in various Areas.

[3]Alpha refers to the exponential decrease of costs with each doubling of manufacturing volume. For details see section 6.1.

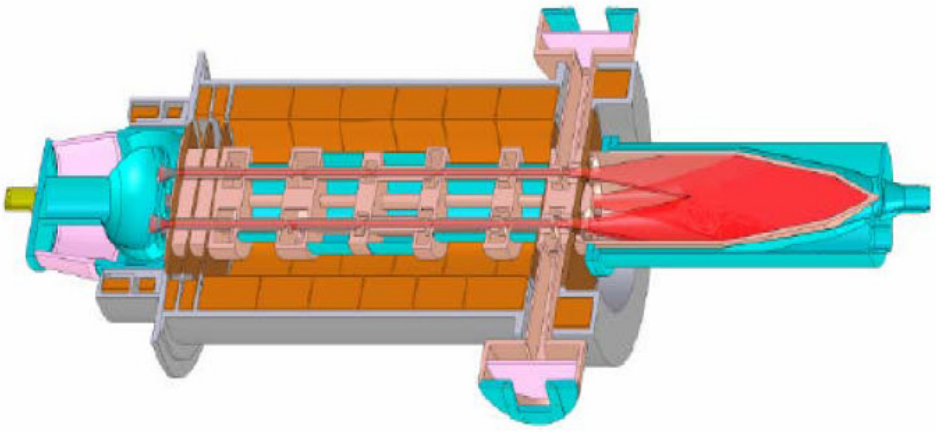

FIGURE 3.4-1. Toshiba E3736 Multi-Beam Klystron.

3.4 KLYSTRONS

3.4.1 Overview

The accelerating gradient for the ILC main linacs is supplied by superconducting 1.3 GHz cavities powered by 560 10 MW RF stations, each with a modulator, klystron and RF distribution system. Another 86 identical klystron/modulator systems are used in the e+ and e- Sources and RTML bunch compressors. The damping ring RF power is supplied by 650 MHz superconducting cavities powered by 1.2 MW CW klystrons. These are fed from a DC charging supply and do not have modulators. There are also a few special purpose S-band RF stations for instrumentation and a 3.9 GHz RF station to power the crab cavities near the Interaction Point. This section describes the 1.3 GHz and damping ring klystrons.

3.4.2 Technical Description

3.4.2.1 L-Band Klystrons

The 10 MW L-band source in the ILC baseline design is a Multi-Beam Klystron (MBK), chosen as a result of ten years of R&D for TESLA and the European XFEL. The MBK is a design approach for linear beam tubes that achieves higher efficiency by using multiple low space charge (low perveance) beams. This allows MBKs to operate at a lower voltage yet with a higher efficiency than simpler single round beam klystrons, and provides a cost-effective and simplified design configuration for the ILC RF systems.

MBK prototypes have been successfully built for the XFEL by three major electron tube manufacturers: Thales, CPI and Toshiba. These prototypes were designed for essentially the same peak RF output power specifications as required at ILC, yet with nearly twice the duty cycle as required for the XFEL. All of these manufacturers have extensive past experience in bringing prototype klystrons of state-of-the-art designs into production models, and they are regarded as fully capable of ramping up and producing the required quantities of MBKs to meet the delivery schedule for the construction of the ILC. A summary of the

Parameter	Specification
Frequency	1.3 GHz
Peak Power Output	10 MW
RF Pulse Width	1.565 ms
Repetition Rate	5 Hz
Average Power Output	78 kW
Efficiency	65%
Saturated Gain	$\geq$ 47 db
Instantaneous 1 db BW	$>$ 3 MHz
Cathode Voltage	$\leq$ 120 kV
Cathode Current	$\leq$ 140 A
Power Asymmetry	$\leq$ 1%
Lifetime	$>$ 40,000 hours

TABLE 3.4-1
10 MW MBK parameters.

MBK specifications is shown in Table 3.4-1.

3.4.2.2 Damping Ring Klystrons

The CW Klystron used in the damping rings is a frequency scaled version of the 1.2 MW 500 MHz CW klystrons currently operating reliably at SLAC and KEK [104]. Frequency scaling of klystrons is a common practice in industry, which has a thorough understanding of the engineering procedures to follow. Therefore, availability of the 650MHz klystrons is not considered to be a technical concern.

3.4.3 Technical Issues

3.4.3.1 L-Band Klystrons

The RF design of the MBK klystron has matured through several iterations of design and testing, and today essentially all aspects of the electrical design are considered solved, in particular, the choice of resonant frequencies to use for the cavities within the klystron body, the beam focusing and others [104], [105], [106], [107], [108]. Test results for all three manufacturers are summarized in Figure 3.4-3.

The three most important technical issues for the MBK are lifetime, manufacturability, and reliability. Lifetime for linear beam tubes is dominated by cathode performance. Both the CPI and Toshiba MBKs have gun designs close to 2 A/cm^2. For an M-type dispenser cathode, this low current density corresponds to a lifetime in excess of 50,000 hours. However, this lifetime has to be confirmed by suitable long-term operation tests. The "lifetime" quoted in Table 1 is the time during which the klystron can operate at the design performance specifications.

FIGURE 3.4-2. (a) CPI VKL-8301 (b) Thales TH1801 (c) Toshiba MBK E3736.

Construction of the MBK is inherently more complex than that of single-beam klystrons due to the several linear beam tubes being built into a single vacuum envelope. The number of braze joints, the fixturing and tooling, and the processes required to successfully construct, bakeout, and test an MBK are issues that require attention in developing an efficient assembly procedure that reduces the unit cost.

For reliable performance, a robust thermal design of the output circuit (output cavity, waveguide, and RF window) is important. Since ILC MBK klystrons are being built for the European XFEL, where they will operate at nearly twice the duty cycle of the ILC, there will be significant thermal/mechanical margin when operated for ILC specifications. The XFEL, however, does not require operation at full power, so reliability at 10 MW must also be demonstrated.

A remaining open issue is that the existing prototypes are vertical klystrons but a horizontal version is required for installation in the tunnel. While this is an engineering challenge, DESY is already working with the manufacturers to produce a horizontal klystron for the XFEL.

An alternate design is being developed to improve on the manufacturability and reliability of the MBK. The Sheet Beam Klystron (SBK) [108] has fewer parts and processes than an MBK. It is focused with a periodic permanent magnet (PPM) system and, as a result, is smaller and weighs less than an MBK.

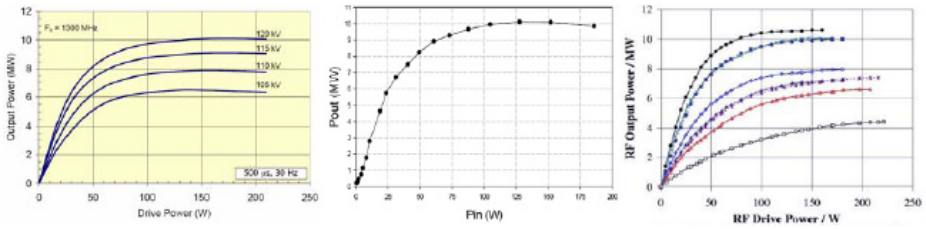

FIGURE 3.4-3. Test results for: (a) CPI VKL-8301 at reduced pulse width; (b) Toshiba MBK E3736 at full spec pulse width; (c) Thales TH1801 at reduced pulse width.

3.4.4 Cost Estimation

The cost estimate for the MBKs was derived from cost estimates from the manufacturers themselves, from the actual costs of the prototypes, and from a bottoms-up factory model. The manufacturers' estimates have inherent in them a set of assumptions that are company specific and not transparent to an outside reviewer. These assumptions cover the spectrum from proprietary processes to corporate policy decisions regarding risk assessment. The actual costs of prototypes are useful to determine the characteristics of possible learning curves a company may have used for quantity discounting, and may be useful in benchmarking models such as those used in the bottoms-up factory model.

The bottoms-up factory model used for the MBK was derived from the model used for the NLC X-band klystron. It is a comprehensive factory model with explicit assumptions about variable costs such as yield and learning curves, and fixed costs, such as up-front costs of tooling and fixturing. Fixed costs are more than 50% of the total cost during the prototype and pre-production stage of manufacturing, and taper off to 10% during the years of maximum production rates. The range of estimates from all sources is well within the risk associated with those estimates.

The cost estimate for the Damping Ring klystrons was based on actual procurement costs for 1.2 MW klystrons already produced by industry.

3.4.5 Components

Klystron	Main linac	RTML	e- source	e+ source	DRs
1.3 GHz	560	36	11	39	0
650 MHz	0	0	0	0	10

TABLE 3.4-2
Klystron requirements by area.

3.5 RF DISTRIBUTION

3.5.1 Overview

The accelerating gradient for the ILC main linacs is supplied by superconducting 1.3 GHz cavities powered by 560 10 MW RF stations, each with a modulator, klystron and rf distribution system. Another 86 similar stations are used in the e+ and e- Sources and RTML bunch compressors. The injector stations have slightly fewer cavities (24-25) per RF unit. This section describes the baseline design for distributing the high-power RF to the cavities.

3.5.2 Technical Description

The high-power L-band RF from each 10 MW klystron is brought to the accelerator cavity couplers through an RF distribution system (see Figure 3.5-1). The standard linac RF unit powers 26 nine-cell superconducting cavities filling three cryomodules. The upstream and downstream cryomodules contain nine cavities each, and the middle one contains eight, with a superconducting quadrupole magnet replacing the center cavity. This three cryomodule unit occupies 37.956 m and, at the nominal 31.5 MV/m cavity gradient, provides 846.6 MeV of acceleration (5° off-crest). With a 9 mA beam current, the total power needed in the cavities is 7.62 MW, so some overhead is included.

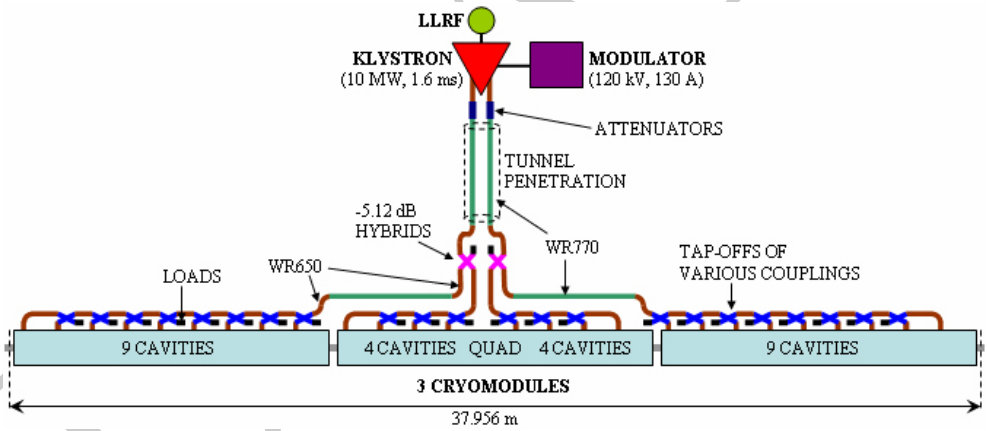

FIGURE 3.5-1. RF unit diagram showing the basic waveguide distribution layout between the klystron and 26 cavities in three cryomodules.

The dual outputs of the klystron feed into two waveguides, each carrying half the power, which run roughly 11 m to the linac through a penetration between the service tunnel and the main tunnel. High-power in-line attenuators allow more power to be sent through one arm than the other to accommodate different average gradient capabilities in the sets of cavities they feed. The penetration emerges approximately at the center of the middle cryomodule of the unit. Here, a hybrid splitter divides the power in each waveguide with a 4:9 ratio (-5.12 dB). The lower power output of each splitter feeds half the center cryomodule and the higher power output is carried approximately 6 m to one of the outer cryomodules.

Along each cryomodule, RF power is equally distributed among the cavities in a linear waveguide system, passing through a series of hybrid-style 4-port tap-offs. These tap-offs couple the appropriate sequential fraction (1/8, 1/7, ...1/2 or 1/4,1/3,1/2) of the power remaining in the line to all but the last cavity, which is directly fed the remainder. The nominal power required in each cavity is 293.7 kW. Between the tap-offs, the remainder of the 1.326 m coupler spacing is filled with modified straight waveguide sections whose width is symmetrically tapered, with 1/4-wave transformer matching steps, varying the guide wavelength to roughly yield the proper inter-cavity phasing.

Between each tap-off output and its associated cavity coupler are a circulator, a three-stub tuner, and a diagnostic directional coupler (see Figure 3.5-2). The three-stub tuner allows fine adjustment of both cavity phase and external coupling. The circulator, with a load on its third port (thus technically an isolator), absorbs RF power reflected from the standing-wave cavity during filling and emitted during discharge. It provides protection to the klystron and isolation between cavities. A couple of E-plane waveguide U-bends are also needed to keep the system compact and feed into the downward pointed coupler flange, and a short semi-flexible section is included to relieve stress and ease alignment tolerances.

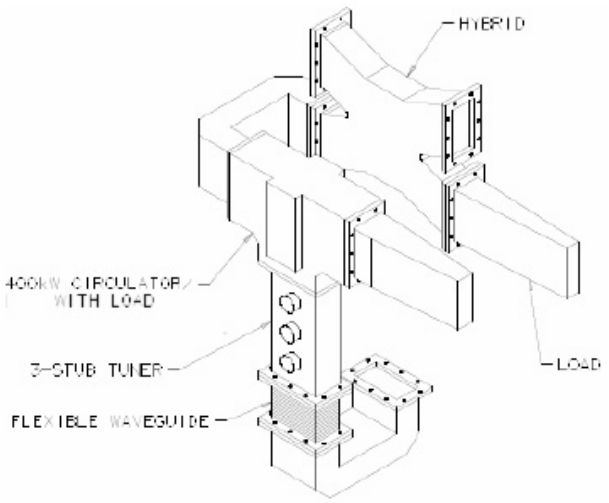

FIGURE 3.5-2. Waveguide circuit from tap-off hybrid to coupler input, showing the various components (except for the directional coupler).

3.5.3 Technical Issues

3.5.3.1 Waveguide

The bulk of the distribution system consists of aluminum WR650 waveguide (6.50" × 3.25") components. This is the standard rectangular waveguide for 1.3 GHz. Larger WR770 waveguide (7.70" × 3.85"), which has 32% lower attenuation, is used, with matched transition sections, for the long runs through the penetration and to the outer cryomodules in order to reduce system losses. The remaining loss, estimated at about 6.5%, may be further reduced

by plating the inner walls of waveguide and/or components with copper, which is 22% less lossy.

The entire waveguide system, from the klystron window to the outer coupler window, is pressurized with dry nitrogen to a pressure of 3 bar absolute. This prevents RF breakdown at the klystron window and potential problems in the circulator or elsewhere. It requires thicker-walled (0.25") waveguide, but is more economical than evacuating the system and also avoids multipactoring. The option of using SF6 was considered undesirable due to safety regulations and the risk of corrosion. Gas loss due to an open connection provides a signal to disable RF operation as a safety measure during installation and maintenance.

Relative phase changes along an RF unit due to temperature change during installation, maintenance or operation are at most about 1.1° per degree Celsius. This can be easily controlled with water cooling and insulation on some waveguide runs and components. In addition to the water cooling required on the loads and circulators, this water removes heat from the system that would be more expensive to remove from the tunnel air.

As a cost-saving measure, electron-beam welding of waveguide joints is used in place of expensive waveguide flanges and gaskets where feasible. This will be particularly useful for the penetration waveguide, which cannot be put through in one piece, as it reduces the effective waveguide cross-section.

3.5.3.2 Components

The tap-offs are compact four-port hybrids with WR650 ports of the type used at TTF. Eight different designs are required, with various coupling fractions: four each with 1/4, 1/3, and 1/2, and two each with 1/9, 1/8, 1/7, 1/6, and 1/5. The 4/13 hybrids providing the 4:9 split of the power from each klystron arm may be of the same type. Alternatively, a "button type" hybrid with slight adjustability of the split ratio might be used to provide added flexibility to tailor the system for unequal cryomodule performance.

The circulators are ferrite-based, with a T-junction configuration that provides a needed H-plane bend. The third port of this device is matched into a water load, which absorbs power propagating backward, away from the cavity. In addition to being the most expensive components in the distribution system, circulators contribute the most loss (2% out of $\sim$ 6.5%). R&D for an alternate distribution system aims at eliminating the need for them.

With three degrees of freedom, the three-stub tuner is a complicated tool to use. It is, however, compact and well tested in TTF. It may be desirable to replace it with an alternate phase shifter, with the moveable coupler antenna providing Q_{ext} adjustment.

3.5.4 Cost Estimation

The cost estimate for the RF distribution system was derived from cost estimates from component manufacturers, from the actual costs of purchased components in small quantities, and from a bottoms-up factory model. The estimates from waveguide component manufacturers have inherent in them a set of company specific assumptions that are not transparent to an outside reviewer. However, it is possible to quantify high quantity discounts and learning curves from a manufacturer if small quantities of a component were already purchased. The actual costs of purchased components were used in two different ways: 1) to calculate learning curves and quantity discounts as mentioned above, and 2) to use in bottoms-up factory models. The bottoms-up factory model approach developed a cost for a single unit

using information from previous experience in constructing components such as loads and couplers. These costs included material, labor and overhead, and fixturing costs. Once a completed first unit cost was computed, a learning curve was applied for high quantities.

The difference between the manufacturers' estimates and the factory model was about 10%. Cost estimates for some components reflected a wide range in capacity and high-volume manufacturing experience among the three regions.

3.5.5 Components

Table 3.5-1 gives a rough part count for the components in the baseline RF distribution system of a single RF unit. There are a total of 560 L-Band RF units in the main linacs and approximately 86 more (some normal conducting) in the injectors and RTMLs.

Component	#/RF Unit	Component	#/RF Unit
Circulators w/loads	26	H-Plane bends	24
3-stub tuners	26	E-Plane bends	4
Dir. Cplrs.	32	E-Plane U-bends	52
Hybrids	24	Meters of WR770	34
Loads	24	Meters of WR650	4
Flex guides	30	WR650-770 trans.	8
Phasing sections	25	Gaskets	306

TABLE 3.5-1
Component Count for a Single L-Band RF Distribution System to 26 Cavities.

3.6 CAVITIES

3.6.1 Overview

The accelerating gradient in the ILC main linac is supplied by over 16,000 9-cell superconducting RF cavities, grouped into approximately 12.6 m long cryomodules. Another ∼1200 9-cell cavities provide acceleration in the sources and bunch compressors. The baseline cavities use the TESLA design developed at DESY over the past 10 years. The cavities are qualified at 35 MV/m gradient in a vertical test and operated at an average gradient of 31.5 MV/m. At these gradients, piezo-electric tuners are required to compensate for Lorentz force detuning.

3.6.2 Technical Description

3.6.2.1 Cavity Design

The TESLA 9-cell superconducting cavity was chosen as the baseline design because it has achieved the highest qualification gradients to date for multi-cell cavities, approximately within the range required for ILC. There is significant operational experience with these cavities and it has been demonstrated with beam that accelerating gradients of greater then 30 MV/m are possible after full installation in a cryomodule. Figure 3.6-1 shows examples of the best vertical test performance for individual cavity structures at DESY (left) and results for a recent DESY cryomodule assembled with the best collection of high gradient cavities (right).

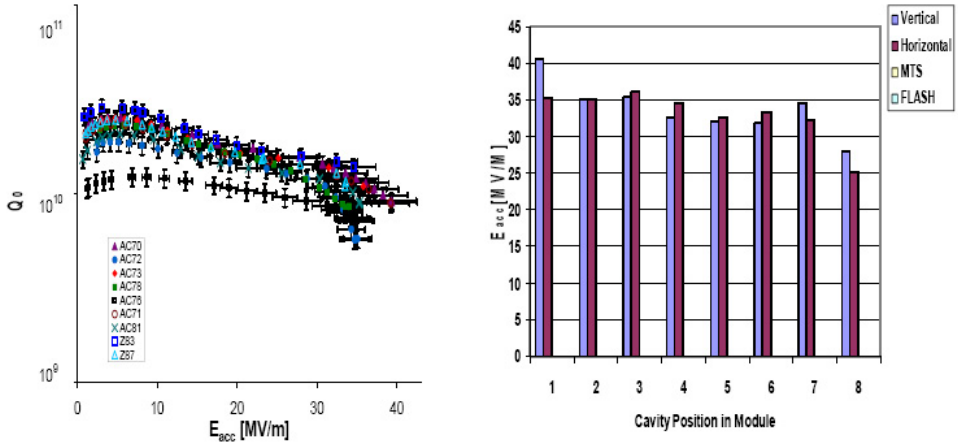

FIGURE 3.6-1. Q_0 vs. E Curves for The Best 9 Cell Vertical Qualification Tests at DESY (left) and Data for a High Gradient Cryomodule Assembled at DESY (right).

Each 9 cell cavity consists of nine accelerating cells between two end group sections. One end group has a port for coupling RF power from the power source into the structure, and the other end has a port for a field sampling probe used to determine and control the accelerating gradient. Each of these ports accepts an electric field antenna required for qualification and operation. Each end group also has a resonant higher order mode (HOM)

coupler structure with a probe port and small electric field antenna for extracting HOM power and for diagnostics. In the process of building a cryomodule, these cavity structures are cleaned, tested and placed in a helium jacket for cooling together with additional peripheral components assembled on them (dressing the cavity). A dressed cavity contains one 9-cell niobium cavity structure, coarse and fine tuners for adjusting the frequency of the structure, magnetic shielding material to minimize the cavity losses, a variable coupling high power input antenna for powering the cavity, an electric field sampling antenna and two higher order mode electric field antennas. Nine of these dressed cavities are usually connected into a string and are a subcomponent of a superconducting cryomodule. Figure 3.6-2 shows a TTF cavity undergoing clean assembly for RF qualification. The basic design parameters for this cavity are listed in Table 3.6-1.

FIGURE 3.6-2. A TTF cavity assembled and prepared for RF qualification testing.

3.6.2.2 Cavity Fabrication

The fabrication of high quality superconducting cavities starts with high quality niobium materials. The cavity accelerating cells and end group components are fabricated from high purity, high RRR niobium sheets. The RRR (residual resistivity ratio) value indirectly indicates the purity of the bulk metal as well as interstitial contamination that can affect the performance of the superconducting properties. An RRR value of 300 is considered desirable Table 3.6-2 shows the typical properties of niobium sheets considered suitable for ILC. The transition joints to the helium vessel are fabricated from a lower grade niobium sheet called "reactor grade" with a RRR value of around 40. The cavity flanges and transitions to the helium vessel are made from bar or round stock niobium alloy, typically NbTi55. The alloy is harder and stronger, and it prevents deformation near the vacuum seals and provides strong transition joints at the cavity connections.

As a final quality assurance check prior to use, the cell material is sometimes eddy-current scanned to a depth of 0.5 mm into the surface of the sheet material. Cavity cells are traditionally formed by deep drawing or hydro-forming methods where the sheets are pressed into dies to form the necessary shapes. These fabrication methods require machining of surfaces

TABLE 3.6-1
ILC 9-Cell Superconducting Niobium Cavity Design Parameters.

Parameter	Value
Type of accelerating structure	Standing Wave
Accelerating Mode	TM_{010}, π mode
Fundamental Frequency	1.300 GHz
Average installed gradient	31.5 MV/m
Qualification gradient	35.0 MV/m
Installed quality factor	$\geq 1 \times 10^{10}$
Quality factor during qualification	$\geq 0.8 \times 10^{10}$
Active length	1.038 m
Number of cells	9
Cell to cell coupling	1.87%
Iris diameter	70 mm
R/Q	1036 Ω
Geometry factor	270 Ω
E_{peak}/E_{acc}	2.0
B_{peak}/E_{acc}	4.26 mT $MV^{-1}m^{-1}$
Tuning range	$\pm$300 kHz
$\Delta f/\Delta L$	315 kHz/mm
Number of HOM couplers	2

to form the weld joints. All cavity subcomponents are joined by electron beam welding in a vacuum chamber. This reduces the contamination at the welds and is considered the cleanest form of joining metals together. Prior to electron beam welding, all subcomponents are inspected, degreased then prepared typically by mechanical polishing of surfaces to be welded, as necessary. The welded components are degreased and chemically etched and rinsed to remove inclusions and surface contamination from the machining and welding steps. The completed cavity has both internal and external chemistry to further remove the damage layer from the fabrication steps of both welding and handling. A smooth outer surface is necessary to provide good thermal contact with the cryogenic bath.

In total about 150-250 μm of niobium material is removed from the interior RF surface of the cavity through several cleaning steps. After each of these acid etchings the cavity has a new superconducting RF surface and can have different RF performance and a different gradient limitation.

The two primary issues with cavity fabrication are quality assurance on the niobium materials and on the electron beam welds. Niobium materials must be scanned to detect and eliminate surface defects, and then protected with care throughout the manufacturing process. Defective material will ultimately limit the gradient performance of a completed cavity. As with the surface defects, impurities in the welds and heat affected zones next to welds will also limit the gradient performance. Welds must have a smooth under-bead and

TABLE 3.6-2
Typical properties of high-RRR Niobium suitable for use in ILC cavities.

Element	Impurity content in ppm (wt)	Property	Value
Ta	≤ 500	RRR	≥ 300
W	≤ 70	Grain size	≈ 50 μm
Ti	≤ 50	Yield strength	> 50 MPa
Fe	≤ 30	Tensile strength	> 100 MPa
Mo	≤ 50	Elongation at break	30%
Ni	≤ 30	Vickers hardness	
H	≤ 2	HV 10	≤ 50
N	≤ 10		
O	≤ 10		
C	≤ 10		

form no surface irregularities, in particular, sharp edges where the weld puddle meets the bulk material. Defects in the equator welds will limit the gradient by thermal quenches due to the high magnetic fields there. Thermal mapping of quench locations suggests that they are typically located at or near the equator region.

3.6.2.3 Cavity Processing

The current technology for preparing cavity surfaces consists of a series of process steps that: remove niobium material damage incurred during the fabrication process or handling; remove the chemical residues left over from the material removal steps; remove the hydrogen from the bulk niobium that has entered during the chemistry steps; remove any particulate contamination that entered during the cleaning and assembly steps; and close up the cavity to form a hermetically sealed structure. The following steps are typical of those used to qualify a cavity structure in a vertical RF test.

Mechanical Inspection:
The cavity is mechanically measured with a coordinate measuring machine to compare dimensional measurements against mechanical tolerances identified on design drawings.

RF Inspection:
The cavity fundamental frequency is measured. A bead is pulled through the beam axis of the cavity to determine and record the stored energy of each cell. The bead disturbs the fields in each cell as it passes through which changes the frequency by an amount equal to the stored energy in that cell.

Bulk Chemistry:
Both the internal and external surfaces of the cavity are ultrasonically treated in hot deionized water to remove grease from the handling and surface particulates that have collected since fabrication. The cavity is then internally chemically etched with electropolishing to remove 150-250 μm of material. The cavity is placed horizontally into an alignment fixture, which levels the cavity and seals the openings while allowing the cavity to rotate. A high

purity aluminum cathode rod is inserted on the beam axis to pump cooled electrolyte into each cell of the cavity through a series of holes in the cathode. The cathode is electrically connected to the negative contact of a DC power supply. The cavity itself is the anode and is typically connected on the cells to the positive contact of the DC supply. The electrolyte is a mixture of hydrofluoric and sulfuric acid in a 1:9 or 1:10 parts by volume respectively. At the start of the process, the cavity is filled to the 60% level covering the entire cathode with the cavity slowly rotating at ≈ 1 RPM. The DC power supply provides a current density of about 50 mA/cm^2 and the cavity is polished for approximately 6-7 hours for an etching depth of 150 μm. Temperatures are monitored during the process to control the current and etch rate which is 0.4 μm/minute at 30 degrees C. After etching, the cavity is rinsed extensively with ultra pure water to remove any chemical residues or chemical safety hazards.

Heat treatment:
After bulk chemistry the cavity is cleaned and dried before inserting into a vacuum furnace for heat treatment. The chamber is evacuated to $approx10^{-7}$ mbar and the bare cavity is heated to 800 °C and soaked at that temperature to remove any excess hydrogen gained during the chemistry. This additional hydrogen, if not removed, lowers the cavity Q-value due to formation of a niobium hydride during cool-down, that adds surface losses. The cavity is then cooled to room temperature and removed from the furnace.

RF Tuning:
The cavity is tuned to the correct warm frequency and the stored energy (field flatness) in each cell equalized. The cells are measured with a bead pull and then plastically deformed by pulling or squeezing in a mechanical tuner. The cavity is mechanically adjusted to correct any alignment errors that would affect tuning for field flatness.

Final Chemistry:
The final internal chemistry refreshes the niobium surface by electropolishing removal of 10-30 μm of material. The processing steps are the same as for the bulk chemistry although the processing time is much shorter. After the standard water rinsing, additional steps should be taken to remove any sulfur particulates from the surface and several methods are now under evaluation.

High Pressure Rinsing:
The cavity is inserted vertically into the high pressure rinse (HPR) system where a wand is moved slowly through the beam axis of the cavity and the cavity is rotated. The head of the wand has small diameter nozzles tilted at angles through which high pressure ultra pure water is sprayed. A water pressure to the wand of 80-100 bar produces up to 40 N of force on the surface at impact. The wand is repeatedly moved up and down spraying all surfaces of the cavity with water to remove surface particulates which are attached on the cavity interior. The HPR process is considered the most effective cleaning method to remove surface contamination.

First Assembly:
Assembly takes place in a Class 10 cleanroom, where the cavity has been left open to air dry over night. Once the cavity has dried, cleaned subcomponents are carefully attached to the cavity by hand. Each flange connection is sealed using a diamond shaped aluminum alloy gasket that is crushed between flange faces with high line loading forces. High strength bolts and nuts with washers provide the force necessary to crush the seal. All subcomponents are assembled to the cavity except the bottom beam-line flange to allow for the second high pressure rinse.

Second HPR:
The second rinse is typically longer then the first rinse and is necessary to remove any additional particulates that have entered during the assembly steps, either from the personnel, the cleanroom environment, or the subcomponents. The cavity is removed from the HPR system after the rinse is completed and is moved to the Class 10 area to dry again overnight, this time with only the lower beam-line flange open.

Second Assembly:
The bottom beam-line flange is connected to the cavity. It typically has an isolation vacuum valve with pump-out port and an RF input probe to power the cavity. The cavity is now hermetically sealed and ready for evacuation.

Cavity Evacuation:
The cavity pump-out port is connected to a vacuum pump and evacuated. The pump system usually has a turbo molecular pump with a scroll type dry mechanical backing pump. The cavity is pumped overnight and the following day tested for vacuum leaks by spraying the cavity flange joints with helium gas and using a residual gas analyzer on the vacuum system to detect helium.

120°C Vacuum Bake:
To improve the high field Q-value, the cavity is baked at 120 degrees C for 12-24 hours while actively being pumped by the vacuum system. After being cooled to room temperature, the cavity is ready for RF testing.

RF Qualification Testing:
The cavity is mounted vertically into a cryogenic test stand, RF cables are connected to the cavity probes and the stand is inserted into a cryogenic dewar. The dewar is cooled to 4.2 K by helium gas and liquid is collected to fill the dewar. The dewar is pumped down, lowering the temperature to 2.0 K where the cavity is RF tested to determine its gradient, Q-value and limitations. Once testing is complete, the dewar is warmed up to room temperature and the stand with cavity is removed. With existing technology and infrastructure, this cryogenic cycle usually takes about 2 days at DESY, and about 4 to 5 days at KEK.

3.6.2.4 Peripheral Components

The DESY variable input coupler has been chosen as part of the baseline cavity design. This coupler features two ceramic RF windows as wells as two bellows which allow the center conductor to be mechanically moved into or out of the cavity structure thus changing the RF coupling of klystron power to the cavity. Further R&D will focus on reducing the cost of construction and adapting it to large scale production in industry.

The ILC cavities have both a mechanical coarse tuner and a piezo electric fine tuner. There are several viable designs for both the mechanical and the piezo electric tuners such as the blade tuner (mechanical). Currently no tuner has been chosen for the baseline design, and R&D is required to determine the reliability and installed performance of current designs.

The ILC cavities use a DESY style helium vessel made from titanium, which is thermally matched to the cavity material to avoid distortion of the cavity shape during cool down.

3.6.2.5 Cavity Performance Requirements

The ILC cavities must meet specific requirements on accelerating gradient and Q-value, both in the vertical qualification test and after assembly in a cryomodule. For the vertical test, each cavity must achieve 35MV/m gradient with a Q-value of 0.8×10^{10} or greater. The Q-value is

a ratio of the stored energy within the cell structure to the losses dissipated in the cell walls. Lower Q-values increase the heat load to the cryogenic system. A cavity assembled within a cryomodule must reach 31.5MV/m on average, with a Q-value of 1×10^{10}. The installed gradient and Q-value requirements are believed to be achievable with current fabrication and processing techniques. The vertical test gradient requirement is higher then that of the cryomodule in order to increase the success rate of assembled cryomodules. The performance of a cryomodule can be limited by additional system variability and administrative interlocks for the protection of peripheral components as well as from the cavity. The baseline design of ILC has been developed under the assumption that cavities qualified at 35MV/m will meet the requirement of 31.5MV/m on average once installed in a cryomodule, with overheard to compensate for microphonics and for limitations from weaker cavities powered by the same RF source.

With current fabrication and process procedures, cavities have a large spread in gradient and Q-value performance and do not reliably reach 35MV/m in the vertical tests. The primary issue is the magnitude and onset of field emission, which lowers the Q-value below specification. Field emission is typically caused by surface contamination located in regions of high electric field. Electrons emitted from the contamination site bombard other cavity surfaces, increasing surface heating and surface losses, thus lowering the cavity Q-value at that gradient. Once field emission starts, it is typically stable and the Q-value continues to drop with increasing gradient.

When not dominated by field emission, the high gradient performance of a cavity is typically limited by a thermal magnetic quench of the niobium material. Quenches can be caused by a variety of surface defects such as bad welds, lossy oxides and imbedded materials entering during fabrication or handling, or even by field emitted electrons from surface contamination.

The highest priority for ILC accelerator cavity R&D is to increase the success rate in producing cavities that reach the required performance. Increased quality control of the processing and assembly steps is expected to address the field emission issues which currently appear to dominate the limitation and variation of cavity performance. Better control of the process variables are being pursued through a global R&D effort. Current emphasis is on understanding and improving the electropolishing process. To reach the desired gradient and Q-value, a high level of quality control must be implemented for the preparation of material used in cavity fabrication, throughout the fabrication of the structures, and during the cleaning and assembly processes.

3.6.2.6 Alternative Cavity Designs

Alternative cavity shapes and fabrication materials are being studied that could potentially reduce the cost of fabrication or increase the achievable gradient. If successful, either could significantly reduce the ILC cost.

By slightly changing the shape of the cavity cell walls, it is possible to reduce the peak magnetic flux on the walls and allow the cavity to reach higher accelerating gradients before reaching a critical field limit on the niobium surface and starting to quench. New cavity shapes have been successfully tested as single cell structures up to gradients of 50MV/m at both Cornell University, with a reentrant shape, and at KEK with the "Ichiro" design. Figure 3.6-3. shows a low loss nine cell prototype RF structure. However, the cavity shape affects many other operational parameters such as the effectiveness of higher order mode damping,

multipactoring, shunt impedance, peak electric fields, energy dissipation, beam impedance and mechanical properties since a different aperture size is to be adopted. These aspects must be reoptimized.

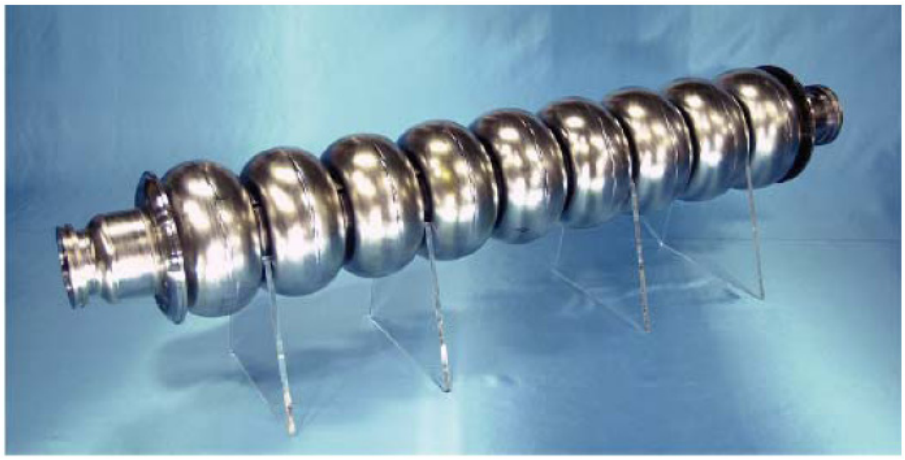

FIGURE 3.6-3. A low loss nine cell prototype RF structure under development.

Recent niobium material studies at Jefferson Lab have led to new methods for cavity fabrication using either large grain or single crystal niobium. These new materials may lead to significant cost savings in cavity preparation as well as simplification of the processing procedures.

3.7 CRYOMODULES

3.7.1 Overview

The accelerating gradient in the ILC main linac is supplied by over 16,000 9-cell superconducting RF cavities. These cavities are grouped into approximately 1,700 12.7 m long cryomodules. Each cryomodule holds nine cavities, their supporting structure, thermal shields, associated cryogenic piping, and the insulating vacuum vessel. Every third cryomodule in the main linac contains a superconducting quadrupole/corrector/BPM package in place of the center cavity. Another 150 cryomodules are located in the e+ and e- sources and RTML bunch compressors. Most of these are the standard linac configuration of 9 cavities or 8 cavities plus quad. A few have special configurations of cavities and quadrupoles.

3.7.2 Technical Description

The cryomodule design is a modification of the type developed and used in the TESLA Test Facility (TTF) at DESY, with three separate vacuum envelopes. The ILC cryomodules contain either nine 9-cell cavities or eight cavities plus a quadrupole package, and have a uniform length of 12.652 m. The cavity spacing within this modified cryomodule is (6-1/4) $\lambda_0 = 1.327$ m. This facilitates powering the cavities in pairs via 3 db hybrids with reflection cancelation in an alternate distribution scheme that may allow the elimination of circulators. Present day accelerators with superconducting RF cavities typically have many separate cryogenic supply boxes and associated warm-to-cold transitions, which represent a significant fraction of the cost. The concept adopted for the ILC is to significantly reduce this number by having a single long continuous string of about 2.5km—called a cryogenic unit—which is connected to one cryogenic supply box at the beginning and one end box.

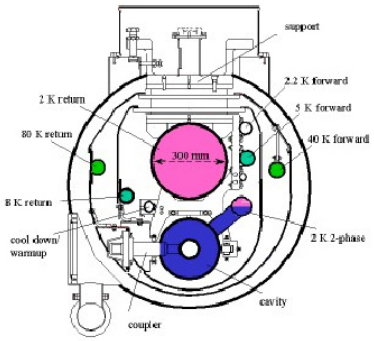

FIGURE 3.7-1. Representative Cryomodule Cross-Section

3.7.3 Technical Issues

3.7.3.1 The Cryomodule

Figure 3.7-1 shows a cross-section of an ILC cryomodule [110]. The 300mm diameter helium gas return pipe (GRP) is the main support structure for the string of cavities and the quadrupole package. The GRP is supported from above by three posts which provide the necessary thermal insulation to room temperature. The posts are fastened to large flanges on the upper part of the vacuum vessel by adjustable suspension brackets, allowing the axis of the cavities and quadrupoles to be correctly aligned, independent of the flange position. The support system is designed to allow the GRP to contract/expand longitudinally with respect to the vacuum vessel during thermal cycling. The center post is fixed to the vacuum vessel, while the two end brackets can move in the axial (z) direction to accommodate differential shrinkage. A post consists of a fiberglass pipe terminated by two shrink-fit stainless steel flanges. Two additional shrink-fit aluminum flanges are provided to allow intermediate heat flow intercept connections to the 5-8K and 40-80K thermal shields; the exact location of these flanges has been optimized to minimize the heat leakage.

Each of the cavities is encased in a titanium helium vessel, supported by the GRP by means of stainless steel brackets connected to four titanium pads on the helium vessel itself; each bracket is equipped with a longitudinal sliding mechanism and adjusting screws and pushers for alignment. A mechanical, coaxial (blade) and a piezo-electric tuner are mounted to the vessel. The inter-cavity spacing—which accommodates RF- and HOM-couplers and a flanged interconnecting bellows—amounts to 291 mm. Manually operated valves required by the clean-room assembly terminate the beam pipe at both module ends. The valves are fitted with simple RF shields.

During cool down the two ends of the $\sim$ 12 m long gas return pipe move by up to 18mm toward the center of the module. To keep the cold input coupler head of each cavity fixed longitudinally within an accuracy of 1 mm, each cavity is anchored to a long invar rod attached to the longitudinal center of the gas return pipe. The beam pipe interconnection between the cryomodules consists of a 0.38 m long section that incorporates a Higher Order Mode (HOM) absorber, a bellows, and a vacuum pumping port; the latter connected to a flange in the vacuum vessel every ninth cryomodule.

The cryostat includes two aluminum radiation shields operating in the temperature range of 5-8K and 40-80K respectively. Each shield is constructed from a stiff upper part (divided into two halves), and multiple lower sections (according to the number of the cold active components, e.g. cavities, magnets). The upper parts are supported by the intermediate flanges on the fiberglass posts; they are screwed to the center post but can axially slide on the other two posts, to which they are still thermally connected. The 'finger welding' technique is used both to connect each thermal shield to its properly shaped aluminum cooling pipe, and the lower shield parts to the upper ones.

Blankets of multi-layer insulation (MLI) are placed on the outside of the 5-8K and the 40-80K shields. The 5-8K shield blanket is made of 10 layers while the 40-80K blanket contains 30 layers. In addition the cavity and quadrupole helium vessels, gas return pipe and 5-8K pipes are wrapped with 5 layers of MLI to reduce heat transfer in the event of a vacuum failure.

The cryostat outer vacuum vessel is constructed from carbon steel and has a standard diameter of 38". Adjacent vacuum vessels are connected to each other by means of a cylindrical sleeve with a bellows, which is welded to the vessels during installation. Radiation shield

bridges are also provided. In the event of accidental spills of liquid helium from the cavity vessels, a relief valve on the sleeve together with venting holes on the shields prevent excessive pressure build-up in the vacuum vessel. Wires and cables of each module are extracted from the module using metallic sealed flanges with vacuum tight connectors. The insulating vacuum system is pumped during normal operation by permanent pump stations located at appropriate intervals. Additional pumping ports are available for movable pump stations, which are used for initial pump down, and in the event of a helium leak. The RF power coupler needs an additional vacuum system on its room temperature side; this is provided by a common pump line for all couplers in a module, which is equipped with an ion getter and a titanium sublimation pump.

The following helium lines are integrated into the cryomodules:

- The 2K forward line transfers pressurized single phase helium through the cryomodule to the end of the cryogenic unit.
- The 2K two phase supply line (made from titanium) is connected to the cavity and magnet helium vessels. It supplies the cavities and the magnet package with liquid helium and returns cold gas to the 300mm GRP at each module interconnection.
- The 2K GRP returns the cold gas pumped off the saturated He II baths to the refrigeration plant. It is also a key structural component of the cryomodule
- The 5-8K forward and return lines. The 5K forward line is used to transfer the He gas to the end of the cryogenic unit. The 5-8K return line directly cools the 5-8K radiation shield and, through the shield, provides the heat flow intercept for the main coupler and diagnostic cables, and the higher-order mode (HOM) absorber located in the module interconnection region.
- The 40-80K forward and return lines. The 40K forward line is used to transfer He gas to the cryogenic unit end and cools the high temperature superconductor (HTS) current leads for the quadrupole and correction magnets. The 40-80K return line directly cools the 40-80K radiation shield and the HOM absorber and, through the shield, provides an additional heat flow intercept for the main coupler and diagnostic cables.
- The warm-up/cool-down line connects to the bottom of each cavity and magnet helium vessel. It is used during the cool down and warm up of the cryostat.

The helium lines connected to the cavities and the magnets withstand a pressure of 4 bar; all other cryogenic lines withstand a pressure of 20 bar. The helium lines of adjacent modules are connected by welding, as was done for the HERA superconducting magnets. Transition joints (similar to those used in the HERA magnets) are used for the aluminum to stainless steel transition on the thermal shield cooling lines. The cryostat maintains the cavities and magnets at their operating temperature of 2 K. A low static heat load is an essential feature of the cryostat design; the total heat load is dominated by the RF losses, and is thus principally determined by cavity performance. Table 3.7-1 lists the heat loads for an RF unit scaled from the 12-cavity cryomodule heat loads calculated for TESLA and documented in the TESLA TDR. For the scaling to the ILC, it was assumed that the gradient is 31.5 MV/m, the cavity Q_0 is 1×10^{10}, and the beam and RF parameters are those listed in section 2.6.

Most losses occur at lower frequencies where the conductivity of the superconducting surfaces is several orders higher than that of normal conducting walls. Part of this power is

TABLE 3.7-1
Heat loads for one RF unit of 3 cryomodules with 26 cavities. All values are in watts.

	2 K		5-8 K		40-80 K	
	Static	Dynamic	Static	Dynamic	Static	Dynamic
RF Load		22.4	4.2		97.5	
Supports	1.8	0.0	7.2		18.0	
Input coupler	1.6	0.5	4.4	4.0	46.5	198.2
HOM coupler (cables)	0.0	0.6	0.9	5.5	5.5	27.1
HOM absorber	0.4	0.0	9.4	1.6	9.8	32.6
Beam tube bellows		1.1				
Current leads	0.9	0.9	1.4	1.4	12.4	12.4
HOM to structure		3.6				
Coax cable (4)	0.2					
Instrumentation taps	0.2					
Diagnostic cable			4.2		7.4	
Sum	5.1	29.0	31.7	12.5	177.6	270.3

extracted by input- and HOM-couplers, but high frequency fields will propagate along the structure and be reflected at normal and superconducting surfaces. In order to reduce the losses at normal conducting surfaces at 2 K and 4 K, the cryomodule includes a special HOM absorber that operates at 70 K, where the cooling efficiency is much higher. The absorber basically consists of a pipe of absorbing material mounted in a cavity-like shielding, and integrated into the connection between two modules. As the inner surface area of this absorber (about 280 cm^2) is small compared to that of all the normal conductors in one cryomodule, the absorber has to absorb a significant part of all the RF power incident upon it. In field propagation studies, which assume a gas-like behavior for photons, it has been shown that an absorber with a reflectivity below 50% is sufficient. Theoretical and experimental studies have suggested that the required absorption may be obtained with ceramics like MACOR or with artificial dielectrics.

The axes of the cavities must be aligned to the ideal beam axis to within ± 0.5 mm. This has been achieved at the TESLA Test Facility [112]. The quadrupole axes must be aligned to within ± 0.2 mm of the ideal beam axis, and must meet a tolerance of ± 0.1 mrad on their rotation about the beam axis. The ambient magnetic field in the cavity region must not exceed 0.5 μT to preserve the low surface resistance. The magnetic field tolerance is achieved by demagnetizing the vacuum vessel before assembly of the cryomodule, and placing a passive shield made of Cryoperm around each cavity's helium vessel.

3.7.3.2 Quadrupole/Corrector/BPM Package

The quadrupole/corrector/BPM package is discussed in Section 2.6. An important feature that must be addressed is the package fiducialization and subsequent transfer of these features to reproducible, external cryomodule fiducials to assure the correct alignment of the package

with respect to the cryomodule string.

3.7.3.3 Damping Ring and Beam Delivery Cryomodules

The damping ring accelerating RF is single 650 MHz cavities in individual cryomodules. The beam delivery also uses superconducting crab cavities with individual cryomodules. This system is discussed in Section 2.4.

3.7.3.4 Shipping of Cryomodules

To date, no engineering design to facilitate the shipping of completed cryomodules exists. It is essential that a reliable method be developed and incorporated into the ILC cryomodule deign.

3.7.4 Cost Estimation

The cryomodules represent nearly one third of the total ILC project cost. Cost studies have been conducted in all three regions , Americas, Asia and Europe. Much of the original effort relied on the TESLA TDR costing as a basis for comparison. However, independent regional studies and the cost study for the XFEL have proved useful in improving the reliability of the ILC cost numbers.

Significant effort has been expended to understand the cost drivers for cryomodules. The cavities are the largest item, with over 40% of the cryomodule cost for cavity fabrication, processing, dressing and qualification. The next largest items are the power couplers, the helium vessel fabrication, the quad package and the tuners, which represent another 30%. It is anticipated that joint studies between ILC engineers and designers and industrial partners utilizing design for manufacture methodology and value engineering principles will lead to significantly reduced cryomodule component and assembly costs.

3.7.5 Table of Cryomodule Types

The different cryomodule types and required quantities of each type are listed in Table 3.8-1. As can be seen in this table, there are basically four types of cryomodules required for the 1.3 GHz portion of the ILC.

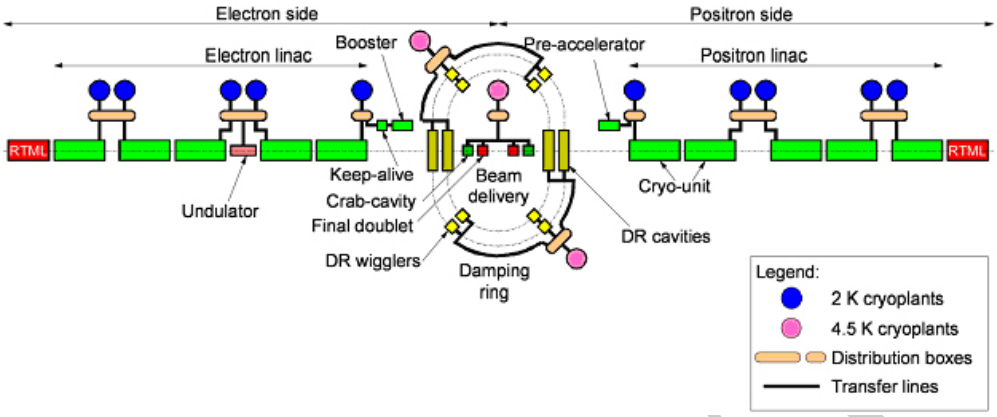

FIGURE 3.8-1. The Overall Layout Concept for the Cryogenic Systems

3.8 CRYOGENIC SYSTEMS

3.8.1 Overview

The ILC main linacs accelerate the beams to their final energy in superconducting niobium RF cavities operating at 2 Kelvin. The main linacs are the largest cryogenic systems in the ILC, but the positron and electron sources, damping rings, RTML, and beam delivery systems also have a large number and variety of liquid helium temperature superconducting RF cavities and magnets. Figure 3.8-1, below, illustrates the concept for the cryogenic system arrangement in ILC. Ten large cryogenic plants with 2 Kelvin refrigeration cool the main linac, RTML and the electron and positron sources. Three smaller cryogenic plants with mostly 4.5 K loads cool the damping rings and beam delivery system.

In addition to the main linac 1.3 GHz RF cavities, the ILC has 1.3 GHz superconducting RF cavities in the sources and RTML, 650 MHz superconducting RF in the damping rings, and 3.9 GHz RF in the beam delivery areas. Table 3.8-1 summarizes the numbers of various types of superconducting RF modules in the ILC.

In addition to the RF modules listed above in Table 3.8-1, there are a variety of superconducting (SC) magnets. As listed in Table 3.8-1, 644 1.3 GHz modules contain SC magnets. As part of the positron source, the electron linac includes about 290 meters of SC helical undulators in 2 to 4 meter length units. The Damping Rings have 8 strings of superconducting wiggler magnets, and there are special SC magnets in the sources, RTML, and beam delivery system.

3.8.2 Technical Issues

3.8.2.1 Cryogenic System Definition

The ILC cryogenic systems are defined to include cryogen distribution as well as production. Thus, components of the cryogenic system include the cryogenic plants, distribution and interface boxes, transfer lines, and non-magnetic, non-RF cold tunnel components. Although

TABLE 3.8-1
Superconducting RF modules in the ILC, excluding the two 6-cavity energy compressor cryomodules located in the electron and positron LTRs

Cryomodules					Total		
(cavities/cryomoule)	8-C	9-C	8-C	6-C		1-C	2-C
(quads/cryomodule)	1-Q	0-Q	2-Q	6-Q			
(frequency, MHz)	1300	1300	1300	1300	1300	650	3900
Main Linac e-	282	564			846		
Main Linac e+	278	556			834		
RTML e-	18	30			48		
RTML e+	18	30			48		
e- Source	24				24		
e+ Booster	12		6	4	22		
e+ Keep Alive	2				2		
e- Damping Ring						18	
e+ Damping Ring						18	
Beam Delivery System							2
TOTAL	634	1180	6	4	1824	36	2

cryomodules, SC magnets, and production test systems also include significant cryogenics, those are not considered in this section of the RDR.

3.8.2.2 Cryogenic Cooling Scheme for the Main Linac

Main linac cryogenic modules each containing eight (with magnet package) or nine (without magnet package) nine-cell niobium cavities, cold helium pipes, and thermal shields are the dominant load to be cooled by the cryogenic system. The magnet package, in one third of the cryomodules, includes a superconducting quadrupole and corrector magnets. The ILC cryomodule design for the 1.3 GHz RF is based on the TESLA Test Facility (TTF) type III design [1] which contains all the cryogenic pipework inside its vacuum enclosure. There are approximately 23 km of 1.3 GHz cryomodules including main linac, RTML, and sources.

Series architecture is mostly used in the cryogenic unit cooling scheme. Like for the TESLA cryogenic concept, saturated He II cools RF cavities at 2 K, and helium gas cooled shields intercept thermal radiation and thermal conduction at 5 - 8 K and at 40 - 80 K. A two-phase line (liquid helium supply and concurrent vapor return) connects to each helium vessel and connects to the major gas return header once per module. A small diameter warm-up/cool-down line connects the bottoms of the He vessels.

A subcooled helium supply line connects to the two-phase line via a Joule-Thomson valve once per string (typically 12 modules). The 5 K and 40 K heat intercepts and radiation screens are cooled in series through an entire cryogenic unit of up to 2.5 km in length. For the 2 K cooling of the RF cavities, a parallel architecture is implemented with the parallel cooling of cryo-strings resulting in operational flexibility. Consequently, each cryogenic unit

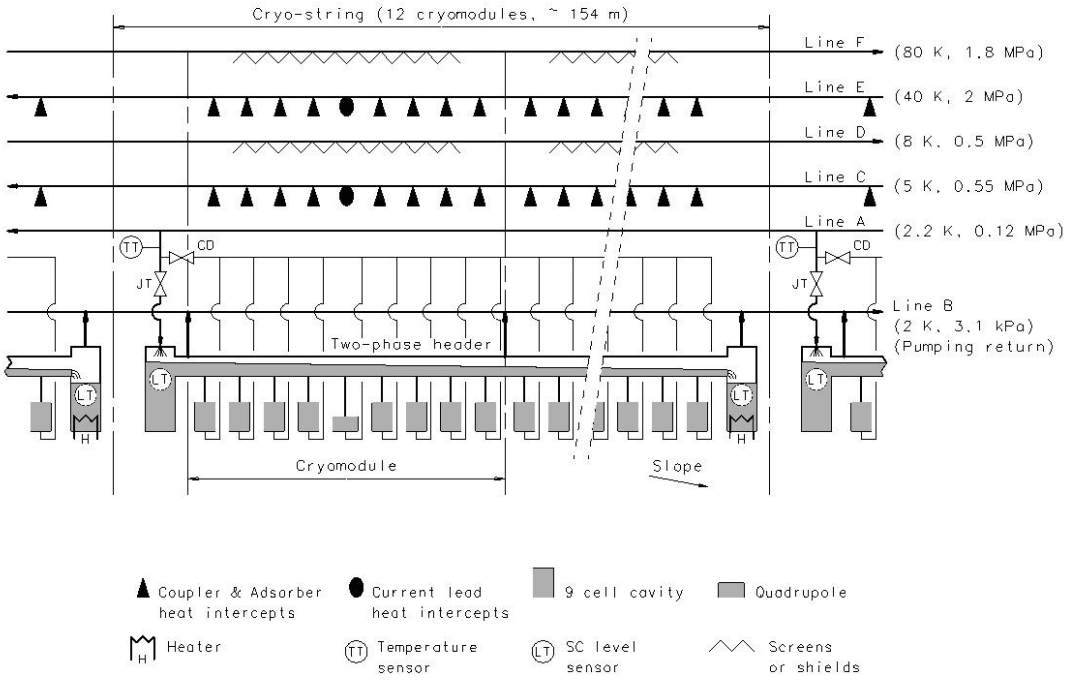

FIGURE 3.8-2. Cooling Scheme of a Cryo-String

is subdivided into about 14 to 16 cryo-strings, each of which corresponds to the 154 meter length elementary block of the cryogenic refrigeration system.

Figure 3.8-2 shows the cooling scheme of a cryo-string, which contains 12 cryomodules. The cavities are immersed in baths of saturated superfluid helium gravity filled from a 2 K two-phase header. Saturated superfluid helium is flowing all along the two-phase header for filling the cavities and phase separators located at both ends of the two-phase header. The first phase separator is used to stabilize the saturated liquid produced during the final expansion. The second phase separator in used to recover the excess of liquid, which is vaporized by a heater. At the interconnection of each cryomodule, the two-phase header is connected to the pumping return line.

The division of the Main Linac into cryogenic units is driven by various plant size limits and a practical size for the low pressure return pipe. A cryogenic plant of 25 kW equivalent 4.5 K capacity is a practical limit due to industrial production for heat exchanger sizes and over-the-road shipping size restrictions. Cryomodule piping pressure drops also start to become rather large with more than 2.5 km distances. Practical plant size and gas return header pressure drop limits are reached with 192 modules in a 16-string cryogenic unit, 2.47 km long. Five cryogenic units divide the main linac conveniently for placing the positron source undulators at 150 GeV. Figure 3.8-3, illustrates the division of the main linac into strings and units.

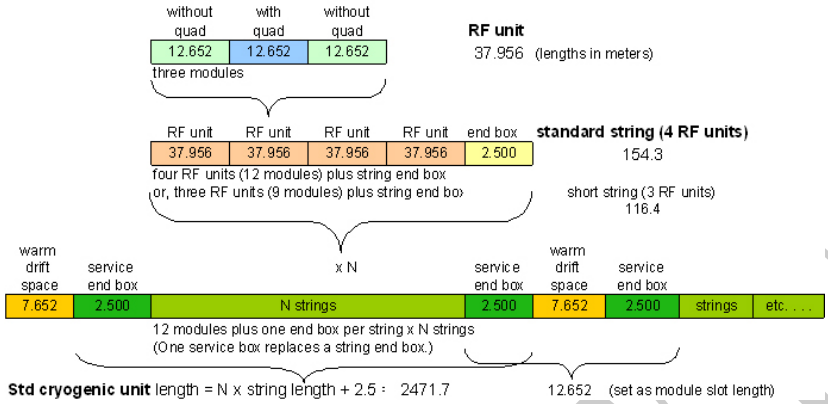

FIGURE 3.8-3. Lengths and Typical Arrangement of Modules in the Electron Main Linac

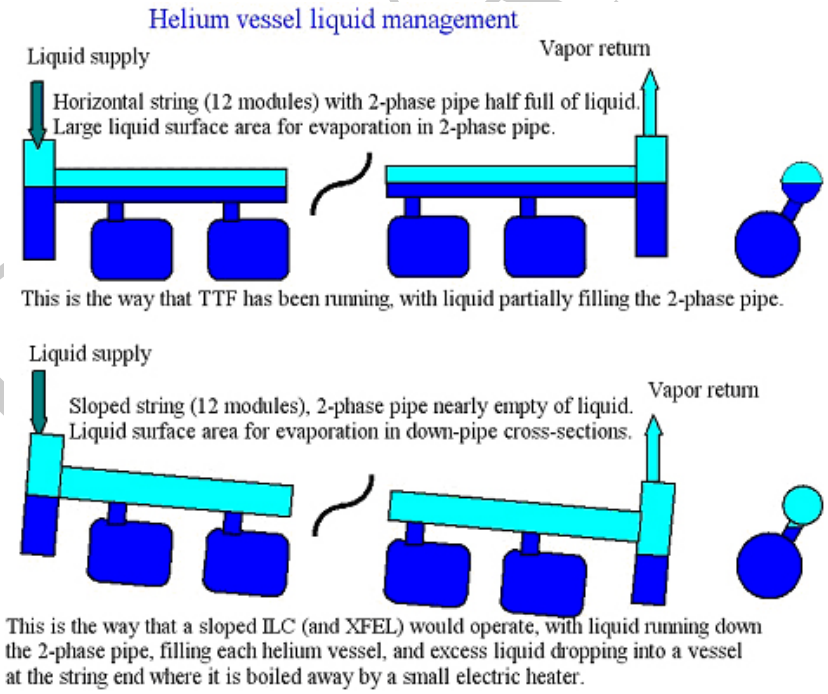

FIGURE 3.8-4. Two-Phase Helium Flow for Level and for Sloped Systems

3.8.2.3 Liquid Helium Management in 1.3 GHz Modules

As the ILC site has not yet been selected, the cryogenic system concept must accommodate different configurations of tunnel and civil works. The tunnel may follow the earth's curvature or be laser-straight with a maximum slope of up to 0.6 % creating large elevation differences. To avoid harmful instabilities, all fluid should ideally be transported over large distances in a mono-phase state. Local two-phase circulation of saturated liquid can be tolerated over limited lengths, within a controlled range of vapor quality. Figure 3.8-4 illustrates two methods of liquid management in the two-phase supply pipe for main linac cryogenic modules, one case for a sloped system and the other for a level system.

3.8.2.4 Sources, Damping Rings, and Beam Delivery Systems

As listed above in Table 3.8-1, electron and positron sources each include just over 20 SRF modules containing 1.3 GHz RF cavities cooled to 2 Kelvin. The sources also include several superconducting magnets, as well as about 290 meters of superconducting positron source undulators. These undulators are cooled by one of the cryogenic plants in the electron linac cryogenic system. The electron and positron source linacs are also cooled from main linac cryogenic plants, as illustrated in Figure 3.8-1.

Damping ring cryogenic loads include 4.5 K superconducting wigglers, 4.5 K 650 MHz cryomodules, associated cryogenic distribution systems, and 70 K thermal shields for all of these. Two cryogenic plants serve the damping rings.

The beam delivery system has one 3.9 GHz cryomodule (containing two cavities) on each side of the interaction point, superconducting final focus quadrupoles, and other special superconducting magnets spaced several hundred meters from the IR. One cryogenic plant serves both sides of the interaction region. This plant could also serve the cryogenic needs of the detectors, but that aspect of these cryogenic systems is not considered here.

3.8.2.5 Heat Loads and Cryogenic Plant Power

Table 3.8-2 shows the predicted heat load for a typical Main Linac Cryogenic Unit. This table lists the uncertainty factor and overcapacity factor, which are multipliers of the estimated heat loads. These are used to estimate a total required cryogenic plant capacity as follows. Installed cryogenic capacity = Fo × (Qd + Qs), where Fo is overcapacity for control, off design operation and seasonal temperature variations. Fud is the uncertainty factor on the dynamic heat load estimate, Fus the uncertainty factor on static heat load. Qd is predicted dynamic heat load, and Qs is predicted static heat load. Note also that cryogenic plant efficiency is assumed to be 28% at the 40 to 80 K level and 24% at the 5 to 8 K temperature level. The efficiency at 2 K is only 20%, however, due to the additional inefficiencies associated with producing refrigeration below 4.2 Kelvin. All of these efficiencies are in accordance with recent industrial conceptual design estimates.

A similar analysis has been done for the sources, damping rings, and beam delivery system in order to estimate size requirements for each. (RTML cooling is included with the main linac.)

Table 3.8-3, below, lists the estimated heat loads and required cryogenic plant size for the damping rings.

Table 3.8-4 summarizes the required capacities of the cryogenic plants for the different area systems. The maximum required plant capacities (equivalent at 4.5 K) are comparable

TABLE 3.8-2
Main Linac Heat Loads and Cryogenic Plant Size

	40-80 K	5-8 K	2 K
Predicted Module Static Heat Load (W/mod)	59.19	10.56	1.70
Predicted Module Dynamic Heat Load (W/mod)	94.30	4.37	9.66
Modules per Cryo Unit	192	192	192
Non-Module Heat Load per Cryo Unit (kW)	1.0	0.2	0.2
Total Predicted Heat per Cryo Unit (kW)	30.47	3.07	2.38
Efficiency (fraction Carnot)	0.28	0.24	0.22
Efficiency in Watts/Watt	16.45	197.94	702.98
Uncertainty & Overcapacity Factor (Fo)	1.54	1.54	1.54
Heat Load per Cryo Unit inc. Fus, Fud, Fo (kW)	46.92	4.72	3.67
Installed Power (kW)	771.7	934.9	2577.6
Installed 4.5 K Equivalent (kW)	3.5	4.3	11.8
Percent of Total Power at Each Level	18.0	21.8	60.2
Total Operating Power for One Cryo Unit Based on Predicted Heat (MW)			3.34
Total Installed Power for One Cryo Unit (MW)			4.33
Total Installed 4.5 K Equivalent Power for One Cryo Unit (kW)			19.57

TABLE 3.8-3
Damping Ring Cryogenics (per ring, two total)

Total Predicted 4.5 K Heat	(W)	1660
Total Predicted 4.5 K Liquid Production (for current leads)	grams/sec	0.80
Total Predicted 70 K Heat	(W)	5080
Uncertainity and Overcapacity (total combined) Margin		1.54
Installed Power	(MW)	1.13
Cryogenic Plant Capacity (converted to 4.5 K equiv)	(kW)	3.45

TABLE 3.8-4
ILC Cryogenic Plant Sizes (sources listed separately here, but may be combined with Main Linac)

Area	# of Plants	Installed Plant Size (each)	Total Installed Power	Operating Power (each)	Total Operating Power
		(MW)	(MW)	(MW)	(MW)
Main Linac + RTML	10	4.35	43.52	3.39	33.91
Sources	2	0.59	1.18	0.46	0.92
Damping Rings	2	1.26	2.52	0.88	1.76
BDS	1	0.41	0.41	0.33	0.33
TOTAL			47.63		36.92

TABLE 3.8-5
Main Linac Helium Inventory

Volumes		Helium (liquid liters equivalent)	Tevatron Equiv.	LHC Equiv.	Inventory Cost (k$)
One Module		370			
String	12 modules	4,500	0.1		13.4
Cryogenic Unit	14-16 strings	68,000	1.1	0.1	203.6
ILC Main Linacs	2x5 cryo units	680,000	11.3	0.9	2,037

with the present state of the art cryogenic plants used in the Large Hadron Collider [3]. Total installed power for the cryogenic system is 48 MW, with an expected typical operating power of 37 MW.

If the tunnel is located near the surface, i.e. with depth of access shafts smaller than 30 m, the entire cryogenic plant can be installed above ground. If the tunnel is deep, certain components must be installed at tunnel level because of the hydrostatic pressure loss.

3.8.2.6 Helium Inventory

As illustrated in Figure 3.8-5, most of the helium inventory consists of the liquid helium which bathes the RF cavities in the helium vessels. The total helium inventory in ILC will be roughly equal to that of the LHC at CERN, about 650,000 liquid liters, or about 100 metric tons.

3.8.3 Cost Estimation

The cryogenic system cost estimate has been generated based on experience in procurement of cryogenic plants and equipment at Fermilab, CERN, DESY, and other laboratories.

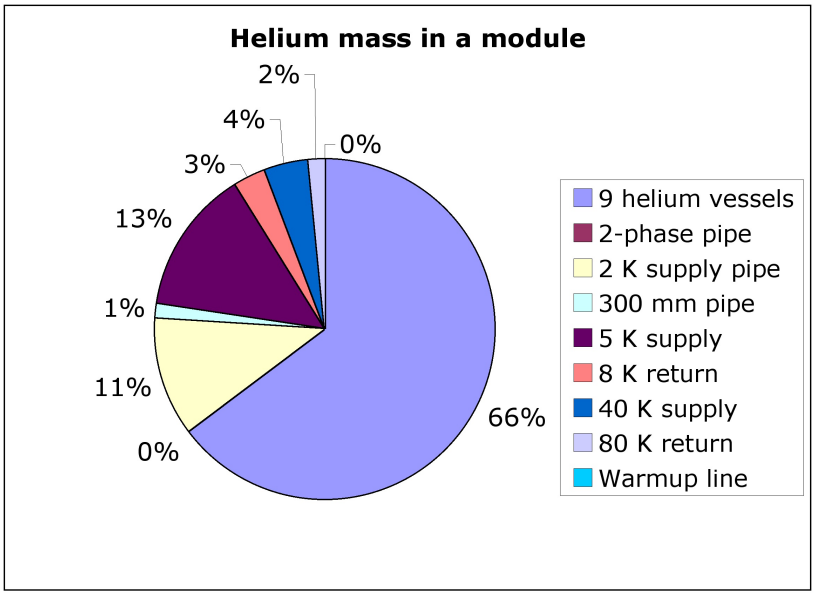

FIGURE 3.8-5. Helium Mass in a Module

3.9 LOW LEVEL RF

This section still under review. Draft to be released by April 1, 2007.

3.10 INSTRUMENTATION

This section still under review. Draft to be released by April 1, 2007.

3.11 DUMPS, COLLIMATORS, AND STOPPERS

This section still under review. Draft to be released by April 1, 2007.

3.12 CONTROLS AND TIMING SYSTEMS

This section still under review. Draft to be released by April 1, 2007.

CHAPTER 4

Conventional Facilities and Siting

4.1 OVERVIEW

This section provides an overview of the ILC Conventional Facilities and Siting (CFS) which has been adopted as the basis of the RDR cost estimate. A more detailed description can be found in [123]. In the absence of a specific ILC site, three reference sites one in each region have been developed in parallel by the CFS Group. The reference sites (described in Chapter 5) are all deep-tunnel sites, but have varying geologies and topographical constraints. An evaluation of an optimized shallow site (either a shallow tunnel or 'cut and cover') was beyond the scope of the current RDR activities, but will be done in the near future. While the focus of the CFS design work has been on the 31 km long 500 GeV machine, the sites are required to support the footprint of the 1 TeV upgrade, both in terms of space and available infrastructure (e.g. power).

The CFS Sample Site designs were generated using criteria provided by each of the ILC Area Systems. Overall tunnel lengths were specifically determined by the machine parameters. However, the size of tunnels, shafts, underground caverns and surface buildings, as well as the related CFS systems, have been developed to accommodate specific equipment installation, maintenance and personnel access and egress requirements. For all these systems, the original criteria have been iterated in order to minimize overall costs while meeting the requirements of the present state of the ILC design. Specific examples include the reduction of Service and Beam tunnel diameters, the number and size of shafts, electrical power and process cooling loads.

Figure 4.1-1 indicates the basic scope of the civil construction of the ILC layout:

- Two parallel 31 km long 4.5m diameter underground tunnels house the main accelerators and the Beam Delivery Systems (Beam Tunnel), and their associated support hardware (Service Tunnel, containing klystrons, modulators, power supplies, controls and instrumentation electronics etc.). The tunnels are generally separated horizontally by ∼11 m (center-to-center), and are connected via small diameter penetrations every 12 m supporting cables, waveguides etc. Personnel access connection tunnels (primarily for safety egress) are located every 500 m.

- A total of 13 shafts along the length of the machine provide access to underground caverns linking to the tunnels. They primarily support the large cryogenics plants required for the superconducting linacs.

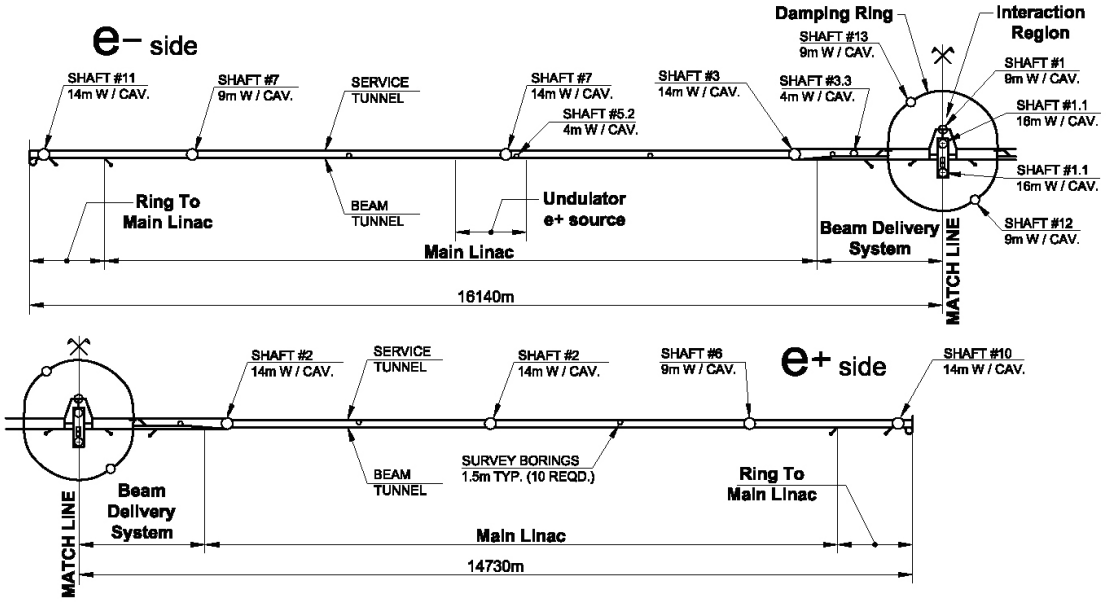

FIGURE 4.1-1. Layout of the Civil Construction, Indicating the Position of Shafts and Caverns

- A single collider hall at the Interaction Region (IR) is large enough to support two physics detectors in a push-pull configuration.
- A single 5 m inner-diameter ∼7 km approximately circular tunnel located around the central IR region and ∼10 m above the BDS elevation houses both the electron and positron Damping Rings in a stacked configuration.
- Several additional tunnels and service shafts house the electron and positron sources and injector linacs (injection into the Damping Ring), and connect the damping ring to the main accelerator housing.

Civil Engineering, Electrical, and Process Cooling Water comprise greater than 90% of the total cost of the CFS. The Civil Engineering portion of the project is almost two thirds of the total CFS cost, with the Underground Facilities equating to 75% of Civil Engineering. The more than 72 km of tunnel is the single largest cost element. Although formal value engineering has not yet been accomplished, the designs have been reiterated with the project team several times to develop a cost efficient, workable design.

4.2 CIVIL ENGINEERING AND LAYOUT

4.2.1 Main Accelerator Housing

The largest underground structures are the two parallel 4.5 m diameter tunnels, which effectively run for the entire length of the machine footprint (∼31 km). One tunnel (the Beam Tunnel) contains the beamline components (SCRF accelerator cryomodules, magnets, vacuum systems etc.) The second so-called 'Service'Tunnel houses the entire support infrastructure:

RF power sources (klystrons, modulators, pulse transformers); dc magnet power supplies; radiation-sensitive instrumentation and controls (electronics). Unlike the Beam Tunnel, the Service Tunnel is designed to be accessed during beam operation, allowing in-situ repairs and adjustment of equipment during running.

Figure 4.2-1 shows a cross-section of the Main Linac twin-tunnel, with the Beam Tunnel on the left. The 4.5 m inner diameter accommodates the cryomodules and RF distribution (waveguides), at the same time as allowing space for cryomodule installation (or removal), while maintaining a minimum 'clear passage'for emergency egress (see Figure 4.2-1 left). The Cryomodules and other floor standing components are placed on short stands mounted to a concrete floor. The beam is centered 1.1 meters above the floor and 0.8 meters away from the wall, which is considered sufficient to allow for cryomodule installation (welding) and the installation of the RF waveguides. Space needed for the survey lines of sight has also been considered. The outer positioning of the cryomodules allows for clear access to the egress passageways connecting the two tunnels, spaced at 500 meter intervals (not shown).

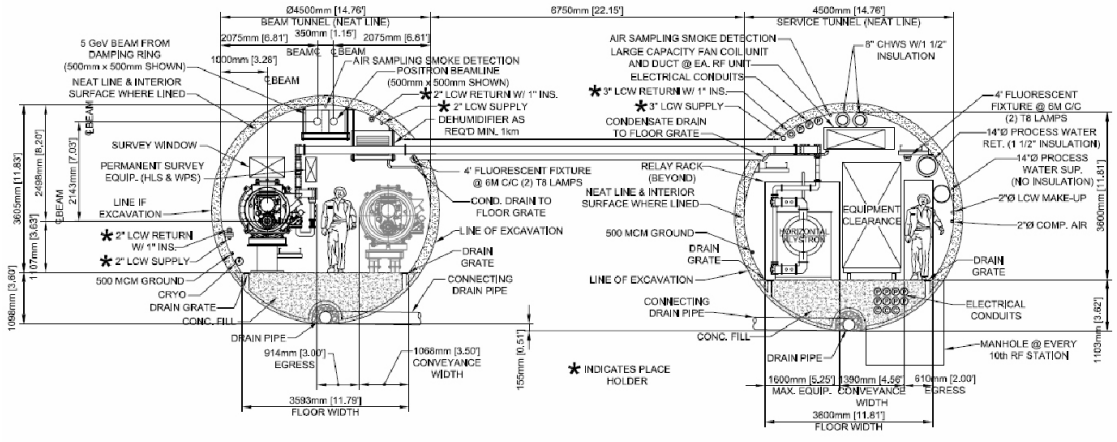

FIGURE 4.2-1. Cross-section of the Main Linac Housing (Beam Tunnel, left) and Service Tunnel, Showing the Connecting Waveguide Penetration

The lateral separation of the tunnels is ∼11 m (center to center). The ∼7 m rock and concrete separation between the Service Tunnel and Beam Tunnel is required for structural reasons and to provide the required radiation shielding mass allowing workers to enter the Service Tunnel while the accelerator is operating. Penetrations between tunnels have been sized and configured to provide the required radiation shielding.

The regions of superconducting RF (accelerator) dominate the length of the main accelerating housing. These sections are made up of many consecutive identical RF units. An RF unit is approximately 38 m long (three cryomodules), and is supplied from the Service Tunnel by three cross penetrations at intervals of approximately 12 m: one for the RF waveguides, and two additional ones for cables and signals. The main RF unit components housed in

TABLE 4.2-1
Main Service Tunnel Equipment for a Single RF Unit

Item Name	Approx. Size (Meters)	Comments
Klystron	1. ×3.38	
Pulse Transformer	1.34 × 1.25	
Modulator	1 × 4.27	
Electronic Racks	9 0.80 × 1.1	Self Contained w/ integral cooling
LCW & CW Skids	1.22 × 2.06	
RF Transformer	1.353 × 1.499	Plus 800 Amp Panel
Charging Supply Trans.	1.22 × 2.44	
Convention Trans.	1.575 × 1.245	Plus 800 Amp Panel
Emergency Transformer	1.575 × 1.245	

the Service Tunnel and their approximate space requirements are given in Table 4.2-1. For the 'warm'sections of the Ring-to-Main-Linac (RTML) as well as the Beam Delivery System (BDS), the Service Tunnel accommodates the many independent magnet power supplies, as well as electronics for controls and instrumentation.

In addition to the RTML, Main Linac and BDS beamline components, the Beam Tunnel also houses the 5 GeV low-emittance transport line (part of the RTML) which transports the beam from the central Damping Rings to the far ends of the machine. The RTML 'turnarounds'at the ends of the machine are housed in a 4.5 m diameter looped tunnel with an average bending radius of ∼30 m in the horizontal plane. The length of each loop is approximately 140 m. On the electron linac side, a third beamline from the undulator-based positron source (nominal 150 GeV point) is required to transport the 400 MeV positrons from the source to the Damping Rings. Both the long 5 GeV low-emittance and the 400 MeV positron transport lines are supported from the Beam Tunnel ceiling, and are positioned towards the center of the tunnel to allow for installation and replacement without removing a cryomodule. Power and cooling services for these elements are provided from equipment in the Service Tunnel.

The RTML and BDS tunnels (a total of ∼12.2km and ∼5.3km, respectively) lie in a plane, while the Main Linac tunnels and associated beamline components (47.8 km) follow the Earths curvature.

The large cryogenic plants (see Section 3.8), required primarily for the SCRF RF cryomodules, are housed in eight underground caverns connected to the surface via shafts (four per side, spaced approximately 5000 m apart): shaft nos. 2, 3, 4, 5, 10 and 11 are 14 m in diameter, while shaft nos. 6 and 7 are 9 m diameter (see Fig. 4.1-1 for shaft locations). Figures 4.2-2 , 4.2-3 shows a schematic of a typical 9 m shaft and cavern. In addition to housing the cryogenic plants, these shafts are also used for: installation of machine components (including cryomodules at the 14 m shafts); normal and safety egress from the tunnels; and for supporting all services such as cooling water, power etc. The 14 m shafts are also used to lower, assemble and prepare the Tunnel Boring Machines (TBM) which are used extensively for tunnel excavation.

Temperature neutral air is routed through the tunnel from the shafts, no additional

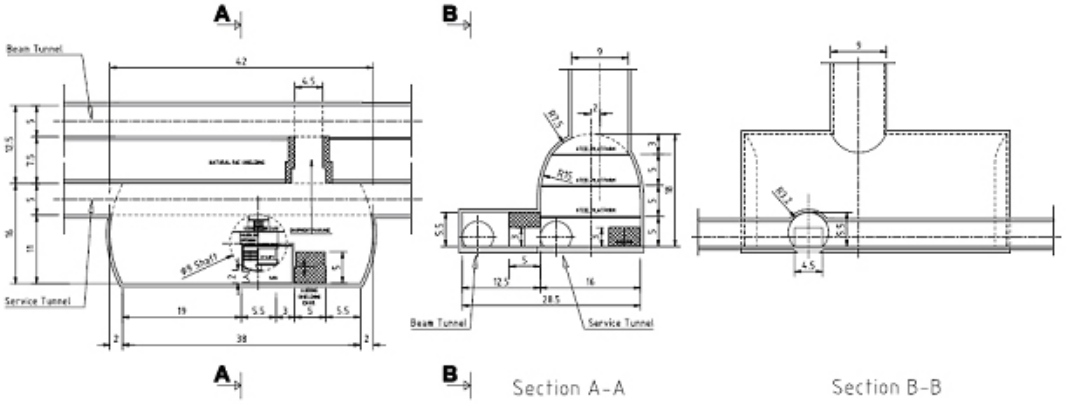

FIGURE 4.2-2. Example of a 9 m Shaft with Underground Cavern, Service and Beam Tunnels (European Sample Site)

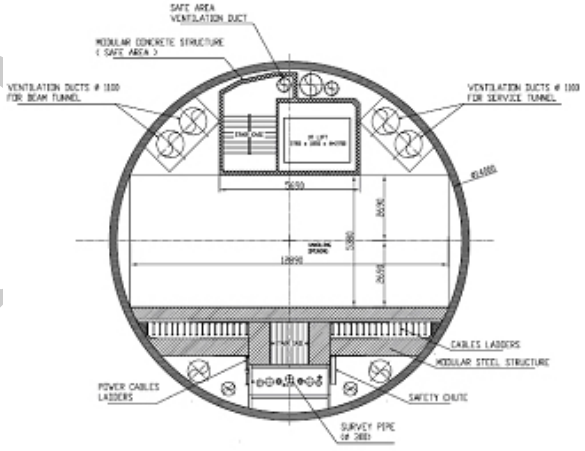

FIGURE 4.2-3. Detailed View of 14 Meter Shaft

heating or cooling is required in the Beam Tunnel. Where needed there is dehumidification equipment installed to maintain humidity levels below the dew point. Seepage is directed to a drain and routed to the sumps located at the shaft caverns.

A special underground cavern is required to service the undulator-based positron source, located at the nominal 150 GeV point in the Main Electron Linac. A 4 m vertical shaft is provided for removal and installation of 'hot'targets.

4.2.2 Central Injectors

The central injector systems include: the 6.7 km circumference Damping Rings; the polarized electron source; the positron Keep Alive Source (KAS); and the electron and positron 5 GeV SCRF injector linacs. Figure 4.2-4 shows the primary tunnel and shaft arrangements.

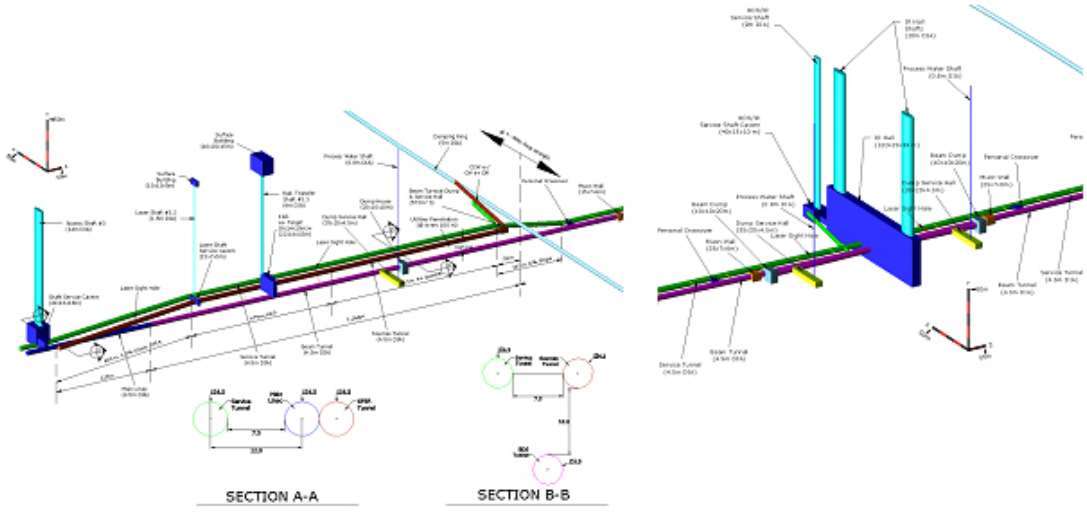

FIGURE 4.2-4. Layout of the Central Injector Complex (electron side)

The electron and positron Damping Rings are housed in a single 5 m inner-diameter quasi-circular tunnel with a total circumference of 6704 m. The tunnel is located in the horizontal plane, approximately 10 m above the plane of the BDS. The ring is made up of six arc sections, two long straight sections for injection and extraction and four short straight sections containing the superconducting damping wigglers and RF. The DR tunnel is connected to the injection tunnels from the sources in the middle of the long straight sections (see Fig. 4.2-4). The tunnel has 6 alcoves in total, located in the middle of the straight sections. Two main alcoves are accessed via two 9 m diameter shafts, and are used to house the cryogenic plants and RF power sources for the wigglers and RF cavities (and are also used for installation). The four smaller alcoves in the remaining straight sections are not connected to the surface, but two of them are vertically connected to the BDS portion of the Service Tunnel 10 m below to allow personnel access. As there is no separate service tunnel for the DR, all service and support equipment are housed in the two shaft caverns and the

four smaller alcoves. A cross-section of the Damping Ring tunnel is shown in Fig. 4.2-5; the 5 m inner diameter is required to house the two rings (vertically stacked), and the emergency egress passage, while allowing enough space for component installation.

The electron and positron 5 GeV injector linacs are each housed in 4.5 m diameter tunnels, and share the main Service Tunnel with the BDS. The sources also make use of the 14 m diameter shafts located directly at the end of each Main Linac, where the connecting tunnel to the Damping Rings has a 2% slope to accommodate the 10 m vertical offset between the Damping Ring and Main Accelerator Housing. The KAS source requires an underground cavern similar to the positron production vault in the electron Main Linac, again with a 4 m diameter vertical shaft for removal and installation of the hot target.

4.2.3 Interaction Region and BDS

The Physics Detector Hall is the largest cavern in the project. It is sized to accommodate two Physics Detectors in a Push Pull type configuration assuming surface assembly of each detector. The hall is connected to the surface assembly buildings via two 16 m diameter shafts, one for each Detector. It is also connected to the Beam Tunnel, to a service cavern through a passageway, and to the survey galleries. The floor slab is thick enough to accommodate the weight of the two Detectors and the weight of the movable shielding wall (2 pieces) in between the Detectors. The walls of the hall are equipped with 3 to 5 levels of steel platforms to be used for services and access at various levels to the Detectors. The hall also has beams and rails for one 400 ton crane and two 20 ton cranes, assuming the surface pre-assembled Detector elements weigh 400 tons at most.

An additional service cavern for the BDS is located next to the Detector Hall (see Fig. 4.2-6). It houses all the equipment needed for the running of the Detectors and ancillary facilities, which need to the shielded from radiation. It has two steel platforms as intermediate floors for equipment, and is connected to the Detector Hall through a shielded passage for personnel and goods, and to the BDS service tunnel on both sides. The service cavern is accessible from the surface via a 9 m diameter vertical shaft, which supports all services, houses a safe staircase and lift for personnel and equipment, and leaves space for lowering all components to be installed in the service cavern.

There are four full-powered Beam Dump facilities in the BDS System, two on each side. For each one there is a cavern which houses the high-pressure water dump itself, and a service cavern located 300-1360 m away to house all electrical, control and cooling equipment.

The inner diameter of the BDS beam tunnels are locally enlarged at four locations (two per side) to house the large magnetized toroids (so-called Muon spoilers) for reducing the muon background to the experimental hall.

4.2.4 Surface Buildings

A total of 120 surface buildings are estimated for the project. The type, number and dimensions of the buildings include only those surface facilities required for construction, installation and operation of the project. Additional infrastructure such as seminar rooms, guest-houses, restaurants, administrative facilities etc. are assumed to be supplied by a nearby (host) laboratory, and are not included in the cost estimate. The Asian sample site does not have a nearby laboratory and that estimate does include such central campus facilities.

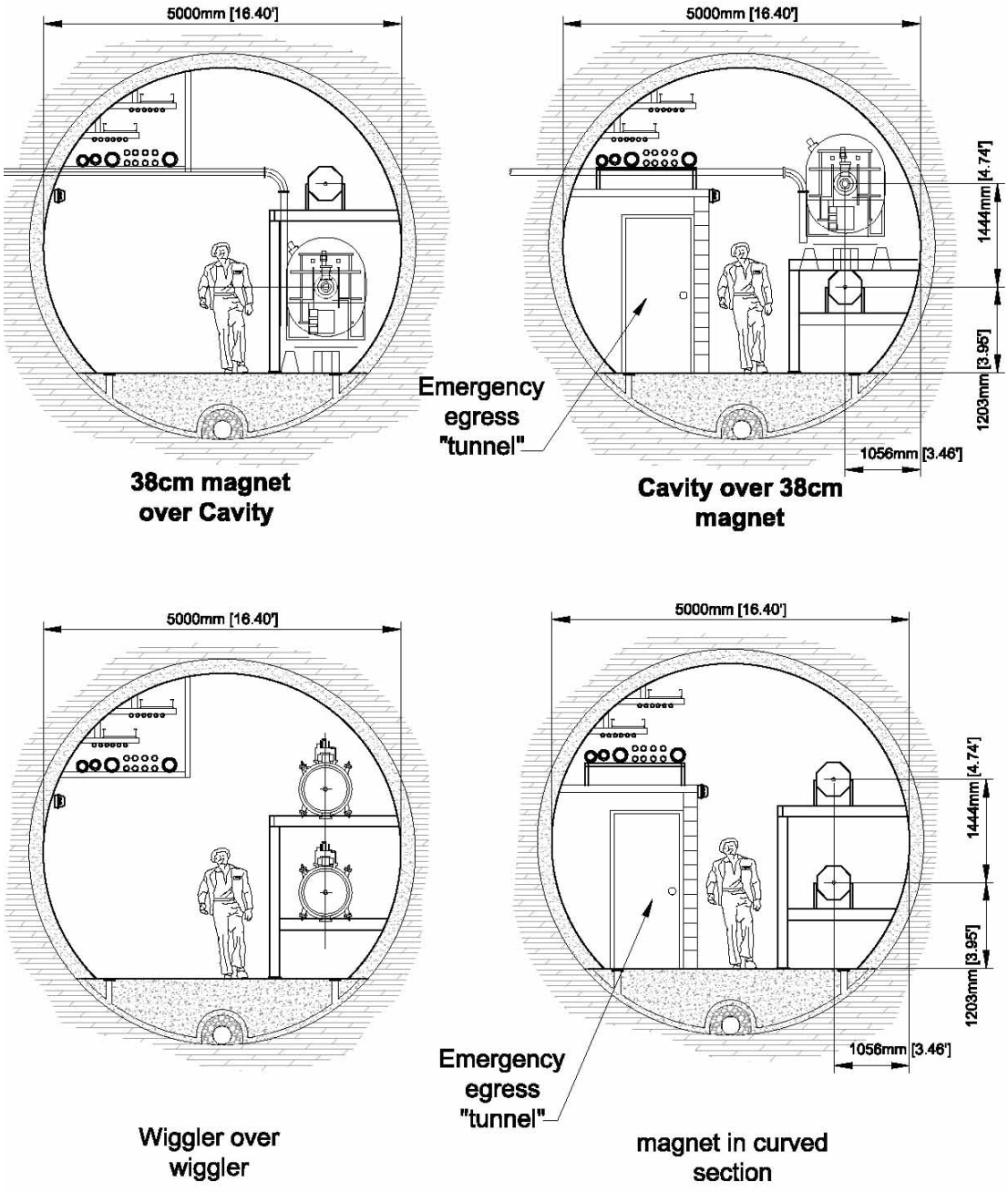

FIGURE 4.2-5. Cross-Sections of the 5 m Diameter Damping Ring Tunnel Showing Vertical Stacked Rings at Several Locations

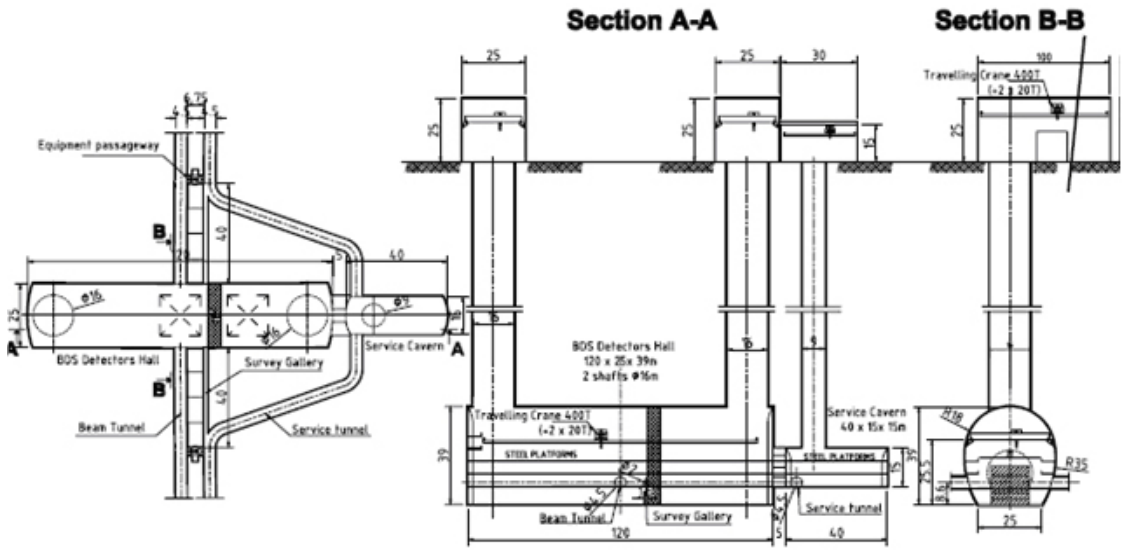

FIGURE 4.2-6. Schematic of Physics Detector Hall, showing BDS Service Cavern Arrangement

Types of surface buildings considered included: surface equipment buildings, including cooling towers and pump stations; shaft head buildings; storage areas; local workshops and assembly areas, local technical offices etc. The majority of these buildings are concentrated at the 'central campus'and specifically at the Interaction Region. The remaining buildings are located at the shafts positioned along the Main Accelerator Housing. Concrete construction with acoustic absorbent material is used for buildings which contain 'noisy'equipment; the remaining buildings have steel structures and insulated steel 'sandwich'type panels for roof and wall cladding on concrete foundations. In all cases, the design of the buildings takes into account the local climatic loads, seismic load (according to local standards) and fixed or moving loads linked to the use of that building. The requirements for each building type have been considered in making the cost estimate. Overhead cranes, gantries, elevators and other lifting gear with appropriate capacity are included where necessary in surface and underground structures. A detailed breakdown of the surface buildings can be found in [123].

4.2.5 Site Development

For the areas where surface buildings are located (central campus, shaft positions), the following items have been included in the cost estimate:

- fences and gates;
- roads and car parks within fences and from fence to existing road network;
- pedestrian walkways;
- lighting for the above and around buildings including buried electrical connections;

- all necessary drains along roads, car parks, including sumps, water treatment facilities and connections to existing mains;
- all necessary water supply pipes, tanks and connection to existing water supply network;
- landscaping and planting of trees, bushes, seeding of grass as required;
- spoil dumps (where applicable) created close to the building areas, including landscaping.

All temporary facilities needed for the construction works as well as the necessary site preparation before start of the works are also included in the cost estimate.

4.2.6 Regional Variants

Both the Americas and European sites are similar deep tunnel sites and both utilize vertical shafts for access as described in the sections above. These shafts are respectively 135-100 m deep. The Asian site is somewhat different, in that it is located along the side of a mountain. With the exception of the two central shafts for servicing the Detector Hall at the IR, long almost horizontal access tunnels are used instead of vertical shafts. The lengths of these access tunnels range from 700 m to 2000 m. Other variants which are due to construction methods depending on local geology are covered in Chapter 5.

4.3 A.C. POWER DISTRIBUTION

Electrical power is categorized by three major systems:

- RF power (modulators);
- conventional power (normal conducting magnet power supplies, cryogenic plants, electronic racks, surface water plant systems and infrastructure components);
- emergency power provided by back-up generators (emergency lighting, sump pumps and ventilation systems for sub-surface enclosures).

The power requirements are dominated by the RF system (modulators) located in the Service Tunnel along the length of the Main Linac. Table 4.3-1 gives an overview of the estimated *nominal* [1] power consumption for 500 GeV center-of-mass operations, broken down by system area and load types. The cost estimate is based on a total nominal power requirement of 227.3 MW. The additional required power for a potential upgrade to 1 TeV centre-of-mass is not included in the current estimate.

High voltage connections to the local utility grid voltage varies by regions, ranging from 275kV (Asia), 345kV (America) and 400kV (Europe). All regions provide for a main substation located at or near the Interaction Region/Central Damping Ring for connection to the local utilitys high voltage transmission system. Standards for GRID, High- and Low-Voltage distribution also tend to vary across the regions; consequently the exact choice of approach to distributing the power to the machine components is slightly different for the three sample sites. However, the salient features remain the same:

[1] Nominal electrical power requirements have been developed (as much as practical) as continuous power, sometimes denoted as wall power. Actual connected or installed power is 30 to 50% higher.

TABLE 4.3-1
Estimated Nominal Power Loads (MW) for 500 GeV Centre-of-Mass Operation

AREA SYSTEM	RF	CONV	NC MAGNETS	WATER SYSTEMS	CRYO	EMER	TOTAL (by area)
SOURCES e-	1.05	1.19	0.57	1.27	0.46	0.06	4.59
SOURCES e+	4.11	7.32	6.52	1.27	0.46	0.21	19.89
DR	14.0	1.71	6.78	0.66	1.76	0.23	25.15
RTML	7.14	3.78	2.84	1.34	0.0	0.15	15.24
MAIN LINAC	75.72	13.54	1.41	9.86	33.0	0.4	134.84
BDS	0.0	1.11	18.48	3.51	0.33	0.20	23.63
DUMPS	0.0	3.83	0.0	0.0	0.0	0.12	3.95
TOTAL (by system)	102.0	32.5	36.6	17.9	36.9	1.4	227.3

- Connection to the main Grid system via a main substation located at the central campus.
- The GRID voltage is stepped down to the High-Voltage (HV, 20-66 kV) for distribution across the site to the shafts (access points);
- From the shaft locations, the power is further distributed into the Service Tunnel. For the Main Accelerator Housing, this implies a distribution of approximately ±2.5 km. The HV is distributed directly to the RF stations (modulators). For the Low-Voltage (LV), local transformers are located along the Service Tunnel which tap-off the HV distribution.

An optimized engineering solution for the power distribution is in general heavily influenced by the choice of site: availability and location of local power substations; regional voltage standards; local (regional) safety regulations. The design work for this report was developed globally by identifying site-dependent and site-independent infrastructure, the former being developed by the regions and the latter being based on a European estimate. Details can be found in [1]. In the following sections, the European solution is generally presented. Important regional variations are briefly dealt with in Section 4.3.6.

4.3.1 Network Configuration

The network is designed to give priority to safety rather than to operations. All trip orders are by under-voltage release, and an emergency stop system is included. The design of the power distribution system is based on operational requirements, and is separated into two networks: machine systems and services. Back-up supplies are included to operate the accelerator safety systems during an interruption in the power network.

The voltage level chosen for the High-Voltage (HV) distribution is 66/6 kV, 36 kV and 69/34 kV for the Asian, European and Americas regions respectively. The local Low-Voltage

(LV) systems are hundreds of volts. The HV substations including the one at the central campus are equipped with two bus-bars connected by a bus-tie. (machine network and the services network). The high voltage protection is based on numerical relays with facilities for programmable automated sequences, and for recording network perturbations; this allows every HV feeder to be monitored by the Supervisory Control and Data Acquisition system (SCADA). Standardized switchboards downstream of the transformers are used to locally distribute the LV.

4.3.2 Distribution for the Main Accelerator Housing

Two HV cable lines are routed along those sections of Service Tunnel containing SCRF cryomodules (Main Linac and RTML):

- One HV line serves the RF itself (Modulator), with an RMU installed every RF unit (∼38 m) connected directly to it.
- The second HV line feeds conventional services, with a HV/LV fused-switch 500 kVA transformer and RMUs located every four RF units (∼152 m). Individual feeders or short power lines along the 152 m section are used. Each power line is protected by a circuit breaker at the switchboard downstream of the transformer. The switchboard is situated next to the power transformer and the RMU in the Service Tunnel, and supplies 152 m of both the Beam and Service Tunnels.

In those sections of the Main Accelerator Housing where there are no RF units (warm sections of RTML and the BDS), only the conventional services HV line is installed. The same 152 m module structure is used in these areas. For the BDS sections, individual transformers are rated 1000 kVA each instead of 500 kVA due to the higher density of the load (larger number of normal conducting magnets)

The required LV power is supplied to the Beam Tunnel via the connecting penetrations, spaced approximately 12 m apart (12 per 152 m distribution unit).

4.3.3 Distribution for the Central Injectors

Power for the central injectors (Damping Rings, sources and injector linacs) is taken directly from the GRID/HV substation located at the central campus.

The SCRF is responsible for about two-thirds of the total power requirement for the Damping Rings, the remaining third being the normal conducting magnets and superconducting wigglers. Due to the restricted tunnel cross section the HV equipment is installed partly on the surface, and partly in the tunnel alcoves (see Section 4.2.2). The Damping Rings tunnel is supplied from a closed HV cable loop originating at one of the two Damping Ring service shafts. A distribution substation is installed on the surface, fed directly from the central area via a HV cable link. The surface equipment at the second service shaft is also fed from the loop. A LV transformer and cable link supplies the power in the shaft base alcoves. RF and other large power consumers are fed from a dedicated HV breaker on the surface.

For the remaining four subterranean alcoves located in the Damping Ring straight sections, an underground substation is created using an RMU. The LV distribution in the Damping Ring tunnel uses power lines with drops to distribution boxes. The LV lines in the tunnel

feed lighting, socket outlets, general power and possibly minor machine system loads. The lines are shorter than 700 m to provide proper protection and obtain a sufficient fault level, even at the end of the line. The switchboard feeding the power lines is situated in the alcoves together with the power transformer and the HV ring main unit.

The sources are essentially concentrated in short tunnels and caverns. The equipment for each of the sources is fed from a short HV line equipped with RMUs. Dedicated transformers are installed for the RF for the source capture sections and SCRF injector linacs, the remaining part of the load is fed from the conventional facilities supply.

4.3.4 Interaction Region

The power needs of the detectors are currently not known. The current design is estimated based on detector equipment of 3 MVA, scaled down from CMS. A HV feeder has been reserved for the detectors.

4.3.5 Emergency Supply Systems

The emergency supply system is based on stand-by diesel generator sets. Each generator set supplies a protected substation, which is normally supplied by the grid. In case of a mains fault, the diesel engines start automatically and take over the critical load when ready. This causes a short break of ∼30 seconds. On return of mains power, the diesel generator sets synchronize to the mains and then the load is commutated back to the grid, after which the diesel generators shut down.

Since certain shafts are located at a distance too far for a LV distribution, the generators must have an output voltage of a few kV. Very critical systems that cannot accept short breaks have to be installed downstream of Uninterruptible Power Supply (UPS) systems, or no-break systems. The Main Linacs and the RTML zones are equipped with a 3.6 kV line with an RMU at regular intervals. The Damping Ring tunnel is equipped with a 3.6 kV line, originating at one access shaft of the ring and with an RMU in each alcove or cavern. Each of the RMUs feeds the critical load through a 3.6kV/LV transformer. A 48 V D.C. system with battery back-up is installed in all substations for network operations. The 48 V is chosen as the highest standard voltage benefiting from VLV regulations.

4.3.6 Miscellaneous Technical Issues

Power quality considerations A separation of pulsed and a non-pulsed systems may be needed to avoid interference between certain loads. Reactive power compensation and harmonics filtering may also be needed, depending on the non-linear load and the dynamic behaviour of the load.

Transformers In general dry transformers are used for HV and LV, either cast resin moulded or impregnated. These transformers require very little maintenance, can be installed in limited space, and offer a reduced level of fire hazards compared to oil-immersed units.

4.3.7 Regional Variations

Table 4.3-2 gives an overview of the various voltages assumed for the regions.

TABLE 4.3-2
Various Voltage Levels Assumed for the Regions. Note that there are two levels of HV distribution assumed for the Americas and Asian sample sites

VOLTAGES	Europe	America	Asia
Transmission	400 kV	345 kV	275 kV
Distribution	36 kV	69 kV	66 kV
Distribution	36 kV	34 kV	6 kV
Distribution	400/230 V	480/277 V	400/200 V

European Sample Site: The description of the power distribution given above is primarily that adopted for the European site (and the cost estimate). The GRID voltages are assumed to be 400 kV, with the HV levels set to 36 kV (a European standard). LV levels are typically 400 V (three phase) and 220-240 V (single phase).

Asian Sample Site: The distribution of power is slightly different to that documented above. The GRID level is 274 kV, and is lowered to 66 kV and distributed via the Service Tunnel to the secondary substations located in each access base caverns. Secondary substations transform the power to 6.6 kV which is distributed through triplex cable to a large number of small converters. A LV of 400 V (three-phase) and 100-200 V (single-phase) is supplied via local transformers from the 6.6 kV. The system applies to power transport and distribution in whole underground areas.

Americas Sample Site: The Americas distribution also varies slightly in that the GRID level of 345 kV is first transformed to 69 kV at the master substation. The 69 kV is routed through the tunnel to each shaft, and then up the shaft to where it is stepped down to the medium distribution voltage (34.5 kV).

4.3.8 Information Network

Site-wide communications are in general be supported via a fiber-optic based LAN system. For the underground areas, local LAN racks are located in the tunnel at an interval of approximately 200 m, which serve as the primary connection point to the end equipment (via electrical cables). From here the signals are sent to sub-center LAN racks located in the Shaft Bases, and finally to the central control center.

The LAN supports the following equipment:

- General digital data transfer.
- Telephone system: 1,800 codeless lines and 240∼360 fixed lines are assumed. Cordless telephones are supported in the underground areas via IP transmitters.
- Public address system (including safety address system): for the underground areas, speakers are mounted every 10 m of tunnel.
- Security CCTV and other video monitoring where needed (both surface buildings and underground areas).
- Fire alarms, smoke detectors etc.

TABLE 4.4-1
HVAC Requirements

Location	Temperature (drybulb)	Dewpoint	RH	Air Flow
e- Source	29 °C	< 13 °C	< 35%	27 m/min
Damping Ring	40 °C	<13 °C	<20%	27 m/min
Main Accelerator Service Tunnel	29 °C	<13 °C	<20%	27 m/min
Main Linac Beam Tunnel (not contr.)	>30 °C	<13 °C	<35%	27 m/min
BDS Beam Tunnel	40-43 °C	<13 °C	<20%	27 m/min
IR Hall	29-32 °C	<13 °C	<35%	27 m/min

In the case of the critical safety-related systems, emergency back-up power is supplied from the standby generator in case of power failure.

4.4 AIR TREATMENT EQUIPMENT

Figure 4.4-1 shows the air-flow and treatment for a typical section of Main Linac. Conditioned ventilation airflow of 68,000 m^3/hr is ducted down every major shaft and routed into the Service Tunnel at the base of the shaft or Access Cavern in both directions. Air flows through the Service Tunnel to the midpoint between the major shafts (∼2.5 km) where it is directed through a protected air passageway into the Beam Tunnel and returned back to the shaft area. The return air is ducted to the surface where 15% (10,200 m^3/hr) of the stale air is vented to the outdoors, and an equivalent amount of fresh conditioned outside air is mixed back in with the remaining circulated air. While at the surface, the air is cooled, dehumidified and/or heated as needed to achieve a neutral dry condition approximately 24-27°C dry bulb and 40% relative humidity. The supply air is then ducted back to the Service Tunnel. This air flow pattern requires evaluation by radiation safety personnel.

The conditioning units are located on the surface and reject tunnel heat and moisture to the ambient air. Air is supplied to the tunnel at a flow rate of approximately 27 m/min; this provides one complete air exchange every 6 hours in the entire tunnel volume. Additional non-conditioning exhaust and supply fans are provided at each shaft to double and/or reverse the airflow during emergency operation. Common ducts are used for both systems separated by configuration control dampers. Elevator shafts and exit vestibules are provided with separate air systems for control and pressurization during emergency operation.

4.4.1 Controls

The temperature and humidity in the Service Tunnel are primarily set by regional standards for allowing personnel to be in the tunnel at moderate work levels with no required rest periods. The requirements for the tunnels in each of the system areas are summarised in Table 4.4-1. In general, air temperature in the Service Tunnel is controlled at 27-29°C using chilled water Fan Coil Units (FCU), as described in Section 4.2.5. In the Main Linac sections, the FCUs are located at every RF unit.

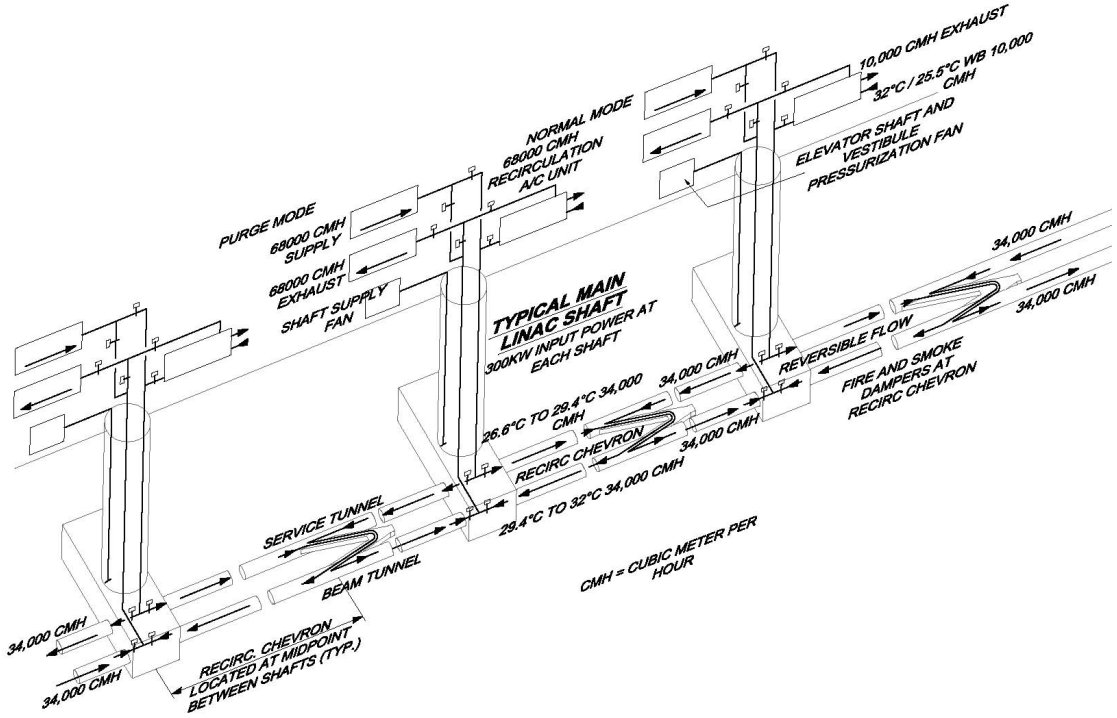

FIGURE 4.4-1. Air Treatment Concept for the Main Accelerator Housing.

TABLE 4.5-1
Summary of Heat Loads broken down by Area System

Area System	LCW	Chilled Water	Total
	(MW)	(MW)	(MW)
SOURCES e-	2.880	1.420	4.300
SOURCES e+	17.480	5.330	22.810
DR e-	8.838	0.924	9.762
DR e+	8.838	0.924	9.762
RTML	9.254	1.335	10.589
MAIN LINAC	56.000	21.056	77.056
BDS	10.290	0.982	11.272
DUMPS	36.000	0.000	36.000
TOTAL HEAT LOAD (MW)			182

Temperature control in the Main Linac Beam Tunnel is not provided because of the relatively low heat loads. The humidity level is maintained by the air circulation from the Service Tunnel and by packaged dehumidification units located approximately every 100 meters. Beam Tunnel temperatures in the BDS are maintained locally at 40-43°C by FCUs.

4.5 PROCESS COOLING WATER

Cooling water is required as a heat rejection medium for technical components such as the water cooled RF components, water cooled magnets, and water dumps in the BDS. The majority if not all of these require low conductivity/deionized water (LCW). Further study is needed to establish water quality requirements. The following descriptions present a reference solution that is generally applicable for all regions, ignoring minor regional site differences.

4.5.1 Heat Loads

Table 4.5-1 summarizes the estimated heat-loads broken down by Area Systems. Of the total load of ∼182 MW, over half is attributed to the Main Linac. Table 4.5-2 lists the heat loads for the Main Linac RF unit.

4.5.2 System Description

There are two water cooling systems; Process Water and Chilled Water. Chilled Water is used for water cooled racks in each RF area and for fan coils that remove the heat rejected to the tunnel air. The Process Water handles the water cooled technical components. The scope of the Process Water cooling included in conventional facilities includes the surface cooling towers, pumps, controls, cavern heat exchangers, skids and piping headers, and distribution and valving up to the water cooled components. Final hose connections to each water-cooled

TABLE 4.5-2
Typical Main Linac RF Component Heat Loads

Components	Tunnel	Total	Average	To Water	To Air
		(KW)	(kW)	(KW)	(KW)
RF Charging Supply 34.5 Kv AC-8KV DC	Service	4.0	4.0	2.8	1.2
Switching power supply 4kV 50kW	Service	7.5	7.5	4.5	3.0
Modulator	Service	7.5	7.5	4.5	3.0
Pulse Transformer	Service	1.0	1.0	0.7	0.3
Klystron Socket Tank / Gun	Service	1.0	1.0	0.8	0.2
Klystron Focusing Coil (Solenoid)	Service	4.0	4.0	3.6	0.4
Klystron Collector/ Body/Windows	Service	58.9	47.2	45.8	1.4
Relay Racks (Instrument Racks)	Service	10.0	10.0	0.0	-1.5
Circulators, Attenuators & Dummy Load	Beam	42.3	34.0	32.3	1.7
Waveguide	Beam	3.9	3.9	3.5	0.4
Subtotal Main Linac RF unit (KW)			120		

technical component are included in the relevant Technical System. The tower system for the cryogenics is considered part of the Cryogenics Technical System.

All water systems are closed loop. The cooling tower type is a closed circuit cooler similar to a dry cooler. The tower works dry by releasing the heat directly to the air during most of the year. During hot periods in the summer seasons, the towers/coolers are wetted with water in order to guarantee the supply temperature. This setup minimizes and conserves water and treatment chemicals and associated cost, as compared to typical open type towers. The closed circuit coolers also minimize plume from the tower. The make-up water to the system and tower is supplied from a well with proper water treatment, from each surface water plant.

Figure 4.5-1 shows a schematic of a typical Process Water Plant. The Process water system has three closed water loops:

- The first is a water/glycol mixture loop from the surface cooling tower to the cavern heat exchanger at 29.4 °C supply temperature.
- The second is a process water loop from the cavern heat exchanger at 32.2 °C supply temperature to the LCW skid in the Service Tunnel. The heat exchanger in the cavern is needed to offset the effect of the static head on system pressure due to the tunnel depth.
- The third is the demineralized/LCW water from the skid at 35 °C supply temperature.

The supply water temperature has a tolerance of ±0.5°C. The basis for pipe sizing and costing is for a ΔT ∼11°C water system. The return pipe is thermally insulated to reduce the heating of the tunnel air. This setup is applicable for the Main Linac; a variation of this scheme is used for other areas. In the case of the Process Water supply to the large BDS

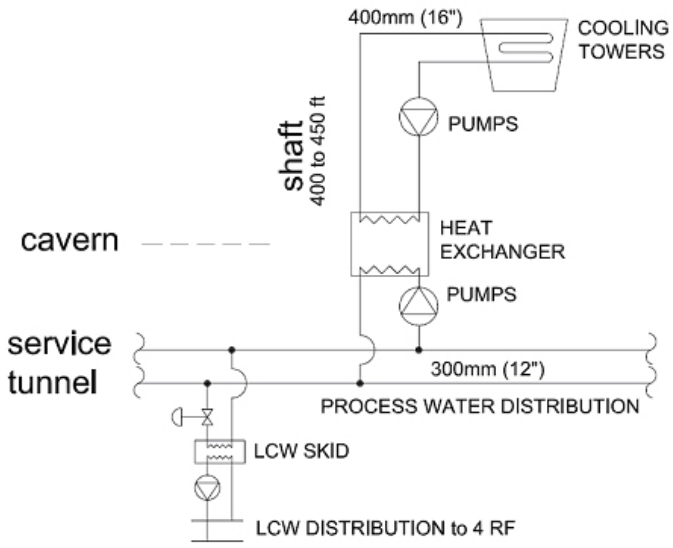

FIGURE 4.5-1. Process Water System at Shaft 7 Plant.

(main) beam dumps, a near surface buried piping distribution from a surface plant at the IR location is fed into each dump cavern hall through individual drilled shafts. (The cooling system for the main high-powered beam dumps is discussed elsewhere.)

The Chilled Water system provides ~6.6°C supply temperature water to fan coils and to the water skid for racks. The water skid, in turn, regulates and provides the proper temperature (above dew point) to the water cooled RF racks. The major components for this system are the same as for the Process Water except for the addition of Chillers on the surface. All chilled water piping is thermally insulated (see Fig. 4.5-2).

4.5.3 Locations and Distribution

The main distribution of the Process Water system follows the major shaft and cryogenic distribution locations. There are twelve surface water plants. For the reference solution, the distribution is simplified to minimize the number of area systems served by each water plant (considered consistent with the current estimate). Only the Main Linac RF system has been considered in any detail. Estimates for other areas have been scaled from the Main Linac model based on their respective loads.

One Low Conductivity Water (LCW) skid is used for cooling all the water cooled technical components for every four Main Linac RF units. Each LCW skid includes one stainless steel centrifugal pump (with no standby), one plate heat exchanger, controls, stainless steel expansion tanks, and miscellaneous fittings and accessories.

Similar to the LCW skid, one chilled water skid for racks is provided for every 4 RF units. This skid is a commercially available package coolant modulating unit typically used in data center rack applications. Each skid includes a multi-stage centrifugal pump, brazed plate heat exchanger, 3-way control valve, expansion tank, flow switch and integrated controls.

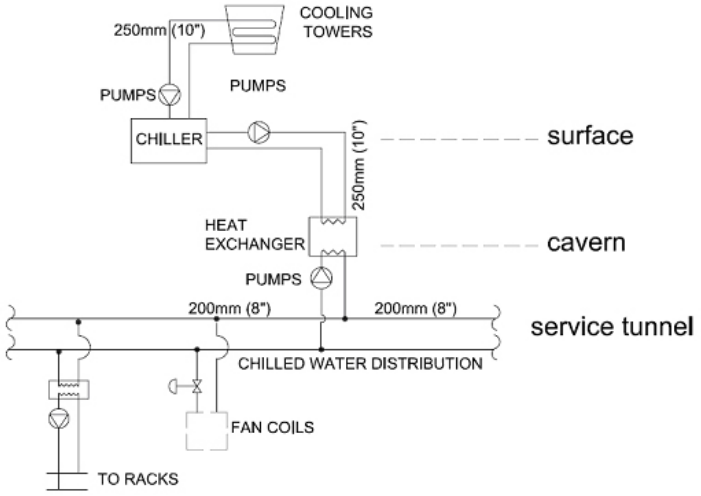

FIGURE 4.5-2. Chilled Water System at Shaft 7 Plant.

4.6 SAFETY SYSTEMS

4.6.1 Radiation safety

The radiation safety systems are described in Section 2.9.4.

4.6.2 Fire Safety

Because there are no existing laws and standards in any region which directly and comprehensively stipulate the safety measures for a facility like ILC, the currently planned safety measures are based on examples of existing accelerator tunnels and the regulations for buildings and underground structures of various types. The final plan will be subject to the approval of the competent authority that has jurisdiction over the selected site.

Evacuation of the underground Service Tunnel is the primary concern, due to the relatively high level of cables. In the event of a fire in the Service Tunnel, personnel can escape to the safety of the Beam Tunnel via the Beam-Service Tunnel personnel cross-overs, located every 500 m (see Figure 4.6-1). Egress to the surface is only possible at the shafts, located every 5 km. Assuming a walking speed of 1 m/s, 500 m between emergency egress points is considered acceptable (∼8 minutes maximum). During beam operations, triggering of a fire alarm will immediately de-energize the machine, making it safe for personnel to enter the Beam Tunnel.

During access periods or installation, when personnel are present in the Beam Tunnel, emergency egress can be either to the Beam or Service Tunnel, depending on the location of the fire.

For the Damping Rings (during installation and maintenance), emergency egress is to a separate safety enclosure behind a fire wall within the tunnel (see Section 4.2.2).

In all cases, personnel can either safely escape to the surface via the nearest shaft, or remain in a fire-safe area until the emergency services respond.

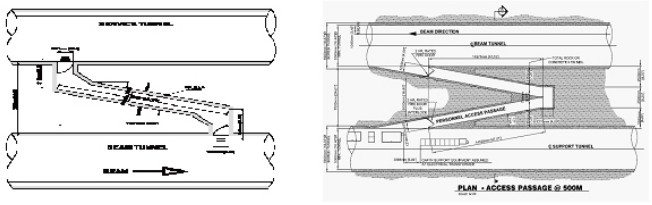

FIGURE 4.6-1. Examples of the personnel cross-connection passages between the Service and Beam Tunnels (left Asia and Europe, right Americas). The geometry of the passage is designed to reduce the radiation levels in the Service Tunnel to acceptable levels.

Smoke detectors are installed in all underground tunnels and halls at intervals of 30 m. Manual alarms (buttons) are located at intervals of 100 m. Alarm bells are also installed at intervals of 100 m. A smoke exhaust fan of 60,000 m^3/hr is installed at each Shaft Access Building on the surface. 1.2 m^2 ducts are installed in the Access Shafts/Tunnels to connect the fans and the Access Hall.

No emergency smoke exhaust system is installed in the tunnels. Instead, movement of the smoke is retarded by 1.5 m high walls mounted to the top of the tunnels at intervals of 50 m. Simulations using software developed and widely used in Japan indicate this solution is more effective than a mechanical exhaust system

Provisions for the required emergency fixtures are also included in the current estimate:

- emergency lighting located every 8 m;
- illuminated exit signs installed above every exit door in the underground spaces;
- illuminated exit direction signs installed at intervals of 20 m in the underground spaces;
- portable chemical powder fire extinguishers (3.0 kg) placed every 30 m in the Service Tunnel, Beam Tunnel and for Asia Site the Access ramps;
- large size fire extinguishing equipment (30 kg) located every 200 meters in the Access Halls and the Experimental Hall.

Sprinklers, hydrants and water curtains have not been specified to avoid possible water damage to the machines.

4.6.3 Safety Access Control

Access control equipment such as a card lock is installed at the entrances to the radiation control areas as required by the radiation safety plan.

4.6.4 Safety for Helium

The helium supply system is equipped with an oxygen meter which activates an alarm and stops the gas supply in case of oxygen deficiency. Air in the Beam Tunnel is automatically pressurized.

4.7 SURVEY AND ALIGNMENT

Survey and alignment covers a very broad spectrum of activities, starting from the conceptual design of the project, through the commissioning of the machines, to the end of operations. The cost estimate developed covers the work necessary until successful completion of the machine installation. It includes equipment needed for the tasks to be performed, and equipment for a dedicated calibration facility and workshops. It also includes the staff that undertake the field work, and the temporary manpower for the workshops. Full time, regular staff is considered to be mainly dedicated to organizational, management, quality control, and special alignment tasks. The cost estimate is mostly based on scaling the equivalent costs of the LHC to the ILC scope.

4.7.1 Calibration Facility

A 100 m long calibration facility is needed for the calibration of all the metrological instruments. The facility is housed in a climate controlled and stable building. Due to the range limit of current day commercial interferometers against which the instruments are to be compared the facility has been restricted to 100 m. A mechanical and an electronic workshop are also needed during the preparation phase and throughout the entire project. They are used for prototyping, calibration, and maintenance of the metrological instruments.

4.7.2 Geodesy and Networks

A geodetic reference frame is established for use across the whole site, together with appropriate projections for mapping and any local 3D reference frames appropriate for guaranteeing a coherent geometry between the different beam lines and other parts of the project. An equipotential surface in the form of a geoid model is also established and determined to the precision dictated by the most stringent alignment tolerances of the ILC.

The geodetic reference frame consists of a reference network of approximately 80 monuments that cover the site. These monuments are measured at least twice, by GPS for horizontal coordinates, and by direct leveling for determining the elevations. The first determination is used for the infrastructure and civil engineering tasks. The second, and more precise determination, is used for the transfer of coordinates to the underground networks prior to the alignment of the beam components. A geodetic reference network is also installed in the tunnel and in the experimental cavern. For costing purposes it is assumed that the reference points in the tunnel are sealed in the floor and/or wall (depending on the tunnel construction) every 50 m. In the experimental cavern, the reference points are mostly wall brackets. The underground networks are connected to the surface by metrological measurements through vertical shafts. The distance between two consecutive shafts does exceed 2.5 km in most cases.

4.7.3 Civil Engineering Phase

The layout points which define the tunnel locations and shapes are calculated according to the beam lines in the local 3D reference frame. The tunnel axes are controlled as needed during the tunnel construction. All tunnels, including profiles, are measured in 3D using laser scanner techniques when the tunnels are completed. The same process is applied to the experiment

cavern(s) and other underground structures. The buildings and surface infrastructure are also measured and the as-built coordinates are stored in a geographical information system (GIS).

4.7.4 Fiducialization

Systematic geometrical measurements are performed on all beamline elements to be aligned prior to their installation in the tunnels. The alignment of elements installed on common girders or in cryomodules is first performed, and the fiducial targets used for the alignment in the tunnels are then installed on the girders (cryomodules) and all individually positioned elements. The positional relation between the external markers and the defining centerlines of the elements are then measured. For this report, an estimated 10,000 magnetic elements were assumed to need referencing. It is also assumed that most corrector magnets do not need fiducialization. This number does not account for instrumentation, collimators, or other special beam elements.

4.7.5 Installation and Alignment

The trajectories of all the beamlines are defined in the local 3D reference frame which covers the entire site. The location of reference markers at the ends of each beam line element to be aligned are defined in this reference system, together with the roll angle giving a full 6 degrees of freedom description of element location and orientation. Likewise the position of all geodetic reference points is determined in this reference frame.

Prior to installation, the beamlines and the positions of the elements are marked out on the floors of the tunnels. These marks are used for installing the services, and the element supports. The supports of the elements are then aligned to their theoretical position to ensure that the elements can be aligned whilst remaining within the adjustment range of the supports.

After installation of services such as LCW and cable trays, the tunnels are scanned with a laser scanner. The point clouds are then processed, and the results inserted into a CAD model. A comparison with theoretical models is used by the integration team to help identify any non-conformity and prevent interference with the subsequent installation of components. The current requirements for the one sigma tolerances on the relative alignment of elements or assemblies are given in Table 4.7-1.

The components are aligned in two steps:

- A first alignment is performed to allow connection of the vacuum pipes or interconnection of the devices. This is done using the underground geodetic network as reference.
- After all major installation activities are complete in each beamline section, a final alignment, or so-called smoothing, is performed directly from component to component in order to guarantee their relative positions over long distances.

To reach and maintain the positioning tolerances of the final doublets in the BDS IR, a 150 m straight reference line is set up as close as possible to the beam components. This line, consisting of a laser or stretched wire and hydrostatic levels, is housed in a dedicated gallery built parallel to the beam tunnel, and goes through the experimental cavern. This allows for the geometrical connection between the beam lines and the detector.

TABLE 4.7-1
Component Alignment Tolerances

Sources, Damping Rings and RTML	Offset Roll	150 μm (horizontal and vertical), over a distance of 100 m. 100 μrad
Main Linac (cryomodules)	Offset Pitch Roll	200 μm (horizontal and vertical), over a distance of 200 m. 20 μrad
BDS	Offset	150 μm (horizontal and vertical), over a distance of 150 m around the IR.

4.7.6 Information Systems

The theoretical positions of all the components to be aligned on the beam lines is managed in a dedicated database. This database is also used for managing all the geodetic and alignment measurements and the instrument calibrations. All measurement data are captured and stored electronically and subsequently transferred to the database. Pre-processing of the measurements are carried out in the database and then dedicated software for data analysis is used to calculate the best fit position of the elements and components. These results are also stored in the database where they can be accessed for further post-processing, analysis and presentation. A geographic information system (GIS) is set up for managing all location data.

4.8 CFS COST METHODOLOGY

The cost for the ILC CFS has been developed internationally with teams in each of the three regions (Americas, Asia and Europe). These teams have worked closely together to optimize the CFS design, based on the requirements supplied by the Area and Technical Systems.

To make use of the available resources for the design and cost work, a detailed WBS for the project was produced, containing up to 5 levels of detail. This WBS was then broken down into site-dependent and site-independent sections. For the site-dependent estimates, the CFS group established a set of uniform definitions for underground construction unit costs. This ensured consistency across all three regions. Estimates for each unit cost were independently produced by experts and consultant engineering firms in each of the three regions (the Civil Engineering falls into this category, for example) and then used to develop each site-dependent design. The remaining site-independent parts were then divided up amongst the regional teams to produce single estimates as follows:

Civil Construction	Regionally developed
Electrical: site-dependent	Regionally developed
Electrical: site-independent	European estimate used
Air treatment facilities	Americas estimate used
Process cooling water	Americas estimate used
Handling equipment	European estimate used
Safety systems	Asian estimate used
Survey and Alignment systems	European estimate used

Cost estimates in all three regions were developed using the same criteria and drawings. information was drawn from consultant engineers, historical data from other accelerator or similar projects, industry standard cost estimating guides, and where applicable the scaling of costs from similar systems. In all cases, the estimates reflect a median value for the work based on the criteria provided to date and the pre-conceptual level of design maturity. There are no factors for contingency contained in any of the CFS costs estimates. Costs for activities that take place prior to the construction start are explicitly not included in the estimate. Some examples of such costs are A/E Services before the start of construction, development costs for geotechnical and environmental investigation, land acquisition costs and cost incurred for compliance with local governmental statutes and regulations. These costs cannot be accurately identified until a specific site selection is made.

4.9 INSTALLATION

This section still under review. Draft to be released by April 1, 2007.

CHAPTER 5

Sample Sites

5.1 INTRODUCTION

For this reference design, three 'sample sites for the ILC were evaluated. Each site was required to be able to accommodate all the conventional facilities for the 500 GeV CM machine; in addition, the sites needed to have the sufficient length to support an upgrade of the machine to 1 TeV CM, assuming the baseline main linac gradient. There were two reasons for the use of three sample sites for this reference design:

- This procedure demonstrates that each region can provide at least one satisfactory site for the ILC. This is important, since it shows that any of the regions has the potential to be a host for the project.
- The cost of, and technical constraints on, the project could depend strongly on the site characteristics. Since the actual site is not yet known, it is important to assess a range of sites with a diverse set of site characteristics, to provide confidence that when the actual site is chosen, it will not present unexpected technical difficulties or major surprises in cost.

In addition to the three sample sites presented, a second European sample site near DESY in Hamburg, Germany, has also been developed. This site is significantly different from the other sites, both in geology and depth (25 m deep), and requires further study.

The Joint Institute for Nuclear Research has also submitted a proposal to site the ILC in the neighborhood of Dubna, Russian Federation.

The three sites reported in detail here are all deep-tunnel solutions. The DESY and Dubna sites are both examples of shallow sites. A more complete study of a shallow site – either a shallow tunnel or a cut-and-cover site – will be made in the future as part of the Engineering and Design phase.

5.2 AMERICAS SITE

5.2.1 Location

The Americas sample site lies in Northern Illinois near the existing Fermi National Accelerator Laboratory. The site provides a range of locations to position the ILC in a north-south orientation. The range is bounded on the east by the Fermilab site, and extends some 30 km to the west. For the purpose of this document and the RDR estimate, a site alignment that is roughly centered on Fermilab was selected. While this site is more developed than an alignment to the west, there is a reasonable construction path and the location benefits more directly from the existing Fermilab site and facilities.

While the routing requires the tunnel to pass below residential areas, the shafts can be located in non-residential areas. It is highly possible that no homes will be physically affected by this project. Roughly one quarter of the alignment is on Fermilab property, including the ILC central campus and IR. The Fermilab site, is located approximately thirty-five miles west of downtown Chicago. The area surrounding Fermilab is comprised of residences, research facilities, light industry, commercial areas, and farmland. Higher population densities are found to the east with more rural and farm communities to the west. The towns and villages around Fermilab vary in population size from ten thousand to over one hundred thousand people. The surrounding communities have established schools, hospitals, infrastructure support functions and local governments.

The Fermilab site borders on a local railroad line with a railroad hub located within four kilometers to the south. Major roads connect Fermilab to the Illinois toll road system within two miles of its gates. Access to OHare International Airport and Midway Airport are via highways with travel times to these airports of less than one hour. Steel mills and other heavy industry are located both in Illinois and in neighboring states.

5.2.2 Land Features

The existing surface of northern Illinois is primarily flat, with surface elevations ranging from 200 meters to 275 meters above sea level. Much of the eastern half of northern Illinois is developed with Chicago suburban communities and municipalities including many commercial, residential and industrial complexes. Underdeveloped areas are currently used for agriculture. Major water bodies include Lake Michigan located approximately 65 kilometers east of Fermilab, the Illinois River approximately 30 kilometers southeast of Fermilab and the Fox River 3 kilometers west of Fermilab. An intricate highway system extends throughout the northeastern Illinois area.

The 2751 hectare (6800-acre) Fermilab site is also relatively flat with less than 15 meters of fall from northwest to southeast. Approximately one-third of the Fermilab site is developed with various high-energy physics accelerator complexes or related experimental areas. The remaining two thirds are equally split between leased agricultural uses and open space including prairies, wetlands and recreational areas. A series of paved roadways exist throughout Fermilab.

5.2.3 Climate

The climate is typical of the Midwestern United States which has four distinct seasons, and a wide variety of types and amounts of precipitation with moderate variations between

monthly and seasonal average values. In summer, temperatures ordinarily reach anywhere between 26°C to 33°C and humidity is moderate. Overnight temperatures in summer are usually around 17°C. Yearly precipitation averages 920 mm. Winter temperature averages -2°C during the daytime, and -10°C at night. T emperatures can be expected to drop below -18°C on 15 days throughout the winter season.

5.2.4 Geology

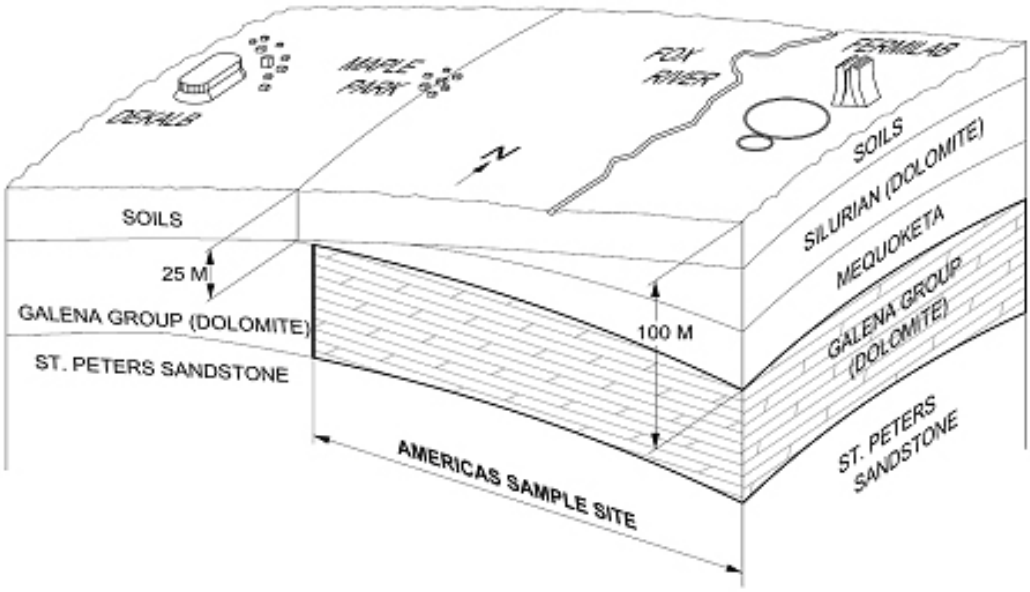

FIGURE 5.2-1. Geology of the Americas Sample Site

The tunnels are located in the Galena Platteville layer (Fig. 5.2-1), which is characterized as a fine to medium grained dolomite, that is cherty. The Maquoketa shales overlaying the dolomite have a low hydraulic conductivity that will act as a hydrogeologic barrier between upper overburden aquifers and the dolomite. At the proposed siting, the Galena Platteville varies from 100 to 125 meters in thickness, gently rising in datum elevation from the south to the north. The Galena is covered by 15 to 30 meters of shale, 15 to 25 meters of Silurian dolomite which in turn, is overlaid by 15 to 45 meters of overburden. The upper Silurian dolomite found at the Fermilab site disappears for alignments further to the west. These geologic conditions should provide a relatively dry tunnel, both during construction and during operations, but it is expected that some grouting will be required. The Galena is the most structurally sound rock in the area and, in general, should not require any extraordinary rock support methods.

5.2.5 Power Distribution

Electric power to the Northern Illinois area is provided by Exelon Generation with access to approximately 35,000 MW of electricity . Electrical power is generated by fossil fuel, hydroelectric, wind and nuclear power generating systems and distributed in Northern Illinois.

5.2.6 Construction Methods

Conventional un-shielded tunnel boring machines are used for the tunnels. No temporary support is required, permanent support can be pattern spaced rock bolts or dowels. Production rate is anticipated to be 30 m /day. Caverns are excavated using drill and blast methods. Temporary supports are required for the largest spans, permanent support is provided by rock bolts. Production rate for medium to large size caverns where mechanized equipment can be employed is estimated at 1,200 cm/wk. Shaft overburden is excavated using standard earth excavators and muck boxes, supported by ring beams and timber lagging, keyed into the underlying rock. Excavation through the limestone and shale to the final depth uses conventional Drill & Blast methods. Support is provided by resin encapsulated rockbolts and the shaft is reinforced and concrete lined.

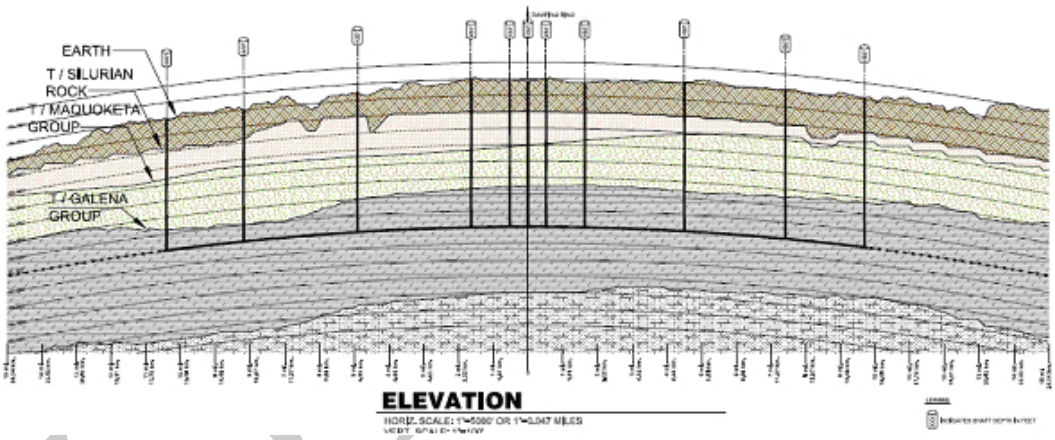

FIGURE 5.2-2. Longitudinal Profile of the Americas Site in Northern Illinois

5.3 ASIAN SITE

5.3.1 Location

A set of about 50 criteria have been used over the past decade to evaluate a large number of ILC candidate sites in Japan. Out of these candidates, a sample site was selected for the RDR with an endorsement by the ILC-Asia group at its 4th meeting in November 2005. It satisfies the following criteria, some overlapping with the criteria matrix developed by the CFS Global Group:

- Firm and uniform geology to ensure stable beam operation at the interaction region.
- Sufficient length to accommodate straight tunnels spanning over 50 km.
- Absence of any known, active faults in the neighborhood.
- Absence of epicenters of any known earthquakes exceeding M6 within 50 km from anywhere in the site since AD1500.
- Uniform altitude of the terrain so that the ILC tunnel depth is less than 600 m throughout.
- Availability of sufficient electrical power for ILC operation.
- Existence of a practical construction plan for the underground tunnels and caverns.
- Suitable environment, in terms of climate and access, for smooth operation.

The Asian site is located in a moderate plateau area (low mountains) in uniform solid rock. It is within 10 to 20 km of cities which provide a living environment with reasonable quality of life. The neighboring cities are connected to an international airport within several hours by both bullet train and highway.

5.3.2 Land Features

The site surface is dominated by woods and is partly occupied by an agricultural area which is crossed by occasional local paved roads. Only a few local residences exist along the tunnel route. There are no major high-ways or streets with heavy traffic and no large river systems which cross the tunnel route. Hence, very few sources of natural or human-made vibrations exist. An adequate flat surface area is available to accommodate surface facilities. Existing local roads can be utilized as access routes to entrances of the tunnel.

5.3.3 Climate

The climate is mild. There is snowfall in winter but only for a short period. It is not too hot in summer. There is no recorded history of major typhoons.

5.3.4 Geology and Tunnel Structure

The 31 km ILC tunnels for the first project phase can be constructed within solid hard rock. In the second project phase, when the tunnels are extended to 50 km, one side of the main linac tunnel will pass through an area with sedimentary rock, but this geology is also solid. The depth of the tunnels, which will be built in a low mountainous part of the site, is in the range between 40 m and 600 m. Most of the access to the tunnel is provided by sloped ramps (Fig. 5.3-1). An exception is the access to the interaction region which has a vertical shaft approximately 112 m deep.

Past experience with Japanese construction projects indicates that the uniform granite has sufficient strength that the tunnels and caverns do not require reinforcement by rock bolts or concrete lining. Shotcrete is used to cover the inner surfaces of the tunnels. Excavation of very large caverns, such as the experimental hall, may require reinforcement by rock bolts.

5.3.5 Power Distribution System

The site is located in the neighborhood of an existing 275 kV power grid. It is considered to be reasonably straightforward to supply the power of 240 MW required for the 500 GeV ILC. Power failures in Japan are very rare, and even if they occur, the system average interruption duration index (SAIDI) [1] has been only 13 minutes, according to the statistics of the Ministry of Economy, Trade and Industry of Japan.

5.3.6 Construction Methods

The geology is uniform hard granite below 20 m of softer topsoil and weathered rock. The access shafts are sloped tunnels excavated by NATM (New Austrian Tunneling Method), except for the IR hall. These tunnels match the mountainous geography and allow vehicle transport of personnel and materials. They are 7.5 m x 7.0 m to accommodate access for the TBM. From the surface to a depth of 20 m, the tunnel is reinforced by rock bolts, a 15-20 cm thick shotcrete liner and steel supports. In the granite, the tunnel is reinforced by rock bolts and 5 cm thick shotcrete.

The IR vertical shafts are excavated by drill and blast, with metal supports and a concrete lining. Caverns are excavated by NATM. The top of the arch is excavated by advancing top drift method with drill and blast. Reinforcement is by rock bolt, pre-stressed bolt and sprayed concrete 20 mm thick with a metal mesh, overlaid by a 1.5 m thick cast concrete liner on the arch. The lower part of the cavern is excavated by drill and blast. After reinforcement in the same method as the top, the side wall is finished with 1.0 m thick concrete, and the concrete floor cast 2.0 m thick. Passageways are excavated manually and finished with sprayed mortar and pre-mixed fiber 20 mm thick.

[1] System average interruption duration index s̄um of customer interruption durations normalized by the total number of customers served

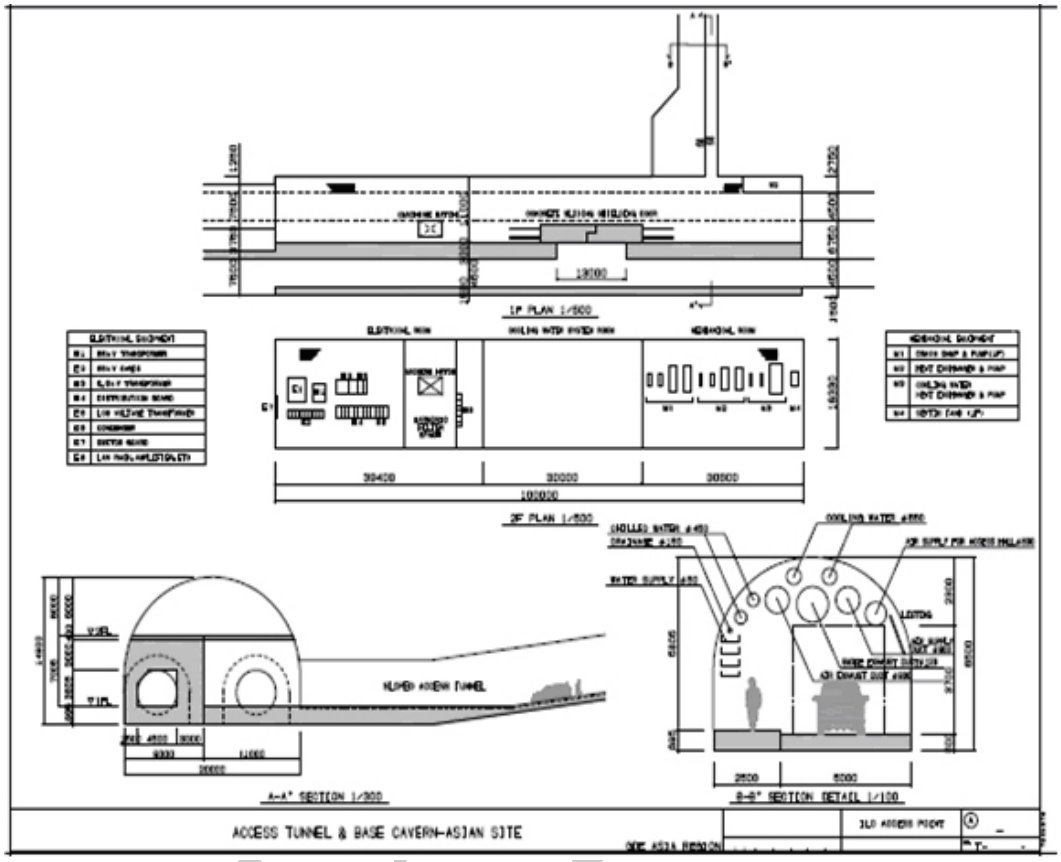

FIGURE 5.3-1. Detail of an Access Ramp for the Asian Sample Site

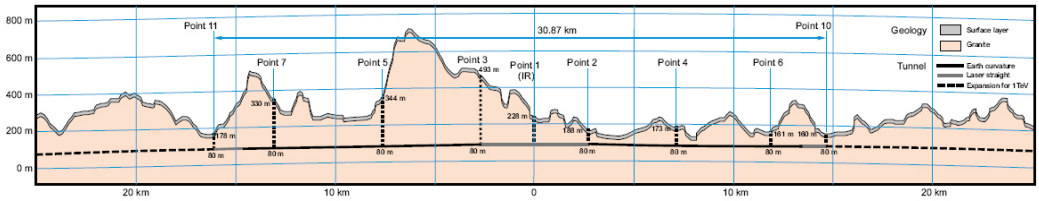

FIGURE 5.3-2. Longitudinal profile of the Asian Sample Site in Japan

5.4 EUROPEAN SITE

5.4.1 Location

The European site for the ILC is located in the north-western part of the Geneva region near the existing CERN laboratory. The area is fairly well populated; the more than 30 km long path of the accelerator crosses the border between France and Switzerland three times and passes under several villages. The region around the accelerator path is mainly covered with agricultural lands and some forests. There are some biologically protected zones and historical places or memorials in the area but the site does not affect national parks.

The proposed site meets all the main requirements of the ILC Project. Colliders have been in operation in this area for more than three decades, including the new Large Hadron Collider (LHC) that will start operating soon. The geological characteristics allow construction of tunnels for the accelerator and its support equipment in a stable rock formation with little seismic activity at a depth of 80 - 110 meters.

CERN and the Geneva area have at their disposal all necessary infrastructure to accommodate specialists for the period of the accelerator construction, to store and assemble the equipment, and to provide for the project-production support during manufacturing of the special-purpose equipment. Due to the importance of Geneva as headquarters of many international organizations and to the existing colliders at CERN, all necessary modern network and information infrastructure is available.

The international airport of Geneva is situated only 5 km away from CERN and is served by Swiss Rail and connected to the European railway network. The highway connecting Switzerland and France (Northern Europe to Southern Europe) passes nearby. The access roads to CERN are suitable for all necessary transportation to deliver the equipment of the accelerator itself and its technical systems.

The governments of France and Switzerland have existing agreements concerning the support of particle accelerators in Geneva area, which make it very likely that the land for the accelerator location could be made available free of charge, as they did for previous CERN projects.

5.4.2 Land Features

The proposed location of the accelerator is situated within the Swiss midlands embedded between the high mountain chains of the Alps and the lower mountain chain of the Jura. CERN is situated at the feet of the Jura mountain chain in a plain slightly inclined towards the lake of Geneva. The surface was shaped by the Rhone glacier which extended once from the Alps to the valley o f the Rhone. The water of the area flows to the Mediterranean Sea. The absolute altitude of the surface, ranges from 430 to 500 m with respect to sea level.

5.4.3 Climate

The climate is warm-continental. The mean temperature of the air of the coldest month (January) is -0.2°C. The mean temperature of the air of the warmest month (July) is +18.4°C. The mean annual rainfall is 928 mm. Snow usually falls in the months of December to February. On the whole, the climate in the vicinity of Geneva is considered to be quite comfortable.

5.4.4 Geology

Most of the proposed path of the ILC is situated within the Molasse, an impermeable sedimentary rock of the Swiss midlands laying over the Jurassic Bedrock. The path crosses a fault at the valley of the Allondon river which is situated South-West of Geneva and filled with sands and gravels. In this valley, the tunnels are built below the groundwater level. For the 1 TeV extension of the projectd, the tunnel will cross a second valley at Gland, situated North-East of Geneva, and will just enter some Jurassic limestone.

. The alignment of the ILC accelerator is placed at a level of 370 m in the Molasse (Fig. 5.4-1). This makes it possible to excavate the tunnels with shielded tunnel boring machines (TBM-S) with a high penetration rate and simultaneous placement of precast concrete segments. For the crossing of the Allondon and Gland valleys, the shielded tunnel boring machines mustl be replaced by hydro mix-shield machines (SM) able to tunnel in closed mode through the sands and gravels below groundwater level and to work in open mode as a normal tunnel boring machine in the Molasse.

5.4.5 Power Distribution System

The European sample site provides sufficient electrical power for the accelerator complex. A nearby 400 kV substation of the French grid will serve as connection point. The availability of the network is considered adequate for the LHC and is thus likely to also be sufficient for the ILC.

5.4.6 Construction Methods

The upper parts of the shafts lie in dry moraines, with total thickness ranging from 0 to 50 m, depending on the situation. Traditional means can be used to excavate down to sound rock, except in water bearing sands and gravels where it will be necessary to use other techniques such as diaphragm walling to allow safe excavation of the shafts. Once in the rock (sandstone) the shafts and caverns are excavated with the use of rock breakers and road headers, with blasting as a possible exceptional resort. After the temporary lining (rock bolts, mesh and shotcrete) is in place, the walls and vaults are sealed with waterproof membranes and covered with cast in-situ reinforced concrete.

Shielded Tunnel Boring Machines (TBM-S) with a prefabricated concrete segment lining are used for the long tunnels. An average daily advance of 25 m/day is assumed. The concrete tunnel floors are then cast in-situ. Short tunnel sections (less than 300 m) and passageways are excavated with road headers or small size rock breakers, then shotcreted. The penetrations between tunnels are excavated with small diameter boring machines, anchored in one of the two tunnels.

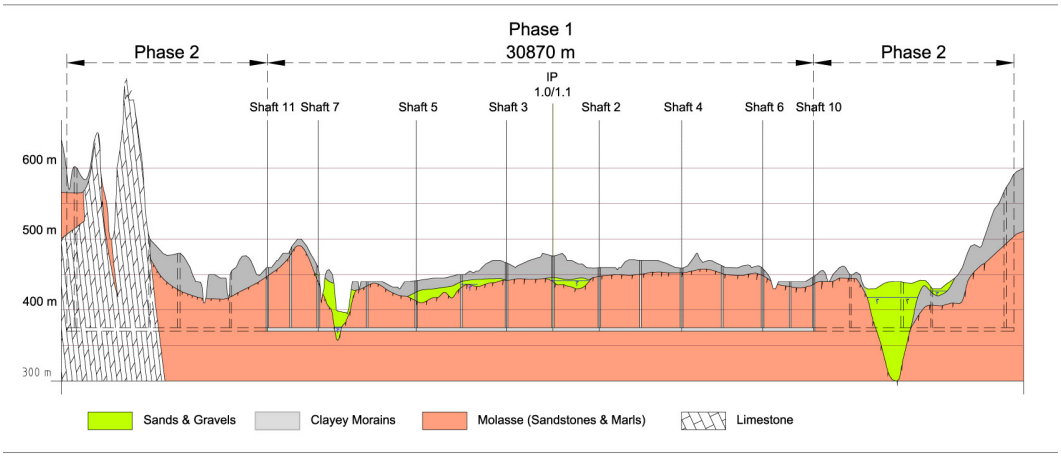

FIGURE 5.4-1. Longitudinal Profile of the European Sample Site near CERN.

5.5 SUMMARY

Although the three sample sites have differences, they all meet the ILC design requirements and at comparable cost. Table 5.5-1 compares some of the salient features.

TABLE 5.5-1
Summary of notable features of the sample sites and construction methodology.

Subject	Americas Region	Asian Region	European Region
Sample Site Location	Northern Illinois; near FNAL.	Japan	Geneva Area, near CERN
Land Features	200 $\sim$ 240m above sea level	120 $\sim$ 680 m above sea level	430 $\sim$ 480 m above sea level
Geology	Dolomite	Granite (Sedimentary rock in phase-2 extension)	Molasse (Sedimentary rock / sandstone)
Tunnel depth from surface	100 $\sim$ 150m	40 $\sim$ 600 m	95 $\sim$ 145m (except 1 valley 30 m)
Access paths to underground caverns	13 shafts (9m, 14m, 16m diam, 100 $\sim$ 135 m deep)	10 sloped tunnels (7.5m $\times$ 7m; 700 $\sim$ 2000 m long) and 3 shafts (for IR)	13 shafts (9m, 14m, 16m diam, 100 $\sim$ 135m deep)
Tunnel construction	TBM	TBM	TBM
Tunnel lining	20% of length Shotcreted	100% of length Shotcreted	100% of length Precast Concrete Segments
Average tunnel excavation speed	30m/day/TBM (boring)	16m/day/TBM (boring + surface work)	25m/day/TBM (boring)
Number of TBMs	9	15 (6 out of 9 access points have two TBMs starting in opposite directions)	9
Cavern construction	Drill and blast	Drill and blast (NATM)	Road breaker/ header
Shaft construction	Earth excavation / Drill and blast	Drill and blast (Step by step method)	Road breaker / header (Moroccan method)
New surface buildings	92	166	120
Distribution Voltage	69/34 kV	66/6.6kV	36kV

CHAPTER 6

Value Estimate

6.1 VALUE ESTIMATING METHODOLOGY

6.1.1 Introduction

The ILC is an international scientific project to be funded by a collaboration of countries or regions around the world, each of which have different traditions and conventions for planning and estimating the cost of large projects. In order to equitably divide up contributions among the collaborators, one must develop a project estimate that is independent of any particular accounting system but compatible with all of them. The "VALUE" methodology has become the standard for such international projects. It was adopted by ITER (the international thermonuclear experimental reactor project) and by the LHC experiments, among others. Value is a particularly convenient concept for dealing with "in-kind" contributions, for which manufacturing costs and labor rates can vary widely between collaborators. Conversion of the value estimate to various national costing practices can only be done by each participating nation.

The ILC estimate consists of two important parts: VALUE (in terms of currency units) for items provided and LABOR (in terms of person-hours or person-years), which may be provided by the collaborating laboratories and institutions, or may be purchased from industrial firms. This is similar to what has been traditionally used for European project proposals. The value of a component is defined as the lowest reasonable estimate of the procurement cost in adequate quality, based on production costs in a major industrial nation. It is expressed in 2007 currency units (not escalated to the years in which the funds are projected to be spent) and does not include R&D, pre- or post-construction or operating costs, taxes or contingency. It is effectively the barest cost estimate that would be used by any of the funding agencies. Individual regions can then add to the base value any other items usually included in their own estimating system.

In this context, LABOR is defined as "explicit" labor, which may be provided by the collaborating laboratories and institutions, or may be purchased from industrial firms. This to be distinguished from a company's "implicit" labor associated with the industrial production of components and contained (hidden) within the purchase price. The implicit labor is included in the VALUE part of this estimate.

The ILC VALUE plus LABOR estimate is the basis on which contributions are apportioned among the collaborators. Each participant makes an agreement with the ILC man-

agement to provide a certain value of components and services. They are then responsible for providing the contracted items, independently of what they actually cost.

6.1.2 Scope of Estimate

The estimate is for a 500 GeV center-of-mass machine but includes some items sized for 1 TeV to enable a later energy upgrade, such as the beam dumps and the length of the Beam Delivery tunnel. The ILC estimate does not include the cost of the detectors. They are assumed to be funded by a separate agreement between the collaborating institutes, in the way the LEP and LHC detectors were built. The estimate does include civil engineering work for the detectors, e.g. assembly buildings, underground experimental halls, shafts, etc.

The estimate covers all aspects of construction, including tooling-up industry, final engineering designs and construction management. The estimate specifically does not include costs for any of the engineering, design, or preparation activities that can be accomplished before construction start. It does not include Research and Development, proof-of-principle or prototype systems tests, pre-construction (e.g. architectural engineering, conceptual and construction drawings, component and system designs and preparation of bid packages), commissioning, operation, decommissioning, land or underground easement acquisition costs. It also does not include items which are treated differently from region to region such as taxes, escalation, or contingency. Table 6.1-1 summarizes the items that are included in, or excluded from, the value and labor estimate.

The estimate assumes a seven-year construction period. The estimate for a given item covers the cost from the day the project obtains funding until that item is installed, tested, and ready for commissioning. Commissioning in one area may overlap with construction elsewhere. The construction period ends when the last component has been installed and tested.

6.1.3 Estimating Approach

The ILC estimate was developed by the RDR matrix of Area, Technical and Global System leaders working with the Cost Engineers. The Area Systems Leaders (AS) defined the requirements for their accelerator systems. The Technical (TS) and Global System (GS) Leaders provided the estimated value and explicit labor per component unit. Specialized components such as the polarized electron gun were estimated by the Area Systems themselves. The AS leaders then compiled the estimate for their areas. The estimates were iterated to optimize cost and performance.

The cost estimates were prepared using a Work Breakdown Structure (WBS) where each item included a description, basis of estimate, quantity required, materials and services estimate and implicit and explicit labor. These could then be summed to produce to an estimated total cost for the component, system, or section of the machine. There were 351 active WBS elements, where each element represented a roll-up of further detailed estimating information provided by the systems leaders. An example of the lower level of detail for one of these WBS elements provided by the Conventional Facilities and Siting group is presented in the Appendix.

TABLE 6.1-1
Summary of the items that are included in, or excluded from. the value and labor estimate.

Included	Excluded
Construction of a 500 GeV machine, including items sized to enable a later energy upgrade	
Tooling-up industry, final engineering designs and construction management	Engineering, design, or preparation activities that can be accomplished before construction start, such as, research & development, proof-of-principle or prototype systems tests, pre-construction
Construction of all conventional facilities, including the tunnels, surface buildings, access shafts and others	Surface land acquisition or underground easement acquisition costs
Construction of the detector assembly building, underground experimental halls and detector access shafts	Experimental detectors
	Commissioning, operations, decommissioning
Explicit labor, including that for management and administrative personnel.	Taxes, contingency and escalation

6.1.3.1 General Guidelines

The ILC estimate is given as the sum of VALUE (in currency units) and explicit LABOR (in person-hours).

Guidelines and Instructions for performing, preparing, and presenting the cost estimate are available at

http://www-ilcdcb.fnal.gov/RDR_costing_guidelines.pdf

http://www-ilcdcb.fnal.gov/RDR_Cost_Estimating_Instructions_23may06.pdf

Estimates are quoted as median or 50%-50% estimates, where, if a given item were to be independently purchased many times, taking the lowest world-wide bid each time, half of the purchases would be below the median estimate and half above.

6.1.3.2 Currency Rates and Raw Materials

Component estimates from all three regions were converted to a common cost basis, the ILC Unit, where one ILC Unit is set equal to $1 U.S. (January 2007 value) The conversion rates used were:

$$1 \text{ ILC Unit} = 1 \text{ US } 2007\$ \ (= 0.83 \text{ Euro} = 117 \text{ Yen})$$

These currency exchange rates are an average of the exchange rates over the five years 2003 through 2007. The value estimates were developed during 2006 and then adjusted to January, 2007 using the official regional cost escalation indices.

Electricity and raw materials such as niobium, steel or copper are assigned fixed prices as of January 1, 2007, as summarized in Table 6.1-2.

electricity:	$0.10 per kWh (including supply cost)
copper:	$8 per kilogram
black steel:	$0.6 per kilogram (up to three times higher price for stainless and magnet steel)
niobium:	$70 per kilogram

TABLE 6.1-2
Assumed prices for electricity and representative raw materials

6.1.3.3 Contingency and Risk

The ILC estimate does not contain contingency. Contingency is a quantitative measure of risk – the final number is set higher than the initial estimate to allow for unexpected or uncontrollable factors that may raise the ultimate price. The ILC project will avoid any future cost increases through R&D, industrial studies, vendor pre-qualifications, and competitive, global calls for tender. The risk analysis is being done and will be included in the final version of this RDR.

6.1.4 Component Estimates

Three different classes of items were identified and approached differently.

- *Site specific*: The costs for many aspects of conventional facilities are site specific and there are separate estimates for sample sites in all three regions: Asia, Europe, and the Americas. These costs are driven by real considerations, e.g. different geology and landscape, availability of electrical power and cooling water, etc. Site dependent costs due to formalities (such as local codes and ordinances) are not included. Common items such as internal power distribution, water and air handling, which are essentially identical across regions although the implementation details differ, have a single estimate. The sample sites have different geologies. Nevertheless, they use similar tunnel-boring machine technologies and the value estimates are very close. Because a site has not yet been chosen, the ILC value estimate is taken as the average of the three site-dependent estimates. Individual estimates for each of the three sites are also provided.

- *High technology*: Items such as cavities, cryomodules, and rf power sources, where there is interest in developing expertise in all three regions, have been estimated separately for manufacture by each region. Costs are provided for the total number of components along with parameters to specify the cost of less than the total number. The European estimate for the cavities and cryomodules is used for the ILC value as it is the most mature, in terms of R&D and industrial studies. Estimates from the other regions provide a crosscheck.

- *Conventional*: Estimates for components, such as conventional magnets and controls, which can be produced by many manufacturers in all regions, are based on a world-wide call for tender. They are the lowest reasonable cost available world-wide, for production in a major industrial nation.

Component estimates include the manufacturer's implicit labor, EDIA (engineering, design, inspection, and administration), quality control/assurance, and technical testing. A single supplier is assumed to be responsible for one deliverable, even though in practice, multiple suppliers may be chosen to reduce risk. The estimates quoted for mass-produced technical systems were generated either by detailed bottom-up industrial studies for the quantities required, or by assuming a learning curve [1] explicitly in an in-house engineering estimate. The basis of estimate and cost estimating methodology for each set of components are discussed in the individual Area System, Global System, and Technical System sections for this report.

6.1.5 Explicit Labor

Explicit labor is estimated separately from component costs, and is given in person-hours. It may be provided by the ILC collaborators as in-kind contributions, drawn from existing laboratories with their own personnel and budgets, or may be purchased from industrial firms. To convert person-hours to person-years, it was assumed that laboratory staff works an average of 1,700 hours per year. Only three classes of manpower are used: engineer/scientist, technical staff, and administrative staff.

6.2 ESTIMATE FOR CONSTRUCTION OF ILC

The value and explicit labor estimates are current as of February 1, 2007, and will be updated in the final report.

6.2.1 Value Estimate

The preliminary value estimate presented here is for the cost of the ILC in its present design and at the present level of engineering and industrialization. The estimate contains three elements:

- 1.78 Billion (ILC Units) for site-dependent costs, such as the costs for tunneling in a specific region
- 4.87 Billion (ILC Units) for shared value of the high technology and conventional components
- 13,000 person-years for the required supporting manpower (= 22 million person-hours)

For this value estimate: 1 ILC Unit = 1 US 2007$ (= 0.83 Euro = 117 Yen)

A common estimate was used for all non site-specific technical components, regardless of region. The three regional site-specific estimates were based on local costs for civil engineering and the primary high voltage electrical power connections, feeds, substations and primary cooling water systems. All three site-dependent estimates are within a few percent of the average.

There are many possible models for dividing the responsibilities among the collaborating regions. The numbers below present one possible model where the estimates are divided into site-specific and shared parts. In this model, the host region is expected to provide the site-specific parts, because of the size, complexity, and specific nature of these elements. The site-specific elements include all the civil engineering (tunnels, shafts, underground halls and caverns, surface buildings, and site development work); the primary high-voltage electrical power equipment, main substations, medium voltage distribution, and transmission lines; and the primary water cooling towers, primary pumping stations, and piping. Responsibilities for the other parts of the conventional facilities: low-voltage electrical power distribution, emergency power, communications, HVAC, plumbing, fire suppression, secondary water-cooling systems, elevators, cranes, hoists, safety systems, and survey and alignment, along with the other technical components, could be shared between the host and non-host regions. Such a model may be summarized as shown in Table 6.2-1.

The value estimates broken down by Area System are shown separately for both the conventional facilities and the components in Figure 6.2-1 and Table 6.2-2. Common refers to infrastructure elements such as computing infrastructure, high-voltage transmission lines and main substation, common control system, general installation equipment, site-wide alignment monuments, temporary construction utilities, soil borings and site characterization, safety systems and communications.

The component value estimates for each of the Area (Accelerator) Systems include their respective RF sources and cryomodules, cryogenics, magnets and power supplies, vacuum system, beam stops and collimators, controls, Low Level RF, instrumentation, installation, etc.. The superconducting RF components represent about 65% of the estimate for all non-CF&S components.

	Region	site-specific	shared	total
	Asia	1.61 B	4.86 B	6.47 B
	Americas	1.89 B	4.87 B	6.76 B
	Europe	1.85 B	4.86 B	6.71 B
and	Average	1.78 B	4.87 B	6.65 B
plus 13 K person-years of explicit labor				
or 22 M person-hours 1,700 hours/year				

TABLE 6.2-1
Possible division of responsibilities for the 3 sample sites (ILC Units).

FIGURE 6.2-1. Distribution of the ILC Value Estimate by Area System and Common Infrastructure. The estimate for the experimental detectors for particle physics is not included. (The Americas region estimate for Conventional Facilities has been used here as an example.)

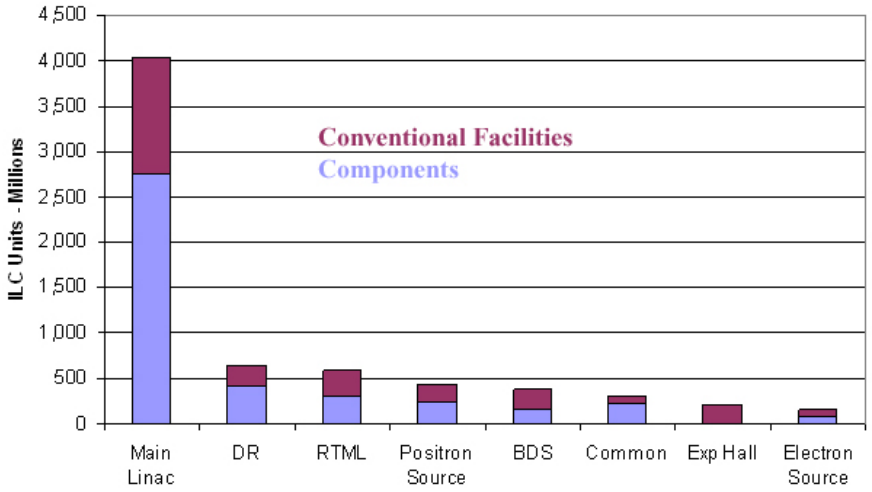

6.2.2 Explicit Labor Estimate

The explicit labor for the Global Systems, Technical Systems, and specific specialty items for Electron Source, Positron Source, Damping Rings, and Ring to Main Linac, include the scientific, engineering, and technical staff needed to plan, execute, and manage those elements including specification, design, procurement oversight, vendor liaison, quality assurance, acceptance testing, integration, installation oversight, and preliminary check-out of the installed systems.

Installation is the largest fraction of explicit labor, about 39%. Management is the second largest fraction at about 18%. At this stage of the ILC design, it is too early for a complete analysis of installation requirements. Instead, the RDR estimate was based on a bottoms-up time and motion study for installation of the cryomodules for the Main Linac. This labor

Area - M	Total	Components	Conventional Facilities
Main Linac	4,038	2,762	1,275
DR	647	415	232
RTML	590	319	271
e^+ source	429	242	187
BDS	383	158	224
Common	323	228	95
Exp Hall	200	0	200
e^- source	151	94	57
Sum	6,760	4,219	2,540

TABLE 6.2-2
Distribution of the ILC Value Estimate by Area System and Common Infrastructure, in ILC Units. The estimate for the experimental detectors for particle physics is not included. (The Americas region estimate for Conventional Facilities has been used here as an example.)

FIGURE 6.2-2. Explicit labor, which may be supplied by collaborating laboratories or institutions, listed by Global, Technical, and some Area-specific Systems.

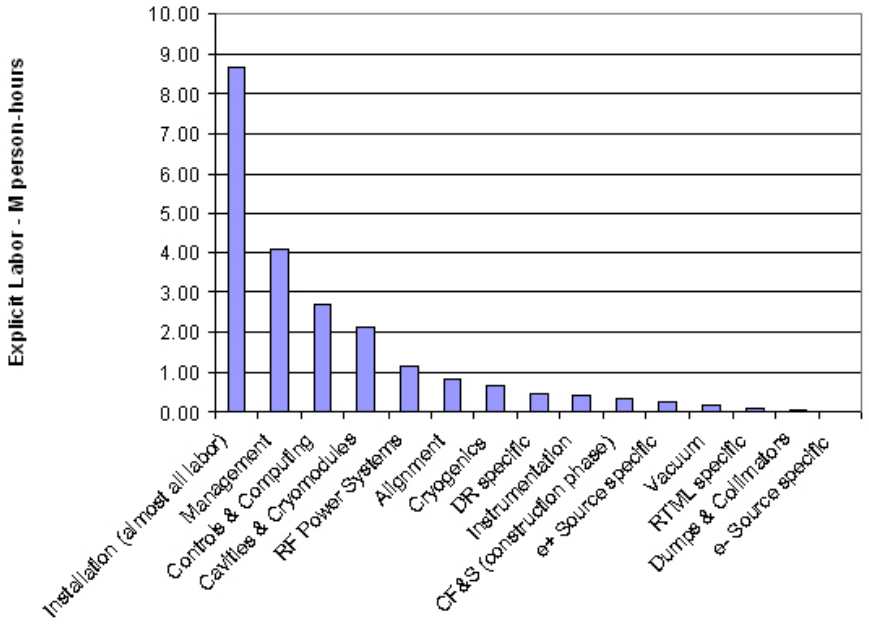

estimate was then scaled to the scope of the capital investment value for the other components in the Main Linac and elsewhere. Some standard tasks were also estimated from published

Explicit labor	M person-hours
Installation (all labor)	8.67
Management	4.09
Controls & computing	2.67
Cavities & cryomodules	2.16
RF Power Systems	1.14
Alignment	0.83
Cryogenics	0.69
DR specific	0.48
Instrumentation	0.44
CF&S (construction phase)	0.36
e^+ Source specific	0.30
Vacuum	0.18
RTML specific	0.09
Dumps & Collimators	0.06
e^- Source specific	0.04
Sum	22.21

TABLE 6.2-3
Explicit labor, which may be supplied by collaborating laboratories or institutions, listed by Global, Technical, and some Area-specific Systems.

construction practices. These estimates were then compared with the actual manpower used for the installation of recent accelerator projects, to check that the estimates were reasonable.

In the present estimate, the installation task is characterized almost exclusively as explicit labor, with minimum costs for material-handling equipment. This is on the assumption that much of the installation and system check-out labor at the ILC site can be contributed by the staffs of collaborating institutions or laboratories. The validity of this assumption depends on the availability of the necessary skilled manpower and local labor regulations. Because of the size of the project, it is likely that many tasks like electrical and plumbing work will need to be outsourced to industry. Trade-offs and translations are likely between using in-house labor and external contracts. It is estimated that a minimum of 10% of the installation task must be management and supervision by in-house manpower.

The management model is similar to that of the construction phase of the Superconducting Super Collider (SSC), but without central computing staff which are included elsewhere. The management personnel is estimated to be half as large as in the SSC model. The ILC staff consists of 345 persons, divided as shown in Table 6.2-4. Personnel for the Area, Global, and Technical System groups are not included in the Project Management Division.

It is the practice in some regions to apply general and administrative overheads to purchases and labor for projects. These overheads are applied as a multiplier on the underlying LABOR and VALUE, and cover the costs of the behind-the-scenes support personnel. In this estimate, such personnel are explicitly enumerated as labor under Directorate, Management

Directorate (30):	Directors Office, Planning, ES&H Oversight, Legal, External Affairs, Education, International Coordination, Technology Transfer;
Management Division (13):	Quality Assurance, ES&H;
Laboratory Technical Services (125):	Facilities Services, Engineering Support, Material and Logistical Services, Laboratory Fabrication Shops, Staff Services;
Administrative Services (94):	Personnel, Finance, Procurement, Minority Affairs;
Project Management Division (83):	Management, Administrative, Project Management Division Office.

TABLE 6.2-4
Composition of the management structure at ILC.

Division, Laboratory Technical Service, and Administrative Services in Table 6.2-4. Therefore, the overheads are included as additional explicit LABOR, rather than as a multiplier on VALUE.

6.2.3 Risk Estimate

This February, 2007 estimate for the ILC is preliminary and does not yet include a complete analysis of the uncertainties and risks associated with the estimates for each cost element; there will be a risk analysis in the final RDR. There are uncertainties in the estimate of the costs of individual components that are simply due to the preliminary stage of the project. In addition, there are three major technical risks which affect the main cost drivers: attaining an economically acceptable performance yield for the superconducting RF cavities (a yield of 80% at a qualification gradient of 35 MV/m was assumed for this estimate); demonstrating adequate power and lifetime for the 10 MW klystrons; and minimizing both the geological and contractual (claims) uncertainties associated with the underground construction. There are additional technical risks to achieving the performance goals of the ILC, with little impact on the overall cost, e.g. the relatively inexpensive crab cavities are required to meet specifications in order to deliver the needed luminosity. Major R&D goals during the engineering design phase are to address and minimize these risks. Additional R&D goals are to reduce the cost estimate by incorporating improved technologies, such as alternative RF power modulators and higher gradient RF cavity geometries, and by cost-performance optimization through value engineering.

6.2.4 Operating Cost

Operating costs are not included in the estimate for the construction project, but a very preliminary estimate is given. It is also to be noted that spare components (those stored in warehouses and not the installed redundant components), although fabricated along with the installed components, are assumed to be financed through operating funds, and are not considered part of the construction projects. Major factors in the operating cost include

personnel costs, electrical power, maintenance and repairs, helium and nitrogen consumables, and components that have a limited life expectancy and need continuous replacement or refurbishment, like klystrons.

The model assumes 9 months of machine operations per year at full power of about 200 MW, corresponding to 500 GeV at design luminosity, plus 3 months standby at reduced power (25 MW) with the superconducting cavities maintained at 4.5K, which is above their operating temperature. At the current electrical power rate of $0.1 per kW-hr, the operating costs for these materials and services are estimated to be approximately 150-180 M$ per year in 2007 Dollars. The continuing operations and administrative staff is expected to be comparable to that at existing facilities (not including support of the scientific program).

Commissioning activities and operating costs are anticipated to gradually increase over the fifth, sixth, and seventh years of construction from zero up to the full level of long-term operations at the end of the 7 year construction phase.

6.3 SCHEDULE

6.3.1 Example Construction Schedule

A detailed schedule for realization of the ILC depends on a variety of factors and milestones including: completion of crucial R&D, completion and review of the conceptual design of the machine (RDR) and detectors, and endorsement of the RDR and cost by international funding agencies so that critical R&D can be funded to completion. Site specific engineering and civil designs require international agreements on site selection which allow land acquisition, environmental assessments, etc. In addition agreements on cost sharing and spending profiles are required to plan the industrial production of components and the preparation of construction contracts.

In the absence of much of this information an attempt was made to construct a technically limited schedule for the construction of ILC assuming that these items have been completed prior to a physical construction start (T0). The RDR cost estimate has been based on this schedule.

6.3.2 Conventional Facilities Schedule

Conventional facilities include Civil Engineering of above and below ground structures, electrical infrastructure, cooling and ventilation, and buildings. In what follows, an assumption was made that a site was selected several years prior to the start of construction and that funding was available such that Architectural & Engineering (A&E) firms can be retained to design the conventional facilities and prepare bid packages prior to the start of construction. In the absence of other financial constraints, the construction schedule for conventional facilities is dominated by the required underground construction. ILC requires about 72 km of underground tunnel construction for the Main Linac, Beam Delivery and Damping Ring systems. For the purpose of this section it was assumed that the tunnel is deep, at a depth of ~100 m and located in dry rock such that standard tunnel boring machines can be employed. (Several possible ILC sites have different local underground conditions. However, these are believed to alter the conclusions in the section in only a minor fashion).

The layout of the ILC is shown in Figure 6.3-1. If it is assumed that all shaft and underground construction can start simultaneously or optimally (i.e. no funding limits) and that at least 9 tunnel boring machines (TBM) of suitable diameter are available and employed simultaneously. Assuming 1 year for the shaft construction (based on LEP/LHC experience), 3 months for TBM setup, and 25 m/day boring speed/TBM, then the actual underground construction time for the ML and Damping Ring is about 3.5 years from ground breaking to beneficial occupancy.

For the purposes of this schedule it was assumed that the finished tunnel can be outfitted with services at the following rate:

1-	Installation of cable trays and pipes supports	4	weeks/km
2-	Installation of cooling pipes	3	weeks/km
3-	Installation of cables + connection	3	weeks/km
4-	Installation of electrical equipment (transformers, switch gear)	4	weeks/km

These rates are based on experience at existing facilities, not independent analysis. It

FIGURE 6.3-1. Schematic Layout of the ILC.

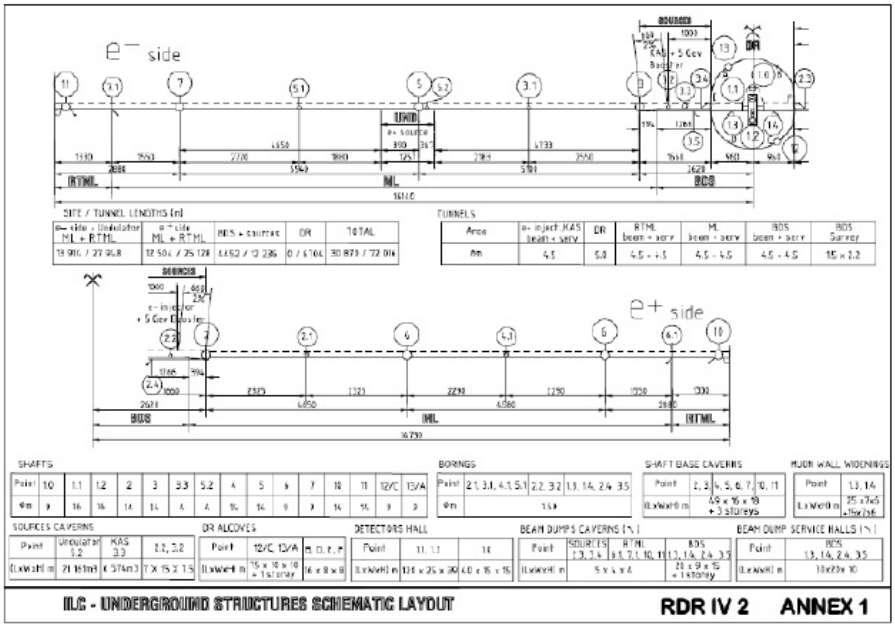

is assumed that these teams do not overlap in the tunnel at the same time, but that a sufficient quantity of trained personnel are available to form teams that can work in parallel at all available locations. The installation of services require about 1 year such that the tunnel is ready to accept technical components after about 3.5 to 4.5 years from the start of construction. (Some areas might be available for component installation a few months sooner, but the start of installation in these areas could disrupt the installation of services. As a result, this was not considered in the modeling.)

About one additional year is required to finish the underground detector enclosure so that detector installation can proceed about 4.5 years after the start of civil construction. It is assumed that detector assembly buildings and detector construction start at the earliest opportunity. Most of the detector assembly is assumed to take place above ground following the general scheme adopted for the CMS detector at CERN. This scheme allows detector construction and commissioning to occur in parallel with the underground construction. In the case of CMS the detector assembly and commissioning took 6 years. In the absence of more detailed information, we assume the same schedule for the ILC detectors.

6.3.3 Technical Component Schedule

It is assumed that the high volume technical components required for the Main Linac and Damping Ring are produced by industry. Components in this category include SCRF cavities, cryomodules, modulators, klystrons, SC and conventional magnets, cryogenic refrigerators, transfer line, cables, piping, etc. The production of even such complex components as klystrons, modulators and conventional magnets are well within the capability of industry. The sequence would probably involve industrial pre-series production by several vendors

FIGURE 6.3-2. Schematic of an example of an ILC civil construction plan using TBMs. Note that TBM #9 is first used to excavate the tunnel for the damping ring (not shown). Five Tunnel Boring machines must be transported in this plan. (Analysis and figure is based upon LEP and LHC experience at CERN)

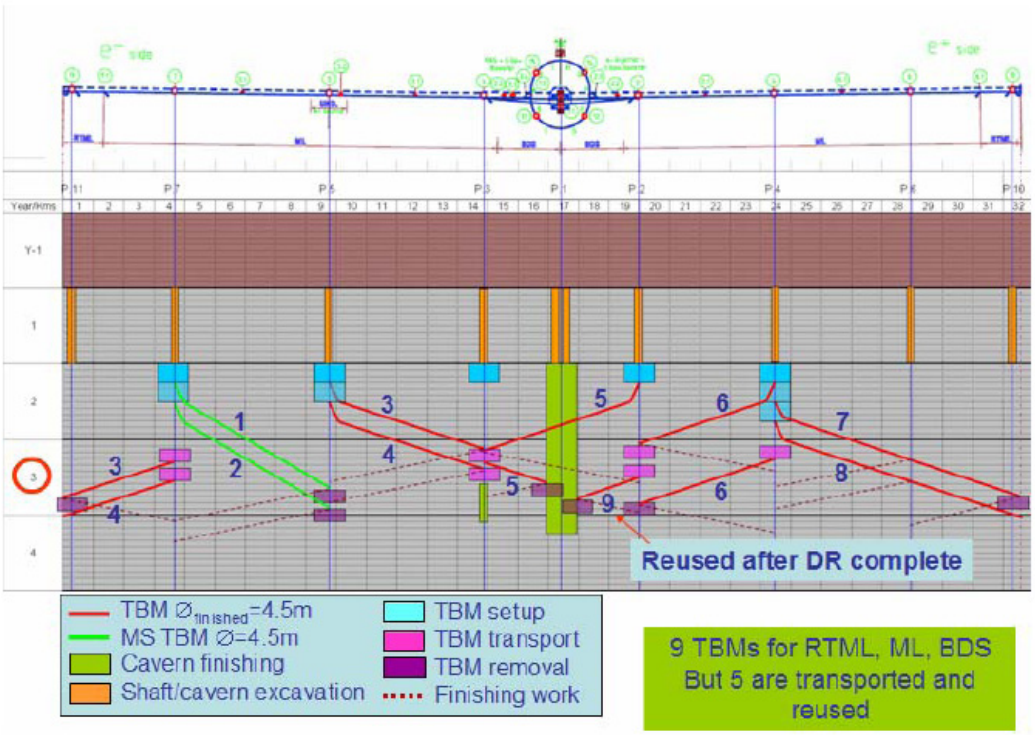

followed by tender for production quantities of components. The number of vendors and the region of production will largely be determined by decisions concerning "in-kind" contributions from the regions participating in the project. The required cryogenic plants are sufficiently similar to those recently acquired for the LHC that they can be procured from industry. Provided funding is available, these components do not determine a technically driven ILC schedule.

The SCRF cavities and cryomodules are the most technically challenging components and require the largest industrial infrastructure and technical ramp up. The overall cost of the cryomodules and associated infrastructure is likely to exceed any one regions production capacity. Regional interest in SCRF technology is also high. Both considerations suggest a model in which three regions of the world provide these cryomodules in equal quantity. Figure 6.3-3 shows one possible model for the ramp up of cryomodule production in one of three regions. Note that the five year production schedule shown in Figure 6.3-3 assumes funding is available prior to construction start so that infrastructure with long lead times can be purchased early. Different regions could have earlier start times and a flatter production schedule.

FIGURE 6.3-3. A possible model schedule for cryomodule production shows 1/3 of the required ILC cryomodules produced in one of three regions. R&D and pre-series devices lead to 5 years of series production (yellow). The position and magnitude of the peak of series production will vary with changes to the available construction and test infrastructure.

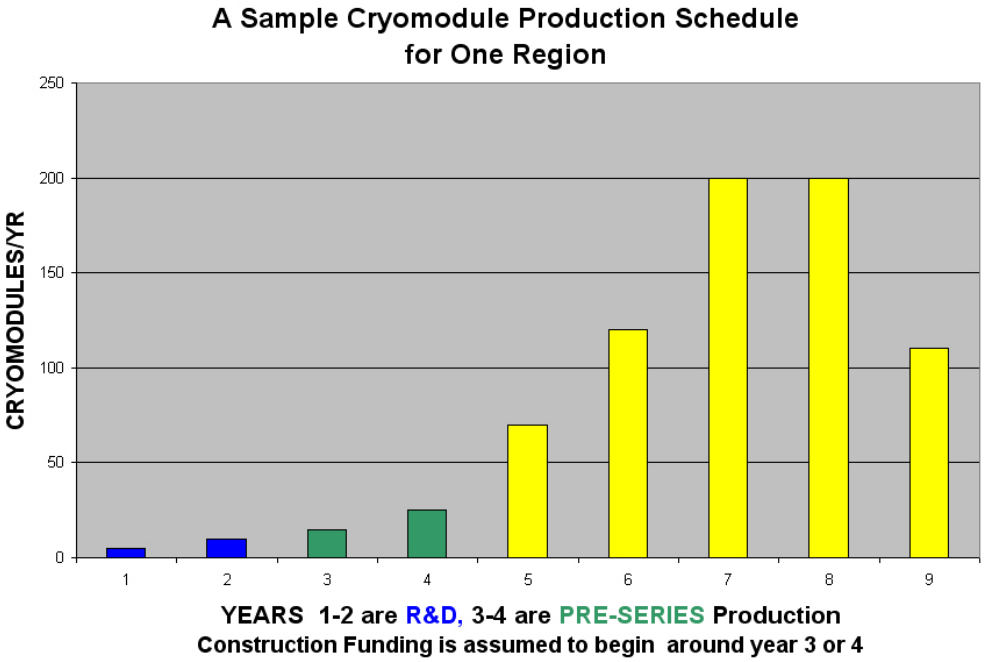

6.3.4 Technical Component Installation Schedule

The installation process follows the civil construction model with parallel ongoing activities in separate areas but planned to minimize interferences with other teams. The general schedule plan is based on experience with the LHC. Transportation of components from surface holding areas into their rough location in the underground tunnels takes place during the evening shift. This minimizes interference with all other activities above and below ground. These components are installed, aligned, interconnected etc. during the day shift.

An example of this schedule for the main linac cryomodules is shown in section 4.9. This is accomplished with specialized crews which are appropriately trained and have all the required support from the technical systems. This manpower versus time profile for the linac installation is also shown in section 4.9. As with the civil construction schedule, installation in the central DR/INJ complex takes place in parallel and is 6 months to 1 year ahead of the main linac schedule.

6.3.5 Example Funding Profile

With the assumptions described above and with the value estimates, one can model a construction schedule with its required funding profile. This was done for a seven year con-

struction project which is consistent with the construction, manufacturing and installation schedules. The civil construction of the underground facilities is concentrated in the first four years and the high technology cryomodules are spread throughout the seven years. The remaining civil construction and technical component manufacture and installation are spread throughout years three to seven.

This plausible plan shows the need for early funding of the two cost drivers, civil construction and the production of cavities and cryomodules. The civil construction schedule drives the overall schedule and therefore this funding, assumed to be mainly from the host country, is on the critical path. The more global distribution of funding of other systems allows flexibility in optimizing construction and installation. This funding profile is, of course, model dependent but it shows that there are no unusual or unattainable requirements in a seven year construction schedule. Operations funding would begin gradually starting in year five and would be at full operating level in year eight.

FIGURE 6.3-4. A funding profile for a model seven year construction schedule.

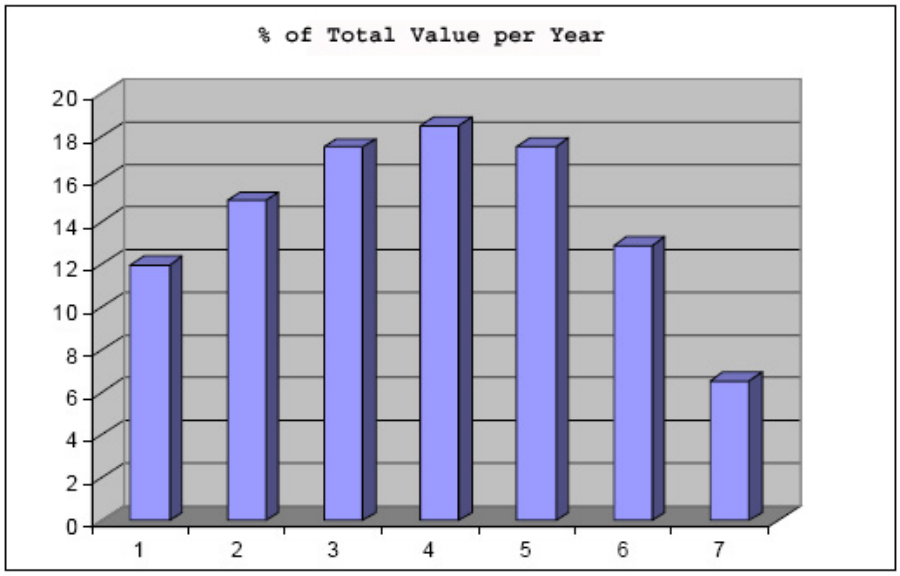

Appendix: Example of the next level of WBS detail for Conventional Facilities and Siting for Civil Engineering for the Main Linac Area System for the Americas site.

TABLE 6.3-1
WBS detail for Conventional Facilities and Siting for Civil Engineering for the Main Linac Area System for the Americas site.

1.7			Conventional Facilities		
				Quantity	Unit
1.7.1			CIVIL ENGINEERING		
	1.7.1.1		Engineering, study work and documentation		
		1.7.1.1.1	In-house Engineering		man-hr
			In-house Engineering	4%	%
		1.7.1.1.2	Outsourced Consultancy Services		
			Outsourced Engineering	6%	%
	1.7.1.2		Underground Facilities		
		1.7.1.2.1	Shafts		
			e- ML 14m dia. Shafts @ Points 5, 3 (2 x 425 vert ft)	259	vert m
			e- ML 9m dia. Shaft @ Point 7 (1 x 425 vert ft)	130	vert m
			e- ML 1500mm dia. Survey Shafts @ Points 3.1, 5.1 (2 x 425 vert ft)	259	vert m
			e+ ML 14m dia. Shafts @ Points 2, 4 (2 x 425 vert ft)	259	vert m
			e+ ML 9m dia. Shaft @ Point 6 (1 x 425 vert ft)	130	vert m
			e+ ML 1500mm dia. Survey Shafts @ Points 2.1, 4.1 (2 x 425 vert ft)	259	vert m
			Surface Grouting of Points 2-5 14m dia. Shafts (4 x 425 vert ft)	4	ea.
			Surface Grouting of Points 6-7 9m dia. Shafts (2 x 425 vert ft)	2	ea.
			Surface Grouting of Points 2.1, 3.1, 4.1, 5.1 Survey Shafts (4 x 425 vert ft)	4	ea.
			Points 2,3,4,5,6,7 - 14&9m dia. Shafts, finishing (stairs, conc. wall, elev.#2)	777	vert m
			ML Underground Potable Water (1/2 of Points 2 & 3)	1	ea.
			ML Underground Potable Water (Points 4,5,6,7)	4	ea.
			ML Underground Sanitary Sewer (1/2 of Points 2 & 3)	1	ea.
			ML Underground Sanitary Sewer (Points 4,5,6,7)	4	ea.
		1.7.1.2.2	Tunnels		
			e- ML 4.5m dia. Beam Tunnel, TBM Excavation (37,162 lin ft)	11,327	lin m
			e- ML 4.5m dia. Service Tunnel, TBM Excavation (37,162 lin ft)	11,327	lin m
			e- ML 4.5m dia. Tunnels, Conc. Inv. (74,324 lin ft)	22,654	lin m
			e+ ML 4.5m dia. Beam Tunnel, TBM Excavation (36,660 lin ft)	11,174	lin m
			e+ ML 4.5m dia. Service Tunnel, TBM Excavation (36,660 lin ft)	11,174	lin m
			e+ ML 4.5m dia. Tunnels, Conc. Inv. (73,320 lin ft)	22,348	lin m
			Provide Tunnel Construction Water Treatment Plant	4	ea.
			Maintain and Operate Tunnel Construction Water Treatment Plant	4	ea.
			Treatment of Tunnel Construction Water	4	ea.

TABLE 6.3-2
CONTINUED : WBS detail for Conventional Facilities and Siting for Civil Engineering for the Main Linac Area System for the Americas site.

1.7			Conventional Facilities (continued)		
				Quantity	Unit
1.7.1			CIVIL ENGINEERING (continued)		
		1.7.1.2.3	Halls		
		1.7.1.2.4	Caverns		
			e- ML Shaft Base Caverns D&B Excavation @ Points 3, 5, 7 (3 x 20,056 CY)	46,003	m^3
			e- ML Points 3,5,7 D&B Exc. for Shield Doors (in Base Caverns) (3 x 959 CY)	2,199	m^3
			e- ML Beam Dump Cavern D&B Excavation @ Point 3 (3,034 CY)	2,320	m^3
			e+ ML Shaft Base Caverns D&B Excavation @ Points 2, 4, 6 (3 x 20,056 CY)	46,003	m^3
			e+ ML Points 2,4,6 D&B Exc. for Shield Doors (in Base Caverns) (3 x 959 CY)	2,199	m^3
			e+ ML Beam Dump Cavern D&B Excavation @ Point 2 (3,034 CY)	2,320	m^3
			Shield Doors @ Base Caverns @ Points 2-7	6	ea.
		1.7.1.2.5	Miscellaneous works		
			e- ML Personnel Crossovers, D&B Excavation (23 X 295.5 CY)	5,196	m^3
			e- ML Waveguides, Drill Excavation (968)	968	ea.
			e+ ML Personnel Crossovers, D&B Excavation (23 X 295.5 CY)	5,196	m^3
			e+ ML Waveguides, Drill Excavation (968)	968	ea.
	1.7.1.3		Surface Structures		
		1.7.1.3.1	Central Lab Buildings		
		1.7.1.3.2	Detector Assembly Buildings		
		1.7.1.3.3	Office Buildings		
			Points 4-7 Office Buildings (4 x 3,750 sq ft)	1,396	sq m
		1.7.1.3.4	Service Buildings		
			Points 2-7 Electrical Service Buildings (6 x 1,500 sq ft)	836	sq m
			Points 2-7 Cooling Towers & Pump Stations Bldgs. (6 x 7,500 sq ft)	4,181	sq m
			Points 2-7 Cooling Ventilation Buildings (6 x 2,500 sq ft)	1,394	sq m
		1.7.1.3.5	Cryo- Equipment Buildings		
			Points 2-7 Cryo - Warm Compressor Building (6 x 4,500 sq ft)	2,508	sq m
			Points 2-7 Cryo - Surface Cold Box Building (6 x 6,250 sq ft)	3,484	sq m
		1.7.1.3.6	Control Buildings		
		1.7.1.3.7	Workshops		
			Points 4-7 Workshop Bldg. - Machine & Detector (4 x 11,250 sq ft)	4,181	sq m
		1.7.1.3.8	Site Access Control Buildings		
			Points 4-7 Site Access Buildings (4 x 750 sq ft)	279	sq m
		1.7.1.3.9	Shaft Access Buildings		
			Points 2-7 Shaft Access Buildings (6 x 9,375 sq ft)	5,226	sq m
		1.7.1.3.10	Miscellaneous Buildings		
		1.7.1.3.11	User Facilities		
	1.7.1.4		Site Development		
		1.7.1.4.1	Off-site Site work		
		1.7.1.4.2	Network of Monuments		
		1.7.1.4.3	Construction Support		
		1.7.1.4.4	Site Preparation		
			Points 2 - 7, Clearing, Grubbing, and Initial Site Preparation (6 sites)	6	ea.
		1.7.1.4.5	Utility Distribution		
			Points 2 - 7, Utility Corridors (Gas, DWS, San., Storm, Elec., Comm.)	6	ea.
			Points 2 - 7, Septic Field / Tank or Sanitary Sewer	6	ea.
			Points 2 - 7, Wells or DWS	6	ea.
			Points 4 - 7, Elevated Water Tank	4	ea.
			Points 4 - 7, Water Pump House	4	ea.
		1.7.1.4.6	Road, Sidewalks & Parking Areas		
			Points 2 - 7, Service Roads (6 sites x 1250 lin ft / site)	2,286	lin m
			Points 2 - 7, Paved Areas (6 sites x 8750 sy / site)	43,896	sq m
			Points 2 - 7, Flatwork (6 sites x 2,500 sq ft / site)	1,394	sq m
		1.7.1.4.7	Landscaping		
			Points 2 - 7, Landscaping	6	ea.
			Points 4 - 7, Security Fencing (4 sites x 5,000 lin ft / site)	6,097	lin m
		1.7.1.4.8	Environmental		
			Points 2 - 7, Sediment & Erosion Control (6 sites)	6	ea.
		1.7.1.4.9	Miscellaneous Site Works		

BIBLIOGRAPHY

[1] http://www.fnal.gov/directorate/icfa/ITRP_Report_Final.pdf

[2] TESLA TDR, March, 2001.

[3] http://www-project.slac.stanford.edu/ilc/techinfo/USLCTOS/

[4] http://www.slac.stanford.edu/xorg/ilc-trc/2002/index.html

[5] http://www.fnal.gov/directorate/icfa/LC_parameters.pdf

[6] Need a reference for the timing document

[7] T. Nishitani et al., J. Appl. Phys. 97, 094907, 2005.

[8] T. Maruyama et al., APL 13, 2640, 2004.

[9] Yu. A. Mamaev et al., SLAC-Pub 12249, 2006.

[10] T. Maruyama et al., Appl. Phys. Lett. 82, 4184, 2003.

[11] R. Alley et al., NIM A 365, 1-27, 1995.

[12] A. Curtoni and M. Jablonca, TESLA 2001-22.

[13] F. Zhou et al., SLAC-Pub 12240, 2007.

[14] K. Moffeit et al., SLAC-TN-05-045, 2005.

[15] L. Young, Parmela Manual, LA-UR-96-1835, 2001.

[16] MAD 8.51, CERN.

[17] M. Borland, Technical Report No. LS-287, ANL, 2000.

[18] BCD, Sept 21, 2006 DR Update (pg.5).

[19] M. Borland, "elegant: A Flexible SDDS-Compliant Code for Accelerator Simulation," Advanced Photon Source LS-287, September 2000.

[20] F. Zhou, Y. Batygin, Y. Nosochkov, J. C. Sheppard, and M. D. Woodley, "Start-to-end beam optics development and multi-particle tracking for the ILC undulator-based positron source", SLAC-PUB-12239, January 2007.

[21] Brechna, H, "150 kOe Liquid Nitrogen Cooled Pulsed Flux-Concentrator Magnet", The Review of Scientific Instruments, 1965

[22] J.W. Wang, et. al."Studies of Room Temperature Accelerator Structures for the ILC Positron Source", PAC05, SLAC-PUB-11767.

[23] A. Wolski, J. Gao, S. Guiducci (eds.) "Configuration Studies and Recommendations for the ILC Damping Rings", LBNL-59449 (2006).

[24] H. Ehrlichmann, S. Guiducci, K. Kubo, M. Kuriki, A. Wolski, "Recommendations for ILC Configuration Satisfying Timing Constraints", `http://www.linearcollider.org/wiki/lib/exe/fetch.php?cache&media=bcd:timingrecommendations-revapril17.pdf` (2006).

[25] G.V. Stupakov, T.O. Raubenheimer, F. Zimmermann, Phys. Rev. E52, 5499-5504 (1995).

[26] T. O. Raubenheimer, private communications.

[27] A. Wolski, J. Gao, and S. Guiducci, LBNL-59449 (2006).

[28] K. Ohmi, F. Zimmermann, and E. Perevedentsev, Phys. Rev. E 65 , 016502 (2002).

[29] L. Wang, G. Stupakov, T. Raubenheimer, in *Proceedings EPAC06*, Edinburgh (2006).

[30] L. Wang, H. Fukuma, S. Kurokawa, M. Pivi, and G. Xia, in *Proceedings EPAC06*, Edinburgh (2006).

[31] D. Rice, et al., "Production and Testing Considerations for CESR-c Wiggler Magnets", *Proceedings of the 2003 Particle Accelerator Conference*, pp. 167-169.

[32] L. Wang, private communication.

[33] F. Le Pimpec, et al., "Properties of TiN and TiZrV thin film as a remedy against electron cloud," Nuclear Instruments and Methods in Physics Research Section A 551, 187 (2005).

[34] T. Naito, H. Hayano, M. Kuriki, N. Terunuma, J. Urakawa, "Development of a 3 ns Rise and Fall Time Strip-Line Kicker, for the International Linear Collider", in preparation (2006).

[35] M. Pivi, T. O. Raubenheimer, L. Wang, K. Ohmi, R. Wanzenberg, A. Wolski, F. Zimmermann, in *Proceedings EPAC06*, Edinburgh (2006); submitted to Phys Rev. Spec. Topic AB.

[36] ZDR Collimator

[37] emma rotator

[38] LOLA

[39] FONT

[40] Juhao paper

[41] Kubo paper

[42] Frisch paper

[43] Lanfa paper

[44] RTML tuning reference 1

[45] RTML tuning reference 2

[46] RTML tuning reference 3

[47] RTML tuning reference 4

[48] Church paper

[49] Sergei paper

[50] ILC Halo Paper

[51] Collimator wakes

[52] Collimator wake jitter

[53] P. Raimondi and A. Seryi, "A novel final focus design for future linear colliders," Phys. Rev. Lett. **86**, 3779 (2001).

[54] P. Tenenbaum, "Collimator Wakefield Calculations for the ILC-TRC Report", LCC-0101, August 2002, SLAC-TN-03-038.

[55] R. Brinkmann, P. Raimondi, A. Seryi, "Halo reduction by means of nonlinear optical elements in the NLC final focus system," SLAC-PUB-8896, PAC 2001.

[56] Y. Nosochkov *et al.*, "ILC Extraction Line for 14 mrad Crossing Angle," SLAC–PUB–11591 (2005).

[57] A. Ferrari, Y. Nosochkov, "Beam losses in the extraction line of a TeV e+e- linear collider with a 20-mrad crossing angle", EUROTEV–REPORT–2005–025, SLAC–PUB–11791 (2005).

[58] Y. Nosochkov and A. Seryi, "Compensation of detector solenoid effects on the beam size in linear collider," Phys. Rev. ST Accel. Beams **8**, 021001 (2005).

[59] B. Parker and A. Seryi, "Compensation of the effects of a detector solenoid on the vertical beam orbit in a linear collider," Phys. Rev. ST Accel. Beams **8**, 041001 (2005).

[60] D. Schulte, PhD. thesis, TESLA-97-08 (1996).

[61] J. D. Fuerst *et al.*, "An RF separated Kaon beam from the main injector : Superconducting aspects," FERMILAB-TM-2060, 1998; M. McAshan, R. Wanzenberg, "RF Design of a Transverse Mode Cavity for Kaon Separation", FERMILAB-TM-2144, 2001.

[62] G. Burt, A. Dexter , P. Goudket, "Effect and tolerances of phase and amplitude errors in the ILC Crab Cavity", EUROTeV Report 2006

[63] M. Liepe, SRF 2005, Cornell N.Y..

[64] A. Dexter, et al., "The Cavity Loaded Waveguide and Beamloading", Cockcroft-07-01.

[65] G. Christian et al, "The electromagnetic background environment for the interaction-point beam feedback system at the International Linear Collider", Proceedings of EPAC 2006, Edinburgh.

[66] P.N. Burrows et al, "Performance of the FONT3 fast analogue intra-train beam-based feedback system at ATF", Proceedings of EPAC 2006, Edinburgh; Eurotev-report-2006-063.

[67] P.N. Burrows et al, "Design of the ILC prototype FONT4 digital intra-train beam-based feedback system", Proceedings of EPAC 2006, Edinburgh; Eurotev-report-2006-062.

[68] G. A. Moortgat-Pick *et al.*, "The role of polarized positrons and electrons in revealing fundamental interactions at the linear collider," arXiv:hep-ph/0507011.

[69] K.C Moffeit, M. Woods, Y. Nosochkov , K.P. Schuler, K. Moenig, and W. Oliver, "Polarization Setup and Polarimetry for 2 IRs, and Status of Downstream Polarimeter Designs", SLAC-PUB-11322, 2005, IPBI_TN-2006-1.

[70] N. Meyners, V. Gharibyan, K.P. Schuler, "Upstream Polarimetry with 4-magnet Chicane", presentation at LCWS05.

[71] K. Bane, "Resistive wall wake in the ILC IR", BDS meeting of 16 May 2006, http://www-project.slac.stanford.edu/lc/bdir/meetings_beamdelivery.asp

[72] L. Keller, T. Maruyama, "Updates on Beam-gas effects in BDS and background", 5 Dec. 2006, http://ilcagenda.linearcollider.org/conferenceDisplay.py?confId=1277

[73] J. Amann, "IR hall deflection study", BDS meeting of 31 October 2006, http://ilcagenda.linearcollider.org/conferenceDisplay.py?confId=1225

[74] K. Kubo. ILC-Asia Note 2006-05

[75] K. Kubo. ILC-Asia Note 2006-05

[76] P. Tenenbaum, A. Latina, K. Kubo, J. Smith. To be published at PAC 2007.

[77] N. Walker. EUROTeV-Report-2005-017

[78] A. Latina et al.. EUROTeV-Report-2006-050

[79] K. Ranjan et al. MOP064 at LINAC 2006.

[80] K. Kubo. ILC-Asia Note 2005-25, ILC-Asia Note 2005-23

[81] J. Smith et al. To be published

[82] J. Smith. PhD thesis. To be published.

[83] K. Kubo. ILC-Asia Note 2006-04

[84] P. Eliasson and D. Schulte. EUROTeV-Report-2005-021

[85] K. Kubo. ILC-Asia Note 2005-18, ILC-Asia Note 2005-17

[86] R. Jones et al. EPAC 2006.

[87] D. Schulte. EUROTeV-Memo-2006-010

[88] G. White, D. Schulte, N. Walker. SLAC-PUB-11340, EUROTEV-REPORT-2005-001, Jul 2005.

[89] G. White, D. Schulte, N. Walker. EUROTeV-Report-2006-088.

[90] L. Hendricksen, A. Seryi, G. White. SLAC-PUB-11661, Feb 2006.

[91] R.M. Jones et al., Proc. Linac 2006, Knoxville,TN.

[92] Reichold et. al. "The LiCAS-RTRS – A Rapid and Cost Efficient Survey System for the ILC" in 9th International Workshop on Accelerator Alignment, September 26-29, 2006; http://www.slac.stanford.edu/econf/C06092511/papers/WE008.PDF

[93] P. Eliasson et al., A STUDY OF FAILURE MODES IN THE ILC MAIN LINAC, EUROTeV Report-2006-040, http://www.eurotev.org/e158/e1365/e1378/e2250/EUROTeV-Report-2006-040.pdf

[94] Mattison, T. NanoBeam 2005 presentation. http://atfweb.kek.jp/nanobeam/files/presen//presen-WG2a-12.pdf

[95] Ross, M., http://www.slac.stanford.edu/cgi-wrap/getdoc/slac-pub-8605.pdf.

[96] http://www-project.slac.stanford.edu/ilc/MPS_design_rules.htm

[97] http://alcpg2005.colorado.edu/alcpg2005/program/accelerator/GG3/peter_tenenbaum20050812215847.ppt

[98] http://lhc-mp-review.web.cern.ch/lhc-mp-review/Review-Programme.html

[99] L. Bertolini *et. al.*, "Design of the Linear Non-Evaporable Getter Pump for the PEP-II B Factory," *Proc. USPAC, IEEE* (1998).

[100] C. Benvenuti *et. al.*, "A novel route to extreme vacua: the non-evaporable getters thin film coatings," *Vacuum* bf 53 (1999).

[101] "The TESLA RF System", S. Choroba, Snowmass 2004 Summary.

[102] "The FERMI SMTF Modulators," H. Pfeffer, C. Jensen & D. Wolff, August 2005 presentation.

[103] ILC Modulator Talk, C. Jensen, H. Pfeffer, D. Wolff, November 14 2004 presentation.

[104] RF System for the ILC Damping Ring, R. Boni and G. Cavallari, Frascati, July 4, 2006, ILC-LNF-001.

[105] Status Toshiba MBK, V. Vogel and S. Choroba, Hamburg, August 9, 2006.

[106] RF Source Selection for the ILC, E. Wright, H. Bolen, S. Lenci, and A. Balkcum, Snowmass 2005.

[107] MBK Testing at DESY - May 22 -June 2 2006, Daryl Sprehn, SLAC, June 15, 2006.

[108] A High Efficiency Long Pulse Multi Beam Klystron for the Tesla Linear Collider, A. Beunas, G. Faillon, Thomson TTE, France and S. Choroba, A. Gamp DESY, Germany, PAC2001.

[109] ILC Klystron Design Options and Klystron Manufacturing, G. Caryotakis, SLAC, Snowmass 2005.

[110] TESLA Technical Design Report, March 2001.

[111] Adolphsen, C. and Peterson, T. , October 2006. Table from a spreadsheet developed to calculate static and dynamic heat loads in an ILC cryomodule

[112] Cavity alignment documentation...

[113] FLASH User facility at DESY.

[114] M. Liepe, "Superconducting Multicell Cavities for Linear Colliders", DESY-THESIS-2001-045, (2001), PhD thesis.

[115] Mike Church, "Phase and Amplitude Tolerances for Crab Cavity"(2006) Internal document.

[116] T. Schilcher, "Vecor-sum Control of Pulsed Accelerating Fields in Lorentz-Force Detuned Superconducting Cavities", TESLA-Report, TESLA 98-05, (1998), PhD thesis.

[117] Marcus E., Stern H., "Blueprints for High Availability" Second Edition, Wiley Publishing Inc. 2003.

[118] Gotz A., Schmidt D., Clausen M., "Middleware in Accelerator and Telescope Control Systems" 9th International Conference on Accelerator and Large Experimental Physics Control Systems, Gyeongju, Korea, Oct. 13-17, 2003, ICALEPCS Conference Proceedings, pp 322-326 (2003).

[119] R.W. Downing, R.S. Larsen, "High Availability Instrumentation Packaging Standards for the ILC and Detectors" SLAC-PUB-12208 http://www.slac.stanford.edu/cgi-wrap/pubpage?slac-pub-12208

[120] Matlab, http://www.mathworks.com/products/matlab/

[121] "Instrumentation – Timing", Rev.1, March 23, 2001 http://docdb.fnal.gov/ILC-public/DocDB/ShowDocument?docid=107

[122] Frisch, J., Bernstein D., Brown D., Cisneros E., "A High Stability, Low Noise RF Distribution System", 2001 Particle Accelerator Conference, Chicago, IL. June 18-22, 2001, PAC 01 Conference Proceedings, pp 816-818 (2001). http://docdb.fnal.gov/ILC/DocDB/0000/000035/001/PhaseAndTiming.pd

[123] ILC Technical Note with details of CFS design

[124] http://www-ilcdcb.fnal.gov/RDR_costing_guidelines.pdf .

[125] http://www-ilcdcb.fnal.gov/RDR_Cost_Estimating_Instructions_23may06.pdf .

[126] Department of Defense, United States of America, Joint Industry Government Parametric Estimating Handbook, Second Edition, Spring 1999.